



UNIVERSITAT DE
BARCELONA

GPR37-ADENOSINE A_{2A} receptor-receptor interaction as a new pharmacological target for Parkinson's disease treatment

Xavier Morató Arús

ADVERTIMENT. La consulta d'aquesta tesi queda condicionada a l'acceptació de les següents condicions d'ús: La difusió d'aquesta tesi per mitjà del servei TDX (www.tdx.cat) i a través del Dipòsit Digital de la UB (diposit.ub.edu) ha estat autoritzada pels titulars dels drets de propietat intel·lectual únicament per a usos privats emmarcats en activitats d'investigació i docència. No s'autoritza la seva reproducció amb finalitats de lucre ni la seva difusió i posada a disposició des d'un lloc aliè al servei TDX ni al Dipòsit Digital de la UB. No s'autoritza la presentació del seu contingut en una finestra o marc aliè a TDX o al Dipòsit Digital de la UB (framing). Aquesta reserva de drets afecta tant al resum de presentació de la tesi com als seus continguts. En la utilització o cita de parts de la tesi és obligat indicar el nom de la persona autora.

ADVERTENCIA. La consulta de esta tesis queda condicionada a la aceptación de las siguientes condiciones de uso: La difusión de esta tesis por medio del servicio TDR (www.tdx.cat) y a través del Repositorio Digital de la UB (diposit.ub.edu) ha sido autorizada por los titulares de los derechos de propiedad intelectual únicamente para usos privados enmarcados en actividades de investigación y docencia. No se autoriza su reproducción con finalidades de lucro ni su difusión y puesta a disposición desde un sitio ajeno al servicio TDR o al Repositorio Digital de la UB. No se autoriza la presentación de su contenido en una ventana o marco ajeno a TDR o al Repositorio Digital de la UB (framing). Esta reserva de derechos afecta tanto al resumen de presentación de la tesis como a sus contenidos. En la utilización o cita de partes de la tesis es obligado indicar el nombre de la persona autora.

WARNING. On having consulted this thesis you're accepting the following use conditions: Spreading this thesis by the TDX (www.tdx.cat) service and by the UB Digital Repository (diposit.ub.edu) has been authorized by the titular of the intellectual property rights only for private uses placed in investigation and teaching activities. Reproduction with lucrative aims is not authorized nor its spreading and availability from a site foreign to the TDX service or to the UB Digital Repository. Introducing its content in a window or frame foreign to the TDX service or to the UB Digital Repository is not authorized (framing). Those rights affect to the presentation summary of the thesis as well as to its contents. In the using or citation of parts of the thesis it's obliged to indicate the name of the author.

PhD Thesis

**GPR37-ADENOSINE A_{2A}
RECEPTOR-RECEPTOR INTERACTION
AS A NEW PHARMACOLOGICAL TARGET
FOR PARKINSON'S DISEASE TREATMENT**

Xavier
Morató Arús

GPR37-ADENOSINE A RECEPTOR-RECEPTOR INTERACTION
AS A NEW PHARMACOLOGICAL TARGET FOR PARKINSON'S DISEASE TREATMENT



UNIVERSITAT DE
BARCELONA

Xavier Morató Arús

2017



GPR37-ADENOSINE A_{2A}
RECEPTOR-RECEPTOR INTERACTION
AS A NEW PHARMACOLOGICAL TARGET
FOR PARKINSON'S DISEASE TREATMENT

XAVIER MORATÓ ARÚS

2017



UNIVERSITAT DE
BARCELONA

**GPR37-ADENOSINE A_{2A}
RECEPTOR-RECEPTOR INTERACTION
AS A NEW PHARMACOLOGICAL TARGET
FOR PARKINSON'S DISEASE TREATMENT**

UNIVERSITY of BARCELONA

FACULTY OF MEDICINE and HEALTH SCIENCES

DEPARTMENT OF PATHOLOGY AND EXPERIMENTAL THERAPEUTICS

NEUROPHARMACOLOGY and PAIN RESEARCH GROUP

This thesis has been submitted in the Doctoral Programme in Biomedicine. Dissertation presented in partial fulfillment of the requirements for the degree of Doctor in Biomedicine by the University of Barcelona. Experimental work and manuscript have been performed by Xavier Morató Arús under the supervision of Dr. Francisco Ciruela Alférez and Dr. Víctor Fernández Dueñas.

Dr. Francisco Ciruela Alférez

Dr. Víctor Fernández-Dueñas

Xavier Morató Arús

Barcelona, June 2017

Foundings

The studies presented in this thesis were supported by the PhD fellowship Formación de Personal Investigador (FPI) (BES-2012-052722) from the Ministerio de Economía y Competitividad. The PhD Student Xavier Morató Arús also was beneficiary of a travel grant and received support for participation in scientific national and international conferences and workshops.

The studies presented in this thesis were carried out at the Unitat de Farmacologia, Departament Patologia i Terapèutica Experimental (Facultat de Medicina, IDIBELL, Universitat de Barcelona, L'Hospitalet de Llobregat, Spain) under the supervision of Professor Francisco Ciruela and Victor Fernandez, at the Departamento de Ciencias Médicas, Instituto de Investigación en Discapacidades Neurológicas (IDINE) (Facultad de Medicina, Universidad Castilla-La Mancha, Albacete, Spain) under the supervision of Professor Rafael Luján, and at the CNC-Center for Neurosciences and Cell Biology (Faculty of Medicine, University of Coimbra, Coimbra, Portugal) under the supervision of Professor Rodrigo Antunes da Cunha.

List of publications

Part of the work presented in this thesis resulted in publications in international peer-reviewed scientific journals:

1. **Morató X**, Rafael Luján, Marc López-Cano, Jorge Gandía, Igor Stagljar, Masahiko Watanabe, Rodrigo Cunha, Víctor Fernandez-Dueñas and Francisco Ciruela. The Parkinson's disease-associated GPR37 receptor interacts with striatal adenosine A2A receptor controlling its cell Surface expression and function *in vivo*. Scientific reports. July 2017. *In press*.
2. Kate Sokolina^{1#}, Saranya Kittanakom^{1#}, Jamie Snider, Max Kotlyar, Pascal Maurice, Jorge Gandía, Abba Benleulmi-Chaachoua, Kenjiro Tadagak, Victoria Wong, Ramy H. Maly, Viktor Deineko, Hiroyuki Aoki, Shahreen Amin, Laura Riley, Zhong Yao, **Morató X**, Sara Rahmati, Hiroyuki Kobayashi, Javier Menendez, Daniel Auerbach, Stephane Angers, Natasa Pržulj, Michel Bouvier, Mohan Babu, Francisco Ciruela, Ralf Jockers, Igor Jurisica, and Igor Stagljar. Systematic protein-protein interaction mapping for clinically-relevant human GPCRs. *Molecular Systems Biology*. 2017 Mar 15;13(3):918.
3. Lopes JP¹, **Morató X**¹, Souza C, Pinhal C, Machado NJ, Canas PM, Silva HB, Stagljar I, Gandía J, Fernández-Dueñas V, Luján R, Cunha RA, Ciruela F. The role of parkinson's disease-associated receptor GPR37 in the hippocampus: functional interplay with the adenosinergic system. *J Neurochem*. 2015 Jul; 134(1):135-46.

During the course of my doctoral work I actively participated in different projects that resulted in international peer-reviewed scientific journals:

4. Eduard Tolosa, **Morató X**, Carles Calatayud, Raquel Ferrer-Lorente, María José Martí, Carles Gaig, Ángel Raya, Antonella Consiglio, Mario Ezquerra, Rubén Fernández-Santiago. MicroRNA changes in iPSC-derived dopaminergic neurons from Parkinson disease patients. *Scientific Reports*. *Under review*.
5. **Morató X**, Marc López, P. M. Canas, R. A. Cunha, Francisco Ciruela. Brain membrane fractionation: An *ex vivo* approach to assess sub-synaptic protein localization. *Journal of Visualized Experiments*. *J Vis Exp*, May 2017, 12 (123).

6. Paulo A. de Oliveira, James A.R. Dalton, Marc López-Cano, Adrià Ricarte, **Morató X.**, Filipe C. Matheus, Andréia S. Cunha, Christa E. Müller, Reinaldo N. Takahashi, Víctor Fernández-Dueñas, Jesús Giraldo, Rui D. Prediger, Francisco Ciruela. Angiotensin II type 1/Adenosine A2A receptor oligomers: a novel target for tardive dyskinesia. *Scientific reports. Sci Rep.* 2017 May 12;7(1):1857.
7. Víctor Fernández-Dueñas, Jhonny Azuaje, **Morató X.**, Begoña Cordobilla, Joan Carles Domingo, Eddy Sotelo, Francisco Ciruela. Synthesis and characterization of a new bivalent ligand based on the combination of caffeine and docosahexaenoic acid. *Molecules.* Feb 2017. 27;22(3).
8. Rial D, **Morató X**, Real JI, Gonçalves FQ, Stagljari I, Pereira FC, Fernández-Dueñas V, Cunha RA, Ciruela F. Parkinson's disease-associated GPR37 receptor regulates cocaine-mediated synaptic depression in corticostriatal synapses. *Neurosci Lett.* Jan 2017. 18;638:162-166.
9. Gandía J, **Morató X**, Stagljari I, Fernández-Dueñas V, Ciruela F. Adenosine A2A receptor-mediated control of pilocarpine-induced tremulous jaw movements is Parkinson's disease-associated GPR37 receptor-dependent. *Behav Brain Res.* 2015 Jul 15; 288:103-6.
10. García-Negredo G, Soto D, Llorente J, **Morató X**, Galenkamp KM, Gómez-Soler M, Fernández-Dueñas V, Watanabe M, Adelman JP, Shigemoto R, Fukazawa Y, Luján R, Ciruela F. Coassembly and coupling of SK2 channels and mGlu5 receptors. *J Neurosci.* 2014 Oct 29;34(44):14793-802.
11. Fernández-Dueñas V, Gómez-Soler M, **Morató X**, Núñez F, Das A, Kumar TS, Jaumà S, Jacobson KA, Ciruela F. Dopamine D(2) receptor-mediated modulation of adenosine A(2A) receptor agonist binding within the A(2A)R/D(2)R oligomer framework. *Neurochem Int.* 2013 Jul;63(1):42-6.
12. Gandía J, Fernández-Dueñas V, **Morató X**, Caltabiano G, González-Muñiz R, Pardo L, Stagljari I, Ciruela F. The Parkinson's disease-associated GPR37 receptor-mediated cytotoxicity is controlled by its intracellular cysteine-rich domain. *J Neurochem.* 2013 May;125(3):362-72.

Other academic publications:

1. Fernández-Dueñas V, **Morató X**, Knöpfel T, Ciruela F. Dynamic recording of membrane potential from hippocampal neurons by using a FRET-based voltage biosensor *Neuromethods*. 2016; 110, 447-454.
2. **Morató X**, Borroto-Escuela DO, Fuxe K, Fernández-Dueñas V, Ciruela F. Co-immunoprecipitation from brain. *Neuromethods*. 2016; 110, 19-30.

The data presented in this dissertation are under preparation for submission:

1. **Morató X**, Paula García-Esparcia, Isidro Ferrer, Víctor Fernández-Dueñas and Francisco Ciruela. Cerebrospinal fluid ecto-GPR37 in Parkinson's disease.
2. **Morató X**, Rafael Luján, Nelio Gonçalves, Ana L. Carvalho, Karen Heyninck, Kathleen Van Craenenbroeck, Rodrigo Cunha, Víctor Fernandez-Dueñas, F. Ciruela. Contactin-associated protein 1 interacts with metabotropic glutamate receptor type 5 and modulates its function in the hippocampus.

I. Table of contents

Foundings	1
List of publications	3

I. Table of contents

List of abbreviations	15
-----------------------	----

II. Introduction

1. G-protein-coupled receptors (GPCRs)	25
1.1. General characteristics	
1.2. Structural features	
1.3. GPCRs classification	
1.3.1. The glutamate receptor family/Class C	
1.3.2. The rhodopsin receptor family/Class A	
1.3.3. The Adhesion receptor family/Class B	
1.3.4. The Frizzled/Taste2 receptor family	
1.3.5. The Secretin receptor family/Class B	
2. Signal transduction	33
2.1. G-protein-dependent signaling pathways	
2.2. G-protein-independent signaling pathways	
3. Post-translational modifications of GPCRs	37
3.1. Glycosylation	
3.2. Proteolytic cleavage	
4. Oligomerization	40
5. Adenosinergic and dopaminergic systems	43
5.1. Adenosine receptors (ARs)	
5.1.1. Adenosine A _{2A} receptors (A _{2A} R)	
5.2. Dopamine receptors (DRs)	
6. GPR37 and GPR37L1	59
6.1. GPR37	
7. Parkinson's disease	63
7.2. History	
7.3. Causes of PD	
7.4. Neuropathology of PD	
7.5. Clinical symptoms	
7.6. Treatment of PD	

- 7.6.1. Dopaminergic drugs
- 7.5.2. Cholinergic drugs
- 7.5.3. Serotonergic drugs
- 7.5.4. Glutamate drugs
- 7.5.5. Adenosinergic drugs

III.Hypothesis and aims 75

IV.Materials and methods

1. Antibodies	79
2. Drugs	80
3. Molecular cloning	81
3.1. Polimerase Chain Reaction (PCR)	
3.2. Restriction enzyme reaction	
3.3. DNA ligation	
3.4. Bacterial transformation	
4. Site directed mutagenesis	86
5. Colony mice C57BL6 GPR37+/+ and GPR37-/-	87
5.1. Animal house conditions/CEEA	
5.2. Strain description	
5.3. Genotyping	
6. Route of administration	90
6.1. Intraperitoneally (i.p.)	
6.2. Intracerebroventricular administration (i.c.v.)	
7. Mice sample obtention	91
7.1. Brain removal	
7.2. Striatum dissection	
7.3. Hippocampal dissection	
7.4. CSF collection	
7.5. Serum collection	
8. Crude membranes obtention	95
9. Co-immunoprecipitation	97
10.Subsynaptic fractionation	98
10.1. Obtaining synaptosomes by discontinuous sucrose gradient	
10.2. Pre-, Post- and Extrasynaptic isolation	

11. Membrane protein biotinylation	102
12. Protein concentration determination	103
13. Western Blot	104
14. Homemade polyclonal rabbit antibody generation	105
14.1. Antigenic peptide preparation	
14.2. Recombinant protein production	
14.3. Protein purification	
14.4. Immunisation	
14.5. Antibody purification	
15. Transfection: PEI	111
16. Cell culture	112
16.1. Culture conditions	
16.2. HEK-293T	
16.3. Primary neuronal culture	
16.3.1. Striatal primary cultures	
16.3.2. Hippocampal primary cultures	
17. Immunofluorescence	116
17.1. Synaptosomes and primary neuronal cultures	
17.2. Coronal brain slices	
18. Proximity Ligation Assay	118
19. Immunohistoblotting	120
20. cAMP accumulation assay	122
20.1. Total striatal synaptosomal membranes	
20.2. Striatal primary cultures	
21. Extracellular electrophysiological recordings	123
21.1. Striatal extracellular recordings	
21.2. Hippocampal extracellular recordings	
22. Behavioral test	129
22.1. Marble burying test	
22.2. Novel object recognition test	
22.3. Elevated plus maze test	
22.4. Open field	
22.5. Catalepsy	
22.6. Cued version of Water Maze	

23. Competitive ELISA	135
23.1. Recombinant protein production and purification	
23.2. Bioluminescence assay measurements	
23.3. Competitive ELISA assay	
24. Statistical analysis	140
V. Results	
Chapter I: A direct A_{2A}R-GPR37 receptor-receptor interaction modulates striatum-mediated activity	145
Chapter II: GPR37-mediated modulation of the adenosinergic system in the hippocampus	171
Chapter III: Ecto-GPR37 as a novel biomarker for Parkinson's disease	181
VI. Discussion	197
VII. Conclusions	213
VIII. References	217
IX. Acknowledgements	243

List of abbreviations

Ab	Antibody
AC	Adenylate cyclase
aCSF	Artificial cerebrospinal fluid
AD	Alzheimer's disease
ADA	Adenosine deaminase
AMP	Adenosine 5'-monophosphate
AMPA	2-amino-3-(3-hydroxy-5-methyl-isoxazol-4-yl) propanoic acid
ANOVA	Analysis of variance
AP	Alkaline Phosphatase
ARs	Adenosine receptors
A ₁ R	Adenosine receptor type 1
A _{2A} R	Adenosine receptor type 2A
AraC	Cytosine β-D-arabinofuranoside
ATP	Adenosine 5'-triphosphate
BBB	Blood Brain Barrier
BCA	Bicinchoninic acid
bp	Base pairs
BSA	Bovine serum albumin
CA1	Cornu ammonis 1
CA3	Cornu ammonis 3
cAMP	3'-5'-cyclic adenosine monophosphate
CB ₁ R	Cannabinoid CB1 receptors

CNS	Central Nervous System
Co-IP	Co-immunoprecipitation
COMT	Catechol-O-methyltransferase
CREB	cAMP response element-binding protein
CSF	Cerebrospinal fluid
DDCI	DOPA-decarboxylase inhibitor
DIV	Days in vitro
DM	Dorsomedial
DMEM	Dulbecco's Modified Eagle's Medium
DMSO	Dymethyl sulfoxide
DRs	Dopamine receptors
D ₁ R	Dopamine D1 receptors
D ₂ R	Dopamine D2 receptors
DG	Dentate gyrus
DNA	Deoxyribonucleic acid
DTT	Dithiothreitol
ECL	Extracellular loop
EDTA	Ethylenediaminetetraacetic acid
EPM	Elevated plus maze
ER	Endoplasmic reticulum
ERK1/2	Extracellular signal regulated kinase
FBSi	Fetal Bovine Serum inactivated
fEPSP	Field Excitatory Postsynaptic Potential

GABA	Gamma-aminobutyric acid
GPCRs	G-protein coupled receptor
GPS	GPCR proteolytic site
h	Hour
HD	Huntington's disease
HEK	Human embryonic kidney
HFS	High frequency stimulation
HRP	Horseradish Peroxidase
I/O	Input/Output curves
IB	Isolation Buffer
ICL	Intracellular loop
i.c.v.	Intracerebroventricular
IFA	Immunofluorescence assay
IHB	Immunohistoblot
IHC	Immunohistochemistry
i.p.	Intraperitoneally
IP3	Inositol trisphosphate
IPTG	Isopropyl β -D-1-thiogalactopyranoside
KO	Knockout
LB	Lewy bodies
L-DOPA	Levodopa, L-3, 4-dihydroxyphenylalanine
LFS	Low frequency stimulation
LID	Levodopa-induced dyskinesia

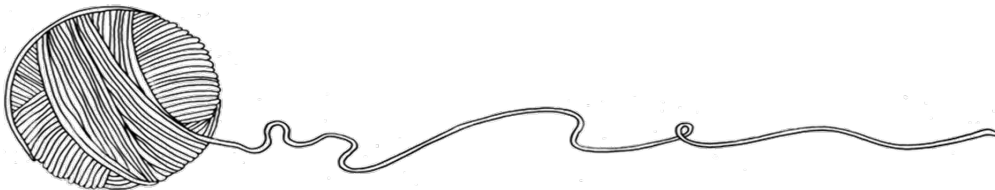
LPS	Lipopolysaccharide
LTD	Long-term depression
LTP	Long-term potentiation
MAO	Monoamine oxidase
MAPK	Mitogen-activated protein kinases
mGlu ₅ R	Metabotropic glutamate 5 receptors
min	Minutes
MPTP	1-methyl-4-phenyl-1,2,3,6-tetrahydropyridine
MSNs	Medium spiny neurons
MWM	Morris Water Maze
MYTH	Membrane Yeast Two-Hybrid
NDS	Normal Donkey Serum
NMDARs	<i>N</i> -methyl-D-aspartate receptors
NOR	Novel object recognition
OD	Optical density
OST	Oligosaccharyltransferase
PBS	Phosphate buffered saline
PCR	Polimerase chain reaction
PEI	Polyethylenimine
PD	Parkinson's disease
PKA	Protein kinase A
PKC	Protein kinase C
PLA	Proximity Ligation Assay
PPI	Protein-protein interaction

PS	Population Spike
PSD-95	Postsynaptic density-95
R	Recording electrode
RIPA Buffer	Radioimmunoprecipitation assay buffer
Rluc	Renilla luciferase
Rpm	Revolutions per minute
S-aCSF	Sucrose artificial cerebrospinal fluid
SDS-PAGE	Sodium dodecyl sulfate–polyacrylamide gel electrophoresis
SE	Stimulation electrode
Sec	Seconds
SEM	Standard error of the mean
SNC	Substantia nigra pars compacta
STV	Streptavidin
TH	Tyrosine hydroxylase
T _m	Melting temperature
7TM	7 transmembrane domain
WB	Western Blot
WT	Wild type

The experimental work presented has been carried out by the author of this thesis. The immunogold electron microscopy experiments were obtained in collaboration with Professor Rafael Luján (Departamento de Ciencias Médicas, Instituto de Investigación en Discapacidades Neurológicas, Universidad Castilla-La Mancha, Albacete) and the extracellular hippocampal and striatal recordings experiments were made in collaboration with Professor Rodrigo Antunes da Cunha (Center for Neurosciences and Cell Biology and Faculty of Medicine, University of Coimbra).

“When you are afraid, your heart beats faster, your blood pressure rises, and you breathe more heavily. This is partly the result of adrenaline forming in your body, which causes your heart rate to accelerate. Adrenaline is a hormone, a substance that manages communication between the cells in your body. Each cell has a small receiver known as a receptor, which is able to receive hormones. What these receptors look like and how they work remained a mystery for many years”.

In 1968, in order to track these receptors, Robert Lefkowitz tagged different hormones with a radioactive isotope. By tracking the radiation emitted by the isotope, he succeeded in finding a receptor for adrenaline. In the 1980s, Brian Kobilka identified the gene that regulates this receptor. The two researchers also discovered that the receptor was similar to receptors located in the eye that capture light. It was later discovered that there is an entire family of receptors that look and act in similar ways - known as G-protein-coupled receptors (GPCRs). Approximately half of all medications used today make use of this kind of receptor. Robert Lefkowitz and Brian Kobilka received the 2012 Nobel Prize in Chemistry for untangling the skein of GPCRs and establishing the basis to understand how they work.



II. Introduction

1. G-protein-coupled receptors

1.1. General characteristics

G-protein-coupled receptors (GPCRs) constitute the largest family of membrane proteins, representing >1% of the human genome and encoding >1000 proteins. Nearly 80% of known hormones and neurotransmitters activate cellular signal transduction mechanisms by activating GPCRs, and it has been estimated that GPCRs represent 30 – 45% of current drug targets (1). Indeed, due to the implication of these receptors in many diseases (2)(3)(4), GPCRs have become the most used targets for drug discovery by the pharmaceutical industry (5). GPCRs share a common seven-transmembrane (7TM) topology and mediate cellular responses for a variety of extracellular signals (**Figure 1**). Thus, extracellular and transmembrane regions contribute to the formation of a pocket within the plasma membrane where selective ligands for the receptor are bound (6). Ligands that bind to GPCR include: photons, hormones, neurotransmitters, nucleotides, odor substances, lipids, small peptides, entire proteins and sugars (7)(8). There still are a large number of GPCRs pending to be de-orphanized, this is, to know the endogenous ligand that binds to the receptor. Also, it is possible that some of them lack an endogenous ligand. Thus, some recent studies have indicated that some orphan GPCRs are not capable of binding any endogenous ligands, but instead they can regulate the function of other non-orphan GPCRs (9).

GPCRs are named based on their ability to recruit and regulate the activity of intracellular heterotrimeric G-proteins. In such way, when GPCRs are activated by its ligand, they transduce the signal to heterotrimeric G-proteins, which transmit the signal to effector proteins, such as enzymes and ion channels, resulting in rapid changes in the concentration of intracellular signaling molecules (i.e. cAMP, cGMP, inositol phosphates, diacylglycerol, arachidonic acid, cytosolic ions) (10)(11)(12). Taking the adenosine A_{2A} receptor (A_{2A}R) as an example, the binding of adenosine leads to the activation of the stimulatory subunit of the heterotrimeric G-protein (G_{αs}), which stimulates the adenylate cyclase that mediates the accumulation of cyclic AMP (cAMP), and thereafter the activation of cAMP-dependent protein kinase A (PKA). Finally, the activation of this signaling pathway, results within other changes, in the phosphorylation of cAMP response element-binding protein (CREB), which has been shown to inhibit nuclear factor-κB transcriptional activity (13).

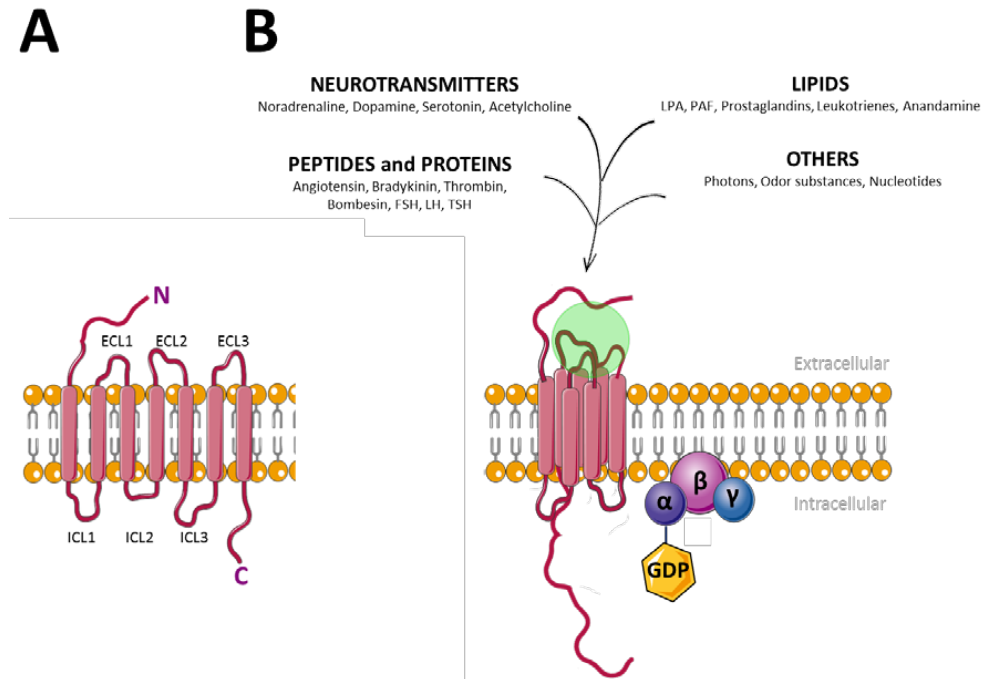


Figure 1. General characteristics of GPCRs. (A) General structural characteristics of GPCRs. Representation of the 7TM α -helices connected by three intracellular and three extracellular loops. **(B)** Ligand diversity for GPCRs. A wide variety of ligands, including neurotransmitters, lipids, peptides and proteins, use GPCRs to stimulate cytoplasmic and nuclear targets through heterotrimeric G-protein-dependent and -independent pathways.

1.2. Structural features

GPCRs do not share an overall sequence homology (14). Thus, the sequence homology shared by over 1000 GPCRs is limited to a number of conserved motifs that are likely to play similar functional roles in most of them (15). Nevertheless, GPCRs share a common tertiary structural signature of 7 hydrophobic transmembrane α -helix segments that span the plasma membrane in an anti-clockwise manner. For this reason these receptors are also named as Seven Transmembrane Receptors (7TMRs). These transmembrane domains are connected with 3 extracellular (ECL1, ECL2 and ECL3) and 3 intracellular (ICL1, ICL2 and ICL3) loops, with an extracellular amino terminus and an intracellular carboxyl terminus (**Figure 2**). The N-terminal segment presents the greatest amino acid diversity (16) and is the site for glycosylation. The C-terminal segment allows palmitoylation and phosphorylation, which are prerequisites for desensitization and internalization. Interestingly, GPCRs share the greatest homology within the TM

segments, while the most variable structures are the carboxyl terminus, the intracellular loop spanning TM5 and TM6, and the amino terminus. Nevertheless, due to the inherent difficulties in crystallizing complex membrane proteins, poor GPCRs high-resolution structural information is available. Recent advances in high quality protein production, protein stabilization by point mutations or antagonist addition, have significantly improved the determination of X-ray crystal structural studies of GPCRs (17), and enriched our understanding of the structure and the process of G-protein signaling. Over the last years, some laboratories have been able to obtain crystals of a number of receptors, such as bovine rhodopsin (18), β 1-adrenergic (19), β 2-adrenergic (20), or A_{2A}R (21). These studies have permitted predicting the helical arrangement within the transmembrane bundle and conformational changes due to GPCR activation.

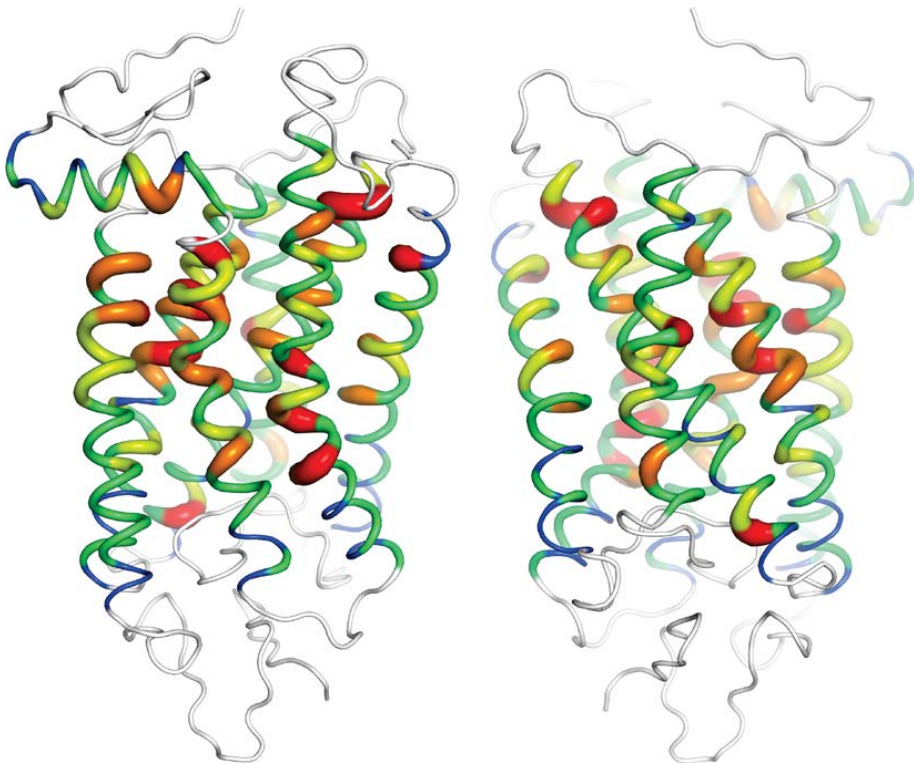


Figure 2. Amino acid homology within the transmembrane region of GPCRs.

Shown are the conserved sequences in all GPCRs mapped onto the rhodopsin structure, ranging from red to yellow to blue to indicate high to low homology at individual positions. For clarity, the thickness of the trace also corresponds to the degree of conservation. Noteworthy, while overall sequence homology between GPCRs is low, many amino acid positions within the transmembrane region are highly conserved and are likely to play similar functional roles in most of them. Figure adapted from (22).

1.3. GPCRs classification

Both physiological and structural features have been used to classify GPCRs. For instance, some classification systems group the receptors based on where the ligand binding pocket is situated. The most frequently used classification system is the A–F, presented in 1994 by Kolakowski and divided into 6 different classes. It contains both vertebrates and invertebrates GPCRs, and each family shares >20% amino acid sequence identity within the TMs (23). A-F classes and their prototype members are as follows: Class A (rhodopsin-like), Class B (secretin receptor family), Class C (metabotropic glutamate), Class D (fungal mating pheromone receptors), Class E (cyclic AMP receptors) and Class F (frizzled/ smoothed). Of note, classes D and E are not found in vertebrates. Recently, after a large scale phylogenetic analysis of the majority of GPCRs present in the human genome, a new classification system was depicted: the GRAFS classification System (**Figure 3A-B**)(24), which is formed by 5 families: Glutamate (G), Rhodopsin (R), Adhesion (A), Frizzled/Taste2 (F) and Secretin(S). Needless to say, despite the similarities, individual GPCRs have unique combinations of signal-transduction activities involving multiple G-protein subtypes, as well as G-protein-independent signaling pathways and complex regulatory processes.

1.3.1. The glutamate receptor family/Class C

This family of receptors consists of 22 human proteins: among them this family includes eight metabotropic glutamate receptors (GRM), two Gamma-aminobutyric acid (GABA) receptors, a single calcium-sensing receptor (CASR), and five receptors that are believed to be taste receptors (TAS1). Most Glutamate family members have the ligand recognition domain in a 280 to 580 amino acids N-terminal region. The glutamate binding region is really conserved within GRMs, CASR and TAS1Rs (25). The ligand-binding mechanism of the extracellular region has been compared to a Venus flytrap mechanism (VFTM), in which the two lobes of the region form a cavity where glutamate binds and thereby activates the receptor. Apart from the structurally similar ligand-binding domain, the extracellular regions also contain a cysteine rich domain (CRD), consisting of nine conserved cysteine residues forming three predicted disulphide bridges important for signal transduction (26).

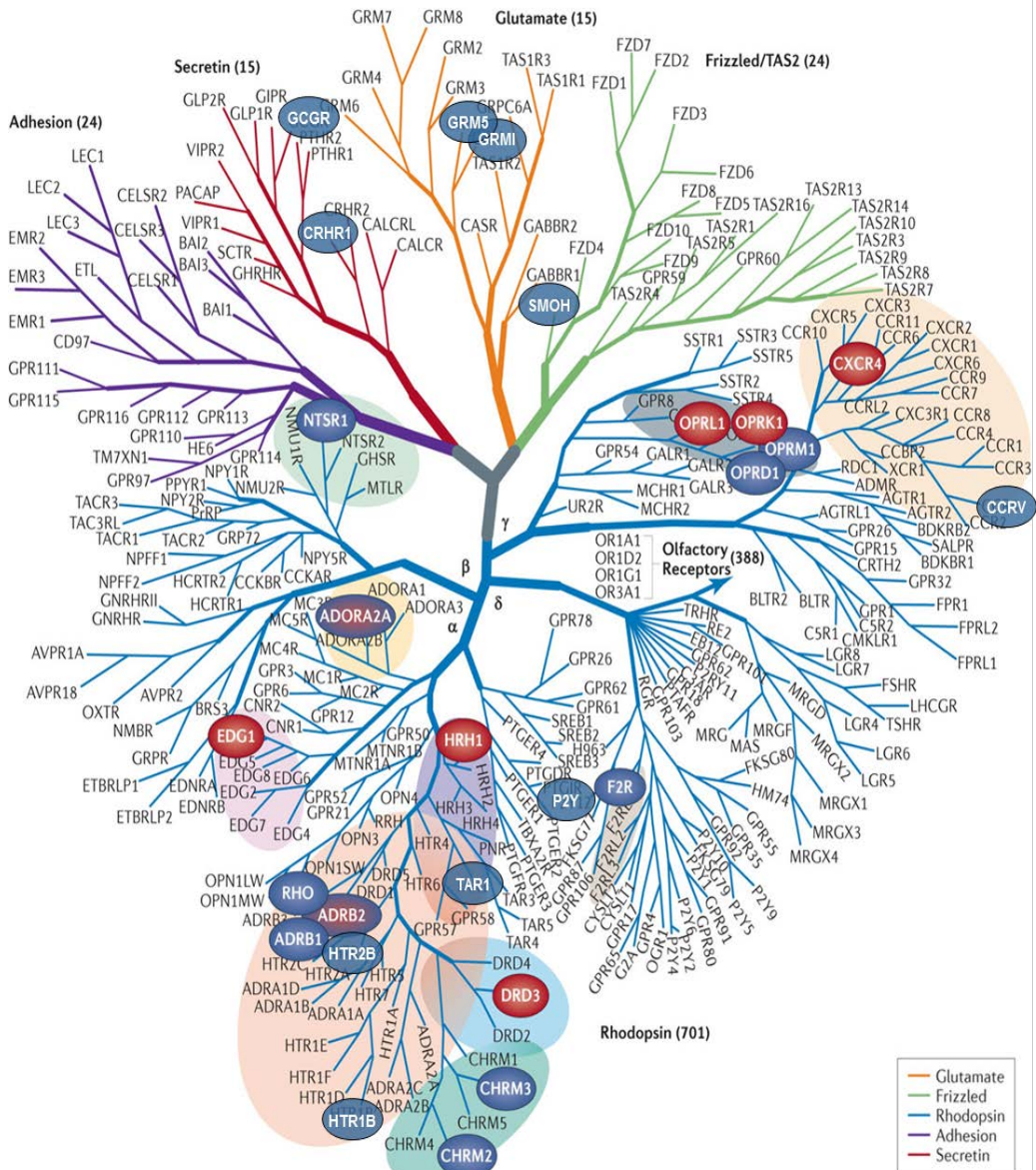


Figure 3A. GPCRs GRAFS classification. Human GPCRs, can be phylogenetically classified into five major families: Glutamate (G), Rhodopsin (R), Adhesion (A), Frizzled/Taste2 (F) and Secretin(S). These families can be further divided into subfamilies on the basis of sequence similarity. This phylogenetic tree was constructed using sequence similarity within the 7TM region. GPCRs are named according to their gene name used by the UniProt database. Crystallographied GPCRs are highlighted in blue or red boxes. Figure adapted from (27).

1.3.2. The rhodopsin receptor family/Class A

The Rhodopsin receptor family is the largest family of GPCRs and contains ~670 full-length human receptor proteins. The rhodopsin family is subdivided into four groups (α , β , δ and γ). In 2000, bovine rhodopsin was crystallized, obtaining the first high-resolution structure of a GPCR (18). It was observed from the X-ray studies that several of the conserved residues within the Rhodopsin family formed interhelical networks that play a central role in the stabilization and activation of rhodopsin. Later, the high-resolution structure of the β 2-adrenoceptor (ADRB2) provided a second model for Rhodopsin GPCRs. Most receptors from this family have a short N-terminal region and share specific sequence motifs within the 7TM regions (28). However, some have a large N-terminal domain that is cleaved prior to receptor activation. For instance, the human thrombin receptor (PAR1/F2R) has an intrinsic cleavage site in the N-terminus, which, upon cleavage by thrombin, reveals a tethered ligand that is able to activate the receptor (29). Similarly, other receptors have been shown to also display a protease-dependent activation mechanism: the protease-activated receptors 2–4 (PAR2–4). However, most Rhodopsin receptors are primarily activated by interactions between the ligand and the TM regions and extracellular loops.

Regarding the distinct subgroups of the rhodopsin family, the α -group contains important drug targets like the histamine receptors 1 and 2 (HR H1-2), the dopamine receptors 1 and 2 (DRD1-2); the serotonin receptors 1A, 1D and 2A (HTR1A-1D-2A), the adrenoceptors 1A, 2A, B1 and B2 (ADR1A-2A-B1-B2), the muscarinic receptor 3 (CHRM3) and the cannabinoid receptor 1 (CBR1). On the other hand, the β -group mainly includes peptide-binding receptors such as endothelin (EDNRA-B), gonadotropin-releasing hormone (GNRHR) and oxytocin (OXTR) receptor ligands. Most of the peptide ligands in this group bind to a binding pocket within the TM regions with participation of the extracellular loops and the N terminus. However, it is challenging to find agonists for peptide receptors, as most endogenous peptides are non-selective and act in multiple subtypes of the receptor (i.e. SRIF peptide activates all 5 subtypes SRIF receptors) (30). Also, neuropeptides use a multitude of interaction sites in the ligand binding pocket, and small molecules are seldom able to mimic the interactions required to induce a full agonistic signal (31). Next, the γ -group includes receptors for both peptides and lipid-like compounds (18), such as the three opioid receptors, somatostatin receptor 2 and 5 (SSTR2 and SSTR5) and angiotensin receptor 1 (AGTR1). Finally, the δ -group mostly contains the P2RYs, the glycoprotein-binding receptors, the PARs and the olfactory receptors.

1.3.3. The Adhesion receptor family/Class B

Despite the Adhesion receptor family is the second largest GPCR family in humans, with 33 members, only few of them have been de-orphanized (32)(33). Adhesion GPCRs are characterized by extremely long N-terminal regions that contain various modular adhesion domains, such as epidermal growth factor-like repeats, thrombospondin-like repeats, and cadherin-like repeats, among others (34). The extracellular N-terminal region also contains the GPCR proteolytic (GPS) domain proximal to the first transmembrane helix. The proteolytic cleavage of the receptor protein occurs in the Golgi apparatus or the endoplasmic reticulum. Mutations in the GPS domain impairs correct folding and transport to the membrane. Proteolytic cleavage of the receptor rise to a membrane-spanning and an extracellular subunit, which reassociate non-covalently, resulting in expression of a heterodimeric receptor at the cell surface (35). Adhesion receptor family share high sequence similarity between the TM regions with the Secretin receptors family.

1.3.4. The Frizzled/Taste2 receptor family

The Frizzled and Smoothened receptors consists of ten frizzled receptors (FZD1–10) and the smoothened receptor (SMO). The FZDs bind the family of Wnt glycoproteins, whereas the SMO protein seems to function in a ligand-independent manner as the signaling unit in the patched, sonic hedgehog (SHH). The other components of this family are the Taste2 receptors (T2Rs), a family of ~30 highly divergent GPCRs. Interestingly, T2Rs are necessary and sufficient for selective responses to bitter tastants. Bitter taste has the onerous task of preventing the ingestion of a large number of structurally distinct toxic compounds (36).

1.3.5. The Secretin receptor family/Class B

Secretin receptor family is a small family of GPCRs formed by 15 members, which name arose because Secretin was the first ligand to be isolated from this group. Secretin family share an extracellular hormone-binding domain and are activated by peptides that vary in length from 24 to 53 amino acids such as hormones and neuropeptides. Secretin-like receptors are characterized by the existence of a large N-terminal domain, with at least six highly conserved cysteines that are proposed to be involved in ligand binding (37). Of note, secretin receptor family and their cognate peptide ligands are implicated as drug targets in many pathologies, such as migraine (calcitonin gene-related peptide),

cardiovascular diseases (adrenomedullin), diabetes (glucagon-like peptide 1), osteoporosis (calcitonin, parathyroid hormone) and inflammation (vasoactive intestinal peptide) (38).

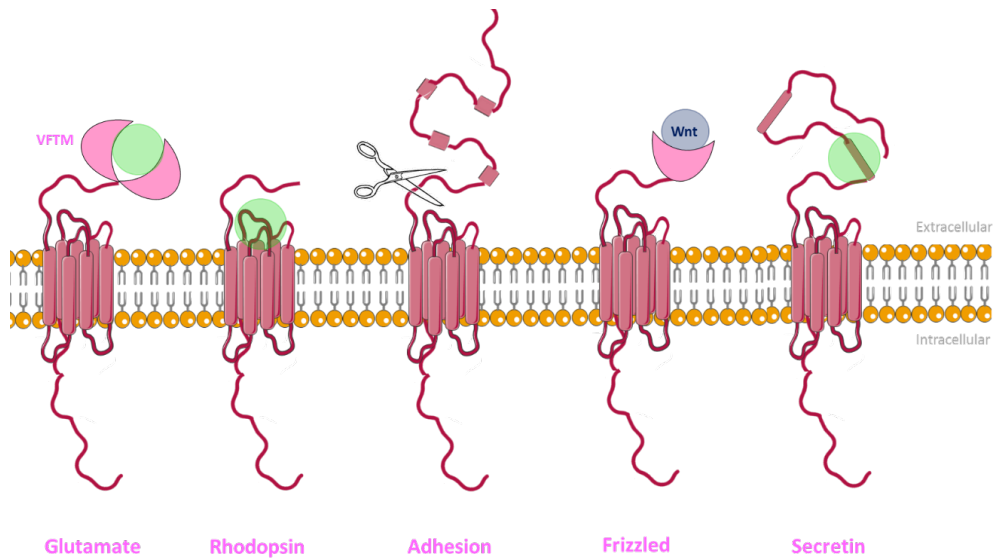


Figure 3B. GPCRs GRAFS classification. The 5 families forming GRAFS classification system show specific structure characteristics. Oversimplification of the N-terminal structure and the ligand binding site for the GPCR activation.

2. Signal transduction

GPCRs activation leads to recruiting and regulating the activity of intracellular heterotrimeric G-proteins (composed of α , β , γ -subunits). However, GPCR signaling is much more complex, and it is now widely accepted that GPCRs may not solely act via heterotrimeric G-proteins, but they also activate G-protein-independent signaling pathways.

2.1. G-protein-dependent signaling pathways

When a ligand interacts with a named GPCR, the activated receptor induces a conformational change that leads to the recruitment and activation of the associated G-protein (14). The heterotrimeric G-protein complex is comprised of a $G\alpha$ subunit, from which there are four main families based on similarities (*Gas*, *Gai/o*, *Gaq/11* and *G α 12/13*), coupled to a combination of $G\beta$ and $G\gamma$ subunits, from which there exist 5 and 12 members, respectively.

In the inactive heterotrimeric state, a GDP molecule is bound to the G α -subunit. After activation, α -subunit undergoes GDP release, followed by binding of GTP. Subsequently, the GTP-bound form of the α -subunit dissociates from the receptor as well as from the stable $\beta\gamma$ -dimer (10). The β and γ subunits of G-proteins form an irreversible heterodimer that functions as a single entity in the G-protein cycle. Both the GTP bound α -subunit and the released $\beta\gamma$ -dimer can modulate several cellular signaling pathways. These include, among others, direct effects on signaling proteins like adenylate cyclases (AC), activation of phospholipase C (PLC) and regulation of potassium and calcium channel activity. The duration of the signal is determined by the intrinsic GTP hydrolysis rate of the $G\alpha$ -subunit and the subsequent reassociation of $G\alpha$ -GDP with $G\beta\gamma$. $G\alpha$ -subunits contain two domains: a GTPase domain that is involved in the binding and hydrolysis of GTP and a helical domain that buries the GTP within the core of the protein. Once $G\alpha$ -GTP has dissociated from the G $\beta\gamma$ -dimer, $G\alpha$ can directly interact with effector proteins to continue the signaling cascade. The specific effector proteins activated by $G\alpha$ are dependent on the $G\alpha$ -subtype. Some $G\alpha$ -subunits have only one identified effector, such as cGMP phosphodiesterase for *Gat*, whereas others more promiscuously couple to several effector proteins.

The signal transduction pathways of G_s, G_i and G_q protein families are well-characterized, whereas signaling properties of G₁₂ proteins have not still been deeply studied (**Figure 4**). The adenylate cyclase family is one of the main intracellular effectors for G-proteins and it is responsible of synthesizing cAMP from ATP. AC responds to GPCR induced stimulatory or inhibitory regulation, mediated either by G_{α_s} or G_{α_{i/o}} respectively. At least 9 mammalian AC isoforms have been functionally characterized and all isozymes can be stimulated by G_{α_s} and, experimentally, by the plant diterpene forskolin (except AC-IX). Of note, G_{α_s} and G_{α_{i/o}} proteins and Forskolin do not compete for the same AC binding sites (39). Many known GPCRs signal through G_s (i.e. A_{2A}R) and G_{i/o} (i.e dopamine D₂ receptor; D₂R). The principal target of the G_q class is phospholipase C (PLC), which is involved in the conversion of phosphatidylinositol (4,5)P₂ to the Ca²⁺-mobilizing second messenger inositol trisphosphate (inositol (1,4,5) P₃, IP₃), and the protein kinase C-activating second messenger diacylglycerol (DAG). This activation results in the activation of PKC by DAG and an increased mobilization of intracellular calcium in response to IP₃, mechanisms that have been related with the modulation of synaptic transmission, cell growth and platelet aggregation. Finally, activation of heterotrimeric G₁₂ and/or G₁₃ proteins stimulates the small GTPases by stimulating specific GEFs (Guanine Nucleotide Exchange Factors), implicated in cytoskeleton reorganization.

It is now recognized that the Gβγ complex, which has been historically considered a stabilizing binding partner for Gα subunits, is involved in an independent signaling pathway upon G-protein activation. Thus, the Gβγ complex directly regulate some AC (40), also participates in the activation of Extracellular signal regulated kinase (ERK1/2) pathway via c-Src activation, recruitment of adaptor protein Growth factor receptor-bound protein 2 (GRB2) (41)(42) and activation of some phospholipases (43).

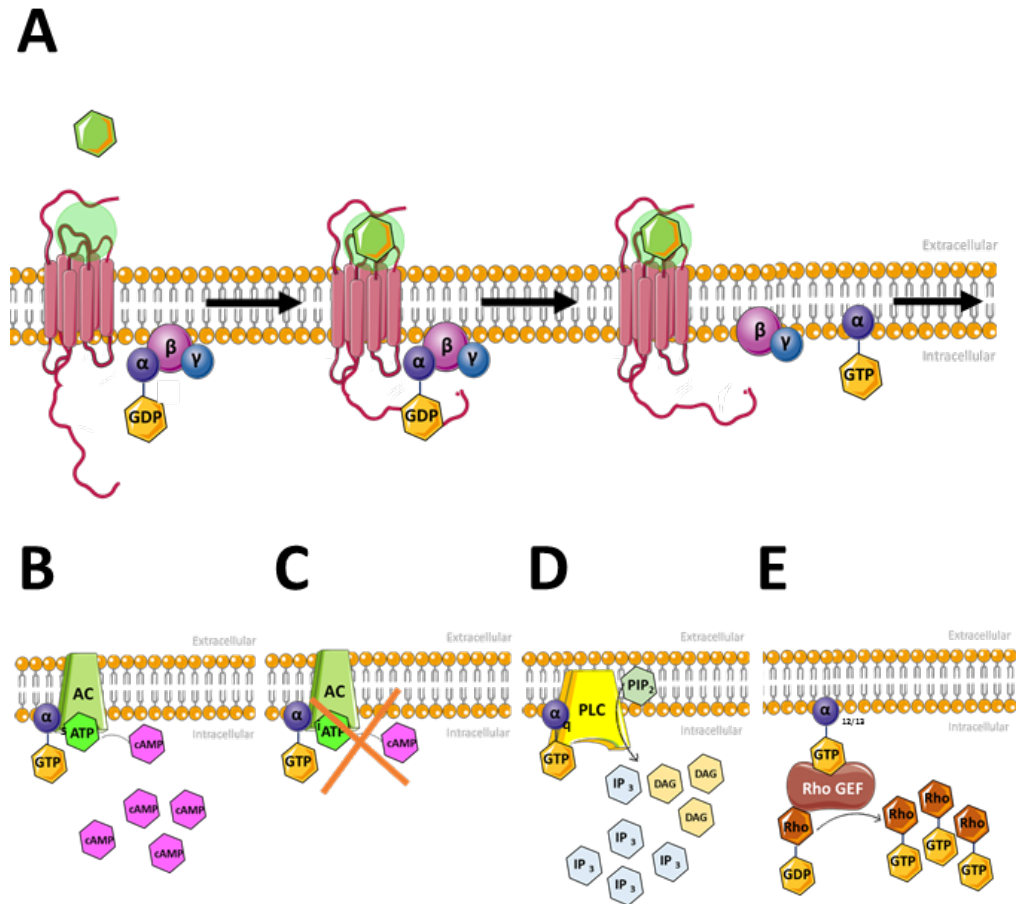


Figure 4. $G\alpha$ -subunit role in the GPCRs G-protein-dependent signaling pathways. (A) The interaction of an endogenous ligand with its specific GPCR promotes conformational changes in the receptor that facilitates the coupling with intracellular heterotrimeric G-proteins. Then, the exchange of GDP for GTP on the $G\alpha$ -subunit, end with the dissociation of the $G\alpha$ -subunit from $G\beta\gamma$. Depending on the $G\alpha$ subunit family, different signaling pathways will be activated. (B) $G\alpha_s$ promotes cAMP formation by AC. (C) $G\alpha_{i/o}$ inhibits AC. (D) $G\alpha_{q/11}$ stimulate formation of IP₃ and DAG by PLC. (E) $G\alpha_{12/13}$ activates Rho GTPase nucleotide exchange factors (RhoGEFs).

2.2. G-protein-independent signaling pathways

Some GPCRs signal via G-protein independent pathways. Thus, besides heterotrimeric G-proteins, other protein families (i.e. G-protein coupled receptor kinases (GRKs) and β -arrestins) have the ability to interact with these kinds of receptors. The GRKs and β -arrestins were first described as molecules that simply desensitized G-protein-mediated signaling. However, they orchestrate GPCRs activities at three different levels: i) silencing: the functional uncoupling of the receptor from its cognate G-protein by a mechanism known as homologous desensitization; ii) trafficking: receptor internalization, 'resensitization' and/or degradation; and iii) signaling: the activation or inhibition of intracellular signaling pathways independently from heterotrimeric G-proteins.

The GRK family consists of seven different genes. Expression of GRK1 and 7 are confined to retinal rods and cones, respectively, and are important for adaptation to light whereas GRK4 has very limited expression in the cerebellum, testis and kidney. By contrast, GRK2, 3, 5 and 6 are widely expressed in mammalian tissues. GRKs phosphorylates a wide range of receptors and are involved in receptor desensitization, which occurs only in agonist-occupied receptors, ensuring that only those receptors that have been activated are desensitized.

On the other hand, the β -arrestin family is formed by 3 different genes (44): The named cone arrestin, which distribution is limited to cones and to the pineal gland, and β -arrestin 1 and β -arrestin 2, which are widely expressed throughout the body. β -arrestin initiates a process known as internalization, endocytosis or sequestration of several GPCRs, acting as adaptors that link the receptors to Clathrin-coated pits. Thus, after the GRK-mediated phosphorylation of GPCRs, β -arrestins bind to the receptor, and recruit clathrin. β -arrestins can serve as adaptor proteins or interact with the Src protein kinase complex that regulates cell proliferation and differentiation (45). Also, they facilitate the activation of Mitogen-activated protein kinase (MAPK)/ERK cascades (46).

3. Post-translational modifications of GPCRs

GPCRs undergo a variety of post-translational modifications, including glycosylations, proteolytic cleavage, palmitoylations, phosphorylations and ubiquitinations (47). Each of these processes have distinct roles in expression and function of GPCRs and highlights the complex regulation of these receptors.

3.1. Glycosylation

The polypeptide chain of a GPCR suffers post-translational modifications when inserted into the membrane of the endoplasmic reticulum (ER). These modifications, which occur during translation process, may be sufficient to establish the proper receptor fold. For instance, asparagine (N)-linked glycosylation of proteins is an important and highly regulated post-translational modification that results in the covalent attachment of an oligosaccharide onto asparagine residues of polypeptide chains (**Figure 5**). It plays a critical role in determining protein structure, function and stability. Many cell surface proteins that transit through the ER are N-glycosylated (95% of GPCRs). Specific consensus tripeptide sequence Asn-X-Ser/Thr are the potential N-glycosylation sites and the acceptors of the oligosaccharide are selected asparagine (Asn or N) residues of this polypeptide chain. The oligosaccharyltransferase (OST) catalyzes the transfer of the oligosaccharide to Asn in the ER lumen. After being covalently linked to proteins, the N-glycan can be modified in a sequential processing coupled to the secretory pathway through the ER and Golgi and results in a species-specific or even cell type-specific diversity of N-linked glycans (48). Proper receptor biosynthesis, trafficking, ligand binding and function depends on this post-translational modifications. A screening of human GPCRs revealed that of the receptors glycosylated in at least one ECL, 66% contained the tripeptide in the ECL2, and only 14% and 20% in ECL1 and ECL3 respectively (49). Protein quality control, correct receptor folding through the alteration of hydrophobicity, protection from protease-mediated degradation and cell–cell interactions, regulating at the end the receptor surface expression are dependent on these glycosylations. Changes in these glycosylations can cause dramatic intracellular receptor accumulation and a decrease in receptor cell surface expression. Glycosylation is absolutely required for the cell-surface expression of the receptors (i.e. N-linked glycosylation of AT1R and FSHR) (50). Several cycles of glycosylation and deglycosylation are repeated until glycoproteins reach its proper folded conformation or are targeted for degradation.

family N-terminal domains contains conserved autoproteolysis sites termed GPS (53). Cleavage of these GPS plays a critical role in intracellular trafficking. Uniquely, the adhesion GPCR, GPR56, undergoes obligate N-terminal cleavage during ER/Golgi trafficking, creating a constitutively active receptor.

On the other hand, some GPCRs contain an N-terminal domain that augment the binding properties of endogenous ligands, like the metabotropic glutamate receptors family. Receptors belonging to this family use their extremely long N-terminal domain to form the glutamate-binding site and modulate ligand selectivity (54). GPCR N-terminal domains can also facilitate proper assembly and impart stability to GPCR macromolecular complexes, thus contributing to the stable formation of the named receptor oligomers. This characteristic has been described for several receptors, including mGluR1 and GABAB R1/R2 receptors (55). In some cases, the proteolytic cut adjacent to the plasma membrane is followed by a release of the extracellular ecto-domain in a process called shedding, in which cleaved fragments may act as ligands in a paracrine or autocrine fashion.

4. Oligomerization

For a long time, GPCRs were assumed to work as monomers, since a single GPCR is sufficient to activate an specific intracellular signaling pathway. Models that describe the interaction of GPCRs with their G-proteins are generally based on the assumption that receptors couple to G-proteins in a 1:1 ratio. The hypothesis that GPCR could interact in cell membranes was initially put forward in the early 1980s. Nowadays, many biochemical, estructural and functional studies, indicate that GPCRs also exist as functional dimers or higher oligomeric units, a phenomenon that is crucial for a proper activity (56)(57). GPCR oligomerization has been generally studied using classical biochemical (i.e. co-immunoprecipitation), electron microscopy techniques (i.e. double-immunogold labeling) and biophysical (resonance energy transfer, i.e. Bioluminescence resonance energy transfer, BRET and Fluorescence resonance energy transfer, FRET) methods. And more recently, by novel techniques such as proximity ligation assay (PLA). The comprehension of oligomeric protein structures and their regulation have significantly progressed due to structures determination by NMR and X-ray crystallography, since they enable detailed characterization of the oligomerization interfaces and the interactions that stabilize oligomers (58)(59). Hence, it is now well accepted that oligomerization is a common property of proteins and takes place in many biological systems.

GPCRs can exist as homodimers, when dimerization includes the association of two identical receptors, or as heterodimers, when two non-identical receptors associate. Also, they may exist as homooligomers and heterooligomers, when more than two proteins associate (**Figure 6**) (60)(61).

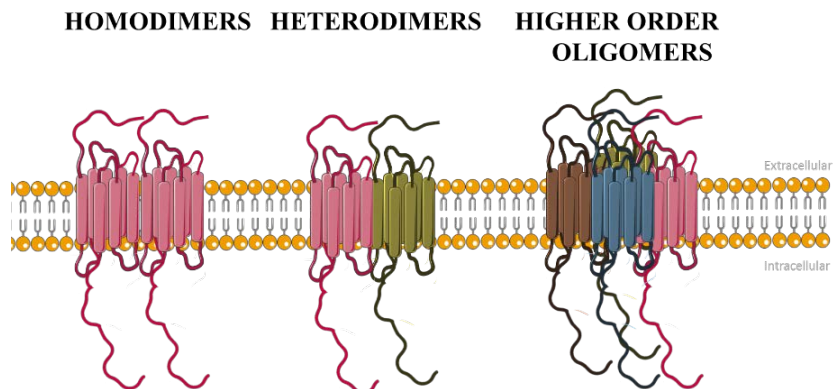


Figure 6. Diversity of GPCR oligomerization. Combination of functional GPCRs can include homo- and hetero-dimers or higher-order oligomers with unique physiological/signaling properties.

Receptor-receptor interactions can be mediated by covalent and/or non-covalent receptor interactions involving extracellular, intracellular and the transmembrane domains. The life of GPCRs begins at the ER, where they are synthesized, folded and assembled. Properly folded receptors are recruited and packaged into vesicles, transported to the ER-Golgi intermediate complex (ERGIC), the Golgi apparatus and the trans-Golgi network (TGN); and finally, mature receptors move to their functional destination at the plasma membrane. During their migration, receptors undergo post-translational modifications to attain mature status. Oligomerization can initially occur in the ER, where it plays an important role in the biosynthesis and quality control of newly synthesized receptors. The formation of oligomeric complexes in the ER can be a determining step in ER exit, as it may mask ER-retention sequences present in the peptide sequence of some GPCRs. A classical example of this obligatory oligomerization in the ER is the case of the GABA B receptor. In such way, the GABA B1 receptor subunit contains the structural elements for ligand binding, but not for G-protein-coupling, thus it is retained in the ER unless it is co-expressed with the GABA B2 receptor subunit. On the other hand, the GABA B2 receptor subunit does not possess the ability to bind ligands, but mediates G-protein-coupling and is able to reach the cell surface alone. Accordingly, dimerization of the two subunits, which involves interactions between the C-terminal domains of the GABA B receptor subunits, masks an ER retention motif located at the C-terminal tail of the GABA B1 receptor subunit. Similar observations indicate that the co-expression of the taste receptors T1R2 and T1R3, or T1R1 and T1R3, are required to generate functional taste receptors that detect sweet and umami, which strongly suggests that heterodimerization is also mandatory for the biogenesis of these sensory receptors. On the other hand, there are also a number of reports in which co-expression of a second GPCR reduces cell surface delivery (62)(63).

GPCR oligomers are generally portrayed as long-lived entities, thus receptors can remain in the oligomeric form when leaving the ER. For instance, association of RTP4 receptors is stable and shows co-localization both intracellularly and at the cell surface (64). On the other hand, increasing evidences show that some GPCRs act as chaperones, promoting a correct protein folding and most of the reported interactions appear to be transient; i.e. calnexin persists in the ER and the interaction with the GPCR is only temporary to the dominant negative effects of certain GPCRs. There are also a number of reports in which co-expression of a second GPCR promotes cell surface delivery.

In most cases, GPCR oligomerization has a marked effect on GPCR function, which may be distinct from that of the constituent receptors. In fact, it may be considered that they confer new pharmacological targets. In this way, it has been described that binding of an specific ligand to a GPCR forming part of a heterodimer can induce changes in ligand affinity to the other receptor. This kind of allosteric modulation can increase (positive allosteric modulation, PAM) or decrease (negative allosteric modulation, NAM) the ligand affinity for the other receptor. PAM- and NAM-based drugs may offer promising therapeutic approaches for the activation or inactivation of GPCRs, since they preserve the physiologic pattern of receptor signaling and are less likely to cause receptor desensitization and/or downregulation than direct ligands; and in parallel they also may modulate other receptor responses (65). Some examples of this PAM and NAM modulation for GPCRs have been described. For example, it has been longly studied the interaction between D₂R and A_{2A}R, in which D₂R agonists exert NAM activity over A_{2A}R functioning (66); similarly, D₃R agonists have been shown to elicit PAM activity over D₂R agonist binding (67).

Overall, appropriate expression and localization of GPCRs is essential for cells to maintain proper communication pathways within an organism. Oligomerization is a dynamic equilibria between several states with different activities, and switching between these states is involved in regulating their normal function. Furthermore, since oligomerization of GPCRs lead to changes in receptor function and play a crucial role in the activity of many disease-related proteins, it may be considered a promising target for therapeutic intervention.

5. Adenosinergic and dopaminergic systems

The release of neurotransmitters from the presynaptic terminal that bind to specialized receptors located postsynaptically is a crucial process in neuronal communication. Of note, a number of these receptors are GPCRs, from which we will next focus on adenosine and dopamine receptors. In the Central Nervous System (CNS), adenosine and dopamine have a wide range of functions; for instance, they are closely related to movement, emotion, reward and memory. Notably, changes on neurotransmitter availability and/or their receptors have been identified to occur in various brain disorders and nervous system diseases, including Parkinson's disease (PD), Alzheimer's disease (AD), autism, schizophrenia and epilepsy. It is also noteworthy that the anatomical localization of adenosine and dopamine receptor subtypes have not only provided the anatomical basis for establishing their functions but it has permitted to elucidate the existence of functional interactions between them in the same neurons. In such way, adenosine and dopamine receptors have been shown to oligomerize in some brain areas, such as striatum. Indeed, it is well-accepted that the functioning of basal ganglia is dependent on the existence of adenosine–dopamine receptor interactions that ultimately influence cellular and behavioral functioning both in physiological and pathological conditions.

5.2. Adenosine receptors (ARs)

Adenosine is an endogenous purine nucleoside present in all mammalian tissues and is an ubiquitous molecule that is directly involved in the key processes sustaining cellular viability and adaptability. To date, adenosine is considered a neuromodulator rather than a neurotransmitter because there are no clear evidences that adenosine is stored in synaptic vesicles or released as a classical neurotransmitter in response to neuronal firing. Thus, adenosine does not trigger direct neuronal responses but fine-tunes ongoing synaptic transmission, controlling the flow of information through different neuronal circuits in the brain (68). Interestingly, adenosine has been shown to be involved in both normal and pathophysiological processes, including regulation of sleep, arousal, neuroprotection, and epilepsy. Adenosine can reach the extracellular space of the brain via dephosphorylation of adenine nucleotides by ecto-nucleotidases and release of adenosine from cells via transporters. ATP is stored in secretory and synaptic vesicles and released from neurons and astrocytes through an exocytotic vesicular process.

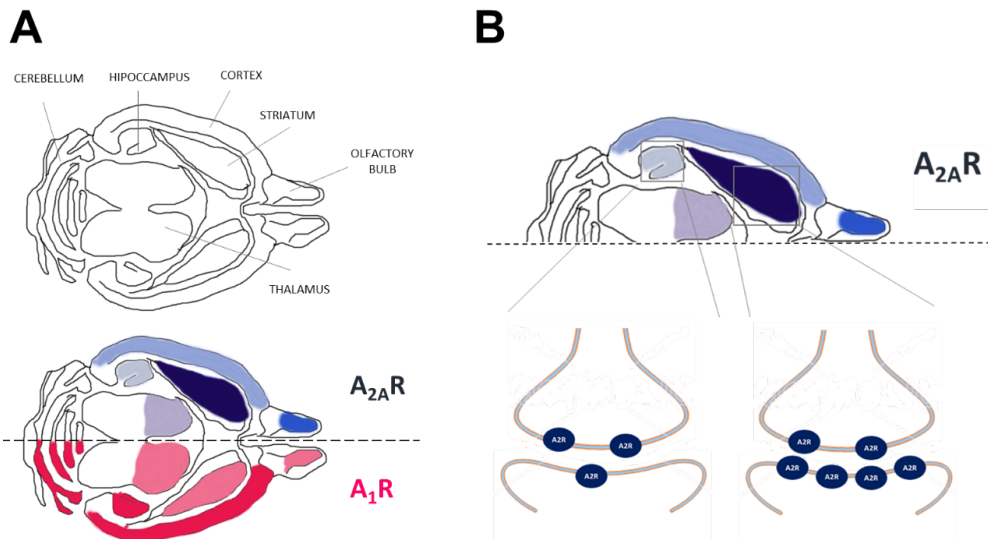


Figure 8. Distribution of A₁R and A_{2A}R in mice brain. A₁R and A_{2A}R have different distribution in brain. **(A)** While A₁R is widely expressed in the brain, A_{2A}R is mainly found enriched in the striatum. **(B)** Furthermore, this A_{2A}R has different subsynaptic distribution in different brain regions. While A_{2A}R is enriched presynaptically in hippocampus it has a preferential postsynaptic distribution in the striatum.

ARs belong to the G-protein-coupled 7TM superfamily of cell surface receptors thus they mainly transduce their signal by heterotrimeric G-proteins that can either stimulate (G_s) or inhibit (G_i) AC, the enzyme that catalyses the formation of cAMP. ARs were first classified by their ability to inhibit (A₁R and A₃R) or stimulate (A_{2A}R and A_{2B}R) AC. Later, ARs were further classified according to their high or low affinity binding sites for adenosine in brain. In synapses, A_{1A}R activation occurs initially at very low adenosine levels, followed by the stimulation of G_s-coupled A_{2A}R and A_{2B}Rs, and finally by G_i-coupled A_{3A}R (85). So far, many reports have provided experimental evidence for the occurrence of A₁R-A₁R and A_{2A}R-A_{2A}R homomers and A₁R-A_{2A}R heteromers. Hence, balanced activation of A₁R and A_{2A}R depends not only on the transient levels of extracellular adenosine, but also on the direct interaction between A₁R and A_{2A}R, which control each other's action.

5.1.1 Adenosine A_{2A} receptor (A_{2A}R)

The crystal structure of the human A_{2A}R in complex with a high affinity subtype selective antagonist, ZM241385, to 2.6 Å resolution was first obtained in 2008 (86)(87). Years later, in 2011, the first crystal structure of the A_{2A}R bound to the agonist UK-432097 was described. Recently, a very high resolution structure of an antagonist-bound A_{2A}R (1.8 Å) has been reported. All these results, together with computational studies have facilitated the characterization of the ligand binding site and the conformational changes that undergo in A_{2A}R after ligand binding. These structural studies also identified that the ICL3 is involved in Gs activation or that the C-terminal fragment of the A_{2A}R is involved in the formation of A_{2A}R-D₂R heterodimer complexes.

As above-mentioned, A_{2A}R is coupled to Gs subunit, which upon activation induces classical second messengers such as cAMP. Gs stimulates AC and subsequently activates PKA. However, the relative low amount of Gs in striatum promotes A_{2A}R signaling through Gα_{off}. In both pathways, an increase in cAMP is observed. In turn, PKA phosphorylates and stimulates CREB1. Activation of A_{2A}R transiently increases phosphorylation of MAPK/ERK (**Figure 9**). All these phosphorylation processes are involved in the regulation of survival, proliferation and cellular differentiation. It has also been described the existence of A_{2A}R G-protein-independent signaling pathways through α-actinin, β-arrestin2 or GRK2.

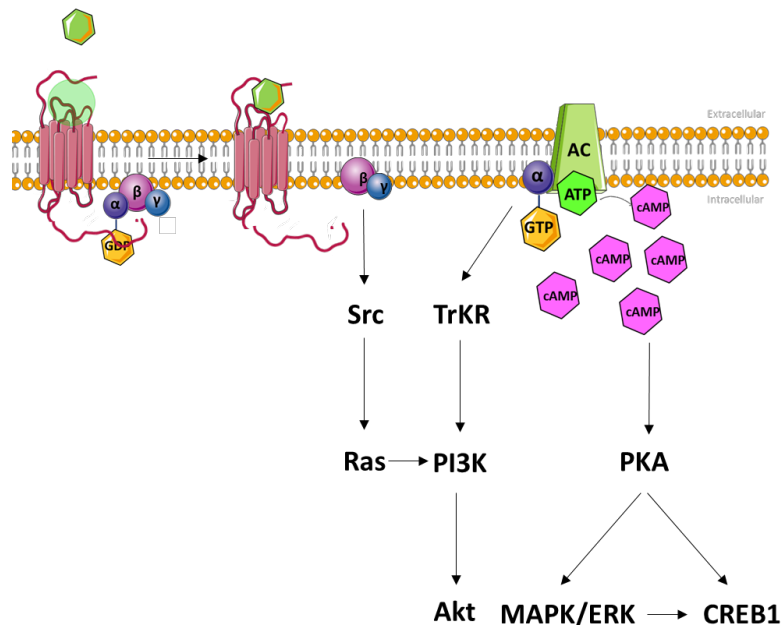


Figure 9. A_{2A}R G-protein-dependent signaling pathway. A_{2A}R activation leads to enhanced phosphorylation of MAPK/ERK1/2 via a cAMP-dependent mechanism.

Furthermore, $A_{2A}R$ activation can trigger alternative signaling pathways via interaction with other receptors and signaling molecules. For instance, functional interactions with A_1Rs , D_2Rs , group I metabotropic glutamate 5 receptors ($mGlu_5R$), *N*-methyl-D-aspartate receptors (NMDARs), and cannabinoid CB_1 receptors (CB_1R) have been reported. From these protein-protein interactions involving the $A_{2A}R$, the most studied is the above-mentioned $A_{2A}R$ - D_2R interaction. As previously described, $A_{2A}R$ is mostly enriched in synapses where it shows different tissue-specific subregional and cellular expression patterns. In the striatum, $A_{2A}R$ is mainly localized in the postsynaptic striatopallidal medium spiny neurons (MSNs) of the indirect pathway, where they interact with D_2Rs . On the other hand, $A_{2A}R$ are also detected at lower levels at presynaptic sites in corticostriatal terminals and in the hippocampus (**Figure 8B**). $A_{2A}R$ and D_2R have been shown to co-localize in the dorsal and ventral striatum (88)(89), where they may act as reciprocal inhibitors. For instance, when the $A_{2A}R$ is activated, conformational changes are transferred to the D_2R , which lead to a reduction in affinity of dopamine analogues and subsequent reduction in signaling; on its own, D_2R activation inhibits cAMP mediated-effects of $A_{2A}R$ by inhibiting AC. These evidences suggest that antagonistic adenosine-dopamine interactions may be important in the regulation of the activity of basal ganglia and could explain the apparently paradoxal depressant and stimulating effects of $A_{2A}R$ (90). Interestingly, it has been shown that the net result of dopamine depletion in the striatum leads to an $A_{2A}R$ oversignaling resulting in typical hypokinetic symptoms of PD, thus blockade of $A_{2A}R$ may be an attractive alternative (or adjunctive) to dopamine-based therapeutic approaches. Indeed, it has been shown an increase in $A_{2A}R$ in the brain of PD patients with dyskinesias.

Focusing on the different actions of adenosine in the CNS, it is well-known that adenosine exerts inhibitory effects on spontaneous locomotor activity. These effects are thought to be mediated acting at $A_{2A}R$ expressed at postsynaptic striatopallidal MSNs of the indirect pathway (91). This anatomic segregation is functionally significant and is relevant for understanding the role of these receptors in motor control (**Figure 10**). Thus, while $A_{2A}R$ antagonism induces motor stimulation and in agreement, $A_{2A}R$ activation induces motor depression (92,93). In addition, it has been shown that $A_{2A}R$ antagonist-induced motor stimulation is absent in striatal $A_{2A}R$ KO mice. Oddly, while $A_{2A}R$ antagonists are well known to induce motor stimulation, genetic $A_{2A}R$ deletion has failed to produce a similar effect on basal motor activity. Instead, adult global $A_{2A}R$ -KO mice consistently exhibit reduced spontaneous motor activity compared to their wild-type (WT)

controls in different genetic backgrounds, probably due to compensatory changes in brain functioning as a result of adaptive effects of constitutive global gene deletion.

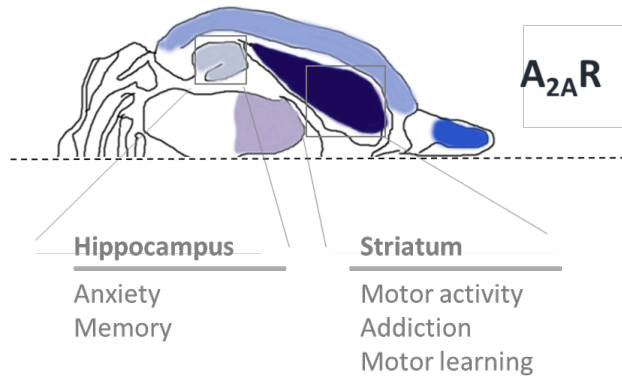


Figure 10. Role of A_{2A}R in different physiologic brain regions. Role of A_{2A}R in different physiologic brain regions have been suggested by KO and pharmacological studies.

Many studies and models of genetically modified rodents have implicated adenosine in the etiology and modulation of different types of anxiety. A growing body of data describes the role of A₁R and A_{2A}R on anxiety. Adenosine and ARs agonists are anxiolytic as assessed by a number of ethological tests in rodent models, such as the elevated zero maze and elevated plus maze (94) and the light-dark box. Conversely, ARs antagonism is responsible for the anxiogenic responses elicited by moderate to high doses of caffeine, theophylline (95)(96), or other ARs antagonists in rodents and humans. Indeed, A_{2A}R-KO mice are considered a valuable model to study anxiety disorders. These mice display reduced exploratory activity and heightened anxiety. The mechanisms underlying the relationship between A_{2A}R antagonists and anxiety and depression remain unclear, although A_{2A}R located at the hippocampus have been hypothesized to be involved (**Figure 10**).

There are many evidences that adenosinergic system, and specifically A₁R and A_{2A}R are related with many different neurological and psychiatric disorders (i.e. epilepsy, HD, PD, AD) (97). Both their altered expression and their ability to control excitatory transmission prompts to consider them as putative therapeutic targets. Several studies have now identified a decreased density and efficiency of synaptic A₁R in models of epilepsy. On the other hand, upon chronic epilepsy it has been observed a robust increase of the density of A_{2A}R. Indeed, some studies showed that blockade of A_{2A}R, either using genetic deletion of A_{2A}R or selective A_{2A}R antagonists (98)(99) induced robust protection against

the seizure evolving severity. Moreover, recent evidence indicates that A_{2A}R polymorphism could influence the age of onset of HD patients (100). Furthermore, post-mortem analysis of frontal cortex and hippocampus of AD patients showed increased levels and a re-distribution of A₁R and A_{2A}R in either early or advanced stages of the disease. Indeed, in a transgenic mice model of AD it was also reported augmented levels of A₁R and A_{2A}R compared with non-transgenic mice. This upregulation of A_{2A}R was also observed after chronic stressful brain conditions. Evidences of altered adenosinergic activity have also been described in schizophrenia, where an upregulation of striatal A_{2A}R has been observed (101), which could be a compensatory response to low adenosinergic activity (102).

A_{2A}R seems to have limited impact on the control of basal synaptic transmission but plays a crucial role in controlling synaptic plasticity. However, mechanisms involved are still under study. Synaptic plasticity is defined as the ability of synapses to strengthen or weaken over time, in response to increases or decreases in their activity. Most forms of plasticity are NMDAR-dependent and, in their early phase, synaptic plasticity events rely on 2-amino-3-(3-hydroxy-5-methyl-isoxazol-4-yl) propanoic acid (AMPA) receptor trafficking with subsequent numeric increase (Long Term Potentiation, LTP) or decrease (Long Term depression, LTD) within the postsynaptic density (103). As above-mentioned, adenosine is produced primarily in the extracellular space from the breakdown of previously released ATP. Notably, ATP is released shortly after a high frequency stimulation (HFS), whereas after a low frequency stimulation (LFS), no ATP is released (104)(105). In hippocampus, many reports have described that caffeine and specific A_{2A}R antagonists inhibit LTP magnitude (106)(107)(108). Furthermore, while low synaptic adenosine concentration or A_{2A}R blockade increased LTD, LTD is impaired whenever there is an increase of the degree of activation of A_{2A}Rs (109) (**Figure 11A**). On the other hand, in the striatum, LTD occurs in response to HFS or LFS. The mechanisms underlying indirect pathway LTD appear to be induced postsynaptically by activation of Gq coupled mGluRs and L-type calcium channels, which together lead to the mobilization of endocannabinoids. Endocannabinoids then travel retrogradely across the synaptic cleft and activate presynaptic CB₁R. Prolonged activation of CB₁R leads to presynaptic expression of LTD as a decrease in release probability. Successful induction of LTD requires activation of dopamine D₂R, but also lack of activation of postsynaptic A_{2A}R (110)(103). Thus, by regulating the activation of these GPCRs, dopamine and adenosine gate LTD induction in MSNs. Similarly, in the striatum LTP has been shown to require A_{2A}R activation as well as a lack of activation of D₂R (111). Hence, high

dopamine levels and low adenosine levels may shift plasticity induction in MSNs towards LTD. By contrast, low dopamine levels and high adenosine levels will promote LTP. Interestingly, SCH442416, a selective $A_{2A}R$ antagonist has been shown to potentiate endocannabinoid-mediated LTD in MSNs, an effect that correlates with an increase in locomotor activity (110) (**Figure 11B**).

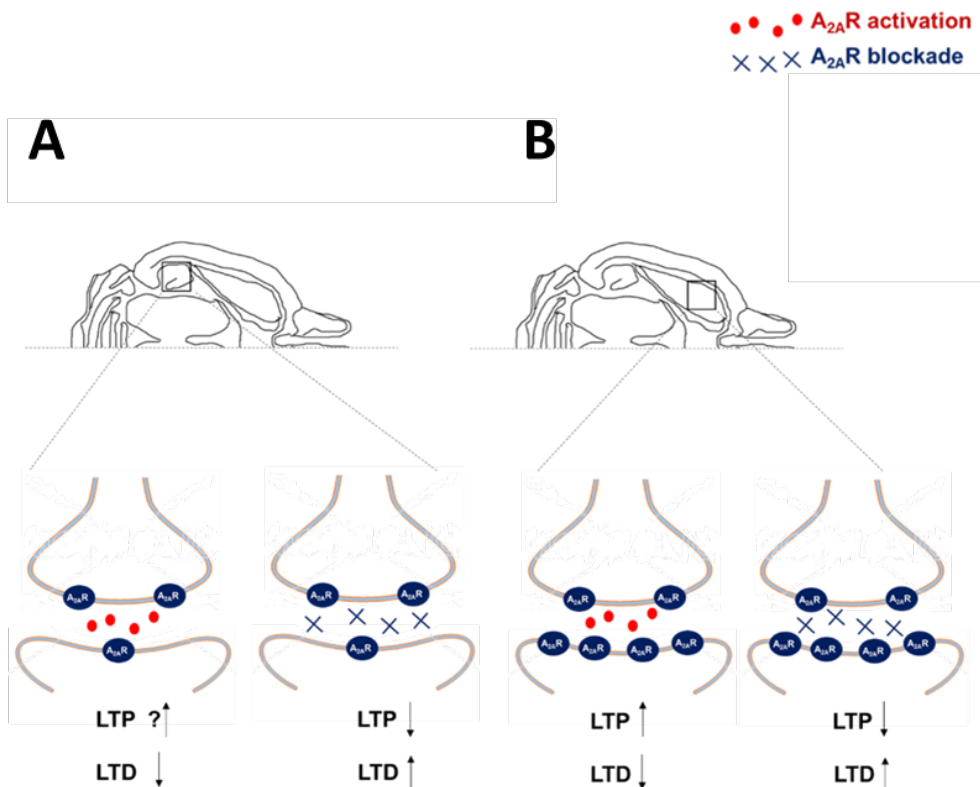


Figure 11. Oversimplification of adenosine and $A_{2A}R$ implication in LTP and LTD induction in hippocampus and striatum. $A_{2A}R$ have a crucial role in controlling synaptic plasticity both in **(A)** hippocampus and **(B)** striatum.

To end with the different actions of adenosine, the involvement of the adenosinergic system in neuromodulation and neurodegeneration in the CNS is well established (97), including its participation in cognitive behavioral functions and in pathological situations. Thus, findings from genetic $A_{2A}R$ studies generally support the notion that suppression of $A_{2A}R$ activity is pro-cognitive and raises the possibility that $A_{2A}R$ may represent a target for improving cognitive function under normal conditions. Thus, while transgenic rats overexpressing $A_{2A}R$ in the cortex exhibited impaired memory function in several behavioral tasks (112), global $A_{2A}R$ knockout (KO) mice showed improved spatial

recognition memory in an elevated Y-maze (113). However, a challenging issue with respect to the functional role(s) played by adenosine in the brain is to understand why antagonizing the effects of endogenous adenosine produce improvements in mental function and performance, whereas antagonism of most other neurotransmitter receptors produce either deficits or pathological effects. Furthermore, inhibition of A_{2A}Rs both by genetic blockade and specific A_{2A}R antagonists has been observed neuroprotective in several experimental models of striatal diseases, which may be of interest for some pathologies such as PD (114).

5.2 Dopamine receptors (DRs)

Dopamine (3-hydroxytyramine) is a catecholaminergic neurotransmitter that is also a precursor for the synthesis of norepinephrine (NE). Dopamine is synthesized through a series of enzymatic reactions, beginning with the hydration of amino acid tyrosine to 3,4-dihydroxyphenylalanine (DOPA) via tyrosine hydroxylase (TH), which indeed is the rate-limiting enzyme in the whole synthetic pathway (115). DOPA is decarboxylated by aromatic amino acid decarboxylase to produce dopamine. The transmitter is then packaged into synaptic vesicles by a vesicular monoamine transporter (VMAT), where it is stored. In these vesicles is where dopamine can be converted to NE by dopamine hydroxylase enzyme. Interestingly, in 1958, Carlsson and colleagues demonstrated that dopamine had signaling properties on its own and was not only a precursor for NE. Thus, they showed that DOPA treatment in rabbits that were previously depleted of catecholamines by means of reserpine, could reverse the reserpine-mediated effects. Importantly, this reversal corresponded to an increase of dopamine, and not of NE, which was the neurotransmitter thought to mediate these effects. Dopamine, similarly to other monoamine neurotransmitters, generally exerts its actions on neuronal circuitry via a relatively slow modulation of the fast neurotransmission mediated by glutamate and GABA. There are four major dopaminergic innervation pathways identified in the mammalian brain: the nigrostriatal, mesolimbic, mesocortical and tuberoinfundibular systems. These neurons are critically involved in several CNS functions, including voluntary movement, feeding, reward, sleep, attention, working memory, and learning. In the periphery, dopamine also plays important physiological roles in the regulation of olfaction, retinal processes, hormonal regulation, cardiovascular functions, sympathetic regulation, immune system, and renal functions, among others.

Once released from presynaptic terminals, the physiological actions of dopamine are mediated by five distinct GPCRs (**Figure 12**), which are divided into two major groups based on structural, pharmacological, and biochemical properties: the D1 subtype comprising the D₁R and D₅R; and the D2 subtype, comprising the D₂R, D₃R and D₄R (116). Members of the D1- and D2-class receptors share a high level of homology of their transmembrane domains. The D₁R and D₅R are 80% homologous in their transmembrane domains, whereas the D₃R and D₄R are 75 and 53% homologous, respectively, with the D₂R. Whereas the N-terminal domain has a similar amino acids length in all DRs, the C-terminal from the D1-class receptors is longer than that from the D2-class receptors.

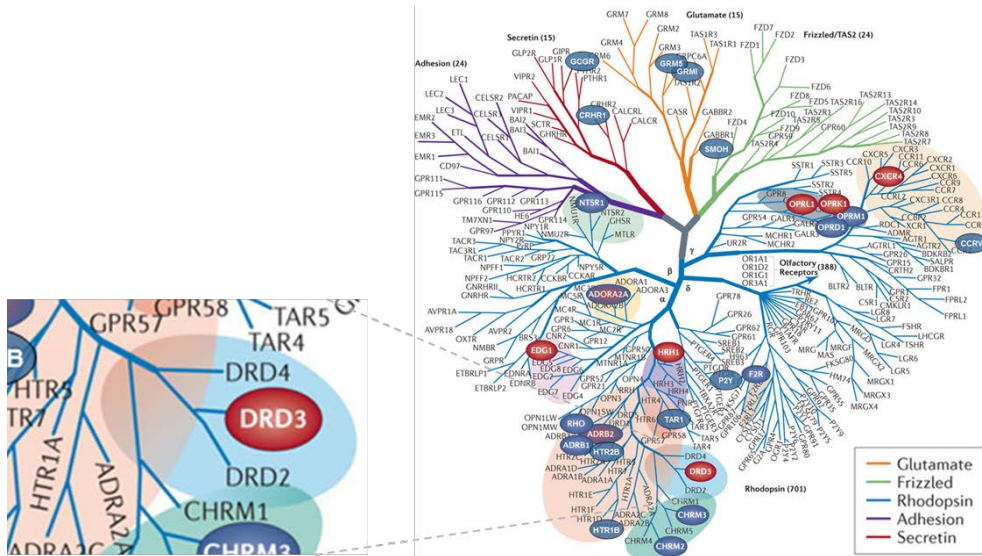


Figure 12. Dopamine receptors belong to the Rodhopsin GPCR family. DRs have structure similarities with rhodopsin. The D₁R and D₅R are 80% homologous in their transmembrane domains, whereas the D₃R and D₄R are 75 and 53% homologous, respectively, with the D₂R.

DRs are able to transduce their signal by means of both G-protein-dependent and independent pathways. It is commonly accepted that the D₁-class DRs activate the G_s/olf family of G-proteins to stimulate cAMP production by AC and PKA and are found exclusively postsynaptically on dopamine-receptive cells, such as GABAergic MSNs in the striatum. Contrary, the D₂-class DRs couple to the G_i/o family of G-proteins and thus induce inhibition of AC. Furthermore, accumulating evidences suggest that these receptors do not signal exclusively through heterotrimeric G-proteins and may also engage G-protein-independent signaling events (**Figure 13**). Finally, there are also evidences that DRs, in addition to their effects on cAMP-regulated signaling, can also couple to G_q to regulate phospholipase C (PLC).

demonstrated that MSNs located at the basal ganglia can be clearly separated into two principal subgroups that are defined by their projection sites and by the proteins that they express. In particular, the MSNs that project to the medial globus pallidus and the substantia nigra pars reticulata comprise a direct striatonigral pathway that selectively expresses the D₁R. Another group of MSNs that project to the lateral globus pallidus and selectively express D₂R forms the indirect striatopallidal pathway (121). And finally, in addition to these main subgroups, there is a population of MSNs that express both D₁R and D₂R in the dorsal striatum (89)(122). The D₃R has a more limited pattern of distribution, being observed in the nucleus accumbens. The D₄R and D₅R have the lowest level of expression in the brain and limited expression pattern in the primary motor regions. In the periphery, all subtypes of DRs have been observed. In varying proportions they are expressed at the kidney, adrenal glands, sympathetic ganglia, gastrointestinal tract, blood vessels, and heart (123).

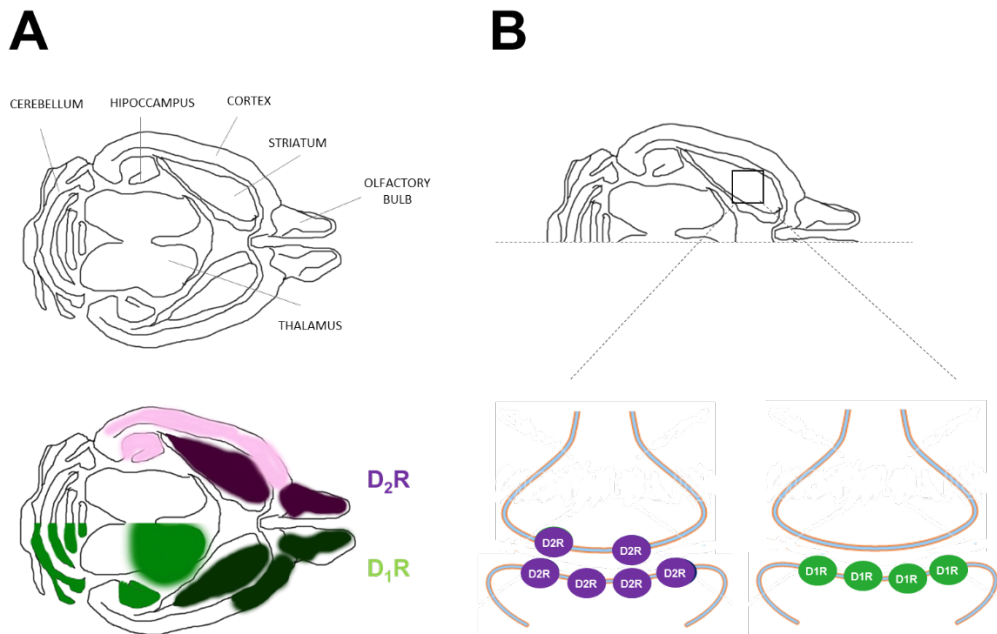


Figure 14. Distribution of D₁R and D₂R in mice brain. D₁R and D₂R have different distribution in brain. **(A)** D₁R is widely expressed in the brain, while D₂R is mainly find enriched in the striatum and olfactory bulb. **(B)** Furthermore, D₁R and D₂R have different subsynaptic distribution in the synapsis. D₁R is found exclusively postsynaptically on dopamine-receptive cells, while D₂R is expressed both postsynaptically on dopamine-target cells and presynaptically on dopaminergic neurons.

Termination of dopamine neurotransmission is mainly regulated by the dopamine transporter (DAT) (**Figure 15**). DAT allows dopamine to be cleared out of the synapse and be transported to the presynaptic neuron, where it can be recycled and repackaged into vesicles. The importance of this transport system was demonstrated in DAT^{-/-} mice, where dopamine clearance was significantly slower than in wild type mice (124), leading to an hyperactive behavior. Due to the important role of DAT in dopamine homeostasis, loss of proper function and regulation of the transporter has been implicated in several dopamine-related diseases. Decreased striatal DAT binding has been reported in first-episode schizophrenic patients. These changes demonstrate that while DAT plays an important role in directly regulating dopamine signaling, it also influences several components of the dopaminergic synapse. Therefore, changes in the activity and functioning of DAT can markedly disrupt dopamine neurotransmission. DAT is also well-known for its role in addiction, including substance abuse of psychostimulants such as amphetamine (AMPH).

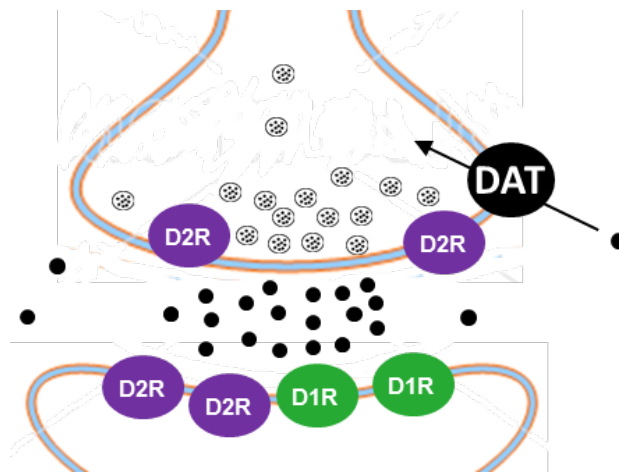


Figure 15. Dopaminergic synapse and dopamine levels are finely regulated. In the presynaptic terminal of dopaminergic neurons dopamine is transferred in vesicles by the vesicular monoamine transporter 2 (VMAT-2). After exocytosis of the dopamine vesicles, it binds to DRs on the postsynaptic membrane, leading to the transduction of the signal in the postsynaptic neuron. Dopamine is then recycled by reuptake via the DAT, or catabolized by the action of MAO or COMT enzymes.

Regarding the effects in the CNS elicited by dopamine, one of the best characterized consists of the control of motor activity (125) (**Figure 16**). Multiple evidences indicate that motor activity is primarily controlled by D₁R, D₂R and D₃R (126)(127). Thus, it is well-defined that the activation of D₁R has a moderate stimulatory effect on locomotor activity, while the roles of D₂R and D₃R are much more complex. A possible explanation relies on the fact that they are both expressed presynaptic and postsynaptically. Presynaptically localized autoreceptors generally provide an important negative feedback mechanism that adjusts neuronal firing rate, synthesis, and release of the neurotransmitters in response to changes in extracellular neurotransmitter levels. For instance, the activation of presynaptic D₂-class autoreceptors generally causes a decrease in dopamine release that results in decreased locomotor activity, whereas activation of postsynaptic receptors stimulates locomotion. Because D₂-class autoreceptors are generally activated by a lower concentration of dopamine agonists than that necessary to activate postsynaptic receptors, the same dopamine agonist can induce a biphasic effect, leading to decreased activity at low doses and behavioral activation at high doses.

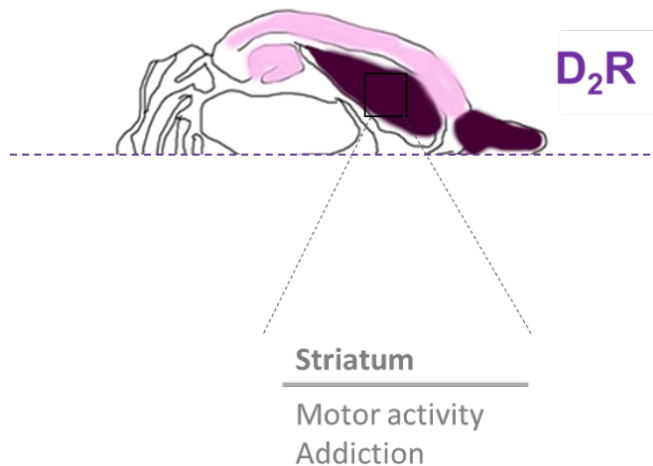


Figure 16. Role of D₂R in different physiologic brain regions. Striatal D₂R have been shown to be involved in the control of motor activity and addiction.

Dopaminergic dysfunctions have been related with the neurobiology and symptoms of a myriad of neurological and psychiatric diseases. One of the most recognized dopamine-related disorder is PD (128). A direct association between the amount of striatal dopamine depletion and motor deficits has been observed in PD. Also, in PD patients, D₂R density in the basal ganglia has been found to be altered, with no changes observed in the density of postsynaptic D₁R. In general, the pattern of changes in D₂R expression is extremely complex and is likely to depend on the stage of the disease, with a slight

increase in D₂R binding observed at the earlier stages and a decrease observed at the later stages. Another brain disorder in which dopamine dysregulation has been described is schizophrenia (129). Again, in these patients, no consistent changes in D₁R binding have been observed, while it has been described that higher levels of D₂R are found in the basal ganglia. Furthermore, decreased striatal D₂R binding has been observed in drug abusers, thus highlighting the relevance of dopamine in addiction (130). Finally, several studies have described alterations in dopamine or DRs levels in the attention deficit hyperactivity disorder (ADHD) (131) and Huntington's disease (HD) (132)(133). Strikingly, in HD patients, in which postsynaptic degeneration occurs in GABAergic MSNs, significant reductions in both the levels of striatal D₁R and D₂R have been observed in essentially all of the studies.

6. GPR37 and GPR37L1

GPR37 is an orphan GPCR that belongs to the Rodhopsin family. It was first described in 1997 by Zeng (134). The receptor was isolated from a human hippocampal library and was first named human endothelin B receptor-like protein (ETBR-LP-1), since it shared 52% similarity and 26.7% identity with the endothelin receptor type B (EDNRB). In parallel, at the same time, it was isolated a novel protein from a human frontal lobe library, which was named G-protein coupled receptor 37 (GPR37) (135). Since then, GPR37 has been the most used name for this receptor. The murine orthologue was next identified, and shown to display 83% identity with the human GPR37 and similar gene organization (136). Finally, a year after the discovery of GPR37, it was found in a human caudate library a shorter and very highly related novel transcript encoding a similar protein to GPR37, which was called ETBR-LP-2 (later termed GPR37L1). Interestingly, GPR37L1 displayed 68% similarity and 48% identity with GPR37 (137) (**Figure 17**).

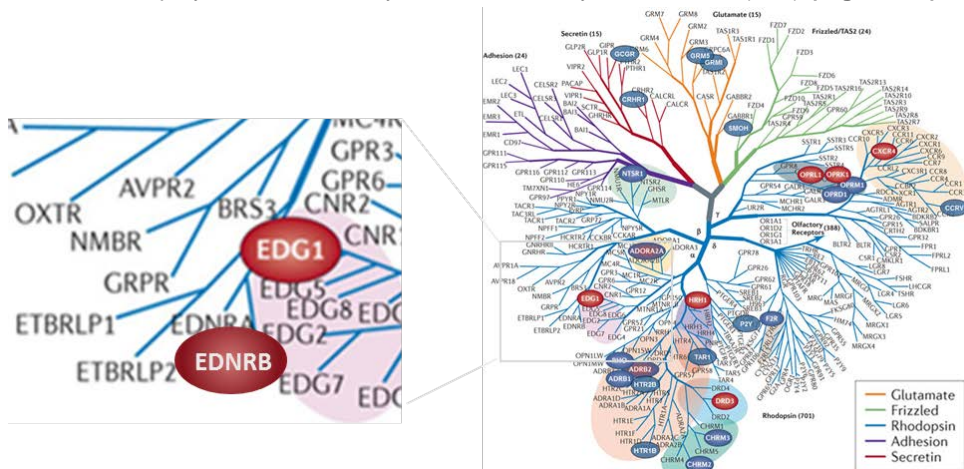


Figure 17. GPR37 and GPR37L1 belong to the Rodhopsin GPCR family. GPR37 and GPR37L1 have structure similarities with rhodopsin. The GPR37 has high sequence identity to the GPR37L1 (48%) and with the Endothelin like receptors (26.7%).

Both GPR37 and GPR37L1 are highly expressed in the CNS, while little peripheral expression has been found in humans and rodents. GPR37 is highly distributed in the brain, particularly at the corpus callosum and substantia nigra. Also, it displays some expression in the spinal cord, and in peripheral tissues it has been found in placenta, liver, stomach and testis (138)(135)(134). In contrast to the predominantly neuronal distribution of GPR37, including the Purkinje cells of the cerebellum, pyramidal cells of the hippocampus and granule cells of the dentate gyrus, GPR37L1 is exclusively expressed in glial cells, being the highest expression within the Bergmann glia of the cerebellum (137) (**Figure 18**).

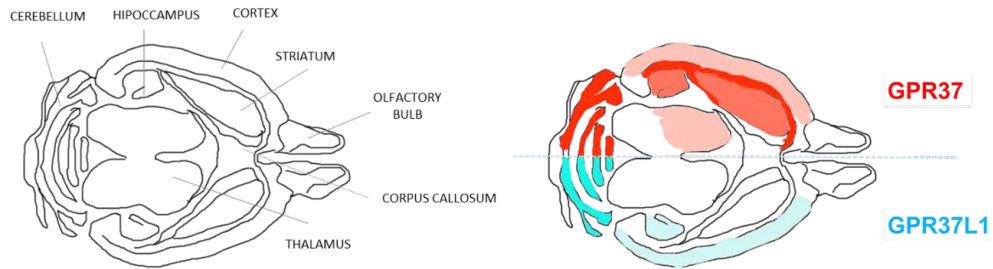


Figure 18. Distribution of GPR37 and GPR37L1 in mice brain. GPR37 and GPR37L1 have different distribution in brain. GPR37 is widely expressed in the brain, but enriched in corpus callosum and cerebellum; conversely, GPR37L1 is mainly find enriched in the cerebellum.

Many efforts have been directed to de-orphanize GPR37 and GPR37L1. Thus, while both receptors are closely related to the endothelin and bombesin receptor families, they are unable to bind to the cognate ligands for these receptors. The first ligand proposed to be the endogenous partner of GPR37 was head activator (HA), an undecapeptide (pGlu-Pro-Pro-Gly-Gly-Ser-Lys-Val-Ile-Leu-Phe) originally discovered in Hydra and reported to have a human homologue (139,140). Many groups attempted to replicate the finding that HA was a specific ligand for GPR37 but did not find evidences for a real interaction. More recently, GPR37 and GPR37L1 were simultaneously paired with the endogenous neuropeptide agonist prosaposin (PSAP) and its active peptide fragment, prosaptide, and also with the synthetic analogue called TX14A, a 14-amino acid neuroprotective peptide that is derived from the saposin C domain of PSAP (141). The assumption that prosaptide and TX14A were selective ligands for GPR37 was based on ERK1/2 phosphorylation and inhibition of forskolin-stimulated cAMP in HEK-293T. Like HA, TX14A was also included in the MRC Technologies β -arrestin-based orphan GPCR screen but was not detected as a ligand for either GPR37 or GPR37L1 (142). Needless to say, these results have been tried to replicate by other groups but no success has been reached, thus it is still doubtful a direct binding of these peptides to GPR37. Indeed, this situation has lead to the fact that little is known about the signal transmission pathways activated by GPR37 (**Figure 19**). Needless to say, although direct agonism and the signals triggered remain to be independently demonstrated, it seems likely that prosaposin and TX14A have some indirect influence on GPR37 localization and activation. Thus, internalization and mobilization of GPR37 has been observed after incubation with these ligands.

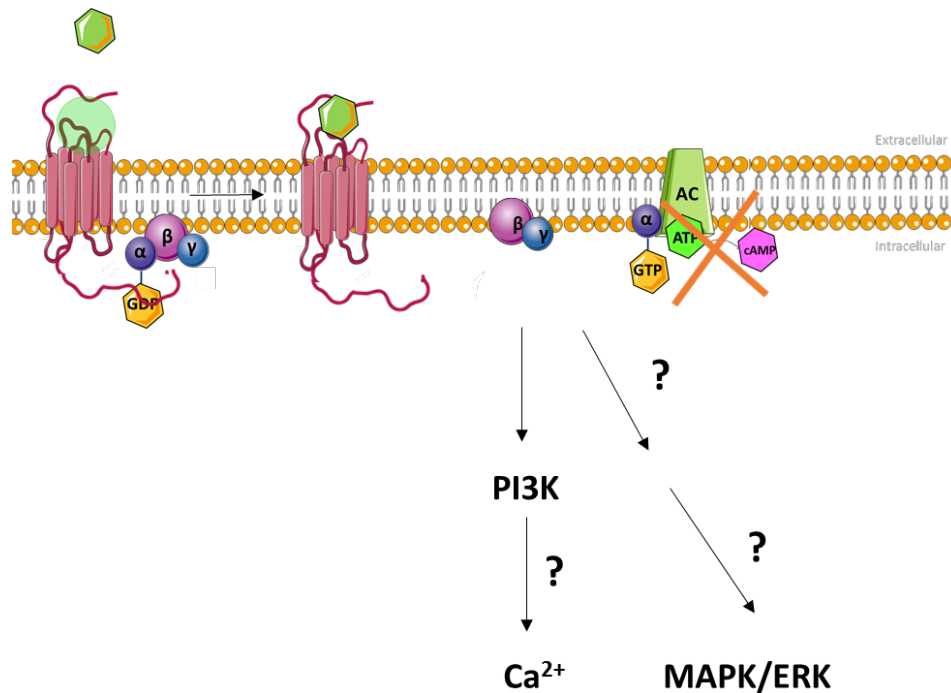


Figure 19. Proposed GPR37 G-protein-dependent signaling pathway. Proposed intracellular signaling pathway after GPR37 receptor activation. This scheme is based on the results obtained after incubation of GPR37 with proposed specific ligands.

6.1. GPR37

The interest on GPR37 biology was bolstered when it was described as a Parkin substrate. GPR37 was isolated from a human brain library in a yeast 2-hybrid screen for novel interacting partners of Parkin, and thus rebaptized as “Parkin-associated endothelin-like receptor” (Pael-R) (143). Parkin is of great interest because mutations in this gene are directly linked to autosomal recessive juvenile Parkinsonism (AR-JP), a form of Parkinsonism without Lewy bodies. It was found that insoluble GPR37 was increased in patients with AR-JP, linking the aggregation of GPR37 to disease pathogenesis. Later, GPR37 aggregates were also found in a variety of inclusion bodies in brains from patients with PD, dementia with Lewy bodies (DLB) and multiple system atrophy (MSA) (144). Parkin is an E3 ubiquitin-protein ligase that was itself first identified in a genetic study of patients with AR-JP, where it was found to be highly expressed, particularly in the substantia nigra (145). Mutations in Parkin that have been associated with AR-JP specifically enhance dopaminergic neuronal cytotoxicity by failing to appropriately remove aggregated proteins via the proteasome, where protein aggregates

trigger the unfolded protein response (UPR) and cause cell death. It is specifically through the loss of E3 ubiquitin ligase activity that Parkin mutations are pathogenic (146)(147), leading to the accumulation of a number of substrates including GPR37. It was described that overexpression of GPR37 in the substantia nigra pars compacta led to neurotoxicity, which was exacerbated in Parkin^{-/-} mice (148). This pathological phenotype was rescued both by overexpression of Orp150, an ER protein-folding chaperone, or by treatment with the dopamine synthetase inhibitor, AMPT (a tyrosine hydroxylase blocker), thus linking GPR37 to ER stress and subsequent dopamine neuron death. While the neurotoxicity seen upon GPR37 overexpression could be explained by GPR37 misfolding and failure to clear aggregated protein from the ER, it has not been already elucidated the mechanisms underlying survival benefits of GPR37 deletion observed in different works. For example, it was described that GPR37^{-/-} mice were resistant to the development of dopamine neurodegeneration and that they developed a PD-like phenotype in the MPTP model of neurotoxicity (149). Similar results were obtained in a recent study, where it was observed that GPR37 overexpression was neuroprotective, an effect that seemed to be directly related to its increased cell surface expression (150). The role of GPR37 in PD has not been still elucidated. However, a number of studies have focused research on finding different strategies to improve its plasma membrane trafficking and reducing receptor-induced cell toxicity. One recent approach consisted of trying to rescue GPR37 membrane expression through the use of a chemical chaperone. As observed in other studies, treatment with 4-phenylbutyrate (4-PBA), increased GPR37 cell surface staining and reduced cytotoxicity that may be caused by GPR37 misfolding and ER stress (151,152). An alternative approach consisted of attempting to rescue cell surface expression by truncation of the long extracellular GPR37 N-terminus (52), an strategy used previously for other GPCRs (153). GPR37 cell surface expression was restored by deletion of the entire N-terminus, as measured by luminometry and flow cytometry against an N-terminal FLAG tag, with the first 210 residues requiring deletion for reaching the rescue. In a similar way, it was described that a cysteine rich domain at the C-terminal fragment of the GPR37 played a critical role in receptor cell surface expression (154). Interestingly, by screening several GPCRs known to form dimers, it was observed that both D₂R and A_{2A}R enhanced GPR37 membrane trafficking (155). Adenosine control of motor function is centered on the ability of A_{2A}R to tightly control D₂R function, both at the level of intracellular signaling as well as by the formation of heteromers with D₂R. Hence, it seems likely that a major aim in GPR37 biology would consist of deciphering its role in the CNS both in physiological and pathological conditions and its implication in A_{2A}R and D₂R functionality.

7. Parkinson's disease

7.1. History

PD is the second most common neurodegenerative disorder after AD (156). PD prevalence increases with age. In such way, about 1:100 of people over age 60 suffer PD, while just 1:1000 of people of 45 or younger develop the pathology. Noteworthy, it is more common in men than in women (157). Also, epidemiological studies have shown that prevalence is much higher in Europe and North America than in Asia and Africa.

First documents reporting description of the major signs of PD date from 1690 by Papai (158). However, the first clear medical description was written by James Parkinson in 1817 (159). A few years later, Charcot added new symptoms to wholly describe the syndrome and proposed the actual name. In the 1950s, a brain region (substantia nigra) was associated with the pathology (**Figure 20**). Thus, substantia nigra, which releases dopamine into the caudate/putamen and regulates motor control, was identified as an important structure in parkinsonian syndromes. Indeed, dopamine levels were found to be decreased in brains of PD patients, thus it was thought that PD treatment would be based on restoring dopamine levels. In 1961, there were conducted the first successful clinical trials using levodopa (L-DOPA), which became the first effective treatment for PD.

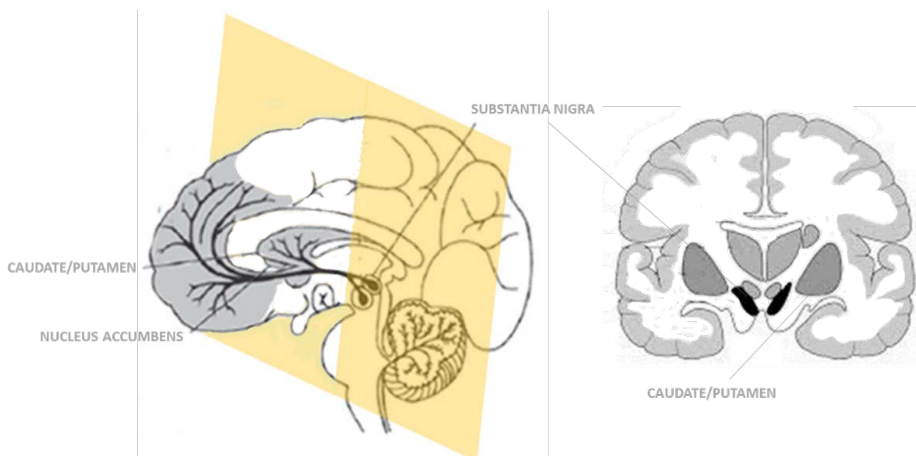


Figure 20. Scheme of the substantia nigra and the nigrostriatal dopaminergic pathway in the human brain. Schematic representation of the substantia nigra pars compacta (SNc) and the innervation of the striatum through the nigrostriatal pathway.

7.2. Causes of PD

The etiology of PD is still unknown, although it has been suggested the participation of genetic factors, hormones, environmental toxins or oxidative stress. Regarding genetic factors, different mutations have been identified in a number of genes studying familial PD, including α -synuclein, parkin, ubiquitin carboxyl-terminal esterase L1 (UCHL1), DJ1, PTEN-induced putative kinase 1 (PINK1) (160) and leucine-rich repeat kinase 2 (LRRK2) (161)(162). Similarly, the Nur-related factor 1 (NURR1) and HTRA2 gene have been proposed to contribute to the biochemical process underlying familial PD but they may not be involved in sporadic/idiopathic PD (163)(164). On the other hand, risk factor studies have pinpointed nicotine (165,166), coffee/tea consumption and alcohol drinking as agents that may lead to lower the risk of suffering PD, while traumatic brain injury (167), long-term exposure to lipopolysaccharide (LPS), well water intake, drug consumption (168) or pesticides may lead to a higher risk of developing PD (169). Some toxins cause parkinsonism (i.e. MPTP) and produce lasting brain damage.

7.3. Neuropathology of PD

PD is a progressive neurological disorder, which pathological hallmark involves the presence of intracytoplasmic proteinaceous neuronal inclusions in neuronal perikarya and neuronal cell processes known as Lewy bodies (LB). LB formation results in the degeneration of dopamine neurons from the substantia nigra pars compacta (SNc), which causes a consequent degeneration of the nigrostriatal dopaminergic pathway and in consequence reduction of dopamine levels in the striatum. Furthermore, adrenergic, serotonergic and cholinergic neurons are also lost. Up to the present, a large number of proteins have been identified in LBs. The main component of inclusion bodies is α -synuclein and after its initial aggregation, additional proteins are captured and accumulated. Indeed, more than 76 LB components from different protein classes have been described so far (i.e. structural elements, components of the ubiquitin-proteasome system, implicated in cellular responses, proteins associated with phosphorylation and signal transduction and cytosolic proteins) (170). Despite most of the α -synuclein immunoreactive cytopathology in PD is within neurons, α -synuclein immunoreactive glia, particularly oligodendroglia, can be detected in small numbers in the midbrain and basal ganglia.

Neuropathologically, PD has been classified into different steps according to LB deposition containing α -synuclein. Thus, in Braak's classification, LBs are first found in lower brainstem nuclei such as the dorsal motor nucleus of the vagus and the olfactory system (stages 1–2); thereafter, the ascending progression leads to changes in the coeruleus complex, substantia nigra pars compacta, basal forebrain magnocellular nucleus, subthalamic nucleus, and amygdala (stages 3–4); and finally, it is affected the cerebral cortex (stages 5–6) (**Figure 21**) (171)(172). The pathophysiology of hyposmia in PD is understood incompletely and may be related to neuronal degeneration with deposition of α -synuclein within the olfactory bulb and anterior olfactory nucleus.

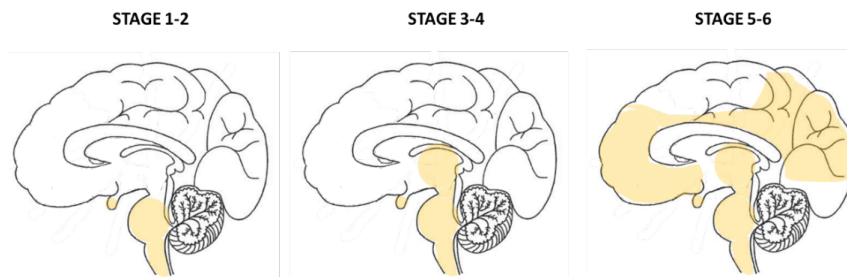


Figure 21. Presence of LB in different stages of the Braak's classification of PD. Scheme representing the progression of LB distribution in human brain.

7.4. Clinical symptoms

The main first clinical features of PD include the asymmetric onset of bradykinesia (slowness of initiation of voluntary movement with progressive reduction in speed and amplitude of repetitive actions), rigidity, resting tremor and posture instability. Furthermore, since muscles are constantly contracted, it is produced a stooped posture, poor balance, and instability. It is currently accepted that the diagnosis of PD requires the identification of bradykinesia plus at least one symptom between rigidity, resting tremor or postural instability. The main cardinal symptoms of PD (i.e. bradykinesia) have been shown to correlate with degree of cell loss in the striatum. Thus, the clinical symptoms appear after approximately 60% of the dopaminergic neurons are damaged, and the dopamine concentration in the striatum drops by about 80%. A symptomatic classification has been established, termed Hoehn–Yahr stages, which aims to define a number of stages that most of the patients may suffer upon the progression of the disease (173). The classification ranges from stage 1 (unilateral onset disease, limited to one side of the body with very few other symptoms) to stage 5 (with severe whole-body shakiness, postural instabilities, and significant mood and mental problems and a high decreased patient autonomy) (**Figure 22**).

PD patients are also afflicted with a host of other non-motor symptoms that are due to the loss of normal autonomic nervous system (ANS) function, which in turn may be due to loss of dopamine innervation that affects the autonomic ganglia, brainstem nuclei and hypothalamic nuclei (174). Some of these problems include gastrointestinal (i.e. constipation, swallowing difficulties that may be disrupted in PD by tremor, rigidity, and bradykinesia of the muscles of the lips, tongue), thermoregulatory dysfunction (i.e. excessive sweating), cardiovascular (i.e. orthostatic hypotension), urogenital (i.e. bladder dysfunction and sexual dysfunction that could be related with depression), sleep abnormalities (175), anosmia and taste sense alterations (176)(177).

The neuropsychiatric symptoms of PD, such as depression (178)(179), apathy, anxiety, hallucinations, cognitive decline (180) and psychosis, characteristically appear at different stages of the disease, and they all exhibit complex relationships with the classic motor deficits. For example, depression is common even before the onset of motor symptoms, and it becomes severe in the mid and late stages. Apathy is more common in later stages, whereas anxiety disorders are more common in early- and mid-stage patients. Speech act deficits appear in the early and mid stages. Finally, most of PD patients that survive more than 10 years develop dementia, although selective cognitive deficits are often present in the absence of clinically diagnosable dementia.

Early stages

Motor symptoms: Bradykinesia (difficulty in initiate actions)
 Reduced power of voice
 Facial expression appear immobile
 Assymetric resting tremor
 Mild rigidity

Loss of autonomic nervous system function:

Constipation
 Swallowing difficulties
 Sleep abnormalities

Anosmia: smell alterations

Taste sense alterations

Neuropsychiatric symptoms: Depression

Mid stages

Motor symptoms Resting tremor
 Severe rigidity
 Postural instability

Neuropsychiatric symptoms: Anxiety
 Depression

Later stages

Motor symptoms Resting tremor
 Severe rigidity
 Postural instability

Neuropsychiatric symptoms: Apathy
 Cognitive decline: Verbal semantic fluency
 Working memory
 Planning,

Figure 22. Early-, mid- and late-stage symptoms in PD. Stages of progression in PD and the corresponding clinical pathological features mainly associated with each PD stage.

7.5. Treatment of PD

At the moment there is no cure for PD, thus treatments available just help to relieve the symptoms and maintain life's quality. It is also important to highlight that PD therapies are individually designed to target the most disabling symptoms of patients and to try slowing the progression of the disease.

7.5.1. Dopaminergic drugs

L-3,4-dihydroxyphenylalanine (L-DOPA) was the first drug used for PD treatment. Its use is based on the fact dopamine can not cross the blood-brain barrier (BBB), thus by using its precursor it is possible to reach the brain and permitting the formation of dopamine. L-DOPA is readily transported across the BBB by an amino acid transporter, system L (181). Needless to say, when taken orally, L-DOPA is absorbed in the small bowel but rapidly decarboxylated in the gastrointestinal (GI) tract and in peripheral tissues. Consequently, only a small proportion would reach the CNS. For that reason, L-DOPA is co-administered in combination with a peripheral DOPA-decarboxylase inhibitor (DDCI), such as carbidopa or benserazide. This association reduces its peripheral conversion to dopamine, thereby also minimizing the predominant side effects of circulating dopamine. Another strategy for improving the bioavailability of L-DOPA and delivery to the brain is to inhibit both peripheral metabolism of L-DOPA and breakdown of dopamine in the synaptic cleft via the COMT pathway. Entacapone, a COMT inhibitor, has been shown to enhance the transportation of L-DOPA across the BBB and its conversion to dopamine. Also, it is possible to use MAO-B inhibitors, such as selegiline and rasagiline, which inhibit enzymatic MAO-B activity that breaks down dopamine (**Figure 23**). Finally, apart from L-DOPA, D₂R agonists can be used in monotherapy, or in combination with L-DOPA at low doses. Interestingly, these ligands (i.e. pramipexole, ropinirole, apomorphine, rotigotine) have been found to be effective in the treatment of advanced PD and also may help to modulate/control some of the undesired effects of long-term L-DOPA administration, this is, levodopa-induced dyskinesia (LID) (182) (**Figure 23**).

Dopamine precursor

Levodopa (L-dopa)

Carbidopa, Benserazide

COMPT inhibitor

Entacapone, Tolcapone

MAO-B inhibitor

Selegiline, Rasagiline

Dopamine agonistsErgot dopamine agonists: Bromocriptine, pergolide, cabergolideNon-ergot dopamine agonists: pramipexole, rapinirole, rotigotine

Apomorphine

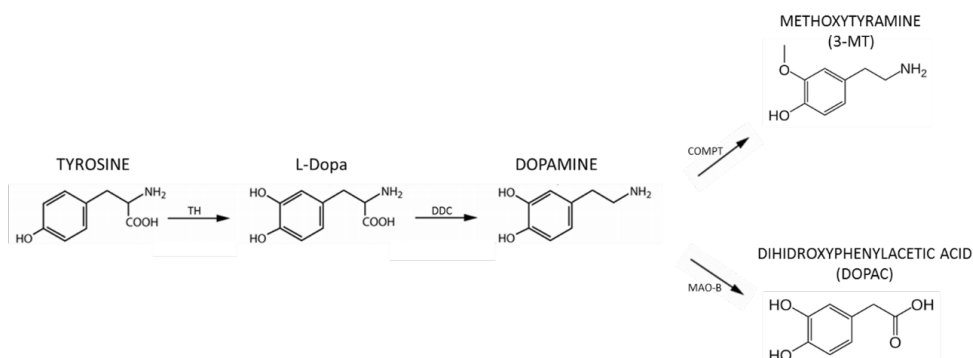


Figure 23. Dopamine-replacement therapy for PD. List of the most commonly dopamine agonists and dopamine precursors used in the treatment and management of PD.

Despite L-DOPA is the most effective drug for PD treatment, after long-term L-DOPA administration, benefits may fluctuate and patients start to notice decreased duration of motor control with each dose of L-DOPA, termed wearing-off. Also, they develop involuntary movements, called LID, and other parkinsonian symptoms such as gait and tremor, which may become resistant to dopaminergic drugs (183). There is ongoing debate regarding when, in the course of PD, it is most appropriate to initiate L-DOPA therapy. Thus, between 50 to 100% of PD patients treated with L-DOPA experience motor fluctuations and dyskinesias after 5-6 years of treatment, which are primarily related with the peak-doses and duration of the L-DOPA treatment.

Noteworthy, some symptoms do not respond to dopaminergic drugs, since other non-dopaminergic neurotransmitters, including acetylcholine, noradrenaline, serotonin, may be involved in the progression of the disease. For that reason, different therapeutic strategies, also aiming to delay the onset of L-DOPA complications and other adverse symptoms, may be used. However, although many non-dopaminergic agents have been evaluated preclinically, very few have shown significant clinical benefits as monotherapy in any PD stage.

7.5.2. Cholinergic drugs

L-DOPA and D₂R agonists have been the most used drugs for PD treatment. However, anticholinergic drugs were the first pharmacological agents used. In such way, PD is primarily viewed as a motor syndrome secondary to nigrostriatal dopaminergic denervation, but other neurotransmission systems also play a relevant role in striatal function. This is the case for cholinergic neurotransmission. Thus, in addition to the well-known reduction in dopamine levels, it also occurs an early alteration in cholinergic neurons. Cholinergic denervation may occur early in PD. In the Braak staging scheme of PD pathology, nigral and basal forebrain pathology occur simultaneously. Most cholinergic systems are affected in PD, such as muscarinic and nicotinic receptors and choline transporters, which are thought to intend correcting the imbalance between dopamine and acetylcholine levels. Of note, nicotinic receptors are not only highly expressed in dopaminergic neurons, but also in the cortex and thalamus (184). These findings support the hypothesis that regulating cholinergic system degeneration and/or dysfunction may be useful to alleviate motor (i.e. balance and resting tremor) and cognitive impairment in PD (185). In fact, nonmotor comorbidities, such as cognitive impairment, are explained better by multi-system denervation. Anticholinergic drugs can be administered as monotherapy in early stages of the disease, and act synergistically with L-DOPA in more advanced stages to correct the imbalance between dopaminergic and cholinergic neurological pathways. Competitive muscarinic receptors antagonists have been extensively used, such as trihexyphenidyl, bethanechol, procyclidine, biperiden, ethopropazine, diphenhydramine and orphenadrine. Importantly, anticholinergic drugs can improve movement symptoms in early stages of PD, but they are not the first choice due to limited efficacy and few clinical studies demonstrating its value. Finally, they also present a major drawback, which consists of the propensity to cause neuropsychiatric side effects.

7.5.3. Serotonergic drugs

Serotonin (5-hydroxytryptamine, 5-HT), glutamate and adenosine are important neurotransmitters within the basal ganglia, and mediate problems occurring after long-term L-DOPA treatment, such as LID. 5-HT receptors are crucial to motor control (i.e. tremor) and modulation of various cognitive functions (i.e. mood, emotion and sleep) (186). The neurodegenerative processes in PD also affect serotonergic neurons from the raphe nucleus, resulting in loss of 5-HT input to the striatum. There are many studies describing 5-HT_{1A}, 5-HT_{1B}, 5-HT_{2A} or 5-HT_{2C} receptors involvement in LID (187). The

diversity of 5-HT receptors involved in PD raises the issue of which is the most effective 5-HT-strategy for PD treatment. Interestingly, the 5-HT_{1A} agonist buspirone has been used in PD patients, in which it was observed a reduction in dyskinesias. Also, 5-HT_{2A/2C} antagonists have shown to regulate dopamine in striatum and extent L-DOPA action (188).

7.5.4. Glutamate drugs

In the brain, glutamatergic transmission plays a key role in the normal physiology regulating motor activity. In PD, glutamatergic transmission is considerably affected and glutamatergic hyperactivity has been observed in some studies (189). Increased glutamatergic transmission involving ionotropic NMDARs and AMPA, and metabotropic glutamate receptors (mGluRs) during PD dyskinesias, has been detected (190). Several subtype-selective NMDA and AMPA receptor antagonists, such as remacemide, amantadine and dextromethorphan have been investigated in preclinical studies and some evidences exist suggesting that NMDARs antagonists might reduce motor complications associated with L-DOPA therapy. Interestingly, the non-selective NMDARs antagonist amantadine is recommended treatment for dyskinesia, although other mechanisms apart from NMDA actions may explain its effects. Also, strategies aiming to potentiate AMPA receptor function have been proposed to provide cognitive enhancement. Finally, the selective mGlu₅R antagonists, mavoglurant and dipraglurant, have been also used with some efficacy against dyskinesia. Further studies are needed to evaluate the clinical potential of this target in PD, but it is mandatory to reduce side effects by selective targeting of glutamate receptor subtypes within affected basal ganglia regions (191).

7.5.5. Adenosinergic drugs

Within the striatum, A_{2A}Rs are expressed at a specific subset of MSNs output that project to the globus pallidus, which co-express D₂R. This discreet anatomical localization reduces the liability of A_{2A}R antagonists to induce central side effects (such as those that limits usefulness of anticholinergic and antiglutamatergic agents in PD) (192). Furthermore, pharmacological modulation of A_{2A}Rs is particularly useful in PD due to their property of antagonizing D₂R activity. In such way, motor effects elicited by A_{2A}R antagonists may be explained by enhancing D₂R activity. A_{2A}R antagonists have been shown to consistently improve motor deficits in all preclinical models of PD, also reducing the development of LID (193). In clinics, A_{2A}R antagonists are being evaluated as add-

on therapy in PD patients with wearing-off (194). Indeed, initial studies using Preladenant and Tozadenant demonstrated modest benefit in reducing the wearing-off as monotherapy (195). On the other hand, it has been proposed that the A_{2A}R might have an important role in the underlying neurodegenerative process. Thus, activation of presynaptic A_{2A}Rs in the glutaminergic endings of the striatum pathway of GABAergic neurons leads to glutamate release (196), which might play a crucial role in the death of neurons resulting from excitotoxicity. Therefore, it would seem likely that drugs inhibiting glutamate release, such as A_{2A}R antagonists, might be efficient in the treatment of neurodegenerative diseases. Noteworthy, some studies have described increased A_{2A}R levels in PD; for instance, A_{2A}R mRNA levels and [³H]SCH 58261-specific binding were shown to be increased in the putamen of dyskinetic patients (197). Accordingly, given the property of interacting and forming oligomers with D₂Rs, it seems likely to use A_{2A}R antagonists in combination with D₂R agonists as multimodal therapies for a better management of PD (198).

III. Hypothesis and aims

Working hypothesis

GPR37 has been identified as a protein that may be involved in the development and/or progression of PD. On the other hand, it has been proposed that GPR37 may modulate adenosinergic and dopaminergic systems. Specifically, it has been suggested that a direct receptor-receptor interaction may occur between GPR37 and D₂R and between GPR37 and A_{2A}R within the brain, specially in the striatum. Our working hypothesis is based on the existence of such GPR37-A_{2A}R oligomerization, which may be relevant both in normal basal ganglia functioning and in PD neuropathology.

Aims

- 1- Elucidating the existence and functional consequences of a direct GPR37-A_{2A}R receptor-receptor interaction in the striatum.
- 2- Establishing the existence of GPR37-A_{2A}R in other brain areas, such as the hippocampus, describing the synaptic distribution of GPR37 and determining its role in A_{2A}R-mediated synaptic plasticity.
- 3- Evaluating GPR37 receptor expression levels in PD and the potential use of this receptor as a PD biomarker

IV. Materials and Methods

This section constitutes a compilation from the materials and methodologies used in the experimental work of this doctoral thesis.

1. Antibodies

The antibodies used in this work are described in **Table 1**.

Primary antibodies					
Protein	Antibody	Brand	Technique	Dilution	Observations
hGPR37	Rb anti-hGPR37	Homemade	WB	1:1000	N-terminal human GPR37
mGPR37	Rb anti-mGPR37 extracell	Homemade	WB	1:1000	N-terminal mouse GPR37
			IFA	1:100	
hGPR37/ mGPR37	Rb anti-mGPR37 intracell	Homemade	WB	1:1.000	C-terminal GPR37
A_{2A}R	Mouse anti-A _{2A} R	Millipore	WB	1:1.000	clone 7F6-G5-A2
	Goat anti-A _{2A} R	Frontier Institute Co	WB	1:1.000	
			IFA	1:200	
TH	Rabbit anti-TH	Millipore	WB	1:1000	
α-Actinin	Rb anti-actinina	Santa Cruz Biotech.	WB	1:5.000	
Synaptophysin	Rb anti synaptophysin	Abcam	WB	1:3.000	Extra-synaptic marker
SNAP-25	Mouse anti-SNAP25	Abcam	WB	1:3.000	Presynaptic marker
			IFA	1:200	
PSD95	Rb anti-PSD95		WB	1:3.000	Post synaptic marker
			IFA	1:200	
Secondary antibodies					
	Goat anti-mouse-HRP	Pierce	WB	1:10.000	
	Goat anti-rabbit IgG -HRP	Pierce	WB	1:30.000	
	Rabbit anti-goat IgG-HRP	Pierce	WB	1:3.000	
	Cy5-conjugated donkey anti-rabbit IgG	Jackson Laboratories	IFA	1/200	
	Cy3-conjugated donkey anti-mouse	Jackson Laboratories		1:200	
	Cy2-conjugated donkey anti-goat	Jackson Laboratories		1:200	
	Alexa Fluor 488 goat anti-guinea pig	Thermo Fisher Scientific		1:500	
	rabbit IgG-Alkaline Phosphatase	Sigma		1:5.000	
	anti goat IgG-Alkaline Phosphatase	Sigma		1:5.000	

Table 1. Primary and secondary antibodies used in this work.

2. Drugs

Different specific ligands for the A_{2A}R and D₂R were used in this study.

Depending on the effect produced upon receptor binding, ligands are classified into full, partial or inverse agonists, or antagonists. Once bound, agonists stabilize receptors in the active conformation, and activates the receptor to produce a either a full or partial biological response. A full agonist results in a maximal response by occupying a fraction of receptors, while a partial agonist results in less than a maximal response even when occupying all of the receptors. On the other hand, antagonists block the action of agonists, while inverse agonists cause an action opposite to that of the agonist.

The A_{2A}R agonist 4-[2-[[6-Amino-9-(*N*-ethyl-β-D-ribofuranuronamidoyl)-9*H*-purin-2-yl]amino]ethyl]benzenepropanoic acid hydrochlorid (CGS21680; Tocris Bioscience, Bristol, UK) was used at 500 nM in mouse primary striatal cell cultures and total synaptosomal membranes for cAMP accumulation assays. For catalepsy induction test 10 μl of a 1 μg/μl CGS21680 solution was injected i.c.v. diluted in aCSF.

For the striatal and hippocampal related behavioral tests, the selective A_{2A}R antagonist 5-amino-7-(2-phenylethyl)-2-(2-furyl)-pyrazolo [4,3-*e*]-1,2,4-triazolo [1,5-*c*]pyrimidine (SCH58261; Abcam, Cambridge, UK), was injected intraperitoneally (i.p.) For the hippocampal related behavioral test, SCH58261 1 mg/kg was administered diluted in saline (0.9% sodium chloride) with 10% dimethylsulfoxide. The dose of 1 mg/kg was used based on previous published studies reporting no motor effects of SCH58261 at this concentration (199). For the striatal related behavioral tasks, an acute administration of 3.75 mg/kg was used (200). In the haloperidol catalepsy induced model, SCH58261 1 mg/kg was administered 15 min before haloperidol. Control animals were injected i.p. with saline (10% DMSO).

The D₂R antagonist haloperidol (Abcam, Cambridge, UK) was administered i.p. at an efficacious dose of 1.5 mg/kg in saline 0.9%.

3. Molecular cloning

Molecular cloning is a process that uses a serial combined set of techniques (such as target DNA isolation, PCR reaction, restriction enzyme reaction, ligation, amplification of the ligation product and sequencing) to insert a recombinant DNA of interest into a replicating plasmid (**Figure 24**). The main elements of this technique are: the target DNA of interest, known as insert, and the plasmid, also known as vector, which are used to obtain copies of the recombinant DNA, to add new properties by adding different tags (i.e. luciferase, GFP, HA, SNAP) or to produce a protein. Plasmids contain a multiple cloning site (MCS). MCS is the area of the plasmid that contains several recognition sites for different restriction endonucleases also known as restriction enzymes. These restriction enzymes are used to open the circular plasmid and introduce the insert by a ligation reaction. The plasmid vector also contains an origin of replication, which allows it to be replicated in bacteria (i.e. *E. coli*) or eukaryotic organisms (i.e. HEK-293T) and an antibiotic gene to allow to specifically select the population of interest.

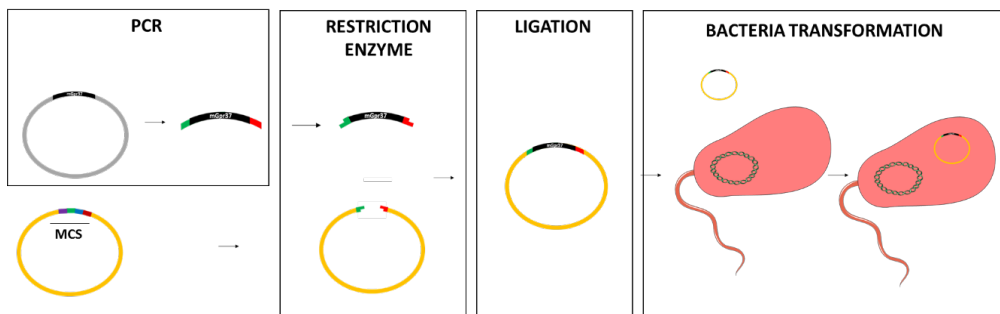


Figure 24. Molecular cloning scheme. Molecular cloning is composed of 4 sequential steps. First, amplification of the DNA of interest is performed; next, the ends of the DNA of interest and the vector are modified to make them compatible; the ligation step permits joining vector and insert through the action of a DNA ligase; and finally, the product is introduced into host bacteria.

3.1. Polimerase Chain Reaction (PCR)

Polimerase chain reaction (PCR) is a biochemical technique used to amplify single or few copies of a specific DNA strand sequence to obtain a high number of DNA fragments of the target DNA.

Primers design. The PCR is used to amplify the final number of DNA copies but it may also permit to introduce point mutations or enzyme restriction sites. Good primer design is essential for a successful PCR reaction. There are many factors to take into account when designing the primers. Some important tips to be considered consists of the following: they should have a length of 20–30 nucleotides, the melting temperature (T_m) of the primers should be between 65°C and 75°C, and within 5°C of each other. It is mandatory to confirm that the target DNA does not contain the restriction enzyme site within its sequence (restriction enzyme sites can be checked online by using the free software *Webcutter 2.0*) and add 3 to 5 nucleotides 5' of the restriction enzyme site in the primer to promote an efficient cutting.

PCR Reaction. Both iProof™ High Fidelity PCR Kit (Bio-Rad) and GoTaq® Green Master Mix (Promega, Fitchburg, WI, EEUU) were used in this thesis. The iProof™ was used in all the molecular clonings described in this thesis, exceptuating in genotyping PCR.

Protocol

PCR reactions were performed following manufacturer instructions (**See Table 2**). PCR mix reactions were prepared in 0.2 ml plastic eppendorfs and proceesed in a MJ mini personal Thermal Cycler (Bio-Rad, Laboratories, Hercules, CA, EEUU). After PCR, a 1% agarose gel stained with Red-Safe™ to allow the visualization of nucleic acids was run in order to confirm presence of the PCR product. A DNA ladder was used to corroborate the weight of the PCR product. The JETQUICK PCR Product Purification Spin Kit was used to purify the double-stranded DNA fragments directly from PCR reaction.

Reagent	Volume (ul)
DNA template 10 ng/ul	1
Forward primer 10 uM	2.5
Reverse primer 10uM	2.5
Iproof 2X	25
H ₂ O milliQ	q.s. 50 µL of final volume reaction

Step	Temperature (°C)	Time
Initial denaturalization	98	4 min
Denaturation	98	10 sec
Annealing	50	30 sec
Extension	72	20 sec/Kb of DNA
Final extension	72	7 min
Stocking	4	-

Table 2. iProof PCR conditions. Mix preparation and cycling conditions for the PCR using iProof™.

3.2. Restriction enzyme reaction

Restriction enzymes, also known as restriction endonucleases, are enzymes that produce a double-stranded DNA cut at or near specific recognition nucleotide sequences of 4-8 nucleotide of length, which are known as restriction sites. Cleavage leaves a 3'-hydroxyl on one side of each cut and a 5'-phosphate on the other. All restriction enzymes used in this thesis were obtained from Promega (Fitchburg, WI, EEUU).

Protocol

Cleavage was performed following manufacturer instructions at 37°C for 2h in Cut-smart Buffer (50 mM Potassium Acetate, 20 mM Tris-acetate, 10 mM Magnesium Acetate, 100 µg/ml BSA pH 7.9) (**Table 3**).

Restriction enzyme	Specific sequence	Extra-close-to-the-end nucleotides
EcoRV	5'---GAT▼ATC---3' 3'---CTA▲TAG---5'	5
HindIII	5'---A▼AGCTT---3' 3'---TTCGA▲A---5'	3
NotI	5'---GC▼GGCCGC---3' 3'---CGCCGG▲CG---5'	3
XbaI	5'---T▼CTAGA---3' 3'---AGATC▲T---3'	3
XhoI	5'---C▼TCGAG---3' 3'---GAGCT▲C---5'	4

By definition, 1 unit of restriction enzyme will completely digest 1 µg of substrate DNA in a 50 µl reaction in 60 minutes.

Reagents	Concentration/Volume
Vector/ Insert	10 µg/All PCR product
Cut-smart Buffer	5 µL
Restriction enzymes (i.e. EcoRV)	1ul
Restriction enzymes (i.e. HindIII)	1ul
H2O	q.s. 50 µL of final volume reaction

Table 3. Restriction enzymes used in this work and reaction conditions.

DNA previously cleaved using restriction enzymes was purified using the JETQUICK Gel Extraction Spin Kit (Genomed), to extract DNA fragments from all types of agarose gels and eluted from the column with H₂O miliQ.

3.3. DNA ligation

Ligase catalyzes the covalently joining of the two strands of DNA between the 5'-phosphate and the 3'-hydroxyl groups of adjacent nucleotides. T4 DNA Ligase (Promega) was used in this work for either cohesive-ended or blunt-ended ligations and was used following manufacturer instructions (See *Table 4. Ligation reaction conditions*).

Protocol

The composition of the 10X ligation reaction buffer is 300 mM Tris HCl (pH 7.8), 100 mM MgCl₂, 100 mM DTT and 10 mM ATP. Ligation reactions were incubated overnight using a ramp temperature gradient from 4°C to 16°C. Generally ligations were performed at 3:1 insert:vector molar ratios following reaction conditions described in **Table 4**.

$$\text{ng de insert} = \frac{3 \text{ insert}}{1 \text{ vector}} \times 100 \text{ ng} \times \frac{\text{Kb insert}}{\text{Kb vector}}$$

Reagents	Concentration/Volume
Vector ADN	100 ng
Inserto ADN	ng de inserto*
Ligasa 10X buffer	1 µL
T4 DNA Ligasa (diluted 1/3 in H ₂ O)	1µl
H ₂ O	q.s. 10 µL of final volume reaction

Table 4. DNA Ligation reaction condition

3.4. Bacterial transformation

Bacterial transformation is a method used to introduce foreign DNA into a bacteria, which can then amplify this exogenous DNA or be used for protein production. Competent bacteria used in this thesis were *Escherichia coli* HB101 or BL21, for DNA amplification or protein production.

Solutions and reagents

Luria broth (LB): 20 g/L of LB broth (Sigma) supplemented with antibiotic of interest: Kanamycin (30 µg/ml) or Ampicillin (75 µg/ml).

LB agar plates: LB broth supplemented with 15 g/L of Bacteriological European Type agar (Cultimed) and with antibiotic of interest: Kanamycin (30 µg/ml) or Ampicillin (75 µg/ml).

BL21 competent cells: Promega

HB101 competent cells: Promega

Protocol

Briefly, bacteria were thawed on ice for 25 min. Then, 5 µl of the DNA and 45 µl of competent bacteria were mixed in a 1.5 ml eppendorf under the flame, and returned the mixture to ice for 25 min. Next, cell and plasmid mixture were heat shocked by placing the mix in a water bath at 42°C for 45 seconds, and rapidly returned to the ice. Next, 950 µL of LB media were added and bacteria placed in a shaking incubator for 37°C for 90 min at 230 rpm. Bacteria were then centrifuged for 10 min at 7000 rpm at room temperature, resuspended in 200 µl of LB medium and spread in a LB agar plate supplemented with the corresponding antibiotic. Plates were incubated upside down overnight at 37°C. Next day, 3-5 colonies were picked and grew overnight at 37°C at 230 rpm in LB supplemented with antibiotic. Subsequently, amplified DNA was extracted using the JETquick plasmid miniprep kit (Genomed, Löhne, Alemania) and sent to be sequenced by the CCIT service. Finally sequence were analyzed using the Blast Sequence Analysis Tool from the NCBI database.

4. Site directed mutagenesis

The Q5® Site-Directed Mutagenesis Kit was used to generate site-specific mutations of double-stranded plasmid DNA.

Protocol

First, the Q5 Hot Start High-Fidelity DNA Polymerase and custom mutagenic primers were used to generate insertions in plasmids. After PCR, the amplified material (PCR product) was added directly to a Kinase-Ligase-DpnI (KLD) enzyme mix for 5 minutes at room temperature to undergo DNA circularization and template removal. Next, 45 µl of NEB 5-alpha Competent *E. coli* bacteria were transformed with 5 µl of the KLD reaction product by heat shock and grown overnight in LB supplemented with antibiotic. Finally, DNA was isolated using the JET Quick Plasmid Miniprep Spin Kit and sequenced for further analysis. Reaction conditions are described in **Table 5**.

Reagent	Volume (µl)
DNA template 10 ng/ul	1
Forward primer 10 µM	1.25
Reverse primer 10 µM	1.25
QS Hot Start High-Fidelity 2X Master Mix	12.5
H ₂ O milliQ	9

	Step	Temperature (°C)	Time (sec)
25 cycles	Initial denaturalization	98	30
	Denaturation	98	10
	Annealing	69	25
	Extension	72	180
	Final extension	72	120
	Stocking	4	-

Reagent	Volume (µl)
PCR Product	1
2X KLD Reaction Buffer	5
10X KLD Enzyme Mix	1
H ₂ O milliQ	3

Table 5 . Site directed mutagenesis reaction conditions.

HA-tag insertion into the pNanoLuc plasmid was generated using the Q5® Site-Directed Mutagenesis Kit. Custom forward and reverse primers were designed by incorporating half of the desired insertion into the 5' ends of the forward and the reverse primers without overlapping of nucleotids.

5. C57BL6 GPR37^{+/+} and GPR37^{-/-} mice colonies

Transgenic and KO animal models represent highly valuable tools to assess protein functions *in vivo*. A big number of experiments and results shown in this work were performed in native tissue from mice. GPR37^{-/-} mice were used both to evaluate the impact of GPR37 deletion and to validate the specificity of the GPR37 detection.

5.1. Animal house conditions/CEEA

C57BL/6J mice were housed in standard cages with *ad-libitum* access to food and water, and maintained under controlled standard conditions (12 h dark/light cycle starting at 7:30 AM, 22°C temperature and 66% humidity). The University of Barcelona Committee on Animal Use and Care approved the protocol and the animals were housed and tested in compliance with the guidelines described in the Guide for the Care and Use of Laboratory Animals (National Institutes of Health, 1996) and following the European Community, law 86/609/CCE.

5.2. Strain description

C57BL/6J Wild type and GPR37^{-/-} male mice (Strain Name: B6.129P2-GPR37^{tm1Dgen}/J; The Jackson Laboratory, Bar Harbor, ME, U.S.A.) were used in this study. To generate the GPR37^{-/-} mice, a fragment of the mouse genomic GPR37 sequence was deleted (5'TTGGGACCGGCATTATTGGCAACTTGGCAGTGATGTGCATCGT3') and replaced by a LacZ-Neo cassette (5140bp) (**Figure 25**).



Figure 25. Representation of the Wild type and Knockout mice GPR37 genomic sequence. Representation of the Wild type (upper) sequence of the GPR37. In **orange**, the fragment deleted for the GPR37 KO mice generation. Representation of the KO sequence (lower) of the GPR37, in which a fragment of the genomic GPR37 DNA was deleted and replaced by a LacZ-Neo cassette.

5.3. Genotyping

Solutions and reagents

Digestion Buffer: 50 mM Tris-HCl pH 8.0, 100 mM NaCl, 100 mM EDTA, 1% SDS.

Saturated NaCl solution: ~5M, used to neutralize the charge of nucleic acid backbone.

Proteinase K: 10 mg/ml (VWR).

Isopropanol: used for DNA and salts precipitation.

Ethanol 70%: used for DNA precipitation.

Protocol

Genomic DNA isolation. The last 2 mm of the mice tail was cut and left in an eppendorf on ice. Then, 750 μ l of Digestion Buffer and 40 μ l of Proteinase K were added and incubated overnight at 55°C with constant shaking. Next day, samples were vortexed and 250 μ l of a saturated solution of NaCl were added. Next, eppendorfs were mixed vigorously and centrifuged for 20 min at 13.200 rpm at room temperature. Then, 750 μ l were transferred to a new clean eppendorf and 500 μ l of ice-cold isopropanol added. Samples were mixed vigorously and returned to the ice for 20 min. Then, samples were centrifuged at 13.200 rpm for 20 min at room temperature and supernatant was discarded. Next, 500 μ l of ice-cold ethanol 70% were added onto the DNA pellet, which was thereafter centrifuged for 13.200 rpm for 10 min at room temperature. Supernatant was discarded and the eppendorf was incubated for 1 h at 42°C to evaporate ethanol. DNA was resuspended in 200 μ l of H₂O miliQ and incubated for 30 min at 42°C, vortexing the samples every 10 min. Finally, samples were centrifuged at 13.200 rpm for 10 min at room temperature and 180 μ l of the supernatant were recovered to a new clean eppendorf. Quantification of DNA was performed using a Nanodrop1000 (Thermo scientific) and diluted to a 50 ng/ μ l working solution.

PCR. A combination of 3 different primers were used to properly genotype and differentiate between GPR37^{+/+} (Wild Type, WT), GPR37^{+/-} (Heterozygous) and GPR37^{-/-} (Knockout, KO) mice with a simple PCR (**Figure 26**). Primer 1 and 2 generated a PCR product of 250 bp (base pairs, bp) while Primers 2 and 3 a 500 bp product. Depending on the genotype different DNA bands in the agarose gel were observed. GPR37^{+/+} mice generated a single 250 bp band; GPR37^{+/-} mice a single 500 bp band; and Heterozygous mice had both the 250bp and the 500 bp DNA bands.

Primer 1 GPR37 Forward 5' AACGGGTCTGCAGATGACTGGGTTTC 3'
 Primer 2 GPR37 Reverse 5' GGCCAAGAGAGAATTGGAGATGCTC 3'
 Primer 3 LacZ-Neo Forward 5' GGGTGGGATTAGATAAATGCCTGCTCT 3'



Figure 26. Scheme of the primers annealing in the PCR reaction and the expected DNA PCR product band agarose profile. (A) Sites of annealing of the different primers used for the GPR37 mice genotyping. **(B)** Characteristic different DNA profile in GPR37^{+/+}, Heterozygous and GPR37^{-/-} animals in an agarose gel stained with Red Safe and observed under the UV.

PCR Reaction. The GoTaq® Green Master Mix (Promega, Fitchburg, WI, EEUU) was used for genotyping, and the PCR reaction was performed following manufacturer instructions (**Table 6**).

Reagent	Volume (µl)
DNA template 50 ng/µl	1
Forward primer 1 10 µM	2.5
Forward primer 3 10 µM	2.5
Reverse primer 2 10 µM	2.5
Green Taq Master Mix	12.5
H ₂ O miliQ	4

Step	Temperature (°C)	Time	
Initial denaturalization	95	30 sec	
35 cycles	Denaturation	95	30 sec
	Annealing	63	30 sec
	Extension	72	25 sec
	Final extension	72	7 min
	Stocking	4	-

Table 6. GreenTaq PCR conditions. Mix preparation and cycling conditions for the PCR using GreenTaq .

After PCR, a 1% agarose gel stained with Red-Safe™ to allow the visualization of nucleic acids was run in order to confirm the PCR product. The DNA molecular weight was used to corroborate the weight of the PCR product.

6. Route of administration

Administration of substances to laboratory animals requires careful consideration to optimize delivery of the agent to the animal while minimizing potential adverse experiences from the procedure. The routes of administration used in this work were the intraperitoneal (i.p.) and the intracerebroventricular (i.c.v.) routes.

6.1. Intraperitoneally

Intraperitoneal injection is used for small species for which intravenous access is challenging. Also, it can be used to administer large volumes (volume injected should not exceed 10 ml/kg for mice) since the drug reach the bloodstream in minutes. Briefly, for i.p. injection, once mice were restrained, a needle (25-27 gauge) was inserted into the abdomen at about a 30-degree angle about half a centimeter depth. Drugs were then slowly injected (201) (**Figure 27**).

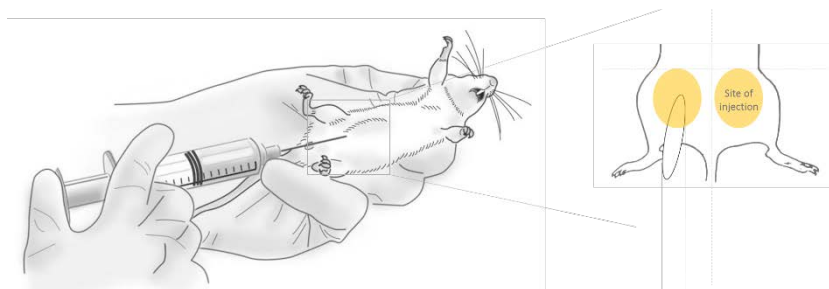


Figure 27. Representation of i.p. injection. Mice were manually restrained and i.p. injection was carefully performed.

6.2. Intracerebroventricular administration

Intracerebroventricular drug administration is an administration route that bypasses the BBB and other mechanisms that may limit brain drug distribution. Instillation of drugs directly into the ventricles of the brain must be done carefully and with full consideration of the osmolarity, pH, volume, and presence of preservatives and diluents of the drug solution being administered. Briefly, mouse were chemical restrained with vaporized isoflurane and placed in a stereotaxic frame. In this work, 10 μ l of CGS21680 in aCSF was administered i.c.v. at a rate of 2 μ L/min using a Hamilton syringe similarly to previously described (202) (**Figure 28**).

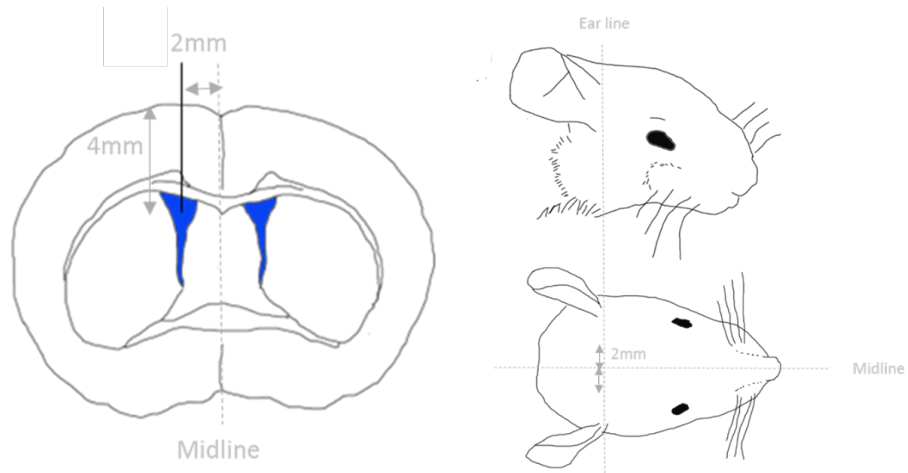


Figure 28. Representation of i.c.v. injection. Mice chemically restrained were placed in a stereotaxic frame and drug was administered using a hamilton needle.

7. Mice sample obtention

The mammalian brain is structurally organized into distinct anatomical regions mostly exerting dedicated control over specific physiological and behavioral functions. For instance, striatum is important for executive control, integration of movement and reward processing; the hippocampus controls formation and retrieval of associative and episodic memories; or the cerebellum is involved in motor learning and coordination. Due to the complexity of the nervous system, the majority of the studies focuses on single brain regions. For biochemical studies (i.e. co-immunoprecipitation, subsynaptic fractionation) or neuronal culture, mice brain was rapidly dissected on ice and hippocampus or striatum were separated. Next, we provide a brief technical description of how dissection was performed.

7.1. Brain removal

Mice were sacrificed by cervical dislocation to prevent pre- and postsynaptic effects of anesthesia (i.e. receptor phosphorylation or changes in receptor distribution). Next, a surgical scissor was used to remove the head with a cut posterior from the ears. A midline incision in the skin was done to expose the skull. Next, a small incision was made starting from the caudal part at the point of the interparietal bone trying to keep the end of the scissors as superficial as possible to prevent perturbing the brain. Then, one side of the parietal bone was tilted with the curved tweezers to expose the brain. Finally, brain was transferred to a plastic plate with ice to cool down the brain immediately, and meninges were removed.

7.2. Striatum dissection

The dissection of striatum (caudate nucleus and putamen) (**Figure 29 A**) was performed with scalpel and tweezers under visual control through a binocular surgical microscope (**Figure 29 B**). Applying the tweezers on the cerebellum, carefully on one hemisphere a superficial cut in the middle-part of the cortex was performed using the tweezers (**Figure 29 C**). Then, cortex was tilted and striatum was exposed (**Figure 29 D-E**). With the help of the scalpel, striatum was carefully dissected (rolled away) and excess of corpus callosum was removed.

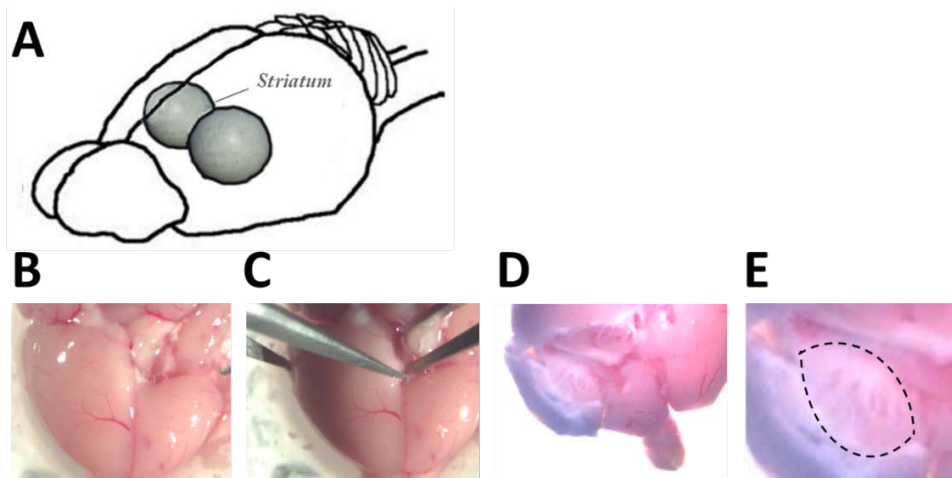


Figure 29. Striatum dissection from mice brain. (A) Schematic representation of the localization of the striatum in mice brain. (B-C) After brain removal, a superficial cut in the middle-part of the cortex was performed on one hemisphere. (D-E) Then, cortex was tilted laterally to expose the striatum and finally non-related brain areas were removed.

7.3. Hippocampal dissection.

The dissection of hippocampus (**Figure 30 A**) was performed using tweezers under visual control through a binocular surgical microscope. Applying the tweezers on the cerebellum, a superficial cut in the posterior part of the cortex was performed (**Figure 30 B-C**). Then, cortex was tilted laterally (**Figure 30 D**) and hippocampus was exposed (**Figure 30 E**). Finally, the hippocampus was pushed out of the cortex (rolled away) and then excess cortex tissue and remaining blood vessels were removed (**Figure 30 F**).

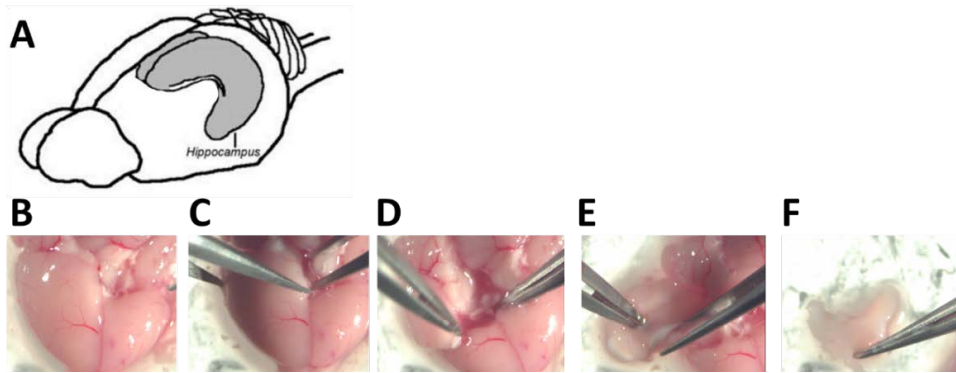


Figure 30. Hippocampus dissection from mice brain. (A) Schematic representation of the localization of the hippocampus in mice brain. (B-C) After brain removal, a superficial cut in the posterior part of the cortex was performed on one hemisphere. (D-F) Then, cortex was tilted laterally to expose the hippocampus and finally the hippocampus was pushed out of the cortex (rolled away) and then excess cortex tissue and remaining blood vessels were removed.

7.4. CSF collection

The epithelial cells of the choroid plexuses secrete cerebrospinal fluid (CSF) which fills the ventricles of the brain, the spinal canal and the subarachnoid space (Figure 31 A). CSF is usually crystal clear because it contains very few, if any, cells. There should be fewer than 5 cells/mm³ (mostly lymphocytes). The CSF has a number of important functions and its composition influence neuronal activity. CSF provides mechanical support for the brain and acts as a drainage pathway for the brain, were products of metabolism or synaptic activity are diluted and subsequently removed (203).

First, mice were anesthetized with Ketamine (100 mg/kg) and Xylazine (10 mg/kg), administered i.p. Secondly, mouse were placed prone on the stereotaxic instrument and the head was secured with the head adaptors forming a nearly 135° angle with the body (Figure 31 B). Next, the skin of the neck was shaved and the surgical site cleaned with 70% ethanol. Then, a sagittal incision of the skin was made in the posterior part to the occiput under the dissection microscope (Figure 31 C), and the subcutaneous tissue and muscles (*m. biventer cervicis* and *m. rectus capitis dorsalis major*) dissected with tweezers. Finally, under the dissection microscope, the duramater of the cisterna magna appeared as a glistening and clear reverse triangle through which the medulla oblongata, a major blood vessel (arteria dorsalis spinalis) (Figure 31 D) and the CSF space were visible. 10 µl of CSF were collected using a Micro-fine 0.3 ml (30G) syringe and stored at -20°C until use.

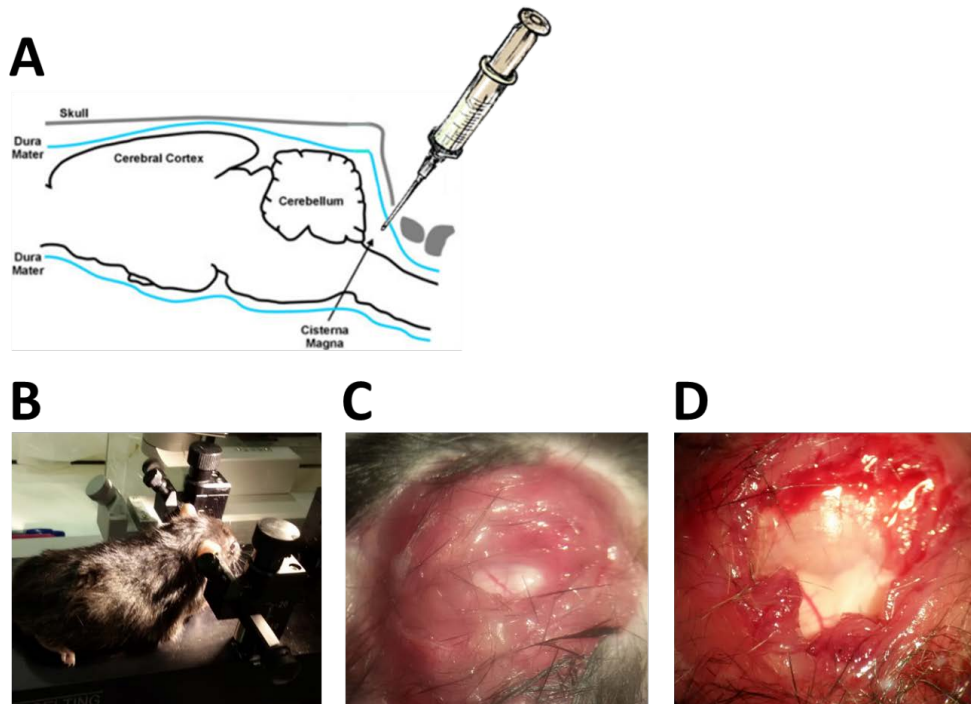


Figure 31. CSF collection from mice brain. (A) Schematic representation of the CSF collection from cisterna magna in mice brain. (B) Mouse were chemically restrained and placed in a *stereotaxic frame*. (C-D) Then, a sagittal incision of the skin was made in the posterior part to the occiput and muscles were dissected. Finally, the duramater of the cisterna magna appeared, and the CSF space was visible. CSF was collected using a Micro-fine 0.3 ml (30G) syringe

7.5. Serum collection

Intracardiac (i.c.) puncture is the best technique to obtain large and good quality blood samples from a mouse under deep terminal anesthesia. Animals were deeply anesthetized and left in dorsal recumbency on a table. Then, we accessed via the left side of the chest to obtain the blood using a 1 ml syringe with a 25-gauge 5/8-inch needle. Before injection, 0.5 cc of air was introduced into the syringe to create a vacuum. Next, the needle was inserted between the ribs at the point of the elbow, parallel to the table (Figure 32). When blood appeared in the syringe, the plunger was carefully pulled back to obtain the maximum amount of blood. Between 0.3 to 1 ml of blood can be obtained depending on the size of the mouse. Finally, the needle was removed and blood was transferred to a 1.5 ml eppendorf. The blood for serum evaluation was allowed to clot at room temperature and centrifuged for 15 min. Then, the serum was separated and stored at -20°C until use.

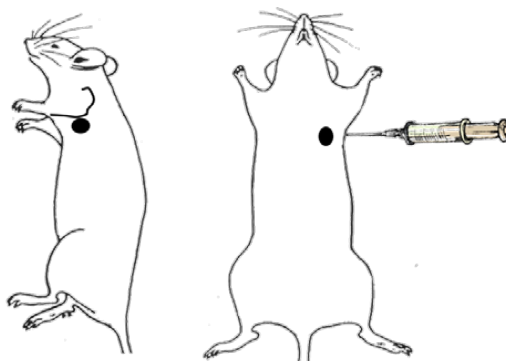


Figure 32. Relative localization of the heart for i.c. injection. Animals were left in dorsal recumbency on a table. Heart (●) was localized using the heartbeat and then the needle was introduced just under the animal's left elbow, at a plane parallel with the table.

8. Crude membranes obtention

The following crude membrane obtention protocol provides effective extraction from total cellular membrane proteins (combinations of plasma and organelle membrane proteins).

Solutions

PBS: 2 mM KH_2PO_4 , 10 mM Na_2HPO_4 , 137 mM NaCl and 2.7 mM KCl and pH was adjusted at 7.2

Tris 50 mM buffer: 50 mM Tris Base, pH 7.4 containing the Protease Inhibitor Cocktail (1:100).

Protease Inhibitor Cocktail Millipore, Set III, EDTA-Free - Calbiochem

Polytron: VDI 12 Adaptable Homogenizer, VWR Radnor, PA, USA.

Protocol

Mice were rapidly sacrificed by cervical dislocation and posterior decapitation. Brain was removed and the area of interest (i.e. hippocampus or striatum) was carefully dissected and kept in a chilled eppendorf on ice. Otherwise, when obtaining total membranes from an heterologue overexpression system (i.e. HEK-293T), cells were washed twice with PBS and detached with Acutase for 4 min at 37°C. Then, cells were centrifuged in a 15 ml falcon tube for 5 min at 1100 rpm.

Next, either for brain tissue sample or cells, 1 mL of ice-cold Tris 50 mM buffer was added and samples homogenized with the help of a polytron for three periods of 10 sec each. Homogenization was performed in an ice bath to preclude sample warming (**Figure 33, Step 1**). Next, samples were centrifuged for 10 min at 1000 *g* at 4 °C to remove the nuclear and tissue debris (**Figure 33, Step 2**). Supernatant containing membrane extracts were recovered in a new eppendorf and centrifuged for 30 min at 12.000 *g* at 4 °C (**Figure 33, Step 3**). Next, the supernatant containing the cytosolic proteins was discarded and the pellet containing the membrane extracts was resuspended in 1 mL of Tris 50 mM with Protease Inhibitor Cocktail (**Figure 33, Step 4 and 5**). Finally, determination of the protein content of each membrane extract was assed by means of the BCA Protein Assay Kit and all membrane extracts were adjusted to the same final concentration, normally between 1 and 2 mg/mL in Tris 50 mM containing the Protease Inhibitor Cocktail. It is recommended to use the membrane extracts freshly obtained. Alternately, they can be frozen down in liquid nitrogen and stored at -80 °C until use.



Figure 33. Scheme of the crude membrane obtention protocol. Brain tissue is homogenized with the aid of the Polytron (**Step 1**). The crude extract (**Step 2**) is then centrifuged at low rpm to eliminate nucleus from the total membrane extract. The supernatant is collected in a new eppendorf and centrifuged at high speed to pellet total membrane proteins (**Step 3**). Supernatant, containing cytosolic proteins, is discarded (**Step 4**) and pellet is resuspended in ice-cold Tris 50 mM (**Step 5**). At this point, the protein concentration is determined using the BCA assay.

9. Co-immunoprecipitation

Co-immunoprecipitation (Co-IP) is one of the most broadly used methodologies to identify, validate and characterize protein–protein interactions (PPIs) biochemically, both in heterologue overexpression systems and in native conditions. In brief, this technique consists of immunocapturing a protein of interest from a tissue lysate using a specific antibody. Subsequently, the immunocomplex containing the antibody, the antigen of interest and the antigen-associated proteins are precipitated by means of a Proteins A/G conjugated resin and analyzed by immunoblot. Of note, since PPIs are extremely dynamic and/or labile, the Co-IP method has to be optimized for each specific PPI. Remarkably, it is mandatory paying special attention to the specificity of antibodies used in the immunoprecipitation and the lysis buffer employed.

Solutions

Radioimmunoprecipitation assay (RIPA) buffer: 50 mM Tris–HCl, pH 7.4, 100 mM NaCl, 1 % Triton-X100, 0.5 % sodium deoxycholate, 0.2 % SDS , and 1 mM EDTA containing the Protease Inhibitor Cocktail.

Protein A-immobilized agarose: Sigma

Protocol

A 1 mg/mL protein suspension of brain membranes (i.e. hippocampus) or heterologue expression system membranes extract was used. First, samples were centrifuged during 30 min at 12.000 g at 4°C, and pellet was resuspended in 1 mL of RIPA buffer, homogenized using the Polytron (**Figure 34, Step 1**), and incubated during 30 min in constant rotation at 4 °C. After incubation, samples were centrifuged for 30 min at 12.000 g at 4°C, and supernatant collected in a new eppendorf. Then, 4 µg of the indicated primary antibody was added to each sample and incubated overnight in constant rotation at 4 °C to allow the formation of the immune complexes (**Figure 34, Step 2**). The following day, 50 µL of a suspension of protein A-immobilized agarose was added to each condition (**Figure 34, Step 3**), and mixture was incubated in constant rotation for 2 h at 4 °C to allow the antibody to bind to the protein complexes. Then, resin was washed three times by centrifuging at 10.000 g for 1 min at 4 °C with RIPA buffer (**Figure 34, Step 4**) and supernatant was carefully discarded (**Figure 34, Step 5**). In the last wash, supernatant was aspirated to dryness with a 28-gauge needle (**Figure 34, Step 6**), and finally, resin was resuspended with SDS -PAGE sample buffer (buffer described in

Section 13. Western Blot (Figure 34, Step 7). Samples were heated for 5 min at 100°C and analyzed by Western Blot (**Figure 34, Step 8**).

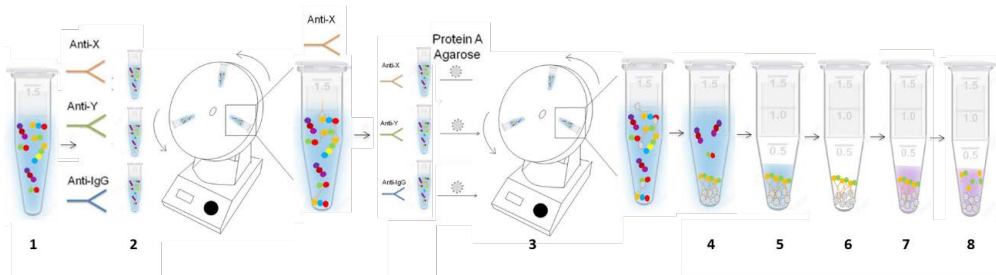


Figure 34. Scheme of the co-immunoprecipitation procedure. After solubilization of crude extracts in RIPA buffer (**Step 1**), supernatant was incubated with the indicated antibody overnight with constant rotation at 4 °C (**Step 2**). Next, Protein A resin was added to each tube and further incubated for 2 h at 4 °C with constant rotation (**Step 3**). Then, resin was washed with ice-cold RIPA by centrifuging at 10.000 rpm for 1 min (**Step 4**) and the supernatant was discarded (**Step 5**). Finally, the supernatant was aspirated to dryness (**Step 6**) and the resin was resuspended in SDS -PAGE (**Step 7**) and heated before loading into the polyacrylamide gel (**Step 8**).

10. Subsynaptic fractionation

Subsynaptic fractionation consists of a protocol to isolate proteins belonging to different synaptic compartments. In other words, it is a biochemical methodology to carry out protein enrichment from presynaptic, postsynaptic and extrasynaptic compartments. Firstly, synaptosomes or synaptic terminals are obtained from neurons that contain all the synaptic compartments by means of a discontinuous sucrose gradient. Subsequently, the isolation of the different sub-synaptic compartments is achieved by combining light solubilization using mild detergents with alterations of pH, which allow the separation by gradient and isopicnic centrifugations. Finally, protein enrichment at the different sub-synaptic compartments (i.e. pre-, post- and extrasynaptic membrane fractions) is validated by means of Western-blot analysis using well-characterized synaptic protein markers (i.e. SNAP-25, PSD-95 and synaptophysin, respectively), thus enabling a direct assessment of the synaptic distribution of any particular neuronal protein (i.e. ion channels, receptors, etc.).

10.1. Obtaining synaptosomes by discontinuous sucrose gradient

Solutions

Isolation buffer (IB): Sucrose 2 M, Sucrose 1 M/CaCl₂ 0.1 mM and CaCl₂ 0.1 mM

Sucrose 2 M: 2M sucrose

Sucrose 1 M/ CaCl₂ 0.1 mM: 1M sucrose and 0.01 mM CaCl₂

CaCl₂ 0.1 mM: CaCl₂ 0.1 mM

Sodium dodecyl sulfate (SDS) 5%: Sodium dodecyl sulfate 5%

Protocol

Solutions containing sucrose were freshly prepared the day of the experiment and chilled on ice. Mice were sacrificed (i.e. five animals) by cervical dislocation and rapidly decapitated. Brain was removed and the brain region of interest (i.e. hippocampus and striatum) dissected and kept into a 5 ml Potter-Elvehjem glass tube in ice, with 1 ml of IB. Then, tissue was homogenized using an overhead stirrer (10 *strokes* at 700-900 rpm) preferentially in an ice-bath (**Figure 35, Step 1**). Next, homogenized tissue was placed into a 15 mL conical tube and 6 mL of sucrose 2 M and 2.5 mL of CaCl₂ 0.1 mM were added and kept at 4°C. Tube was homogenized slowly by inverting it and the solution was placed in an Ultra-clear centrifuge tube and 2.5 mL of sucrose 1 M/CaCl₂ 0.1 mM was added on top of each tube, very slowly, to form the sucrose gradient (**Figure 35, Step 2**). Then, tubes were centrifuged for 3 hours at 100.000 *g* at 4°C using an Ultra-Swinging Bucket SW41Ti rotor in a Beckman Coulter Optima Ultracentrifuge L-90K. After centrifugation, top layer containing myelin was discarded, and with the help of a Pasteur pipette the white ring between the 1.25 M and 1 M sucrose interphase corresponding to the synaptosome fraction was collected (**Figure 35, Step 3**). Synaptosomes were diluted 9 times its volume with IB in an Ultra-clear centrifuge tube and centrifuged again for 30 min at 15.000 *g* at 4°C using an Ultra-Swinging Bucket SW41Ti rotor. Finally, supernatant was discarded and pellet was resuspended with 1.1 mL of IB solution. Then, 100 µL of this synaptosomal solution was collected and centrifuged at 11.000 *g* for 5 min at 4°C and the synaptosomal pellet was resuspended in 5% SDS and stored at -20 °C. This sample correspond to the total synaptosome fraction for further Western-blot analysis. The remaining synaptosomal fraction (~1 ml) was frozen down at -20°C until use or processed for subsequent subsynaptic fractionation.

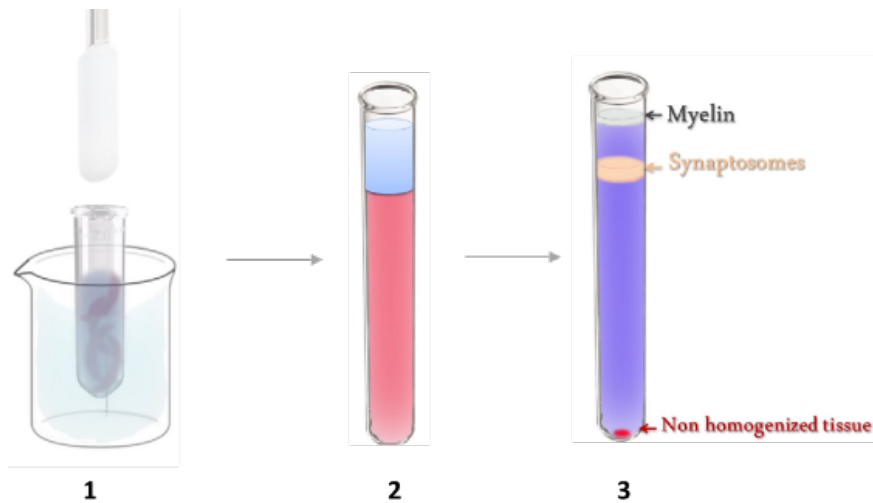


Figure 35. Scheme of the brain synaptosomes obtention. After tissue dissection (i.e. 5 hippocampus), tissue was homogenized in a Potter-Elvehjem glass tube (**Step 1**) and the sucrose gradient was formed in a Ultra-clear centrifuge tube (**Step 2**). After centrifugation total synaptosomes fraction observed as a white dense ring between the 1.25 M and 1 M sucrose interphase were isolated (**Step 3**).

10.2. Pre-, Post- and Extrasynaptic isolation

Solutions

Isolation buffer (IB): Sucrose 2 M, Sucrose 1 M/CaCl₂ 0.1 mM and CaCl₂ 0.1 mM

Solubilization buffer 2x pH 6.0: 40 mM Trizma Base (Sigma-Aldrich) and 2% Triton X-100, and carefully adjust pH at 4°C.

Solubilization buffer 1x pH 6.0: 20 mM Trizma Base and 1% Triton X-100, and carefully adjust pH at 4°C.

Solubilization buffer pH 8.0: 20 mM Trizma Base and 1% Triton X-100, and carefully adjust pH at 4°C.

SDS 5%: SDS 5%

Protocol

The day of the experiment, solubilization buffer 2x pH 6.0, solubilization buffer 1x pH 6.0, solubilization buffer pH 8.0 and CaCl₂ 0.1 mM were freshly prepared. Of note, pH was adjusted carefully and chilled on ice. The 1 ml-resuspended synaptosomal fraction was diluted slowly with 5 mL of CaCl₂ 0.1 mM and the same volume (5 mL) of ice-cold solubilization buffer 2x pH 6.0 was added and incubated for 50 min in ice, under high agitation in a beaker with ice. After agitation, solution was placed in an Ultra-clear centrifuge tube. Tubes were equilibrated with CaCl₂ 0.1 mM and solubilization buffer 2x pH 6.0 solution and centrifuged for 30 min at 40.000 g at 4°C using an Ultra-Swinging Bucket SW41Ti rotor. After centrifugation, the resulting supernatant represented the extrasynaptic fraction and the pellet the synaptic junctions (i.e. both the pre- and postsynaptic fractions). Supernatant containing the extrasynaptic fraction was concentrated to a final volume of 200 µl by using a 15 ml Amicon Ultra.10K Filter Falcon by centrifugation at 4000 g at 4°C and the resulting concentrated extrasynaptic fraction (200 µl) were precipitated with 5 volumes (1mL) of pre-chilled (-20°C) acetone overnight at -20°C. Next day, extrasynaptic fraction was centrifuged at 18.000 g for 30 min at -15°C. After centrifugation acetone supernatant was discarded and the pellet was left to dry to remove any trace of acetone. Finally, pellet containing extrasynaptic proteins was resuspended with 200 µl of the 5% SDS solution.

The pellet containing the pre- and postsynaptic fractions was carefully washed with 2 ml of solubilization buffer 1x pH 6.0, without disrupting it, and buffer was discarded. Then, pellet was resuspended with 10 mL of solubilization buffer 1x pH 8.0 with a glass Pasteur pipette and the suspension incubated for 50 min in ice, under high agitation in a beaker with ice. After agitation, solution was placed in an Ultra-clear centrifuge tube. Weight and tubes were equilibrated with solubilization buffer 1x pH 8.0 solution and centrifuged for 30 min at 40.000 g at 4°C using an Ultra-Swinging Bucket SW41Ti rotor. The resulting supernatant corresponding to the presynaptic was processed as described for the extrasynaptic fraction. Pellet containing postsynaptic fraction was resuspended with 200 µl of the SDS 5% solution. Finally, the enrichment in synaptophysin, SNAP-25 and PSD95 within the extra-, pre- and post- subsynaptic fractions, respectively, was analyzed by immunoblot using specific antibodies against these proteins.

11. Membrane protein biotinylation

Labeling of cell surface proteins with biotin represents a powerful tool to study plasma membrane receptors expression or cellular transport pathways involved in regulating membrane proteins. Biotin is a water soluble and membrane impermeable reagent with negative charge that reacts with primary amines at pH 7.0-9.0 in an irreversible way generating an amide bound.

Solutions

Sucrose-supplemented artificial CSF (S-aCSF): 2.5 mM KCl, 1.2 mM NaH₂PO₄, 1.2 mM MgCl₂, 2.4 mM CaCl₂, 26 mM NaHCO₃, 11 mM glucose, and 250 mM sucrose

aCSF: 125 mM NaCl, 2.5mM KCl, 1.2mM NaH₂PO₄, 1.2mM MgCl₂, 2.4 mM CaCl₂, 26 mM NaHCO₃, and 11 mM glucose.

Sulfo-NHS-SS-biotin: Thermo Scientific

RIPA: 50 mM Tris-HCl, pH 7.4, 100 mM NaCl, 1 % Triton-X100, 0.5 % sodium deoxycholate, 0.2 % SDS , and 1 mM EDTA.

Streptavidin immobilized on agarose, CL-4B: Sigma-Aldrich

Protocol

Brains were removed and immediately chilled in S-aCSF solution saturated with 95%O₂/5%CO₂ (**Figure 36, Step 1**). Then, 300 µm coronal sections were made on a Leica vibratome 1200S sectioning system (**Figure 36, Step 2**). Sections containing striatum were recovered and incubated in aCSF at 31°C at 300 rpm for 90 min with 95%O₂/5%CO₂ (**Figure 36, Step 3**). Surface proteins were covalently labeled with 0,5 mg/ml sulfo-NHS-SS-biotin in ice-cold aCSF for 45 min at 4°C (**Figure 36, Step 4 and 5**). Following biotinylation, slices were washed 3 times in ice-cold aCSF and three times in ice-cold aCSF supplemented with 100 mM glycine. Residual reactive biotin was quenched by incubating twice in ice-cold aCSF supplemented with glycine for 25 min at 4°C, with 95%O₂/5%CO₂ bubbling. Next, slices were washed four times with ice-cold aCSF. Tissue was lysed with the help of a polytron in RIPA buffer and rotating 30 min at 4°C (**Figure 36, Step 6**). Cellular debris were cleared by centrifugation at 18.000 g for 20 min at 4°C, and protein concentrations were determined using the BCA protein assay. A bead:lysate ratio of 25 µl streptavidin agarose:50 µg striatal lysate was used and incubated overnight in rotation at 4°C. Afterwards, beads were washed three times with RIPA by centrifugating at 18.000 g for 2 min at 4°C and resuspended in SDS-PAGE sample buffer for Western Blot. This protocol was adapted from (204).

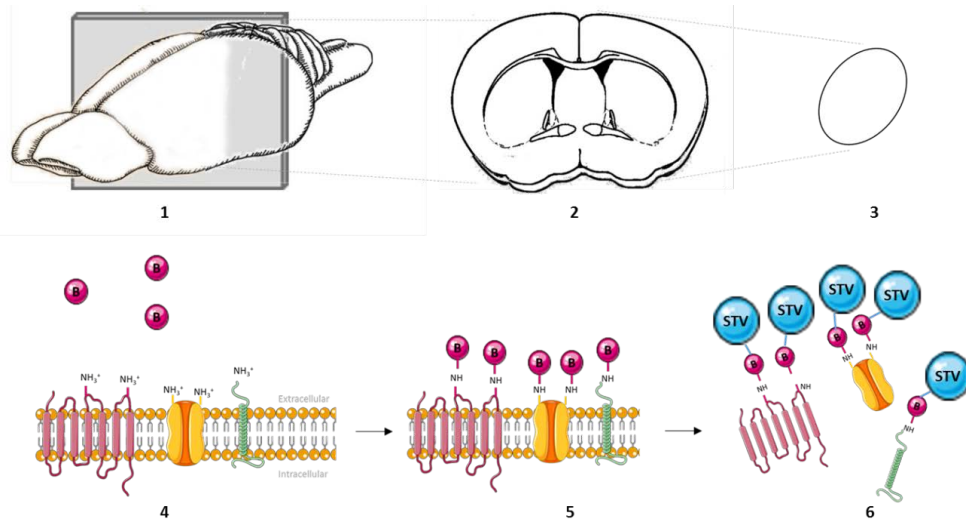


Figure 36. Scheme representing membrane protein biotinylation protocol in corticostriatal slices. Mice brain was rapidly removed (**Step 1**) and 300 μm corticostriatal sections were performed (**Step 2**). With the help of a microscalpel striatum was dissected and incubated for 1h at 31°C for membrane recovering (**Step 3**). Surface proteins were covalently labeled with biotin, an impermeable membrane reagent (**Step 4-5**) and then tissue was lysed. Finally streptavidin agarose, which has the ability to bind with high affinity the *biotin*, was added to each sample to isolate membrane proteins (**Step 6**).

12. Protein concentration determination

Using the bicinchonic acid (BCA) protein assay (Thermo Scientific), duplicate 10 μl samples of known BSA standards in the range 0 to 2 mg/ml and unknown protein samples were added to a 96-well plate. Then, 200 μl BCA solution (1 % (w/v) 4,4 dicarboxy-2,2 biquinoline disodium salt, 2% (w/v) sodium carbonate, 0.16% (w/v) sodium potassium tartrate, 0.4% (w/v) sodium hydroxide, 0.95% (w/v) sodium bicarbonate pH 11.25, 0.08% (w/v) copper (II) sulphate) was added to each well. Protein concentration was determined by measurement of the absorbance at 495 nm using a POLARStar plate reader. Plates were incubated for 30 min (specific reduction of Cu^{2+} to Cu^{1+} allowed the BCA sodium salt to bind the Cu^{1+} ion forming an intense purple colour) at 37°C. The absorbance of the standards was used to determine a straight line from which unknown protein concentrations were calculated.

13. Western Blot

The gels contain two different polyacrylamide phases (i.e. stacking or concentrating and separating gels). Separating gel acrylamide/bis-acrylamide % depends on the size of the protein under study. In this work 7.5 and 10% separating gel acrylamide/bis-acrylamide were used. Stacking gel was done at 1% acrylamide/bis-acrylamide.

Solutions

Stacking gel Buffer: 25 mM Tris Base, pH 6.8.

Separating gel Buffer: 1.5 M Tris Base, pH 8.8

Anode Buffer: 300 mM Tris Base, 20 % methanol

Catode Buffer: 40 mM 6-aminocaproic acid, 20 % methanol.

Electrophoresis Buffer: 25 mM Tris Base, pH 8.0, 180 mM glycine, 0.1 % SDS.

PBS: 2 mM KH_2PO_4 , 10 mM Na_2HPO_4 , 137 mM NaCl and 2.7 mM KCl and pH was adjusted at 7.2

IB Blocking solution: PBS with 0.05 % Tween 20 and 5 % (w/v) of nonfat dry milk.

IB Washing solution: PBS containing 0.05 % Tween 20

2X SDS -PAGE sample buffer (for 20 ml): 4 ml of Glycerol, 8 ml of a 10% SDS solution, 5 ml of Stacking Buffer, 3 ml of H_2O and a small amount of bromophenol blue.

Protocol

Protein marker and samples were loaded into the gel wells. Gels were run at 75 V until samples reached the separating gel and then voltage was increased until 120 V. SDS-PAGE running was stopped when the downmost band of the protein marker reached the foot line of the glass plate. Following electrophoresis, gel was equilibrated in anode buffer for 5 min. Meanwhile, immobilon-P transfer membranes and two immunoblot thick filter papers were cut in 9 cm x 6 cm sheets. Membranes were completely soaked in methanol for 5 sec to activate them and finally equilibrated in anode buffer. An anode buffer pre-soaked sheet of filter paper was left onto the anode cassette; then, the anode buffer pre-wetted membrane was transferred on top of the filter paper; next, gel was placed carefully on top of the transfer membrane; and finally, the other cathode buffer pre-soaked extra thick filter paper was placed on top of the gel. A plastic pipet was rolled over the surface of the filter paper in both directions to eliminate air bubbles and to ensure

complete contact between polyacrylamide gel and the transfer membrane. Carefully, the cathode top was placed onto the cassette. Mini gels were transferred for 30 min at 25 V. Next, membrane were transferred in IB blocking solution for 45 min at room temperature with continuous shaking and incubated overnight at 4 °C with the indicated primary antibody diluted in IB blocking solution with continuous shaking. The following day, membranes were washed three times for 10 min with IB washing solution to eliminate unbound primary antibody and incubated with the indicated secondary antibody for 90 min at room temperature in continuous shaking. Membranes were washed 3 times for 10 min with IB washing solution to eliminate unbound secondary antibody. Finally, membranes were incubated with SuperSignal west pico chemiluminescent substrate (the mix was prepared following the proportion 1:1 of solution A and B provided by the manufacturer in dark conditions). Membrane was developed in an Amersham Imager 600.

14. Homemade polyclonal rabbit antibody generation

Briefly, the production of polyclonal antibodies consists of the molecular cloning of the peptide, production of peptide antigens, immunisation, serum preparation, affinity purification and a specificity/validation test. Good specific antibodies are often easily produced against the *N*- and *C*-terminal regions of proteins, probably because the extremities of many endogenous proteins are prone to adopting conformations similar to those formed by short peptide antigens. Therefore, *N*- and *C*-terminal sequences should be considered as primary candidates for immunogens. Of note, it is mandatory to check for the presence of PEST domini on the sequence. PEST domini are proteic motifs found in a big number of proteins of short half-life. Presence of this PEST domini on the peptide can impair in a minor or major way its stability and production/degradation. One of the main characteristics of these regions are that they are rich in proline, glutamate/aspartate, serine, treonine residues close to basic amino acids. Presence of PEST domini can be checked online in this website: <http://emboss.bioinformatics.nl/cgi-bin/emboss/pepfind>

14.1. Antigenic peptide preparation

To produce the peptide for immunisation, the gene fragment was cloned into the pGEX-4T1 plasmid to generate a GST fusion tag protein. Then, protein induction was performed in BL21 bacterias, and finally, the recombinant protein was purified using affinity columns.

Molecular cloning

Plasmid: pGEX-4T1 plasmid vector (GE Healthcare). This vector allows the cDNA fragments to be fused in frame with glutathione S-transferase (GST), thereby enabling their purification via glutathione-affinity chromatography.

A gene fragment (i.e. N-terminal or C-terminal fragment of the mouse GPR37) was cloned into the pGEX-4T1 plasmid. In brief, DNA fragments obtained from PCR were cleaved with restriction enzymes for 2 h at 37°C and after using a PCR Purification Kit, ligation with the T4 Ligase was performed overnight at a ramp temperature from 4 to 20°C. Next day, HB101 were transformed and a MAXIprep was done. After sequencing, DNA was transformed into BL21 and protein production was induced.

14.2. Recombinant protein production

Isopropyl β -D-1-thiogalactopyranoside (IPTG) is a molecular biology reagent that mimics a lactose metabolite, stably binds to the Lac repressor, and triggers transcription of the Lac operon. It is therefore used to induce recombinant protein expression when a gene is under the control of the Lac operator.

Solutions and reagents

LB and LB agar plates supplemented with antibiotic

IPTG (Isopropyl β -D-thiogalactopyranoside, Sigma-Aldrich)

E.coli BL21 competent cells (Promega). BL21 (DE3)pLysS Competent Cells allowed high-efficiency protein expression.

Protocol

A single colony from the agar plate of the BL21 already transformed (i.e. with the pGEX 4T-1 N-terminal mGPR37) was picked using a sterile yellow tip and grown overnight in 50 ml LB supplemented with Ampicillin at 37°C with vigorously agitation. The following day, the overnight culture was diluted to OD₆₀₀ 0.05 in 1 L of LB supplemented with Ampicillin, and grown at 37°C with agitation until OD₆₀₀ reached 0.6-0.7. Then, induction of the peptide expression was elicited with 0.3 mM IPTG and grown for 6 hours at 30°C (temperature should be optimized for each protein production from a range of 20 – 37°C). Finally, the culture was harvested at 8000 rpm for 20 min and supernatant discarded. In this step, pellets could be kept at -20°C or processed for protein purification.

ABC solutions for affinity column cleaning

Glutathione-Superflow and Aminolink resin were used for gravity flow purification of GST-tagged proteins or antibody purification from rabbit serum, respectively. Impurities from the resin were eliminated using the ABC cleaning protocol.

Solutions

Solution A: 0,1M Acetate, 0,5M NaCl. pH is adjusted to 4.5 using Acetic acid

Solution B: 0,1M Borate, 0,5M NaCl. pH is adjusted to 8.5 using NaOH

Solution C: 2M NaCl

Storage solution: 2M NaCl, 1mM Sodium azide

Protocol

To prepare the column 4 ml of a 50% Glutathione-superflow resin (Clontech) were loaded to a 10 ml chromatography column (Bio-Rad), and washed with 20 ml of Solution B, then 20 ml of Solution A and finally 20 ml of Solution C. Column was then ready to use.

14.3. Protein purification

Solutions

STE Buffer: 10 mM Tris-Base, 150 mM NaCl, 1mM EDTA, pH is adjusted to 8.

Lysis Buffer: 1% N-Lauroilsarcosine (Sigma-Aldrich), 8.5 mM DTT in STE

Wash Buffer: 0,1% N-Lauroilsarcosine (Sigma-Aldrich), 8.5mM DTT in STE

Elution Buffer: 0,1% N-Lauroilsarcosine (Sigma-Aldrich), 8.5mM DTT and 10mM L-Glutathione reduced (Sigma-Aldrich) in STE

Glutathione-superflow resin (Clontech)

Dialysis tubing cellulose membrane (avg. flat width 10 mm, Sigma-Aldrich)

Staining solution: 0.25% Comassie, 10% glacial acetic acid, 50% Methanol.

Destaining solution: 15% glacial acetic acid, 20% Methanol

Protocol

The chromatography column containing the Glutathione-agarose resin was equilibrated with 20 ml of Wash Buffer. Pellets containing BL21 induced bacterias were resuspended in 20 ml Lysis buffer and frozen using liquid nitrogen. Then, they were thawed using a 37°C water bath. The freezing-thaw cycle was repeated at least 3 times. Then, samples were sonicated 5 times in an ice bath in cycles of 20 seconds (80% of each second) using a Branson Sonifier 250. Then, samples were centrifuged during 15 min at 12.000 rpm at 4°C using a Beckman centrifuge with the JA-20 rotor. Supernatant was filtered using a 0.22 µm filter and loaded 3 times to a 20 ml plastic column with 2 ml resin Glutathione-agarose resin. Then, column was washed with 50 ml of Wash Buffer. Finally, GST-fusion proteins were eluted from the column using 10 ml of Elution Buffer in 1 ml fractions and analyzed by polyacrilamide gel. Known amounts of BSA ranging from 0.2-2 µg and eluted proteins were analyzed by SDS-PAGE. The gel was stained for 20 min at room temperature with the staining solution, and subsequently destained overnight with the destaining solution. Finally, it was scanned and the density of BSA bands was used to generate a standard curve. The BSA standard curve was used to estimate the concentration of protein fractions, which were dialyzed 48 h in PBS at 4°C. Finally, protein was quantified using the BCA assay.

14.4. Immunisation

Solutions and reagents

PBS: 2 mM KH₂PO₄, 10 mM Na₂HPO₄, 137 mM NaCl and 2.7 mM KCl and pH was adjusted at 7.2.

Freund's complete adjuvant (Sigma-Aldrich).

Freund's incomplete adjuvant (Sigma-Aldrich).

Host animals for immunisation: 2 male White New Zealand White rabbits weighing 2.5 Kg were used for each polyclonal antibody of interest, due to variability of the antigenic response in different individuals. Rabbits were housed in standard cages with ad-libitum access to food and water, and maintained under controlled standard conditions (12 h dark/light cycle starting at 7:30 AM, 22°C temperature and 66% humidity). The University of Barcelona Committee on Animal Use and Care approved the protocol and the animals were housed and tested in compliance with the guidelines described in the Guide for the Care and Use of Laboratory Animals (National Institutes of Health, 1996) and following the European Community, law 86/609/CCE.

Protocol

The first day of immunisation (I_1) a 1:1 (v/v) 1.5 ml mixture of Freund's complete adjuvant and 750 μ g of the peptide of interest in PBS was injected subcutaneously distributed in 0.2 ml/site of injection (**Figure 37 A**). The same day, pre-immune blood sampling was extracted from the marginal ear vein to be used as negative control during the immunisation process (S_0). Booster immunisations (I_2 , I_3 , I_4 and I_5) were done 15 days after I_1 and given every 2 weeks intervals. A 1:1 (v/v) 1.5 ml mixture of Freund's incomplete adjuvant and peptide in PBS was injected (**Figure 37 B**). Blood samples collection were obtained 1 month after S_0 and 7 days after booster injections.

Finally, after reaching the desired immunogenic response, rabbits were anesthetized and i.c. puncture was performed for a large blood collection. Then, blood was kept at room temperature for 2 h and centrifuged at 3000 rpm for 10 min at room temperature. Finally, serum was recovered and stored at -80°C .

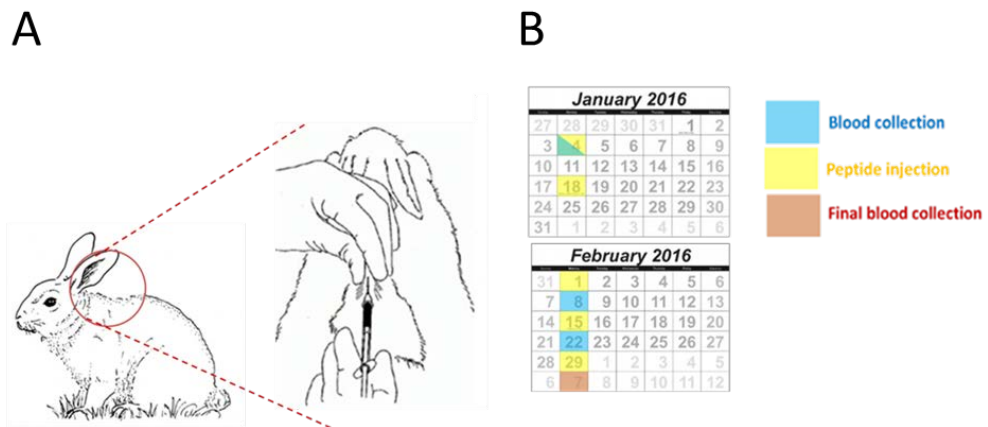


Figure 37. Multiple peptide injection and blood sample collecting schedule for polyclonal antibody generation in White New Zealand rabbits. (A) Site of administration of the peptide suspension. **(B)** Exemple of a typical time distribution for peptide administration and blood sample extraction during the polyclonal antibody production.

14.5. Antibody purification

Solutions and reagents

AminoLink Coupling resin (Thermo Scientific)

Coupling Buffer: 0.1 M Sodium phosphate buffer, pH is adjusted to 7-7.5

Quenching Buffer: 1M Tris-HCl, pH is adjusted to 7.4

Washing Buffer: 1M NaCl

Cyanoborohydride Solution: 1M NaCNBH₃ in 0.01N NaOH. Prepare the same day of use in a fume hood.

Storage Buffer (PBS): 2 mM KH₂PO₄, 10 mM Na₂HPO₄, 137 mM NaCl and 2.7 mM KCl and pH was adjusted at 7.2.

Elution Solution: 100mM Glicine, pH is adjusted to 2.5

Neutralizing solution: 1M Tris-Base, pH is adjusted to 8.8

Protocol

Aminolink column preparation

For the specific antibody purification from rabbit serum, we first produced two different Aminolink purification columns: the first one to capture the specific antibodies generated against the GST and the other one to capture the antibodies of interest (i.e. GPR37).

For each column we used 2 ml of Aminolink resin and made 3 washes with the Coupling Buffer. Then, 1-2 mg of the GST or GST-tagged protein (i.e. GPR37-GST) produced in BL21 in PBS and 25 µl of the Cyanoborohydride Solution/ml were incubated in a 15 ml falcon tube in a end-to-end rocker at 4°C for 2 h.

Then Aminolink remaining active sites were blocked by making two washes of the resin with Quenching buffer for 30 min at room temperature in a end-to-end rocker. Finally, columns were washed with Washing Buffer.

Antibody purification

For the antibody purification, 3 ml of rabbit serum were diluted in a final volume of 20 ml of PBS. Then, the 20 ml mixture were loaded through the GST-Aminolink column to retain all GST specific antibodies and the flowthrough was subsequently applied to the GST-tagged fusion protein-Aminolink column (i.e. GPR37-GST). Then GST-tagged fusion protein-Aminolink column was washed with 50 ml of PBS and antibody was finally

eluted with 10 ml of Elution solution in fractions of 1 ml and immediately neutralized with the Neutralizing solution to achieve a basic pH. Finally, fractions were analyzed by polyacrilamide gel as described previously. Fractions containing the antibody, which were recognized by a 50 kDa protein band, were dialysed for 24 h in PBS at 4°C and then 24 h in 0.1X PBS. Protein concentration was determined by BCA. Aliquots were lyophilized to a 1/10 of the initial volume to concentrate the antibody.

15. Transfection: PEI

Polyethylenimine (PEI) is a linear polycationic polymer with repeating units composed of the amine group and two carbon aliphatic CH_2CH_2 spacer. PEI condenses DNA into positively charged particles, which bind to anionic cell surface residues and are brought into the cell via endocytosis. Once inside the cell, protonation of the amines results in releasing the polymer-DNA complex into the cytoplasm. When the polyplex unpacks the DNA is free to diffuse to the nucleus. Of note, PEI is extremely cytotoxic, thus it may be carefully used.

Solutions

NaCl 150 mM

Polyethylenimine linear (PEI) 1mg/ml (Polisciences, Inc)

Protocol

Cells were seeded in an appropriate plate culture dish and transfected at 70-80 % of confluence for an optimal transfection efficiency. DNA/NaCl and PEI/NaCl mixtures were prepared in different 1.5 ml eppendorfs tubes. Then, DNA/NaCl and PEI/NaCl solutions were mixed and incubated for 25-30 min at room temperature to generate a DNA/PEI complex. After incubation, the medium of the cells was replaced with half of the volume of DMEM supplemented medium. The DNA/PEI mixture was added drop by drop homogeneously in all the plate and cells were placed in the incubator at 37°C for 4 hours. Finally, medium was replaced with fresh DMEM supplemented medium and cells and placed in the incubator at 37°C.

Reagent/ Culture vessel size	100 mm/10 ml plates	35 mm/ 6 well plate
PEI/NaCl	94.25 µl PEI + 231.84 µl NaCl	14.5 µl PEI + 35.5 µl NaCl
DNA/NaCl	19.5 µl DNA (1µg/µl) + 306.59 µl NaCl	3 µl DNA (1µg/µl) + 47 µl NaCl

Table 7. Reagents quantities for different sizes of plates/wells. PEI/DNA and NaCl proportions suggested for HEK-293T cells transfection.

16. Cell culture

16.1. Culture conditions

The manipulation of HEK-293T and primary neuronal cultures were performed in Biological Safety Cabinet Class 1. Maintenance was done in an incubator at 37°C, 5% CO₂ and 90% relative humidity.

16.2. HEK-293T

The human embryonic kidney (HEK-293T) cell line used in the present work (35) were obtained from ATCC (American Type Culture Collection, Rockville, MD, USA) (**Figure 38**) and cultured in the medium described in **Table 8**. The T after the number indicates that cells were stably transformed with the SV40 large T antigen gene (205). The protein that is expressed by this gene interferes with the p53 and Retinoblasma tumor suppressor proteins causing the cells to enter the S phase and proliferate. When an expression vector is carrying an SV40 promotor, it can greatly increase gene expression and protein production, and the vector can replicate episomally (outside and independent of the host DNA). HEK-293T are neomycin resistant due to the presence of a neomycin resistance cassette together with the SV40 Large T.

Reagent	Concentration	Brand
Dulbecco's Modified Eagle's Medium – high glucose (DMEM)		Sigma Aldrich
L-glutamina	2 mM	GIBCO® Thermo Fisher scientific
Penicilin/Streptomycin	100 U/ml, 100 µg/ml	GIBCO® Thermo Fisher scientific
FBSi (inactivated Fetal Bovine Serum)	5 %	GIBCO® Thermo Fisher scientific
MEM Non essential aminoacids solution 100X	1%	Gibco® MEM Non-Essential Amino Acids
Sodium Piruvate 100 mM	1 mM	Gibco® Sodium Pyruvate (100 mM)

Table 8. Supplemented DMEM medium composition

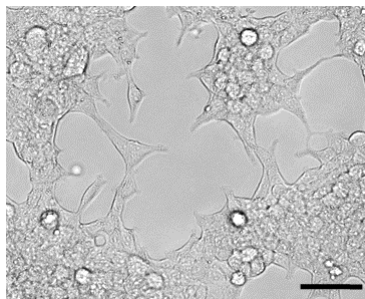


Figure 38. HEK-293T cell line grown for several days in DMEM medium. Picture showing uniform and health growth of HEK-293T cells. Scale bar = 100 µm.

16.3. Primary neuronal culture

Animal and cell culture model systems are used to further understand neuronal mechanisms. These *in vivo* and *in vitro* systems have advantages and limitations. Animal models can be used to reveal many aspects of neuronal development and degeneration and different behavioral aspects can be analyzed; however, definitive comprehension of molecular, biochemical, and structural observations is often obscured, due to the inherent complexity of nervous system tissue. Primary neuronal culture is a powerful tool for isolating cellular and molecular mechanisms. Primary cultures are desirable because they are not tumor-derived and hence are more likely to recapitulate the properties of neuronal cells *in vivo*.

16.3.1. Striatal primary cultures

Solutions

HBSS: Hanks Balanced Salt Solution (+CaCl₂ and MgCl₂, GIBCO)

Growing media: DMEM (Sigma-Aldrich) supplemented with 5% horse serum (GIBCO), 5% Fetal bovine serum (GIBCO) and 2 mM L-Glutamine (GIBCO)

Maintenance media: Neurobasal-A medium (GIBCO) supplemented with penicillin (100 U/mL), streptomycin (100 µg/mL), 0.5% Glutamax (GIBCO), 0.59% glucose, and B27 supplement (Invitrogen).

Trypsin from bovine pancreas: Sigma-Aldrich, St. Louis, MO, USA

Ovomucoid solution: 10mg/ml BSA, 10 mg/ml of Trypsin inhibitor from chicken egg white (Sigma), 10 mM HEPES diluted in HBSS.

Protocol

Primary striatal neurons were cultured from E18 GPR37^{+/+} and GPR37^{-/-} mice embryos. Briefly, after dissection of the striatum with the help of a LEICA M50, as described previously (**See Section 7. Mice sample obtention, B: Striatum**) in a horizontal laminar flow cabinet, they were kept in ice-cold HBSS until all striatum were collected. Striatums were then treated with 1.25 % trypsin for 10 min at 37°C in a incubator and trypsin was removed by washing the striatums twice in HBSS. Next, they were mechanically dissociated with a flame polished Pasteur pipette and neuron suspension was added drop by drop over an Ovomucoid solution in a 15 ml falcon tube and

centrifuged for 10 min at 800 rpm at room temperature. Neurons were plated at a density of 80.000 cells/cm² onto both poly-D-lysine-coated (0.1 mg/mL) and laminin (0.01 mg/ml) treated 12 well plate for cAMP accumulation assay or 12 well plate with treated glass coverslips for immunocytochemistry, in Growing media. After 4–14 h, the medium was 2/3 substituted with Maintenance media. Neurons were kept at 5% CO₂, 37°C and 95% humidity for 21 days before the experiments (**Figure 39**) (206).

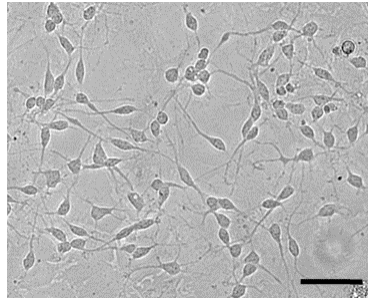


Figure 39. Primary striatal cultures. Primary striatal neurons were cultured on Poli-D-lysine / Laminin coated 96 well plates or coverslips for over 20 days, showing uniform and health growth of pure primary neurons. Scale bar = 100 μ m.

16.3.2. Hippocampal primary cultures

Protocol

Primary hippocampal neurons were cultured from 0- to 3-day-old mice. First, it was dissected the hippocampi with the help of a LEICA M50, as described previously (**See Section 7. Mice sample obtention, C: Hippocampus**), in a horizontal laminar flow cabinet. They were kept in ice cold HBSS, until all hippocampi were collected. Next, they were treated with 1.25% trypsin for 10 min at 37°C in a incubator, and trypsin was removed by washing with HBSS. Next, they were mechanically dissociated with a flame polished Pasteur pipette and neuron suspension was added drop by drop over an Ovomuroid solution in a 15 ml falcon tube and centrifuged for 10 min at 800 rpm at room temperature. Finally, cells were plated onto poly-D-lysine-coated (0.1 mg/mL) glass coverslips at a density of 80 000 cells/cm² in Growing media. After 4–14 h, the medium was 2/3 substituted with Maintenance media. Neurons were kept at 5% CO₂, 37°C and 95% humidity for 21 days before the experiments (**Figure 40**). Cytosine arabinofuranoside (AraC, 5 μ M; Sigma-Aldrich) was added at day 3 in vitro (DIV3).

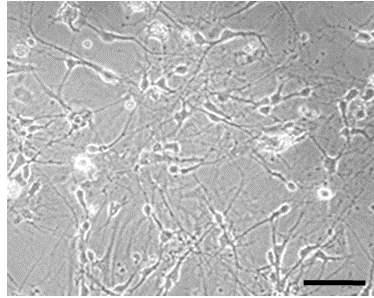


Figure 40. Primary hippocampal neurons. Primary hippocampal neurons were cultured on Poli-D-lysine coated coverslip for over 20 days, showing uniform and health growth of pure primary neurons. Scale bar = 100 μ m.

17. Immunofluorescence

17.1. Synaptosomes and primary neuronal cultures

Solutions

PBS: 2 mM KH_2PO_4 , 10 mM Na_2HPO_4 , 137 mM NaCl and 2.7 mM KCl and pH was adjusted at 7.2.

Paraformaldehyde 4%: Formaldehyde solution diluted in PBS

Permeabilization solution: PBS with 0.3% Triton X-100

Blocking solution: PBS with 0.05% Triton X-100 and 10% of Normal Donkey serum (NDS, Sigma).

Protocol

Both total striatal synaptosomes and neuronal primary cultures, cultured in coverslips, were fixed with 4% paraformaldehyde for 15 min and washed twice with phosphate buffered saline (PBS) medium. Total striatal synaptosomes or primary neuronal cultures were permeabilized in PBS with 0.3% Triton X-100 for 10 min and then blocked for 1 h in PBS with 10% NDS to prevent nonspecific binding. Samples were then immunolabeled with rabbit anti-GPR37 (1:200) and guinea pig anti- $A_{2A}R$ (1:200), or mouse anti-SNAP25 (1:200) and rabbit anti-PSD95 in blocking solution for 16 h at 4°C. Next, they were washed three times with PBS 0.05% Triton X-100, 5% NDS and incubated for 1 h at room temperature with AlexaFluor-488 goat anti-guinea pig, a Cy3-donkey anti-mouse or a Cy5 donkey anti-rabbit (1:200). After washing and mounting on slides with Vectashield immunofluorescence medium (Vector Laboratories, Peterborough, UK), samples were examined using a Leica TCS 4D confocal scanning laser microscope (Leica Lasertechnik GmbH, Heidelberg, Germany). (207).

17.2. Coronal brain slices

Immunohistochemistry (IHC) allows visualizing the distribution and localization of specific cellular components within cells and in the proper native tissue context.

Solutions

PBS: 2 mM KH_2PO_4 , 10 mM Na_2HPO_4 , 137 mM NaCl and 2.7 mM KCl (pH 7.2).

Paraformaldehyde 4%: Formaldehyde solution diluted in PBS.

Walter's Antifreezing solution: 12 mM NaH_2PO_4 , 31 mM Na_2HPO_4 , 30% Glycerol, 30% Ethylene glycol diluted in H_2O

Permeabilization solution: PBS with 0.5% Triton X-100

Blocking solution: PBS with 0.1% Triton X-100 and 10% of NDS (Sigma)

Antibody solution: PBS with 0.1% Triton X-100 and 1% of NDS.

Protocol

Mice previously anesthetized with Ketamine (100 mg/kg) and Xylazine (10 mg/kg) were administered with 20 ml of cold PBS followed by 80 ml of cold 4% paraformaldehyde, which was intracardiacally perfused. The clearing of the liver and increasing rigidity of the different mice body organs and muscles was used as indicator of a good perfusion. Once fixed, brain was removed and preserved overnight at 4°C in 4% paraformaldehyde, and the following day medium was replaced with PBS and stored at 4°C. Subsequently, brains were mounted on a Leica vibratome 1200S sectioning system and 50 μm coronal sections were made. Coronal sections were stored in antifreezing solution at -20°C until use. Immunofluorescence staining of the free floating brain sections was performed with constant agitation at 300 rpm using a Thermomixer C (Eppendorf). First, coronal slices were transferred to 1.5 ml eppendorf with the help of a fine paintbrush and slices were washed 3 times in PBS. Next, slices were permeabilized for 2 h and thereafter blocked for 2 h to prevent nonspecific binding. The coronal slices were then immunolabeled with rabbit anti-GPR37 (1:200) and guinea pig anti- $\text{A}_{2\text{A}}\text{R}$ (1:200) in the antibody solution for 48 h at 4°C. The slices were then washed three times with PBS 0.1% Triton X-100, 1% NDS and incubated for 1 h at room temperature with AlexaFluor-488 goat anti-guinea pig or a Cy5 donkey anti-rabbit (1:200). After washing and mounting on slides with Vectashield immunofluorescence medium (Vector Laboratories, Peterborough, UK), they were examined using a Leica TCS 4D confocal scanning laser microscope (Leica Lasertechnik GmbH, Heidelberg, Germany). (207).

18. Proximity Ligation Assay

Most in vivo protein-protein interactions are transient and occur only briefly to facilitate signaling or metabolic function. Capturing these momentary or weak contacts is not an easy task. The use of transfected overexpression systems may result in the artificial generation of many more oligomers than naturally exist. In some cases, BRET may detect interactions between receptors that are in close proximity in a compact structure rather than forming real dimers. Furthermore, GPCRs contain hydrophobic regions that can oligomerize even after solubilization. Hence, receptor dimerization or oligomerization may occur after solubilization in detergent and not be representative of receptor structure and organization in native tissue membranes. Thus, it is important to study receptors in their natural environment. Precisely, the Proximity Ligation Assay (PLA) is used for in situ detection of heteromers in native tissue. Primary antibodies used are specific for the receptors under study and the two secondary antibodies, each recognizing a specific species epitope, are covalently coupled to oligonucleotides; the proximity MINUS and PLUS probes. When both secondary antibodies are near each other, proximity dependent ligation and rolling circle amplification of a circular DNA reporter molecule occurs, which can be visualized (208).

Solutions and reagents

Permeabilization solution: PBS with 0.5% Triton X-100

Blocking solution: PBS with 0.1% Triton X-100 and 10% of NDS (Sigma)

Antibody solution: PBS with 0.1% Triton X-100 and 1% of NDS.

Duolink In situ PLA Probe donkey anti-rabbit PLUS

Duolink In situ PLA Probe donkey anti-goat MINUS

Ligation buffer: 1:40 Ligase (1U/ μ l, Duolink) and 5X Ligation Buffer (Duolink), diluted in H₂O.

Buffer A and Buffer B: diluted in H₂O.

Amplification buffer: 1:80 Polymerase (10U/ μ l, Duolink) Amplification Red 5X(Duolink) and diluted in H₂O.

TO-PRO-3 Iodide (642/661)Thermo Fisher Scientific: 1:1000 diluted in PBS.

Protocol

The first part of the PLA protocol was performed as previously described in the Immunofluorescence section. First, coronal slices were transferred to a 1.5 ml eppendorf with the help of a fine paintbrush and slices were washed 3 times in PBS. Next, slices were permeabilized for 2 h and then blocked for 2 h to prevent nonspecific binding. The coronal slices were then immunolabeled with rabbit anti-GPR37 (1:200) and guinea pig anti-A_{2A}R (1:200) in the antibody solution for 48 h at 4°C. Then, slices were washed three times with PBS 0.1% Triton X-100, 1% NDS and incubated for 1 h at 37°C with the donkey anti-rabbit PLUS (1:5) and the donkey anti-goat MINUS (1:5) diluted in antibody solution. Next, slices were washed with Buffer A and ligation was performed for 30 min at 37°C in Ligation Buffer. Thereafter, slices were washed using Buffer A and amplification was performed for 2 h at 37°C in amplification buffer. Then, slices were incubated with TO-PRO 3 for 30 min and washed with Buffer B. Finally, slices were washed subsequently with 0.01X Buffer B and PBS and mounted on slides with Vectashield immunofluorescence medium (Vector Laboratories, Peterborough, UK). The presence of heteromers was examined using a Leica TCS 4D confocal scanning laser microscope (Leica Lasertechnik GmbH, Heidelberg, Germany) at λ_{ex} 594 nm/ λ_{em} 624 nm. (207). High-resolution images were acquired as a z-stack with a 0.2 μm z-interval. High-resolution (60X) images from single scans were analyzed in ImageJ (NIH) to calculate the density of PLA puncta. Images were first smoothed and a threshold was selected manually to discriminate PLA puncta from background fluorescence. Once selected, this threshold was applied uniformly to all images in the sample set. The built in macro 'Analyze Particles' was then used to count and characterize all objects in the thresholded image. Objects larger than 5 μm^2 were rejected, thereby effectively removing nuclei. The remaining objects were counted as PLA puncta. An unpaired t-test was used for the comparison of PLA signal density between GPR37^{+/+} and GPR37^{-/-} mice striatum.

19. Immunohistoblotting

The histoblot method is a convenient way to compare brain regional distribution and expression levels of different proteins without compromising the integrity of antibody binding sites by tissue fixation, which is required for conventional immunocytochemistry. Histoblot technique provides more accurate and direct information about the anatomical localization of the receptors.

Solutions and reagents

Transfer Buffer: 48 mM Tris-base, 39 mM glycine, 2% (w/v) SDS and 20% (v/v) methanol

PBS: 2 mM KH_2PO_4 , 10 mM Na_2HPO_4 , 137 mM NaCl and 2.7 mM KCl and pH was adjusted at 7.2.

TBST-8 pH 8.0: 10 mM Tris-HCl, 150 mM NaCl and 0.05% Tween 20.

Blocking solution: 5% (w/v) non-fat dry milk in TBST-8.

RIPEA pH 7.5: 20 mM Tris-HCl, 60 mM NaCl, 0,4% Tritón X-100, 0,1% SDS, 0,4% deoxycolic acid and 2 mM EDTA

DNAsaI solution (Deoxyribonuclease I from bovine pancreas, Sigma) pH 5.0: DNase I, 5 U/mL diluted in 5 mM MgSO_4 and 100 mM Sodium acetate.

Stripping solution: 2% (w/v) SDS, 100 mM β -mercaptoethanol in 100 mM Tris-HCl (pH 7.0)

AP buffer pH 9.5: 0.1 M Tris-HCl, 0.1 M NaCl and 5mM MgCl_2 .

AP Developer: 264 μl of NTB solution, 132 μl of BCIP solution and 40 ml of AP buffer.

AP Stopper: 1.5 mM KH_2PO_4 , 8.5 mM Na_2HPO_4 , 137 mM NaCl and 3 mM KCl.

Protocol

For immunohistoblotting, mice brain was rapidly removed and frozen in isopentane at -20°C . Then, sagittal cryostat sections ($10\ \mu\text{m}$) were prepared using a Leica CM1860 Cryostat at -20°C . Nitrocellulose membranes $0.45\ \mu\text{m}$ (Whatman) were moistened with Transfer Buffer at room temperature. Thereafter, sagittal sections were transferred to the membranes by pressing the slide against the nitrocellulose membrane during 60 s. Membranes were blocked in blocking solution for 1 h without agitation. Next, membranes were washed with TBST-8 and treated with DNAsal solution at 37°C for 20 min. Then membranes were washed in RIPEA and TBST-8 and incubated in stripping solution for 60 min at 45°C to remove adhering tissue residues. After extensive washing with RIPEA and TBST-8, blots were incubated overnight at 4°C with rabbit anti-mGPR37 ($5\ \mu\text{g}/\text{ml}$) or goat anti- $\text{A}_{2\text{A}}\text{R}$ antibodies ($5\ \mu\text{g}/\text{ml}$) in blocking solution. The following day, membranes were washed and incubated for 90 min at room temperature with AP-conjugated secondary antibodies. Finally membranes were washed and developed with the AP developer. All nitrocellulose membranes were processed in parallel, using the same incubation times and antibody/reagent concentrations. Reaction was terminated by washing membranes with AP stopper. Digital images were acquired with a Stereo Lumar.v12. (209)(210).

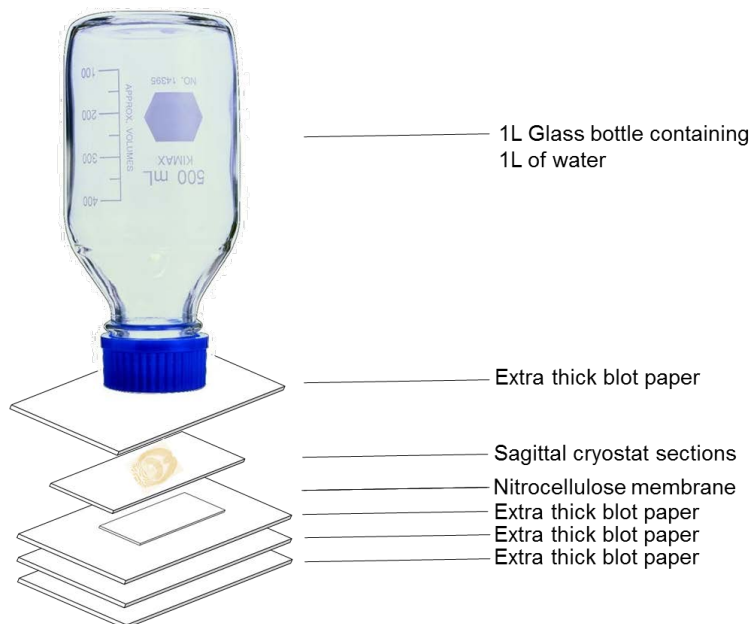


Figure 41. Scheme of the immunohistoblot transfer. Sagittal cryostat sections were transferred to nitrocellulose membranes by pressing the slide against the nitrocellulose membrane during 60 s with help of a 1L glass bottle.

20. cAMP accumulation assay

Typically, GPCRs preferentially activate only one type of G-protein, which transmit the information intracellularly. Both G α i and G α s subunits produce changes (decreasing and increasing, respectively) in the intracellular levels of cAMP which can be measured.

20.1. Total striatal synaptosomal membranes

Total synaptosomal cAMP accumulation was measured using the LANCE Ultra cAMP kit (PerkinElmer, Waltham, MA, USA). Total striatal synaptosomal membranes (0,5 μ g/ μ l) were resuspended in stimulation buffer (HBSS 1X, 5 mM Hepes pH 7.4, 10 mM MgCl₂, 0.1 % BSA and 5 μ g of Adenosine Desaminase from calf intestine (ADA, Roche)) and incubated for 20 min at room temperature to eliminate endogenous adenosine. Afterwards, zardaverine (10 μ M), GTP (10 μ M), and ATP (150 μ M) were included into the extract and were incubated for 10 min at room temperature. Subsequently, the ligands (Vehicle, 1 μ M Forskolin or 500 nM CGS21680) were added for 30 min at room temperature prior to lysis. Eu-cAMP tracer and ULight™- anti-cAMP reagents were prepared and added to the sample according to the LANCE® Ultra cAMP Kit instruction manual. Samples were seeded in 384-well plates and incubated 1 h at room temperature in dark conditions. Finally, the signal resulting from cAMP accumulation was read in a POLARstar microplate reader (BMG Labtech, Durham, NC, USA). Measurements at 620 and 665 nm were used to detect the TR-FRET signal, and the concomitant cAMP levels were calculated following the manufacturer's instructions

20.2. Striatal primary cultures

DIV21 mice striatal neurons were used to determine cAMP accumulation using the cAMP HiRange assay Kit (CISBIO). Primary striatal maintenance media was changed for Neurobasal with 5 μ g/well of ADA and incubated for 1h in the incubator to eliminate endogenous adenosine. Afterwards, zardaverine (50 μ M) was included into the media and incubated for 30 min at 37°C into the incubator. Subsequently, the ligands (Vehicle, 1 μ M Forskolin and 500 nM CGS21680) were added for 30 min at 37°C prior to lysis with 250 μ l of Lysis buffer. After scrapping the neurons they were centrifuged for 30 min at 4°C at 13.200 rpm. Then, 10 μ l of the supernatant was added to the 384-well plate. D2 and Cryptate reagents were prepared and added to the sample according to the assay Kit instruction manual. The plate was incubated 1 h at room temperature in the dark and then read in a POLARstar microplate reader (BMG Labtech, Durham, NC, USA). Measurements at 620 and 665 nm were used to detect the TR-FRET signal, and the concomitant cAMP levels were calculated.

21. Extracellular electrophysiological recordings

Synaptic plasticity is defined as the biological process by which specific patterns of synaptic activity result in changes in synaptic strength. Both pre- and postsynaptic mechanisms contribute to the expression of synaptic plasticity. Synaptic plasticity is crucial for the development of the nervous system and thereafter to the ability of an individual to learn and remember new information and to accordingly adjust behavior. Distinct stimuli elicit different changes in synaptic efficacy. While high frequency stimuli produce synaptic strengthening called long-term potentiation (LTP), low frequency stimulation has been shown to produce synaptic weakening, called long-term depression (LTD). Paired pulse facilitation (PPF), Long-term potentiation (LTP), depotentiation and long-term depression (LTD) are commonly used experimental models for understanding the synaptic basis of learning and memory. PPF is the simplest form of plasticity and is defined as an increase in the size of the synaptic response to a second pulse delivered within a short interval of time following the first pulse. PPF is maximal at short interstimulus intervals (i.e. 50 ms) and declines exponentially over a period of ~500 ms. It is well established that PPF is a purely presynaptic phenomenon (211). LTP is the most extensively studied form of synaptic plasticity in the brain. LTP is induced rapidly (within a sec-min) after a conditioning stimulus and is characterized by a persistent increase in the size of the synaptic response that often lasts for many hours. Synaptic potentiation refers to an increase in the size of the field excitatory postsynaptic current (fEPSP) when recorded extracellularly as a population event. LTD is the converse of LTP, namely a persistent decrease in AMPA (and NMDA) receptor-mediated synaptic transmission measured as field responses. Under certain circumstances, LTD cannot be induced unless LTP is first induced, in which case the process is generally referred to as depotentiation. Under certain circumstances, the induction of LTP in one input is associated with LTD in a separate input.

Solutions

aCSF: 124 mM NaCl, 4.4 mM KCl, 1 mM Na₂HPO₄, 25 mM NaHCO₃, 2 mM CaCl₂, 2 mM MgCl₂, 10 mM glucose, 0.4 μM L-ascorbic acid and 3 μM pyruvic acid. aCSF was prepared fresh the day of the experiment and osmolarity of the solution was checked using a Vapor pressure osmometre (Vapro, Wescor) and values should be 300±10 mmol/kg.

Sucrose aCSF (S-aCSF): aCSF with 210 mM Sucrose. Solution used during brain dissection.

NaCl 4M: solution for the Recording electrode.

Micropipettes for the recording electrode: Borosilicate glass capillaries used for micropipettes were from Harvard (GC150F-10, 30-0057) using a pipette puller Model P-87. Micropipettes had a resistance of 2-5 M Ω .

21.1. Striatal extracellular recordings

The striatum is the major input nucleus of the basal ganglia and is composed mainly of GABAergic projecting MSN. Striatal synaptic plasticity depends on dopaminergic and glutamatergic neurotransmission. Recent clinical and experimental studies have provided evidence that striatum is related in formation of motor memory. Within the striatum, two forms of long-lasting synaptic plasticity have been described at glutamatergic corticostriatal synapses near the dorsolateral striatum, namely LTD and LTP. By far, the most commonly reported form of corticostriatal plasticity is LTD, which can be induced in response to LFS in vitro leading to a long-lasting reduction in synaptic strength at MSNs synapses. In contrast, it has been challenging to induce striatal LTP in vitro, thus little is known about the molecular pathways underlying its induction.

Protocol

Following decapitation, brain was quickly removed and placed in ice-cold, oxygenated (95% O₂, 5% CO₂) S-aCSF. Corticostriatal slices (400 μ m-thick) were obtained using a Vibratome 1500 (Leica, Wetzlar, Germany) and allowed to recover in aCSF for at least 90 minutes prior to recording, when they were transferred to a submerged recording chamber and superfused at 3 mL/min with oxygenated aCSF kept at 30.5 °C (**Figure 42 A-C**). The configuration of the recordings was as previously described (212), with the stimulating electrode placed in the *Corpus callosum* and the recording electrode, filled with 4 M NaCl (2-5 MW), placed in the dorsomedial (DM) portion of the striatum. Stimulation was performed using a Grass S44 square pulse stimulator (Grass Technologies, RI, USA). After amplification (ISO-80, World Precision Instruments, Hertfordshire, UK), the recordings were digitized (BNC-2110, National Instruments, Newbury, UK) and analyzed using the WinLTP version 2.10 software (WinLTP Ltd., Bristol, UK) (Anderson and Collingridge, 2001). The relationship between dendritic responsiveness to the synaptic input was determined on the basis of input/output (I/O) curves in which the population spike (PS) was plotted *versus* the stimulus intensity. Stimulus intensity was increased in 50 mA increments from those that produced no detectable postsynaptic response to the stimulus until those producing a maximal postsynaptic response. The intensity of stimulation was selected to yield 70% of the

maximum response. Striatal slice baseline was stabilized during 30 min, and then LTD induction was evoked. All evaluations of striatal plasticity in this study were subsequently conducted based on measurement of the PS amplitudes (**Figure 42 D**). Significant increase or decrease in population spike amplitude relative to average baseline amplitude indicates LTP or LTD, respectively.

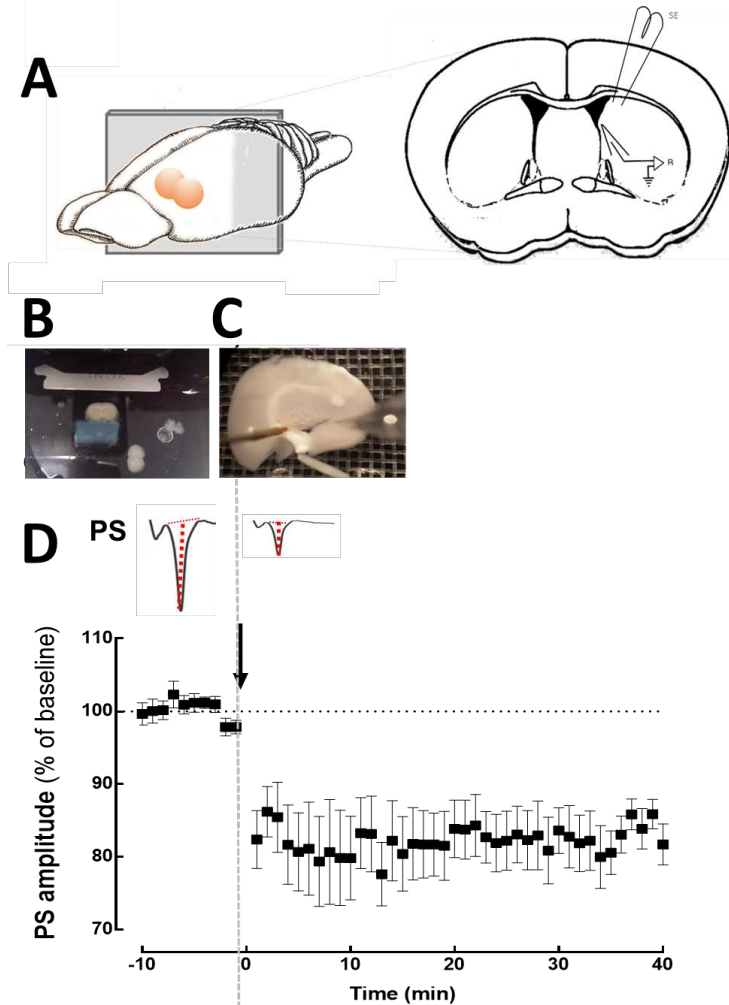


Figure 42. Stimulation and recording electrodes disposition for extracellular corticostriatal field recordings for LTD generation. (A) Schematic representation of the stimulation and recording electrodes in dorsal striatum extracellular recordings. **(B)** Brain was rapidly removed and 400 μm -thick slices were performed using a vibratome in ice-cold aCSF and **(C)** stimulation and register electrodes were settled. **(D)** A typical LTD experiment. The traces at the top of the graph show representative population spike (PS) responses extracted from the plot at the times indicated on the graph. Amplitude of each trace is represented with a **red line**.

21.2. Hippocampal extracellular recordings

Critical for memory formation, the hippocampal slice is the principal preparation for studying synaptic plasticity. This is due to its orderly anatomical arrangement, which facilitates experimentation. The anatomy of the hippocampus consists of three sequential synaptic pathways (perforant, mossy fiber and Schaffer collateral pathways), each with discrete cell body layers and axonal and dendritic projections. When placed, the stimulating electrode activates a parallel band of fibers that evoke, first, a presynaptic fiber volley (caused by the inward current of the action potentials in the presynaptic fibers and, second, a fEPSP. LTP is observed as an increase in the size of the fEPSP. When the fEPSP reaches a certain size, a population spike (reflecting the synchronized firing of action potentials) is evoked. The appearance of the population spike complicates the measurement of fEPSP amplitude because it goes in the opposite direction and limits the amplitude of the fEPSP. Therefore, fEPSP slope is the preferred measure of response size as it is generally unaffected by the population spike.

Protocol

Following decapitation, the brain was quickly removed and placed in ice-cold, oxygenated (95% O₂, 5%CO₂) artificial S-aCSF. Slices (400 μm-thick) from the dorsal hippocampus were cut transverse to the long axis of the hippocampus using a Mc Ilwain tissue chopper and placed in a holding chamber with oxygenated aCSF. Slices were allowed to recover for at least 1 h prior to recording at 30°C, when they were transferred to a submerged recording chamber and superfused with oxygenated aCSF at 3 mL/min kept at 30.5°C (**Figure 43, A-C**). The configuration of the recordings was described previously (108), with the stimulating electrode placed in the proximal CA1 stratum radiatum for stimulation of the Schaffer fibers and the recording electrode, filled with 4 M NaCl (2–5 MΩ), was placed in the CA1 stratum radiatum, targeting the distal dendrites of pyramidal neurons (**Figure 43 D**). The depth of the recording electrode was set where the maximal signal was observed. Stimulation was performed using either a Grass S44 or Grass S48 square pulse stimulator (Grass Technologies, Warwick, RI, USA). After amplification (ISO-80, World Precision Instruments, Hertfordshire, UK), the recordings were digitized (BNC-2110, National Instruments, Newbury, UK) and analyzed using the WinLTP version 2.10 software (WinLTP Ltd., Bristol, UK) (Anderson and Collingridge 2001). The relationship between dendritic spine density and sensitivity to synaptic input was determined on the basis of input/output (I/O) curves in which the field excitatory

postsynaptic potentials (fEPSP) slope was plotted versus the stimulus intensity. Stimulus intensity was increased in 20 mA increments from those that produced no detectable postsynaptic response to a stimulus that produced a maximal postsynaptic response (no observation of population spike). We decreased the stimulus intensity until it evoked 50% of the maximum response and used this intensity for the whole experiment. Hippocampal slice baseline was stabilized during 30 min. To elicit PPF, Schaffer fibers were stimulated twice with a 25–200 ms inter-pulse interval and the synaptic facilitation was quantified as the ratio (P2/P1) between the slopes of the fEPSP elicited by the second (P2) and the first (P1) stimuli. LTP was induced by high-frequency stimulation (HFS) train (100 Hz for 1 s). Depotentiation was induced by a low frequency stimulation (LFS) train (900 pulses at 1 Hz for 15 min) applied 60 min after LTP induction. The intensity of the stimulus was not changed during these stimulation protocols. LTP was quantified as the percentage change between two values: the average slope of the five potentials taken between 55 and 60 min after LTP induction in relation to the average slope of the fEPSP measured during the 10 min that preceded LTP induction (**Figure 43 E**). Averages of 3 consecutive responses were continuously monitored. The effect of SCH58261 was assessed by comparing the slope of LTP and depotentiation in untreated versus treated slices from the same mouse. N values refer to the number of mice used.

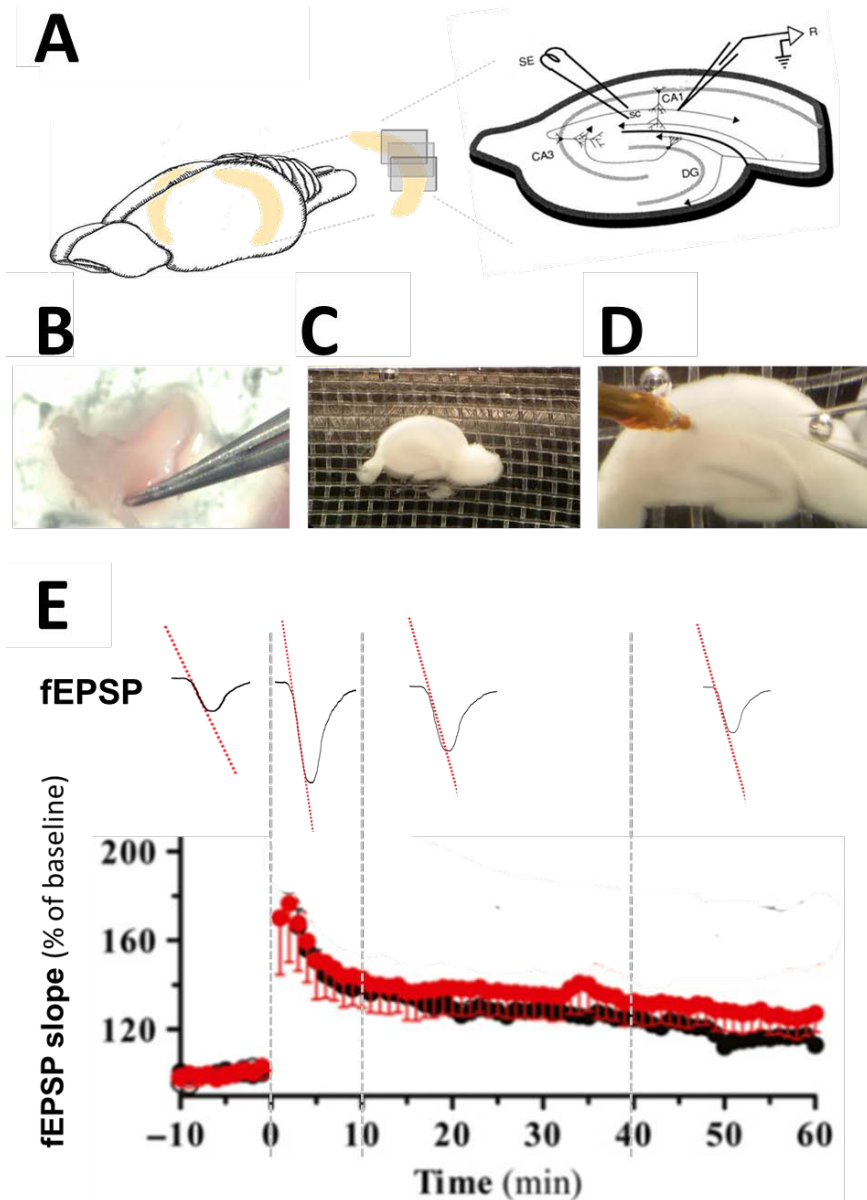


Figure 43. Stimulation and recording electrodes disposition for extracellular hippocampal field recordings for LTP generation and posterior depotentiation. (A) Schematic representation of the stimulation (SE) and recording (R) electrodes for CA1 hippocampus extracellular recordings. In brief, **(B)** Hippocampus is rapidly dissected in ice-cold aCSF, **(C)** slices 400 μm -thick were performed using a chopper and allowed to recover for at least 1 h prior to recording at 30°C. **(D)** Finally stimulation and register electrodes were settled. **(E)** A typical LTP experiment. The traces at the top of the graph show representative fEPSP responses extracted from the plot at the times indicated on the graph. Slope of each trace is represented with a **red line**.

22. Behavioral testing

The behavioral testing was performed during the light period of the cycle, in a silent room, under dim light (15 lux).

22.1. Marble burying test

The marble burying test (MBT), a test of anxiety and/or obsessive-compulsive behavior (213), was conducted at 8 weeks of age. In brief, clean cages (40x20x20 cm) were filled with 4 cm of wood chip bedding lightly tamped down to make a flat-even surface. Nine identical black marbles (1.2 cm diameter) were placed in a regular pattern on the surface, evenly spaced, each about 3x5 cm apart (**Figure 44**). Mice were left to explore this environment for 30 min and the number of marbles buried (to 2/3 their depth) was counted. Mice (n = 9/group) were treated with either vehicle or SCH 58261 (i.p.; 1 mg/kg) 15 min before the test.

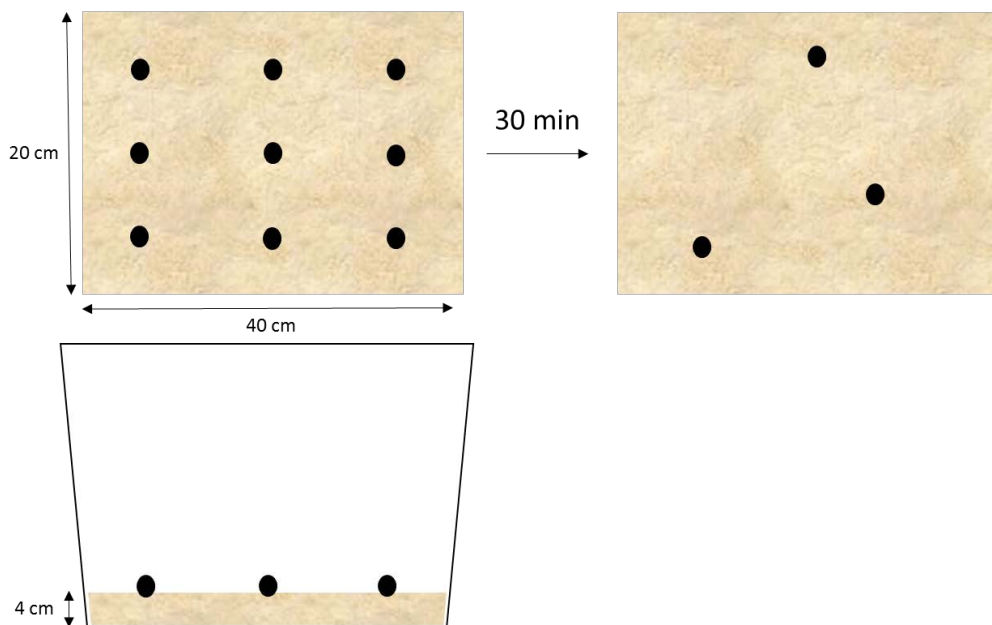


Figure 44. Disposition of the marbles in the Marble burying test. Marbles were distributed in the cage in the disposition shown in the picture. Then, mice were left to explore during 30 min and finally total number of marbles buried were quantified.

22.2. Novel object recognition test

To evaluate the reference memory, we performed the novel object recognition test (100). In brief, mice were first habituated to the open field arena (25 cm long, 25 cm wide and 50 cm high) twice a day (separated by 6 h) during three consecutive days. The test consisted of two 5-min sessions: in the first session (i.e., familiarization session) mice were exposed to two identical objects (two 100 mL blue bottles) and in the second session (test session, 120 min after) mice were exposed to two dissimilar objects (a familiar and a novel one, i.e., the 100 mL blue bottle and a 50 mL green tube) (**Figure 45**). Mice were treated with either vehicle or SCH 58261 (i.p.; 1 mg/kg) 15 min before being placed in the open field for the familiarization test. Each session was recorded and the time exploring each object was manually scored. Object exploration was defined as the orientation of the nose to the object at a distance ≤ 2 cm, touching with forepaws or nose, sniffing and biting the objects, but climbing on the objects was not considered. The preference for exploring the novel object (time exploring novel object/time exploring both objects) was calculated and expressed as percentage.

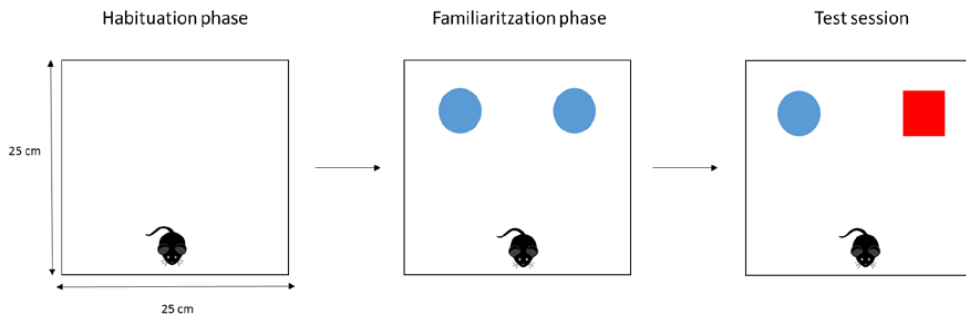


Figure 45. Habituation, familiarization and test session scheme of NOR test. Graphical representation of the open field arena and the different stages of the NOR test (habituation, familiarization and test session).

22.3. Elevated plus maze test

Unconditioned fear was assessed as previously described using the elevated plus maze (EPM) test to evaluate anxiety behavior (215,216). The apparatus was 40 cm elevated from the ground and consisted of 4 arms (30 x 5 cm), connected by a common central area (**Figure 46**). Two opposite facing arms were open, while the other two were enclosed by 15 cm high walls. Mice were habituated to the room thirty minutes prior to the test. Then, they were treated with either vehicle or SCH 58261 (i.p.; 1 mg/kg) 15 min before being placed in the center of the maze facing one of the open arms, preferably the one opposite to the experimenter. The time spent in the open arms and the number of arms entries was monitored during 10 min.

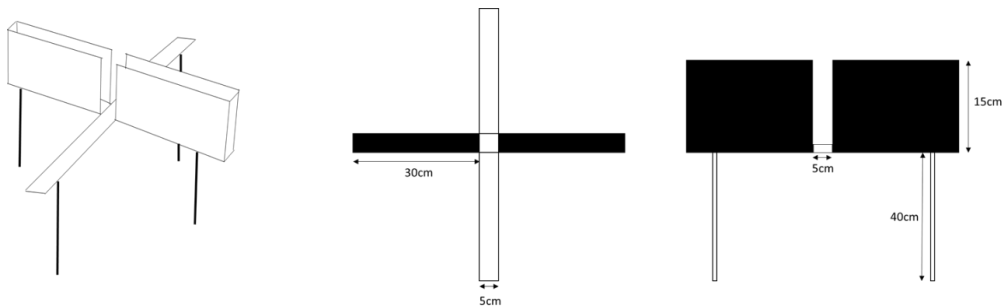


Figure 46. Elevated plus maze. Graphical representation of the EPM instrument showing the open and closed arms.

22.4. Open field

Since rodents are gregarious animals, which usually live in small spaces, its separation from its social group/cage and placing in a large arena (new and unknown arena normally) trigger an anxious behavior. In these situations, they naturally display a propensity to walk close to the walls and to avoid open spaces, a behavior called thigmotaxis. Based on this, it is considered that increased time spent on the central zone of the open field represents a less anxious behavior. Similarly, mice display a natural pre-disposition toward protected, enclosed areas, which is in conflict with their innate motivation to explore new environments. The open-field test was used to evaluate locomotion behavior.

In brief, thirty minutes prior to the test the animals were acclimatized to the room. Then, mice were placed in a corner facing the wall of an activity field arena (30 x 30 cm) equipped with a camera above to record activity under lim light conditions. The arena was divided into a central field (center, 10 x 10 cm) and an outer field (periphery) (**Figure 47**). The exploratory behavior of the animals was evaluated during a 10 min period and the analysis included the total distance traveled and the activity within the outer and inner zone of the open field. All behavioral tests were carried out in a sound attenuated room with 15 lux illumination. All the apparatus were cleaned with a 10% alcohol solution and rinsed with water after each session. The ImageJ (Spot Tracker plugin) was used to assess the total distance traveled, as well as the time spent in the center area.

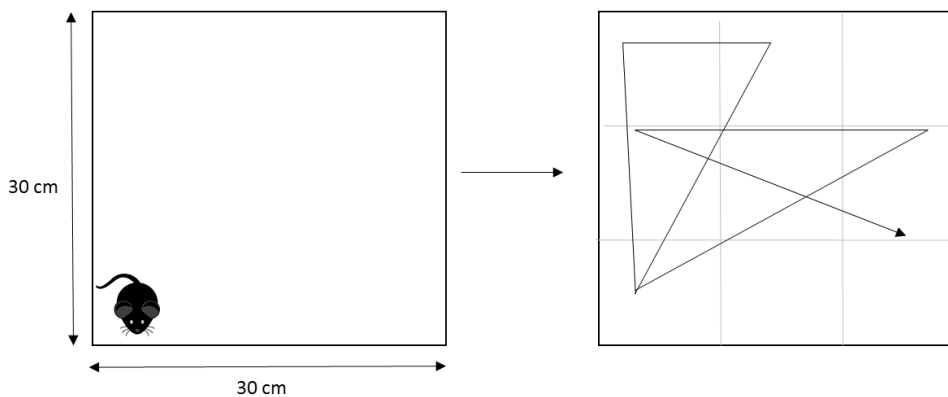


Figure 47. Representation of the Open field. Graphical representation of the open field arena and the starting position of the mice.

22.5. Catalepsy

Catalepsy is a pharmacological model of PD. Haloperidol works by antagonizing D_2R in the MSN and the resultant block of striatal dopamine transmission results in abnormal downstream firing within the basal ganglia circuits that is manifest as symptoms of muscle rigidity and catalepsy. On the other hand, $A_{2A}R$ agonists are known to induce catalepsy and inhibit dopamine mediated motor hyperactivity. Catalepsy, which is expressed as the inability of an animal to correct itself from an abnormally imposed posture, reproduce the rigidity and the inability of PD patients to initiate movements and so could be considered a worthwhile measure. Two different methods for catalepsy induction were used in order to assess the impact of the GPR37 in the adenosinergic system: **i)** male mice were injected with either the selective $A_{2A}R$ antagonist SCH58261 (i.p., 1 mg/kg) 15 min before Haloperidol (i.p., 1,5mg/kg) **ii)** the selective $A_{2A}R$ agonist

CGS21680 was injected i.c.v. (10 μ g). The cataleptic response was measured as the duration of an abnormal imposed upright posture in which the forepaws of the mouse were placed on a horizontal wooden bar (0.6-cm-diameter) 4.5 cm above the box floor (**Figure 48**). The latency to move at least one of the two forepaws was recorded with a stopwatch (in seconds) 2 h after CGS21680 or Haloperidol injection and a cutoff time was set at 180 s. The inability of an animal to correct an externally imposed posture was measured at a single interval time (2h) to avoid induction of pseudocatalepsy (217)(93).

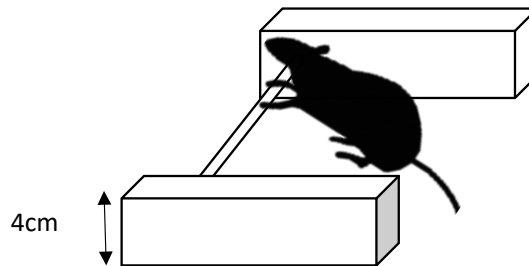


Figure 48. Catalepsy test. Mice were with their two forelimbs on a wood rod (0.56 cm diameter) elevated 4.5 cm from the chamber floor.

22.6. Cued version of Water maze

Mice were submitted to a working memory version of the water maze task (218)(219). Tests were performed in a circular swimming pool made of grey painted fiberglass, 97 cm in diameter and 60 cm in height. For the tests, the tank was filled with water maintained at $20 \pm 1^\circ\text{C}$. The target platform (10-9-10 cm^2) was made of transparent Plexiglas and it was submerged 1.5 cm beneath the surface of the water. The platform was marked with a visible cue, consisting of a 4 cm high black plastic cylinder. No distant visual cues were placed on the walls of the water maze room. The apparatus was located in a room with dim illumination. A monitor and a video-recording system were installed in an adjacent room. The experiments were videotaped and the scores for latency of escape from the starting point to the platform and swimming speed were later measured through an image analyzer (CEFET, Curitiba, PR, Brazil). Mice were submitted to a working memory version of the water maze consisting of 4 training days, 4 consecutive trials per day (Platform and animal initial position change in each trial. **Trial 1:** Plat: NW; Animal: S, **Trial 2:** Plat: NE; Animal: E, **Trial 3:** Plat: SE; Animal: N, **Trial 4:** Plat: SW; Animal: W), during which the animals were left in the tank facing the wall, then allowed to swim freely to the submerged platform placed in the centre of one of the four

imaginary quadrants of the tank (**Figure 49**). The initial position in which the animal was left in the tank was one of the four vertices of the imaginary quadrants of the tank, and this was varied among trials in a pseudo-random way. If a mouse did not find the platform during a period of 60 s, it was gently guided to it. The animal was allowed to remain on the platform for 30 s and then moved to the next initial position without leaving the tank. Starting points for animals were marked on the outside of the pool as north (N), south (S), east (E), and west (W).

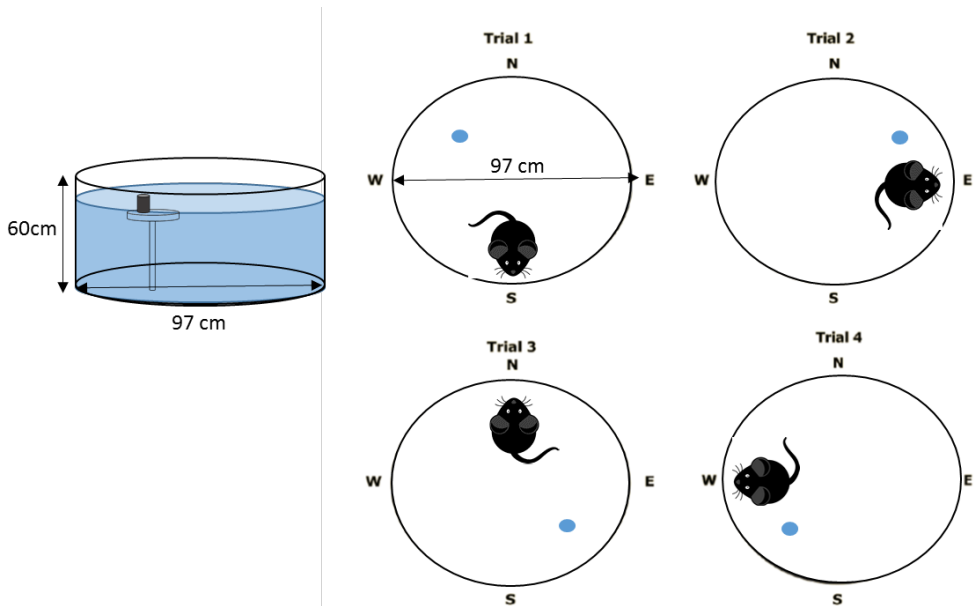


Figure 49. Representation of the 4 consecutive trials of the memory version of the water maze behavioural test. Mice underwent 4 trials every day. Platform position and starting mice position is represented in the picture.

23. Competitive ELISA

ELISA is used to measure metabolites, hormones and proteins in cell, tissue, organ or body fluids (i.e. blood, CSF or urine). The central event of competitive ELISA is a competitive binding process executed by original antigen present in the sample of interest (unlabeled) and an add-in antigen (labeled). In a competitive ELISA, higher sample antigen concentrations leads to weaker signals.

23.1. Recombinant protein production and purification

Solutions and reagents

DMEM Complete: DMEM medium supplemented with 5% FBS, Pen/Strep, 2mM L-Glutamine, 1mM Sodium Pyruvate and MEM non Essential amino acids.

Serum free DMEM: DMEM Complete without FBS.

TBS Solution: 50 mM Tris Base, 150 mM NaCl, pH 7.6

Neutralization solution: Tris Base 1M pH 8,8

Elution Solution: Glicina 100 mM pH 2.5

ELISA Wash Buffer (EWB): 25 mM Tris Base, 150 mM NaCl, 0,1% BSA, 0,05% Tween-20, pH 7.2

Amicon Ultra-15 10K Centrifugal Filter Devices

Pierce anti-HA Agarose 21680: 1 ml of anti-HA agarose resin for each purification product.

Dialysis tubing cellulose membrane D9277-100FT, Sigma-Aldrich

Protocol

HEK-293T were cultured in 10 cm culture dishes and transiently transfected with the i) HA-pNFL-hGPR37, ii) HA-pNFL-mGPR37, iii) SNAP-HA-pRK-hGPR37 or iv) SNAP-HA-pRK-mGPR37 using PEI, as described previously. Cells were maintained overnight in DMEM Complete. Next day, medium was replaced with serum-free DMEM medium and supernatant was collected 48 and 72 h after transfection. For recombinant protein purification, first, supernatant was centrifuged at 1100 rpm for 5 min to remove cell debris. Secondly, supernatant was concentrated and dialysed in TBS buffer using an Amicon-Ultra-15 10K falcon tube by continuous centrifugation at 3000 rpm, at 4°C until red phenol was not observed.

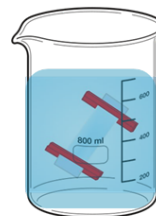
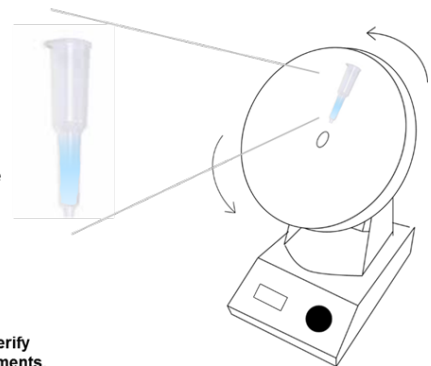
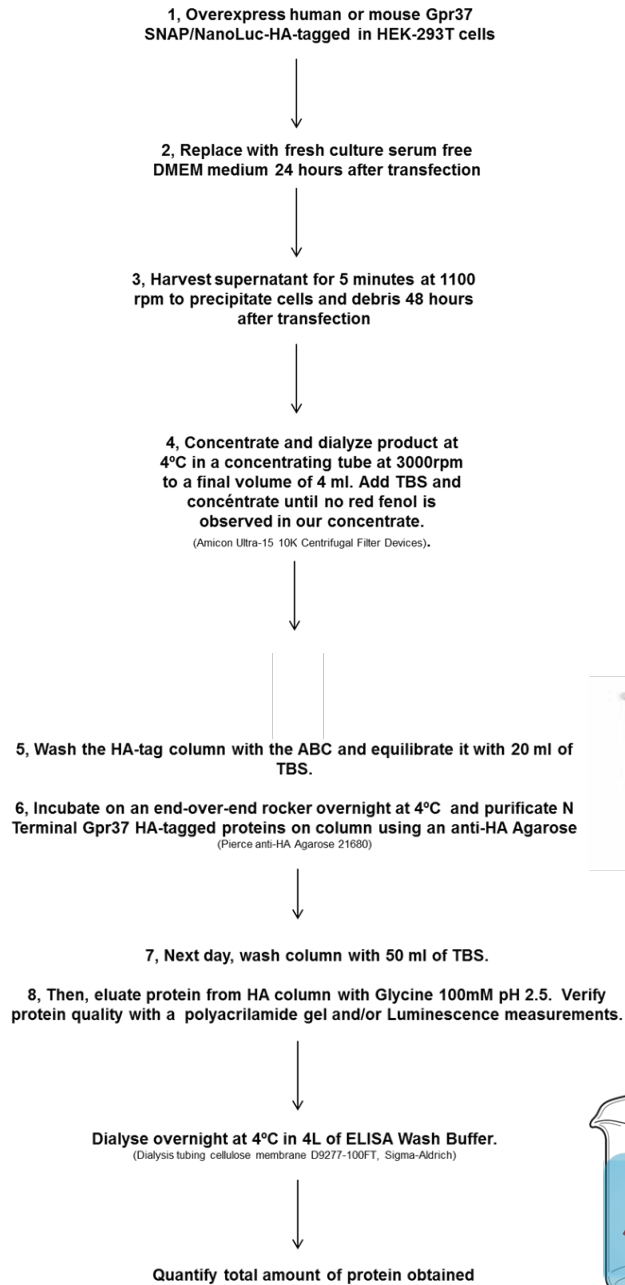


Figure 50. Protocol for the production and purification of human and mouse N-terminal GPR37 NLuc-ELISA reagents. Production of the NanoLuciferase HA-GPR37 and the SNAP HA-GPR37 cleaved fragments for the competitive assay. In brief, pNFL-HA-mGPR37/pNFL-HA-hGPR37/pRK-HA-SNAP-mGPR37 or pRK-HA-SNAP-hGPR37 were transiently transfected in HEK-293T cells and supernatant was collected 48 and 72 hours later. Supernatants were centrifuged to remove cell debris. Then, supernatants were concentrated and dialyzed using an Amicon 10K centrifuge tube. Next, the concentrate was incubated overnight with a HA-tag column. The following day, column was eluted with Glycine and dialysed overnight in ELISA WASH Buffer. Finally, ecto-GPR37 purification was validated by immunoblot analysis and/or luminescence measurements.

At this point, supernatant was incubated overnight in a column with the Pierce anti-HA column in an end over end rotator at 4°C. Subsequently, recombinant protein was eluted in 1 ml fractions from HA-tagged resin by washing column with Glycine-HCl pH 2.5 and rapid neutralization with Tris-Base (pH 8.8). Finally, eluted fractions were analyzed by luminescence measurements and/or Western Blot analysis. The containing recombinant protein fractions were dialyzed overnight in ELISA Wash Buffer at 4°C. A graphical representation of this protocol is shown in **Figure 50**.

23.2. Bioluminescence assay measurements

Bioluminescence is a phenomenon involving light emission by live organisms. It is caused by the oxidation of a small organic molecule, luciferin, with molecular oxygen, which is catalyzed by the enzyme luciferase (**Figure 51**) (220).

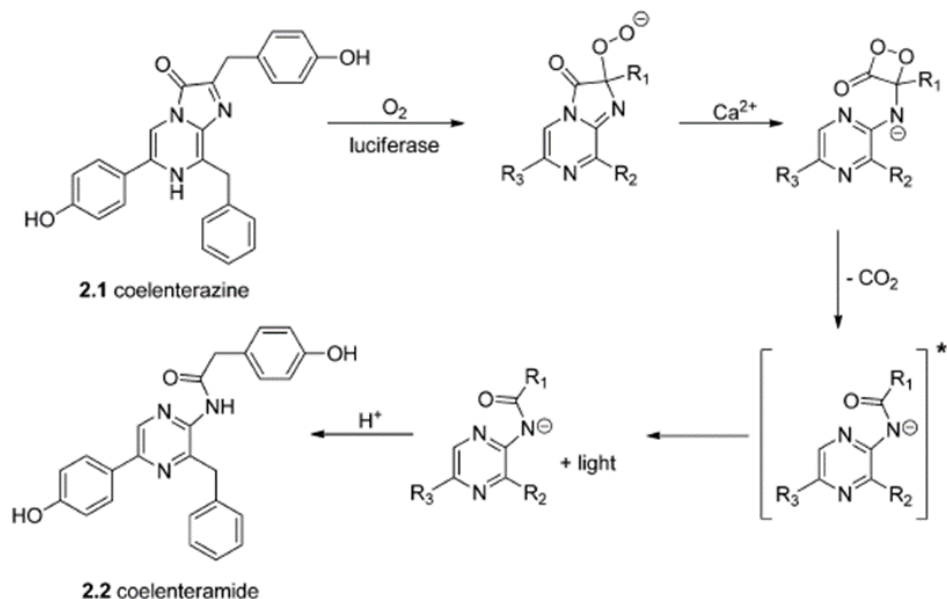


Figure 51. Bioluminescent reactions catalyzed by Luciferase. *Renilla luciferase* or *NanoLuciferase* catalyze the oxidation of coelenterazine to coelenteramide, which yields light at 480 nm.

From coelenterazine substrate bioluminescence systems, a number of natural luciferases were isolated and sequenced. Among these diverse luciferases, *Renilla luciferase* (*Rluc*) was the first described and found to be used in broad applications (i.e. BRET assays). *Rluc* is a protein with a mass of 36 kDa and a bioluminescence I_{max} of 480 nm. Recently, it was described NanoLuciferase (NLuc), with small size, 19 kDa, and high bioluminescence intensity, which makes it a better candidate for fusion protein constructs and quantitative assays (221).

Solutions

ELISA Wash Buffer (EWB): 25 mM Tris Base, 150 mM NaCl, 0,1% BSA, 0,05% Tween-20, pH 7.2

Coelenterazine-h: Coelenterazine-h was diluted in ELISA Wash Buffer at a final concentration of 5 μ M. Coelenterazine-h stock solution was dissolved in ethanol (250 μ M) and stored in aliquots at -80°C for long-term stability. Coelenterazine is sensitive to light.

Protocol

After purification of the NLuc-HA ecto-GPR37, we added 90 μ l of a 1/10 product solution diluted in Elisa Wash Buffer. Then, we added 10 μ l/well of the 5 μ M Coelenterazine-h solution and measured luminescence after 1 min of incubation at $\sim 485\text{nm}$. NLuc-HA ecto-GPR37 were diluted at 7500 RLU/ μ l (Relative Light Units, RLU) in EWB and stored at -20°C until use.

23.3. Competitive ELISA assay

Solutions and reagents

ELISA Wash Buffer (EWB): 25mM Tris Base, 150mM NaCl, 0,1% BSA, 0,05% Tween-20, pH 7.2

Pierce Streptavidin Coated White 96-Well plate (Thermo scientific)

Anti-rabbit IgG (whole molecule)-biotin antibody Sigma-Aldrich

Coelenterazine-h: Coelenterazine-h was diluted in ELISA Wash Buffer at a final concentration of 5 μ M.

Protocol

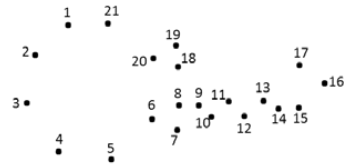
First, white 96-well plates were blocked with 200 μ l/well of DMEM complete for 2h at room temperature. Secondly, wells were washed 3 times with 200 μ l/well of EWB and incubated with 100 μ l/well of 10 μ g/ml anti-rabbit IgG (whole molecule)-biotin antibody and incubated for 1 h at room temperature. Then, wells were washed again with 200 μ l/well of EWB 3 times. Next, 100 μ l/well of a 1 μ g/ml solution of the anti N-terminal hGPR37 or mGPR37 primary antibody was added in each well and incubated for 1 h at room temperature. Thereafter, plates were washed 3 times with 200 μ l/well of EWB and

finally 47 μl of EWB + 3 μl of human or mouse CSF were incubated in the plate overnight at 4°C in a humid chamber. Increasing amounts of SNAP-HA ecto-GPR37 used as unlabeled antigen/standard were incubated in parallel to perform the standard curves to allow quantification. The following day, the plate was washed 3 times with 200 μl /well of EWB and 100 μl of a 7500 RLU/ μl solution of NLuc-HA mGPR37 or hGPR37 were incubated for 1 h at room temperature. Again, wells were washed 3 times with 200 μl /well of EWB and finally 90 μl /well of EWB were added. Finally, 10 μl of a 5 μM solution of Coelenterazine h was added and luminescence was measured 1 min later.

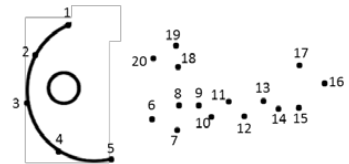
24. Statistical analysis

GraphPad Prism 6 software was used for statistical analysis and significance was considered as $P < 0.05$. The number of samples (n) in each set of experimental conditions is indicated in figure legends and data was expressed as means \pm SEM. Statistical analysis was performed by Student's t -test when used for comparison between two groups. For multiple comparisons, statistical analysis was performed by two-way ANOVA followed by Bonferroni's *post hoc* test or one-way ANOVA followed by Newman-Keuls *post-hoc* test. Student's paired t -test was also used to analyze differences between subsynaptic enrichment or membrane biotinylation within the same experiment.

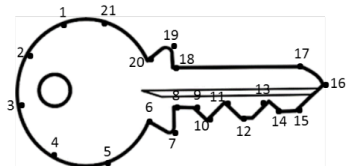
A recent study suggested that people with red hair had an approximately two-fold higher risk for PD relative to those with black hair.



People who carried a gene mutation that influences both skin and hair color (MC1R Arg151Cys variant allele) had a significantly increased risk for PD. This gene modulate/regulate melanin levels and neuromelanin. Independent studies of the cell loss in PD have demonstrated that severity of PD is associated with loss of pigment-containing cells of the substantia nigra — the cells that produce dopamine. If people with red hair have lower baseline levels of these pigmented cells in the substantia nigra, then they would be more vulnerable to PD if and when it strikes (Gao, Simon, Han, Schwarzschild, & Ascherio, 2009)



"Small disconnected facts, if you take note of them, have a way of becoming connected". Walker Percy



V. Results

Chapter I

A direct A_{2A}R-GPR37 receptor-receptor interaction modulates striatum-mediated activity

GPR37 is an orphan GPCR distributed throughout the brain, but its function remains unknown. Interestingly, GPR37 expression has been almost restricted to the CNS, thus being enriched in the cerebellum, corpus callosum, putamen, caudate nucleus, substantia nigra, and hippocampus. However, the precise neuronal, non-neuronal and subsynaptic distribution of this orphan receptor still is under study.

The development of specific antibodies has greatly contributed to unravel the molecular and cellular functions of unknown-function proteins, including orphan GPCRs. Since the anti-GPR37 antibody we previously produced in the lab (222) only detected the human GPR37, we aimed to generate a new anti-GPR37 antibody against the mouse GPR37. Accordingly, we immunized rabbits with the mouse GPR37 N-terminal domain (amino acids 27-250) fused to glutathione S-transferase (GST). Interestingly, this N-terminal amino acid sequence shared a 90% of identity with the rat GPR37, but only a 60% with the human GPR37. In order to avoid a PEST domain present within this N-terminal tail, which impaired protein production in *E.coli* BL21, two GST-tagged proteins were designed instead, namely peptide 1 (aa: 27-136: ALSFVPEPRNGTCLGESCSFLI QRRSRDARGPGNSAKDALRVHVPREKLEAEVARGATSWDLPPPARGGDTGVIEEAAAA AGPGPPTKPPSAWRWKSQQKEPSGHLRRR) and peptide 2 (aa 153-250: (KRDGIPQSRQEHSVKTEPRDLFYWPRRTGQLQDSQHRPSAVHEGRILAPPGRALPQ NGSADDWVPDQGGPRRGNTTRRVRLKNPFYPLTQESYGAYA) (**Figure 52 A**). To this end, the cDNA fragments encoding the corresponding peptide 1 and 2 were cloned into the pGEX-4T-1 plasmid using the *Sall-NotI* restriction sites. Subsequently, the two GST-tagged fusion protein, with theoretical weight of 38.66 and 38.05 kDa, respectively, were produced in *E.coli* BL21 (**Figure 52 B-C**).

Reagent	Volume (µl)
pCDNA3-mGPR37 10 ng/µl	1
Forward primer 10 µM	2.5
Reverse primer 10 µM	2.5
2X Iproof Master Mix	25
H ₂ O miliQ	19

Peptide 1

Forward 1: 5'CCGTCGACTCGCCCTGAGCTTTGTCCCTGAGC 3'

Reverse 1: 5' GTGCGGCCGCCCTTCTCCTCAAATGCCCGGA 3'

Peptide 2

Forward 2: 5' AAGTCGACTCAAGCGCGATGGGATTCCCCAG 3'

Reverse 2: 5' AAGCGGCCGCGACCGCATAGGCTCCGTAGG 3'

Table 9. PCR conditions and primers used in the cloning of the two N-terminal mGPR37 cDNA inserts. Two different GST-tag recombinant peptides from the N-terminal domain of the mouse GPR37 were designed and cloned in the pGEX-4T1 vector as described previously in the *Molecular cloning* section.

In brief, PCR amplification products (See **Table 9** for PCR reaction conditions) were purified using a PCR purification kit. Then, both pGEX-4T-1 and the PCR products were cut with the restriction enzymes *SaI* and *NotI*, purified from the agarose gel with the purification extraction gel kit and ligation reaction was performed overnight at 12-16°C. Next day, ligation product of each reaction was used to transform *E. coli* HB101 which were then plated into LB agar plates containing ampicillin. Next day, the presence of the DNA insert was determined by screening bacterial colonies using PCR. PCR-positive clones of each cloning was grown overnight in LB with ampicillin and following day, DNA was extracted for sequencing. For protein production, the cDNA encoding the fusion protein was transformed into *E.coli* BL21. The bacteria were grown in LB containing IPTG upon constant shaking for 6 hours at 30°C. Subsequently, bacteria were centrifuged and the fusion proteins purified.

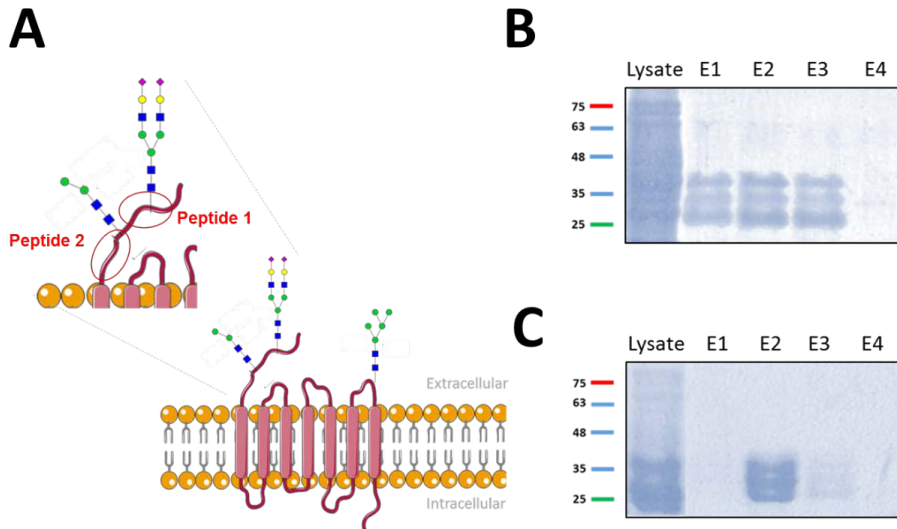


Figure 52. Purification of the N-terminal mGPR37-GST fusion proteins. (A) Schematic representation of the mouse GPR37 and the two peptidic sequence used for the antibody generation. **(B-C)** Purified N-terminal GPR37 GST-tagged fusion peptide 1 and peptide 2 were analyzed by sodium dodecyl sulfate–polyacrylamide gel electrophoresis (SDS-PAGE).

Two male New Zealand White rabbits, were immunized with a Freund's adjuvant emulsion containing 750 μg of a mixture 1:1 of both GST-tagged fusion proteins, as described previously in the "Immunisation" section. After 6 immunisations, serum from rabbits was obtained and the anti-mGPR37 antibody generation was confirmed by immunoblot using striatal extracts. Interestingly, the GPR37 antibody revealed a specific band of ~ 60 kDa, consistent with the predicted molecular weight of mouse GPR37 **(Figure 53 A)**. Finally, once the anti-mGPR37 antibody generation was confirmed the rabbits were sacrificed and the serum kept at -80°C . Importantly, after serum purification the specificity of the antibody was validated by the lack of immunoreactivity in striatal extracts from GPR37^{-/-} mice and by the absence of labeling mock transfected HEK-293T cells **(Figure 53 B)**. Interestingly, besides the ~ 60 kDa band a ~ 40 kDa band was also observed in HEK-293T expressing the mouse GPR37 **(Figure 53 B)**.

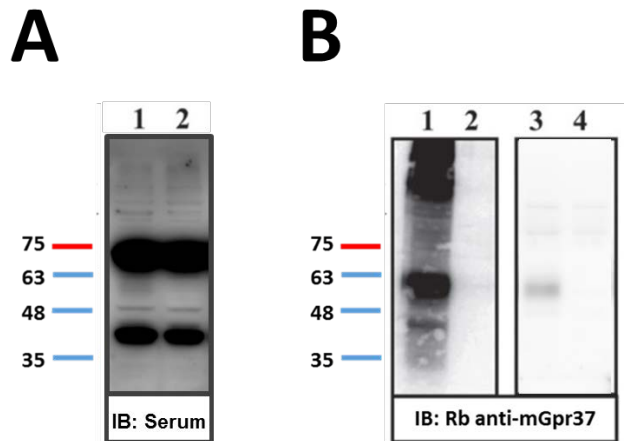


Figure 53. Validation of the rabbit anti-mGPR37 N-terminal polyclonal antibody. (A) Membrane extracts (50 μ g) from the striatum of GPR37^{+/+} (lane 1) or GPR37^{-/-} mice (lane 2) were analyzed by SDS-PAGE and immunoblotted using serum from immunized rabbits. **(B)** Crude membrane extracts (20 μ g) from HEK-293T cells transiently transfected with the mouse GPR37 (lane 1) or empty pCDNA3 plasmid (lane 2), and membrane extracts (50 μ g) from the striatum of GPR37^{+/+} (lane 3) or GPR37^{-/-} mice (lane 4) were analyzed by SDS-PAGE and immunoblotted using a rabbit anti-mGPR37 antibody (1 μ g/mL). The primary bound antibody was detected using a horseradish peroxidase (HRP)-conjugated goat anti-rabbit antibody (1/30.000). The results are representative of western blot analysis carried out in samples from three mice and three cell batches.

We recently demonstrated that A_{2A}R and GPR37 form heteromeric complexes in living cells (223). However, the physiological impact of this potential receptor-receptor interaction has not been elucidated. Therefore, we aimed to unravel the existence and functional consequences of A_{2A}R/GPR37 heteromers *in vivo*. Interestingly, it has been demonstrated that GPR37 deletion increases presynaptic DAT cell surface expression in the striatum (63). Similarly, it has been observed that the adenosinergic-dependent control of anxiety behavior is modified in GPR37 deficient mice and, upon deletion of GPR37, A_{2A}R antagonists cannot revert pilocarpine-induced tremor, which is a model for parkinsonism (224). Importantly, while the GPR37-dependent mechanism modulating these neurotransmission systems has not been fully characterized, some data point to the existence of direct receptor-receptor interactions. Thus, it was firstly proposed that GPR37 may interact with D₂R (52). Indeed, it was postulated that GPR37 and A_{2A}R might form receptor-receptor complexes or heteromers in the striatum, a fact that has not been

still wholly demonstrated. Indeed, the existence of a direct receptor-receptor interaction between $A_{2A}R$ and D_2R in the striatum was recently demonstrated and proposed as a pharmacological target for PD management (225). Hence, it could be postulated that the involvement of GPR37 in PD could be related to its interaction with striatal $A_{2A}R$ and/or D_2R .

GPR37 is widely distributed throughout the brain with a high degree of expression in myelinated tracts including corpus callosum and cerebellar white matter tracks (**Figure 54 B**), as previously described by means of *in situ* hybridization. In addition, a moderate labeling was consistently detected in cortex, striatum and hippocampus (**Figure 54 B-C**). Interestingly, no immunostaining was observed when brain sections from $GPR37^{-/-}$ were used (**Figure 54 B**), thus demonstrating the specificity of the antibodies used. Finally, under the same experimental conditions we found that $A_{2A}R$ expression was mostly concentrated in the striatum (**Figure 54 B-C**), as expected (226). Overall, these first experiments pinpointed the striatum as a brain region to assess GPR37- $A_{2A}R$ interaction.

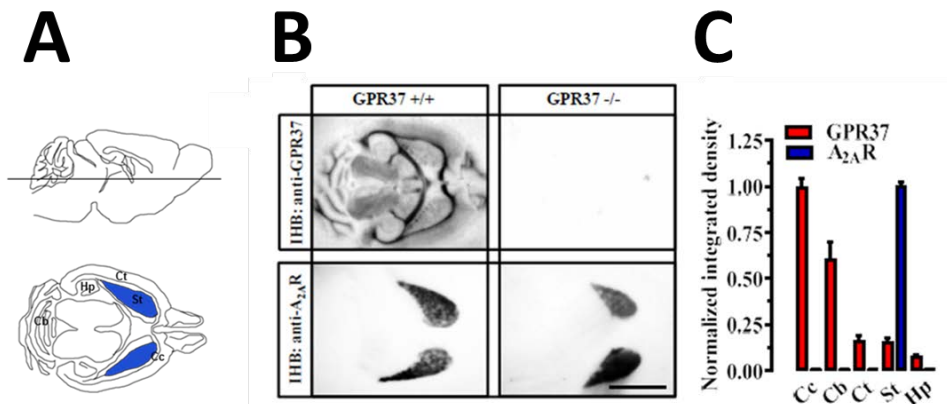


Figure 54. Co-distribution of GPR37 and $A_{2A}R$ in mice brain. (A) Schematical representation of a horizontal brain mice section and the distribution of the different brain regions. Striatum is highlighted in **BLUE**. (B) Histoblots from horizontal sections of $GPR37^{+/+}$ and $GPR37^{-/-}$ mice brain. GPR37 and $A_{2A}R$ were detected using a rabbit anti-GPR37 antibody (10 μ g/ml) and a goat anti- $A_{2A}R$ antibody (10 μ g/ml) (see “*Materials and Methods*”). (C) The histoblots were scanned and densitometric measurements from six independent experiments were averaged to compare the GPR37 and $A_{2A}R$ protein densities. Results are expressed as mean \pm SEM. Scale bar: 0.4 cm. Cc, *Corpus callosum*; Cb, *Cerebellum*; Ct, *Cortex*; St, *Striatum*; Hp, *Hippocampus*.

Thus, to evaluate the proximity and the potential receptor-receptor interaction between GPR37 and A_{2A}R we performed co-immunoprecipitation experiments in crude membranes from striatum. Immunoprecipitation of striatal GPR37 yielded a band of ~45 kDa corresponding to the A_{2A}R (**Figure 55**). Notably, A_{2A}R co-immunoprecipitation was not observed when an unrelated antibody was used, or in striatal membranes from GPR37^{-/-} mice, thus validating the specificity of the interaction in native tissue.

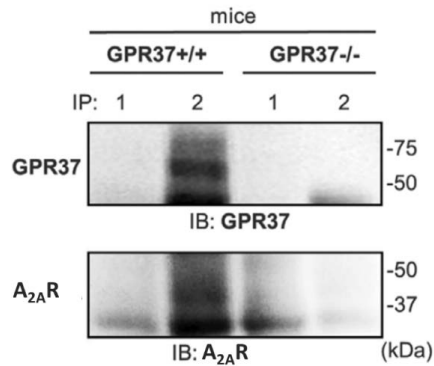


Figure 55. Co-immunoprecipitation of GPR37 and A_{2A}R from C57BL/6J GPR37^{+/+} and GPR37^{-/-} mice striatum. Crude membrane extracts from GPR37^{+/+} and GPR37^{-/-} mice striatum were obtained and GPR37-A_{2A}R co-immunoprecipitation was performed using a rabbit anti-Flag antibody (4 µg/ml; lane 1) or a rabbit anti-GPR37 antibody (4 µg/ml; lane 2) as described in the methods section. The immunoprecipitates (IP) were analyzed by SDS-PAGE and immunoblotted (IB) using a rabbit anti-GPR37 (1 µg/ml) or mouse anti-A_{2A}R antibody (1 µg/ml).

Next, we aimed to ascertain the subsynaptic striatal locus where the interaction between these two receptors might be relevant. To this end, we first evaluated the subcellular localization of GPR37 within the striatum by means of immunogold electron microscopy. In dendritic spines of striatal neurons, GPR37 immunoparticles were mostly found at the extrasynaptic plasma membrane (**Figure 56 A, arrows**), with few immunoparticles present at intracellular sites (**Figure 56 A, crossed arrows**). Similarly, in axon terminals establishing asymmetrical synapses with striatal spines GPR37 immunoparticles were also localized at the extrasynaptic plasma membrane (**Figure 56 A, lower panel, arrowheads**). Finally, in dendritic shafts, immunoparticles for GPR37 were mainly found at the plasma membrane (**Figure 56 A, lower panel arrows**). Interestingly, quantitative analysis showed that 26±0.9% of immunoparticles were located presynaptically while 73±0.9% showed a postsynaptic distribution (**Figure 56 B**), thus matching with A_{2A}R distribution within the striatum (227).

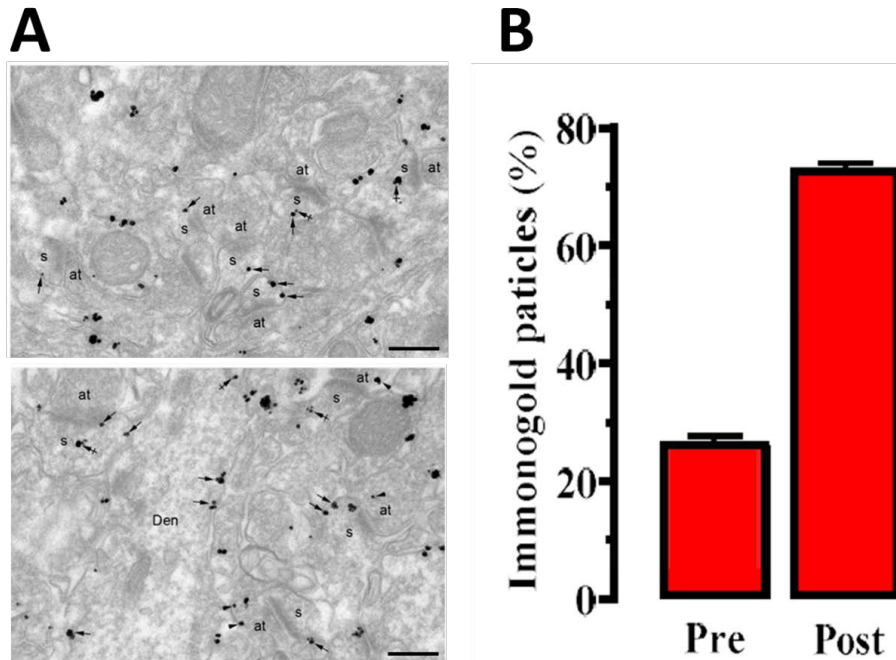


Figure 56. Subsynaptic distribution of GPR37 in mice striatum. (A) Electron micrographs showing immunoparticles for GPR37 in the striatum of GPR37^{+/+} mice using the pre-embedding immunogold technique. GPR37 immunoparticles were abundant on the extrasynaptic plasma membrane (arrows) of dendritic spines (s) of striatal neurons contacted by axon terminals (at). Few immunoparticles were observed at intracellular sites (crossed arrows) in dendritic spines (s) (upper panel). Immunoparticles for GPR37 were also localized to the extrasynaptic plasma membrane (arrowheads) of axon terminals (at) establishing asymmetrical synapses with spines (s). In dendritic shafts (Den), immunoparticles for GPR37 were mainly found in the plasma membrane (arrows) (lower panel). Scale bars: 200 nm. **(B)** Bar graphs showing the percentage of immunoparticles for GPR37 at post- and presynaptic compartments. A total of 5,837 immunoparticles were analyzed, and 73.2% were postsynaptic and 26.8% presynaptic. These experiments were performed by Prof. Rafael Luján, Universidad de Castilla la Mancha, Spain.

Subsequently, we performed subsynaptic fractionation of striatal nerve terminals, which allowed identifying the localization of GPR37 and A_{2A}R in pre-, post- and extrasynaptic enriched fractions (**Figure 57**). Interestingly, immunoblot analysis of the different striatal subsynaptic fractions revealed an enrichment at the postsynaptic over the presynaptic fraction of both GPR37 and A_{2A}R (**Figure 57 B**), thus showing correspondence with its subsynaptic distribution within the striatum.

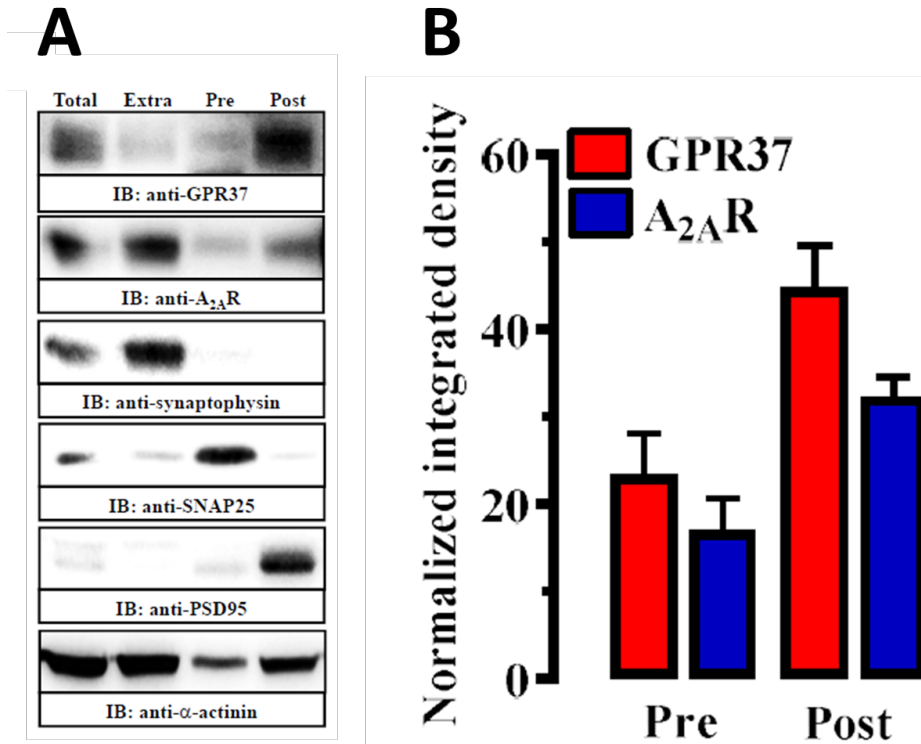


Figure 57. Subsynaptic distribution of GPR37 in mice striatum. (A) Representative immunoblots showing GPR37 and A_{2A}R immunoreactivity in striatal synaptic fractions. Striatal synaptosomes (Total) were subcellularly fractionated (see “Materials and Methods” section) into extrasynaptic (Extra), presynaptic active zone (Pre) and postsynaptic density (Post) fractions, which were analyzed by SDS-PAGE (20 μ g of protein/lane) and immunoblotted using rabbit anti-GPR37 (1 mg/ml), goat anti-A_{2A}R (1 μ g/ml), rabbit anti-synaptophysin (1 μ g/ml), mouse anti-PSD-95 (1 μ g/ml), mouse anti-SNAP-25 (1 μ g/ml) and rabbit anti- α -actinin (0.5 μ g/ml) antibodies. The primary antibodies were detected using a horseradish peroxidase (HRP)-conjugated goat anti-rabbit IgG (1/30.000), HRP-conjugated goat anti-mouse IgG (1/10.000), HRP-conjugated anti-goat IgG (1/3.000) and chemiluminescence detection (see “Materials and Methods”). **(B)** Relative quantification of GPR37 enrichment in striatal presynaptic and postsynaptic fractions. The intensities of the immunoreactive bands on the immunoblotted membranes corresponding to extrasynaptic, presynaptic (Pre) and postsynaptic (Post) fractions were measured by densitometric scanning. Values were normalized using the amount of GPR37 or A_{2A}R in the total fraction. Data from three independent experiments are shown.

While biochemical approaches are useful to establish the subsynaptic distribution of neuronal proteins they do not provide spatial information. Thus, we aimed to determine the proximity between GPR37 and A_{2A}R within striatal neurons by means of double-labeling immunogold electron microscopy and proximity ligation *in situ* assay (P-LISA). First, it was observed that GPR37 and A_{2A}R closely co-distributed along the extrasynaptic plasma membrane of dendritic shafts and dendritic spines, establishing excitatory synaptic contact with axon terminals (**Figure 58 A-D**). This result agreed with the previous subsynaptic fractionation experiments. Importantly, in GPR37^{-/-} mice striatum no GPR37 detection was observed (**Figure 58 E**), thus again demonstrating the specificity of the anti-GPR37 antibody used. Overall, these results revealed close and selective anatomical proximity for GPR37 and A_{2A}R within striatal spines.

Accordingly, we next aimed to validate the existence of GPR37/A_{2A}R heteromers in striatum by means of P-LISA, a well described technique that provides enough sensitivity to evaluate receptor close proximity (i.e. GPCR oligomers) in native conditions (229). The effectiveness of P-LISA depends on antibody specificity. Thus, to improve P-LISA detection we designed and produced a new antibody against the C-terminal domain of GPR37. The pan GPR37 C-Terminal antibody was raised by immunizing 2 male rabbits with a GST-fusion protein containing amino acids 541-600 of human GPR37 (KPF₂SRAFMECCCCCEECIQKSSTVTSDNDNEYTTELELSPFSTIRREMSTFASVTH). The human GPR37 amino acid sequence shared a 98% of identity with the mouse and rat. Protocol was followed as described previously for the polyclonal rabbit anti mGPR37 N-terminal antibody production.

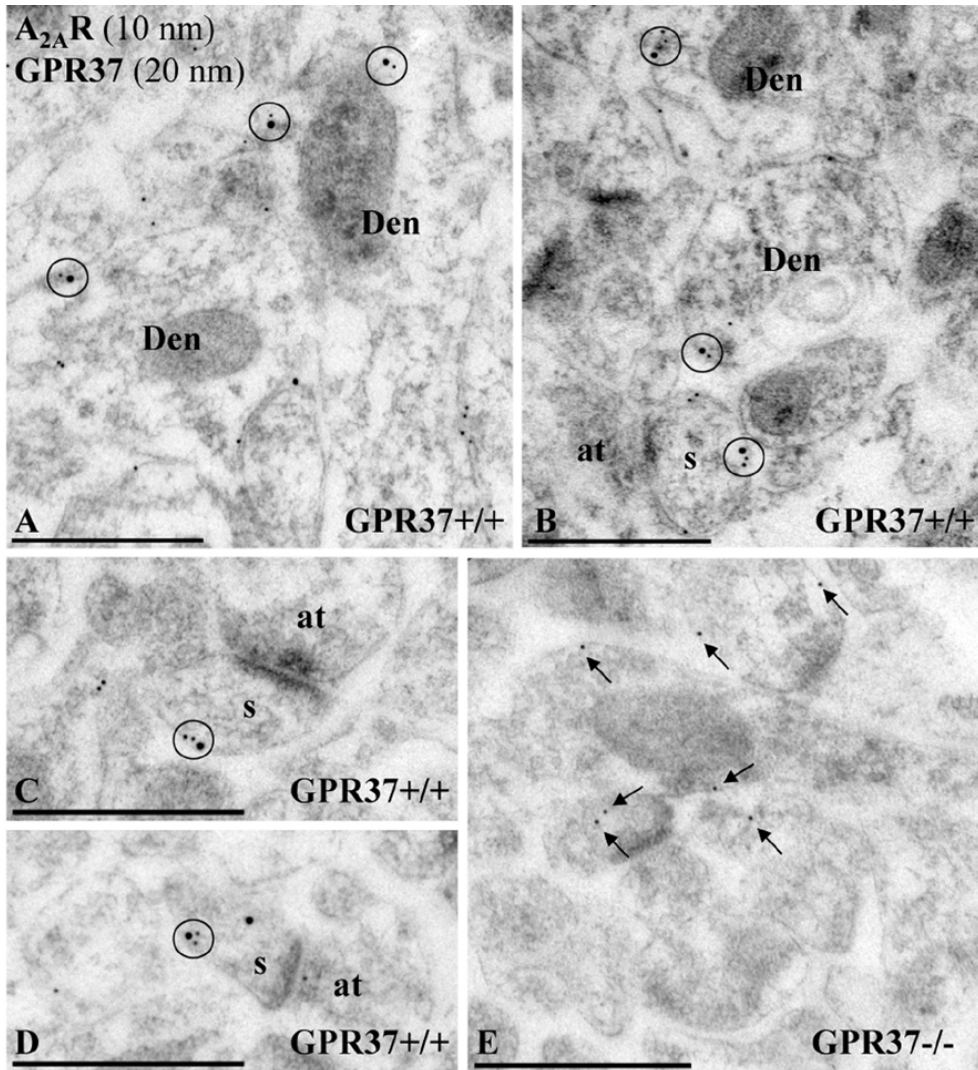


Figure 58. Post-embedding electron microscopy showing GPR37 and A_{2A}R co-distribution in mouse striatum. Electron micrographs from GPR37^{+/+} and GPR37^{-/-} showing immunoreactivity for GPR37 and A_{2A}R in striatum revealed using a double-labeling post-embedding immunogold technique. **(A-D)** In GPR37^{+/+} mice, immunoparticles for A_{2A}R (10 nm size) and GPR37 (20 nm size) were closely co-distributed (circles) along the extrasynaptic plasma membrane of dendritic shafts (Den) and dendritic spines (s) establishing excitatory synaptic contact with axon terminals (b). **(E)** In GPR37^{-/-} mice, immunoparticles for A_{2A}R (10 nm size) were present in the tissue but not immunoparticles for GPR37 (20 nm), demonstrating the full specificity of the antibody anti-GPR37. Scale bars: A-E, 500 nm.

Reagent	Volume (μ l)
pCND3-hGPR37 10 ng/ μ l	1
Forward primer 10 μ M	2.5
Reverse primer 10 μ M	2.5
2X Iproof Master Mix	25
H ₂ O miliQ	19

Peptide 3

Forward: 5' ACGCGGATCCAAACCCTTCAGTCGGGCCTTC 3'

Reverse: 5' CGGACTCGAGTCAATGAGTTCCGACAGAAGC 3'

Table 10. PCR conditions and primers used for the molecular cloning of the C-terminal hGPR37 cDNA insert. GST-tag recombinant peptide from the C-terminal domain of the human GPR37 was designed and cloned in the pGEX-4T1 vector as described previously in the “*Molecular cloning*” section.

The cDNA encoding the C-terminal GPR37 tail (**Figure 59 A**), was cloned into the pGEX-4T-1 plasmid using the *Bam*HI and *Xho*I restriction sites to produce a GST-tagged fusion protein with a theoretical molecular weight of 33 kDa. The recombinant protein was produced in *E-coli* BL21 and purified (**Figure 59 B**). Subsequently, two male New Zealand rabbits were immunized as described before.

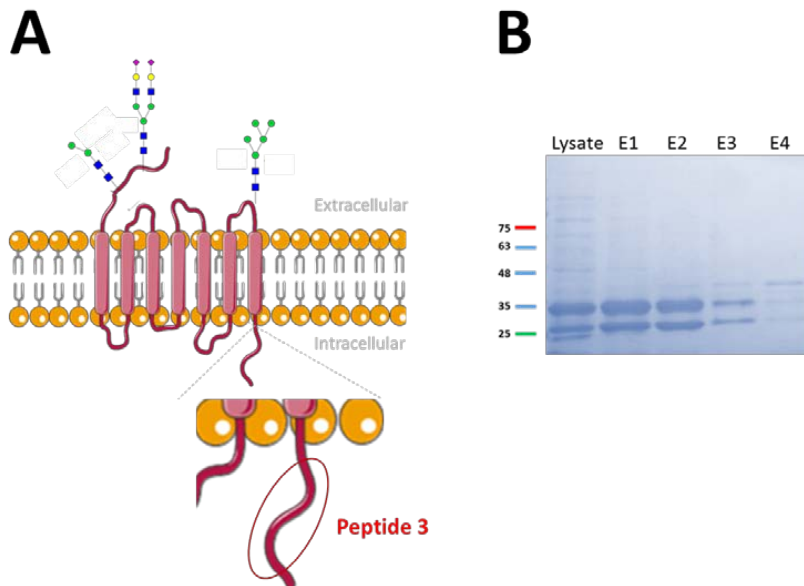


Figure 59. Purification of the C-terminal hGPR37 fusion protein. (A) Schematic representation of the human GPR37 and the peptidic sequence used for the antibody generation. **(B)** Purification of the GST-tagged fusion protein produced using a glutathione-agarose column.

Upon immunization, rabbits were sacrificed and the serum was purified and stored at -80°C . Surprisingly, the GPR37 antibody revealed a specific band of ~ 40 kDa, instead of the ~ 60 kDa consistent with the predicted molecular weight of mouse GPR37. Specificity of the C-terminal GPR37 antibody was confirmed by immunoblot analysis by the lack of immunoreactivity in striatal extracts from GPR37^{-/-} mice and by the absence of labeling mock transfected HEK-293T cells. Interestingly, besides the ~ 40 kDa band a ~ 60 kDa band was also observed in HEK-293T expressing the mouse GPR37 consistent with the predicted molecular weight of mouse GPR37 (**Figure 60**).

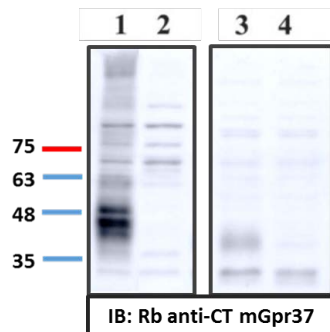


Figure 60. Validation of the Rb anti-mGPR37 C-terminal. Crude membrane extracts (20 μg) from HEK-293T cells transiently transfected with the mouse GPR37 (lane 1) or empty pCDNA3 plasmid (lane 2), and membrane extracts (50 μg) from the striatum of GPR37^{+/+} (lane 3) or GPR37^{-/-} mice (lane 4) were analyzed by SDS-PAGE and immunoblotted using a rabbit anti-mGPR37 C-terminal antibody (1 $\mu\text{g}/\text{mL}$). The primary bound antibody was detected using a horseradish peroxidase (HRP)-conjugated goat anti-rabbit antibody (1/30.000).

Accordingly, we next aimed to validate the existence of GPR37/A_{2A}R heteromers in striatum by means of P-LISA (229). We first conducted corresponding immunohistochemistry detection of GPR37 and A_{2A}R in the striatum. As expected, both receptors showed a high degree of co-distribution throughout the striatal neuropil (**Figure 61 A**). Subsequently, we implemented the P-LISA approach. Thus, by using proper antibody combinations, GPR37/A_{2A}R heteromer expression in the mouse striatum was addressed. Interestingly, red dots reflecting a positive P-LISA signal were observed in the striatum of GPR37^{+/+} mice (**Figure 61 B, upper panel**), thus allowing the visualization of the GPR37/A_{2A}R receptor-receptor interaction. Importantly, in striatal slices from GPR37^{-/-} mice the P-LISA signal was negligible (**Figure 61 B, lower panel**), thus reinforcing the specificity of our P-LISA assay. Indeed, when the P-LISA signal was quantified, 6.5 ± 1.6 dots/nuclei were observed in GPR37^{+/+} mice, while GPR37^{-/-} mice

displayed only 0.9 ± 0.3 dots/nuclei under the same experimental conditions (**Figure 61 C**). Thus, a marked and significant ($P < 0.05$) reduction in the P-LISA signal was observed in GPR37^{-/-} striatal slices, which strongly supported the existence of GPR37/A_{2A}R heteromers in the mouse striatum.

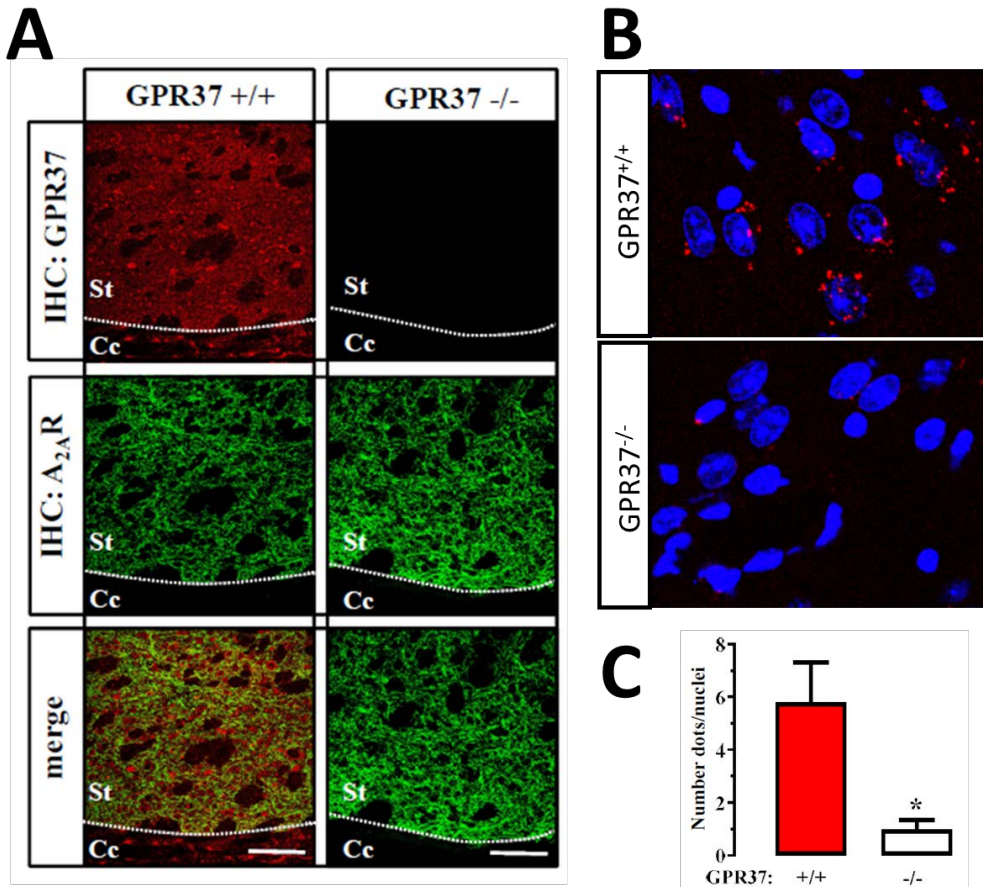


Figure 61. GPR37 and A_{2A}R co-distribute and interact in the striatum. (A) Immunohistochemistry detection of GPR37 and A_{2A}R in mice striatum. Representative confocal images of GPR37 (red) and A_{2A}R (green) immunoreactivities in the dorsal striatum of GPR37^{+/+} and GPR37^{-/-} mice. Superimposition of images revealed receptor co-distribution in yellow (merge). Scale bar: 350 μ m. Cc, Corpus callosum; St, Striatum. **(B)** Representative photomicrographs of dual recognition of GPR37 and A_{2A}R with P-LISA in striatal sections from GPR37^{+/+} (upper) and GPR37^{-/-} (lower) mice. **(C)** Quantification of P-LISA signals for GPR37 and A_{2A}R proximity in GPR37^{+/+} and GPR37^{-/-}. Values in the graph correspond to the mean \pm SEM (dots/nuclei) of at least five animals for each condition. Asterisk indicates statistically significant differences ($p < 0.05$; Student's *t*-test) when comparing GPR37^{-/-} with GPR37^{+/+}.

However, the function of the GPR37-A_{2A}R interaction in native tissue is still enigmatic. Therefore, we aimed to ascertain the impact of GPR37 expression on A_{2A}R trafficking and function in native conditions. To this end, we first assessed A_{2A}R cell surface expression by means of biotinylation of striatal slices, thus enabling the selective quantification of surface expressed receptors in GPR37^{+/+} and GPR37^{-/-} mice. Interestingly, while total A_{2A}R was unaltered, the receptor's cell surface expression was increased in the striatum of GPR37^{-/-} mice (**Figure 62 A and B**). Of note, the absence of tyrosine hydroxylase immunoreactivity in the biotinylated surface fractions indicated that the integrity of slices was maintained and no major cell damage occurred during striatal slice preparation. Thus, our results demonstrated that GPR37 deletion potentiates A_{2A}R cell surface targeting.

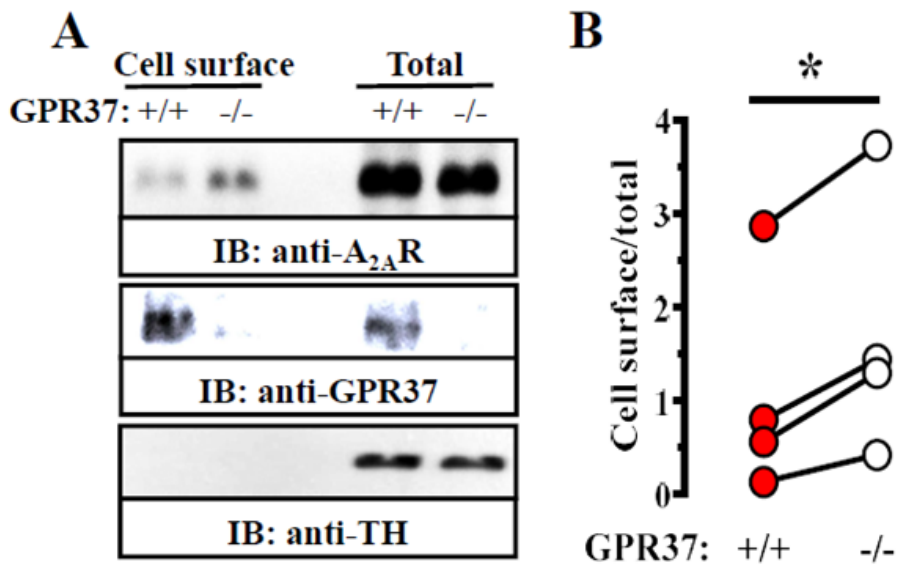


Figure 62. GPR37 deletion promotes A_{2A}R cell surface expression in striatum. (A) Coronal brain slices (300 μ m) from GPR37^{+/+} and GPR37^{-/-} mice were prepared and biotinylated as described in “*Material and methods*” section. Total and cell surface extracts were analyzed by SDS-PAGE and immunoblotting. **(B)** Quantification of A_{2A}R cell surface expression in GPR37^{+/+} and GPR37^{-/-} striatum. Cell surface expression was normalized using the total amount of A_{2A}R. The asterisk indicates statistically significant difference from the control condition ($P < 0.05$; paired Student’s *t* test).

Next, we examined whether A_{2A}R increased cell surface expression in GPR37^{-/-} striatum had any impact in A_{2A}R-receptor function. To this end, we evaluated A_{2A}R-dependent cAMP accumulation in striatal nerve terminals from GPR37^{+/+} and GPR37^{-/-} mice. First, we undertook a complementary double immunocytochemistry study in individual striatal nerve terminals to identify synaptosomes endowed with both GPR37 and A_{2A}R (**Figure 63 A**). We observed that around 9±1.1% of total population of striatal nerve terminals (immunopositive for both SNAP25 and PSD95), presented immunoreactivity for both GPR37 and A_{2A}R (**Figure 63 B**). Subsequently, we determined A_{2A}R agonist-mediated cAMP accumulation in striatal nerve terminals from GPR37^{+/+} and GPR37^{-/-} mice. A significant 2.5-fold increase in A_{2A}R-mediated cAMP accumulation was observed in synaptosomes from GPR37^{-/-} mice (**Figure 63 C**).

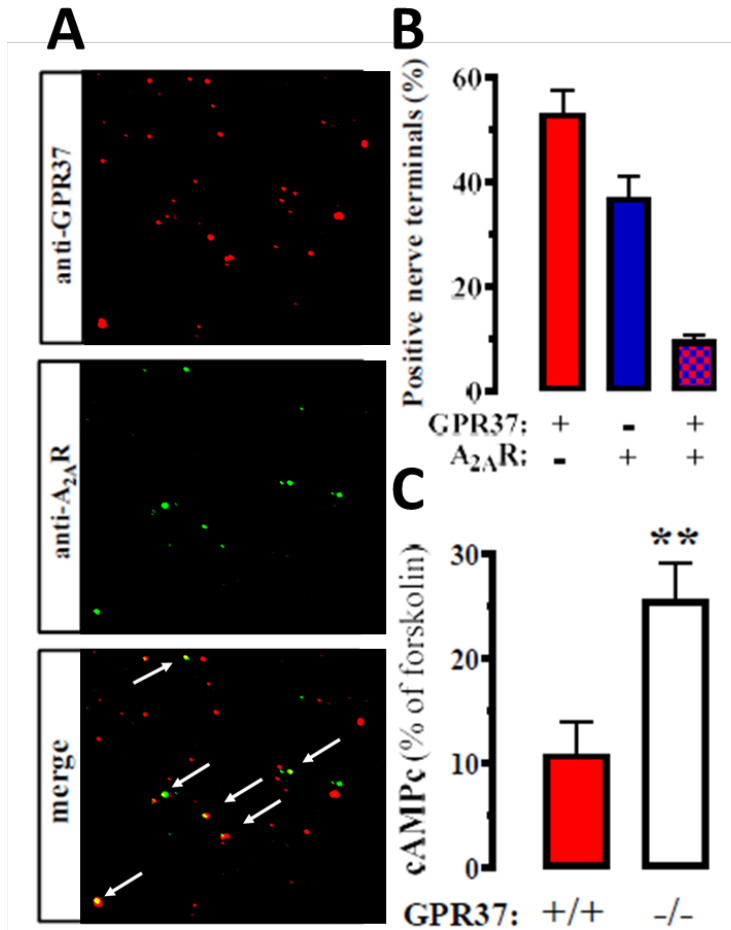


Figure 63. GPR37 deletion bolsters striatal A_{2A}R function in synaptosomes. (A) Co-distribution of GPR37 and A_{2A}R in striatal synaptosomes. Immunofluorescence detection of GPR37 (red) and A_{2A}R (green) in striatal total synaptosomes was performed as described in “Materials and Methods” section. Superimposition of images (merge) reveals co-localization in yellow (arrows). (B) Quantification of synaptosomes expressing GPR37 and/or A_{2A}R. The data are expressed as the percentage (mean ± SEM) of total number of synaptosomes that are endowed with GPR37 and/or A_{2A}R, quantified in 3-4 different synaptosomal preparations from different mice, in which four different fields acquired from two different coverslips were analyzed in each preparation. (C) A_{2A}R-mediated cAMP accumulation in synaptosomes. Total striatal synaptosomes from GPR37^{+/+} and GPR37^{-/-} mice were stimulated with 500 nM CGS21680 for 30 min at 37°C and the cAMP accumulation was measured as described in “Materials and Methods”. The data are expressed as percentage (mean ± SEM) of forskolin-induced cAMP accumulation, which was similar ($P > 0.05$) in both genotypes. The asterisks indicate statistically significant difference from the control condition ($P < 0.01$; Student’s *t* test).

Finally, similar $A_{2A}R$ -based functional assays were performed in striatal primary neurons from $GPR37^{+/+}$ and $GPR37^{-/-}$ mice (**Figure 64 A**). Again, a significant increase in $A_{2A}R$ -mediated cAMP accumulation was observed in primary cultures from $GPR37^{-/-}$ striatum (**Figure 64 B**). Overall, these results demonstrated that $GPR37$ deletion promotes striatal $A_{2A}R$ cell surface expression and function.

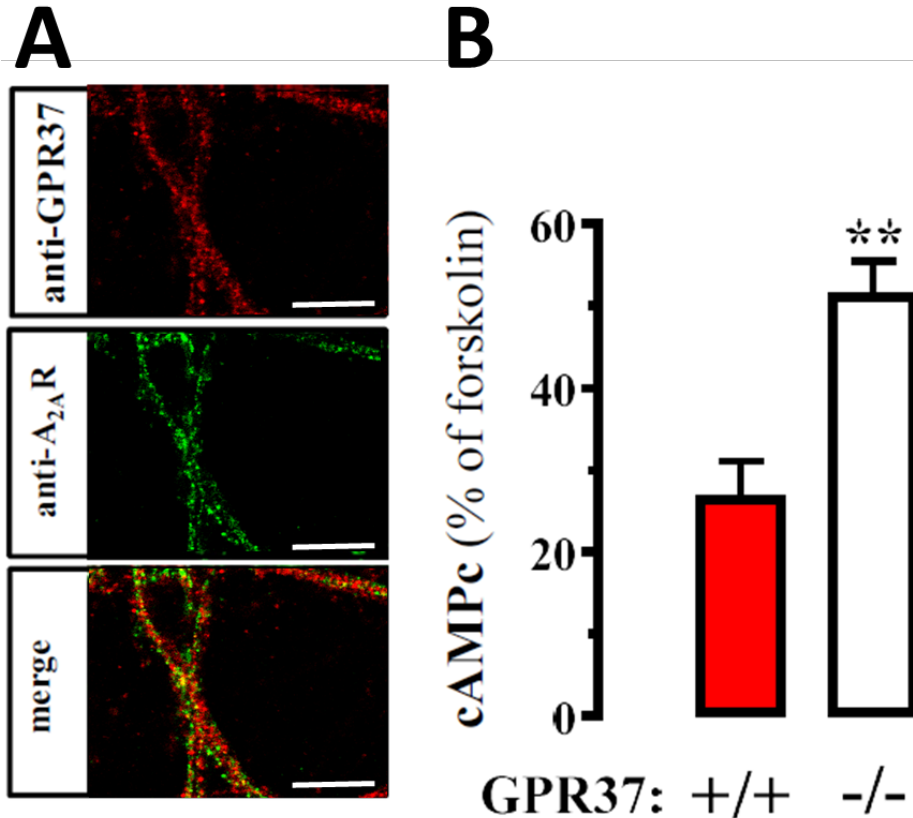


Figure 64. GPR37 deletion bolsters striatal $A_{2A}R$ function in striatal primary cultures (A) Co-distribution of $GPR37$ and $A_{2A}R$ in striatal neurons. Immunofluorescence detection of $GPR37$ (red) and $A_{2A}R$ (green) in primary cultured striatal neurons (DIV21) was performed as described in “*Materials and Methods*”. Superimposition of images (merge) reveals co-localization in yellow. Scale bar: 100 μ m. (B) $A_{2A}R$ -mediated cAMP accumulation in striatal neurons. Striatal primary neurons from $GPR37^{+/+}$ and $GPR37^{-/-}$ were stimulated with 500 nM CGS21680 for 30 min at 37°C and the cAMP accumulation was measured as described in “*Materials and Methods*”. The data are expressed as percentage (mean \pm SEM) of forskolin-induced cAMP accumulation, which was similar ($P > 0.05$) in both genotypes. The asterisks indicate statistically significant difference from the control condition ($P < 0.01$; Student’s t test).

Once confirmed the striatal $A_{2A}R$ enhanced activity in $GPR37^{-/-}$ mice, we aimed to determine its impact in the behaving animal. It is well established that striatal $A_{2A}R$ modulates the central processes involved in locomotor activity and psychomotor behaviors due to its interplay with the dopaminergic system (230). Our hypothesis consisted of expecting an enhanced modulation of locomotor activity by striatal $A_{2A}R$ in $GPR37^{-/-}$ mice. Since it is well-known that blocking of $A_{2A}R$ increases spontaneous locomotor activity in mice (231), we assessed $A_{2A}R$ antagonist-induced hyper-motility in $GPR37^{+/+}$ and $GPR37^{-/-}$ mice. To this end, we administered $GPR37^{+/+}$ and $GPR37^{-/-}$ mice with SCH58261 and the spontaneous locomotor activity in an open field arena was monitored (**Figure 65 A**). Interestingly, our results showed that $A_{2A}R$ antagonist-mediated locomotor activity potentiation was significantly ($P < 0.05$) higher in $GPR37^{-/-}$ mice (**Figure 65 B**), thus suggesting an increased $A_{2A}R$ basal activity in the absence of GPR37.

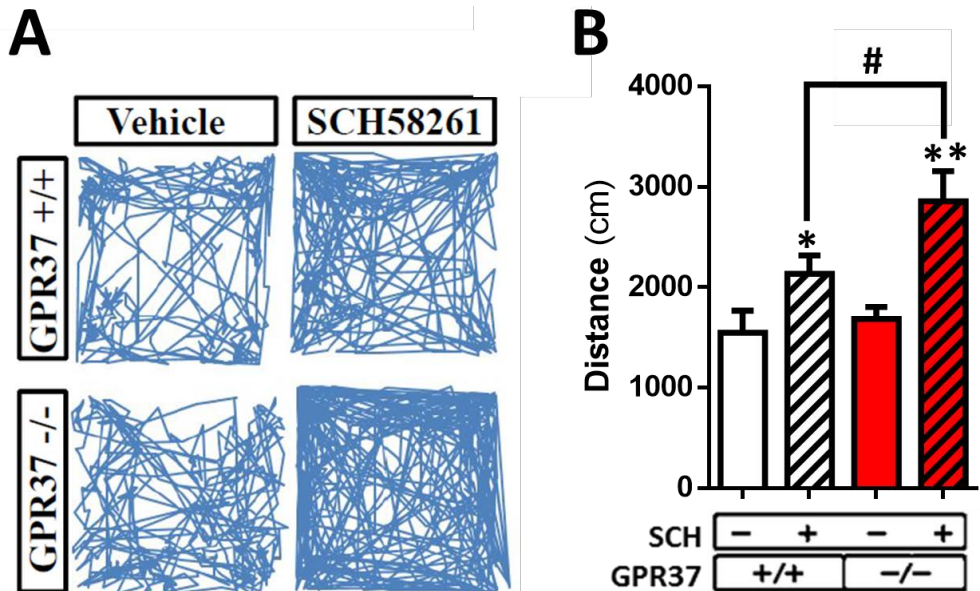


Figure 65. GPR37 deletion promotes $A_{2A}R$ -mediated behavior. (A) $A_{2A}R$ antagonist-induced locomotor hyperactivity in $GPR37^{+/+}$ and $GPR37^{-/-}$ mice. Representative 10 min trajectories in an open field arena of $GPR37^{+/+}$ and $GPR37^{-/-}$ mice administered with vehicle or SCH58261 (3.75 mg/kg, i.p.). (B) Quantification of the horizontal locomotor activity shown in (A). The distance travelled is expressed as mean \pm SEM ($n=10$ animals) * $P < 0.05$, ** $P < 0.01$ SCH58261 treatment effect, # $p < 0.05$ phenotype effect by two-way ANOVA and Bonferroni post-hoc test.

GPR37 deficient mice showed lower haloperidol-induced catalepsy, thus suggesting an altered functioning of postsynaptic striatal D₂R in GPR37^{-/-} mice (63). In addition, the well-known effects of A_{2A}R antagonists blocking haloperidol-induced catalepsy were higher in the absence of GPR37, thus suggesting a GPR37-dependent A_{2A}R modulation of dopaminergic transmission (**Figure 66 A**) (232). Indeed, GPR37 may play a key role in defining the A_{2A}R-D₂R interplay and consequently it could be considered as a novel target for PD management. Conversely to hyperlocomotion induced by A_{2A}R antagonists, activation of striatal A_{2A}R with selective agonists can suppress motor activity, thus producing effects that resemble those yielded by D₂R antagonists (i.e. haloperidol) or DA depletion (i.e. reserpine) (233). For instance, administration of the A_{2A}R agonist CGS 21680 blocked acquisition and expression of wheel running behavior (234), depressed locomotor activity (235) and induced catalepsy (236). Accordingly, we assessed whether A_{2A}R agonist-induced catalepsy was increased in GPR37^{-/-} mice. Interestingly, our results showed that upon CGS21680 administration (i.c.v.) the catalepsy scores of GPR37^{-/-} mice were significantly higher ($P < 0.001$) to that observed in GPR37^{+/+} mice (**Figure 66 B**), thus demonstrating an increased activity of striatal A_{2A}R in GPR37^{-/-} mice. Overall, our results suggested that GPR37 may modulate A_{2A}R control of locomotor activity and psychomotor behavior through a putative GPR37/A_{2A}R heteromer.

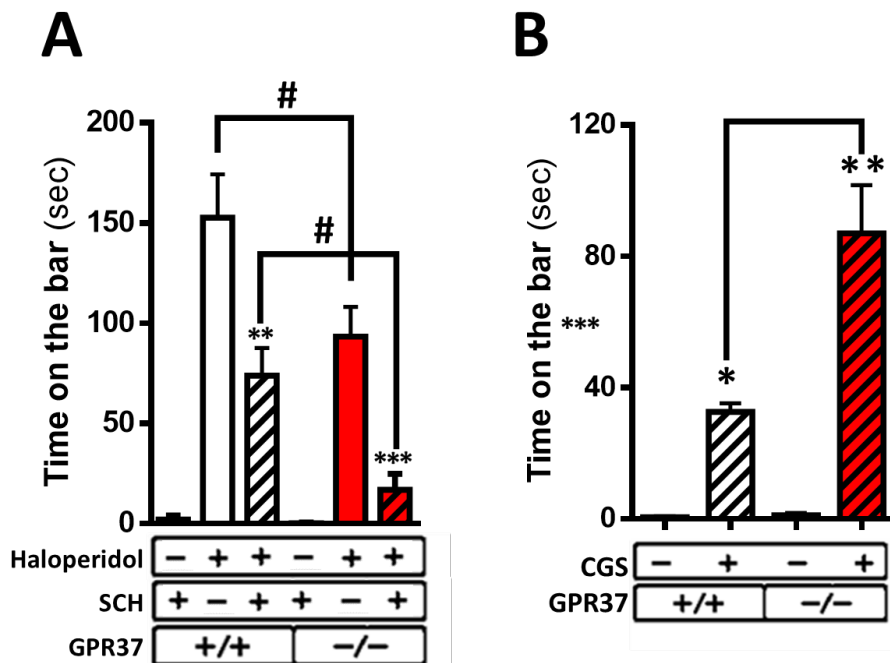


Figure 66. Involvement of GPR37 in haloperidol- and CGS58261-induced catalepsy. (A) The influence of systemic injection of $A_{2A}R$ antagonist SCH58261 (1 mg/kg, i.p.) on the catalepsy induced by haloperidol (1.5 mg/kg i.p.) was assessed in both GPR37^{+/+} and GPR37^{-/-} mice as described in “*Materials and Methods*”. The data indicate the mean \pm SEM (n = 6 per group). Asterisks denote data significantly different from the haloperidol-treated mice: **P < 0.01 and ***P < 0.001 by one-way ANOVA with Bonferroni multiple comparison post hoc test. In the GPR37^{-/-} mice, the haloperidol plus SCH 58261 group were not significantly different (P > 0.05) from the control (i.e. SCH 58261 alone). #P < 0.01 by two-way ANOVA with Bonferroni multiple comparison post hoc test for genotype and treatment comparisons. **(B)** $A_{2A}R$ agonist-mediated catalepsy in GPR37^{+/+} and GPR37^{-/-} mice. The cataleptic response induced by i.c.v. administration of CGS21680 (10 μ l of a 1 μ g/ μ l CGS21680 solution) in GPR37^{+/+} and GPR37^{-/-} mice was measured as the duration of an abnormal upright posture in which the forepaws of the mouse were placed on a horizontal wooden bar. The time spent with both front paws resting on the bar is expressed as mean \pm SEM (n=10 animals); a cut off time was set at 200 s. The asterisk (one-way ANOVA, followed by Newman-Keuls test). ** P<0.01, *** P<0.001 CGS21680 treatment effect, # P < 0.05 phenotype effect (Two-way ANOVA, Bonferroni post-hoc test).

The $A_{2A}R$ has been involved in the control of synaptic plasticity processes (108)(106). Thus, after determining the precise synaptic localization of GPR37 and its functional relationship with the adenosinergic system in the striatum, we next aimed to determine whether GPR37 can modulated basal striatal synaptic plasticity and/or its modulation, by $A_{2A}R$ s. To this end, we performed electrophysiological experiments using corticostriatal slices from GPR37^{+/+} and GPR37^{-/-} mice (**Figure 67 A**). Therefore, the impact of GPR37 expression in synaptic transmission and short-term plasticity was assessed by recording corticostriatal fEPSPs (**Figure 67 C**). Interestingly, a similar input–output curve for the fEPSP population spike amplitude as function of the stimulus intensity was observed in GPR37^{+/+} and GPR37^{-/-} mice (**Figure 67 B**), thus the GPR37 deletion does not modify synaptic transmission. Next, the effect of GPR37 deletion on short-term synaptic plasticity (paired-pulse facilitation, PPF) in corticostriatal slices was evaluated (**Figure 67 C**). Thus, the comparison of PPF in mice striatum revealed that GPR37 deletion did not alter the striatal short-term plasticity at any of the inter-pulse intervals tested (i.e., 20 and 160 ms) (**Figure 67 D**). Overall, GPR37 expression do not impinge into the striatal synaptic transmission and short-term plasticity.

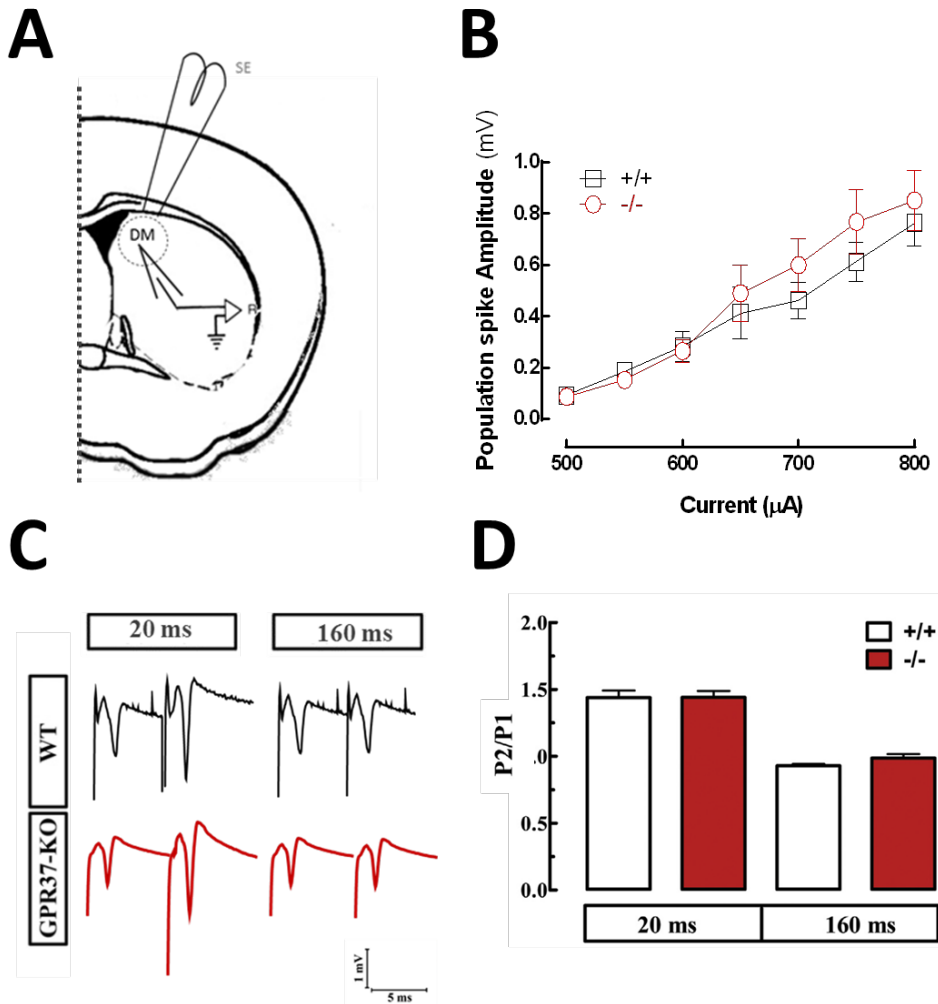


Figure 67. Impact of GPR37 deletion on synaptic transmission and short-term plasticity in corticostriatal slices. (A) Schematic diagram of a striatal hemislice and the placement of stimulating electrode (SE) and recording electrode (R) in dorsolateral (DM) subregion of the striatum. **(B)** Input–output curves of the population spike (PS) amplitude of fEPSP as function of the stimulus intensity (current) in corticostriatal slices from GPR37^{+/+} and GPR37^{-/-} mice. **(C)** Representative traces of fEPSP paired with an inter-pulse interval of 20 ms and 160 ms recorded in the stratum of GPR37^{+/+} and GPR37^{-/-} mice. **(D)** The ratio of the second vs. the first fEPSP (P2/P1 ratio) for both 20 ms or 160 ms inter-pulse intervals shown in (C) was quantified. Data are expressed as mean \pm SEM (n = 4 per group).

The molecular mechanisms underlying striatal plasticity remain elusive. Thus, while the mechanisms governing LTD have been studied (111)(103), the LTP assessment in the striatum still is limited due to the difficulty in evoking reliable long-lasting LTP. Interestingly, in medium spiny neurons, low-frequency stimulation (LFS) of corticostriatal afferent fibers leads to a different form of LTD (237)(238)(239). Therefore, we assessed the role of GPR37 expression in LFS-induced LTD in the striatum and no significant differences between GPR37^{+/+} and GPR37^{-/-} were found (80% ± 5% vs. 80% ± 4%, respectively) (**Figure 68**). Again, GPR37 by itself does not seem to play a role in striatal synaptic plasticity (i.e. LTD). Next, since GPR37 interacts with A_{2A}R and its deletion facilitates striatal A_{2A}R cell surface expression *in vivo*, we aimed to investigate a possible gain of function of A_{2A}R in the control of synaptic plasticity in corticostriatal synapses, which is the most relevant neurophysiological role of A_{2A}R (240). Accordingly, we preincubated corticostriatal slices with SCH58261 (50 nM) for 20 min prior LTD induction. Indeed, SCH58261 didn't alter striatal LTD amplitude in wild-type mice, as previously described (212), but also it was ineffective in GPR37^{-/-} mice (85% ±4% vs. 79% ±4%, respectively) (**Figure 68**). Overall, bath superfusion with SCH58261 failed to modify striatal LTD.

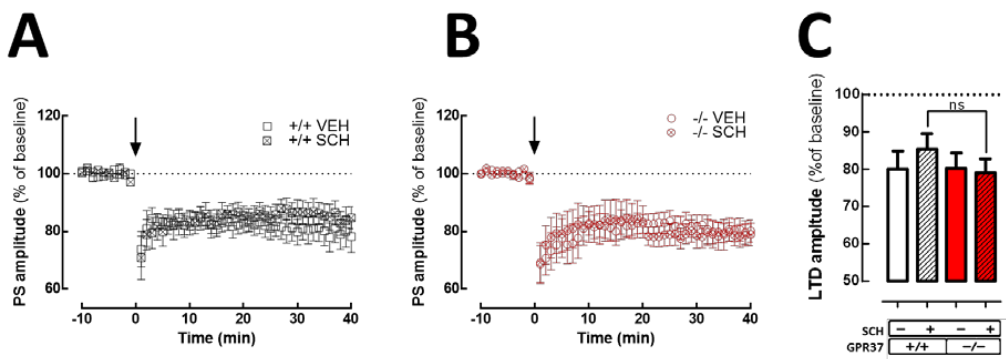


Figure 68. Effect of acute A_{2A}R blockade on LTD in corticostriatal synapses of GPR37^{+/+} and GPR37^{-/-} mice. Plot of normalized PS amplitudes during experiments examining the effect of applying a low frequency stimulation (LFS) train (900 pulses at 1 Hz for 15 min) in DM striatum in GPR37^{+/+} (**A**) or GPR37^{-/-} (**B**) perfused with vehicle (Veh) or SCH58261 (SCH, 50 nM) for 20 min prior LTD induction. (**C**) Quantification of the last 10 minutes after LTD induction. Plotted data are mean ±SEM (n= 5-7). Arrow indicates the time of LTD induction.

Importantly, while our previous results revealed an increase in the expression and function of A_{2A}R in GPR37^{-/-} mouse striatum, the acute incubation of corticostriatal slices with the A_{2A}R antagonist (i.e. SCH58261) didn't modify LTD both in GPR37^{+/+} and GPR37^{-/-} mice. Indeed, this might be considered an unpredicted result in view of the described ability of A_{2A}Rs to control synaptic plasticity in excitatory synapses, but a similar study didn't observe changes in LTD after acute perfusion of SCH58261 in corticostriatal slices (212)(241). Interestingly, it has been demonstrated that low doses of either caffeine (10 mg/kg/day, i.p.) or SCH58261 (2 mg/kg/day, i.p.) during 10 consecutive days elicited locomotor sensitization with concomitant elevation of striatal dopamine concentration (200)(242). Therefore, chronic A_{2A}R blockade may play an important role in the striatal neuroadaptation observed upon caffeine consumption.

Accordingly, we aimed to assess the impact of GPR37 expression in A_{2A}R-dependent striatal neuroadaptations. To this end, we evaluated locomotor activity sensitization in GPR37^{+/+} and GPR37^{-/-} mice treated with SCH58261 (1 mg/kg/day, i.p.) for 10 days. We measured spontaneous locomotor activity 24h after the last SCH58261 administration (i.e. day 15). Interestingly, while chronic SCH58261 treatment did not alter spontaneous locomotor activity in GPR37^{+/+} mice, the GPR37^{-/-} showed SCH58261-mediated spontaneous locomotor sensitization (**Figure 69**). The two-way ANOVA analysis revealed effect of genotype [$F_{(1,24)} = 5.737, P = 0.0248$], treatment [$F_{(1,24)} = 13.10, P = 0.0014$] and interaction between both factors [$F_{(1,24)} = 6.445, P = 0.018$]. Bonferroni post-hoc analysis showed significant differences in the GPR37^{-/-} mice upon SCH58261 treatment ($P < 0.01$) and when compared to GPR37^{+/+} mice either vehicle or SCH58261 treated ($P < 0.001$ and $P < 0.05$, respectively) (**Figure 69 B**), thus indicating a GPR37-dependent SCH58261-mediated locomotor sensitization. A close analysis of the trajectories in the open field test revealed significant effect of genotype [$F_{(1,26)} = 11.82, P = 0.002$] but not treatment [$F_{(1,26)} = 0.946, P = 0.339$] in the total time spent in the center of the arena (**Figure 69 C-D**). Hence, GPR37^{-/-} mice showed a significant increase in the exploration of the arena center independently of SCH58261 treatment (**Figure 69 C-D**). Overall, these results suggested that GPR37 deletion reduced anxiety-like behavior, as previously reported (228).

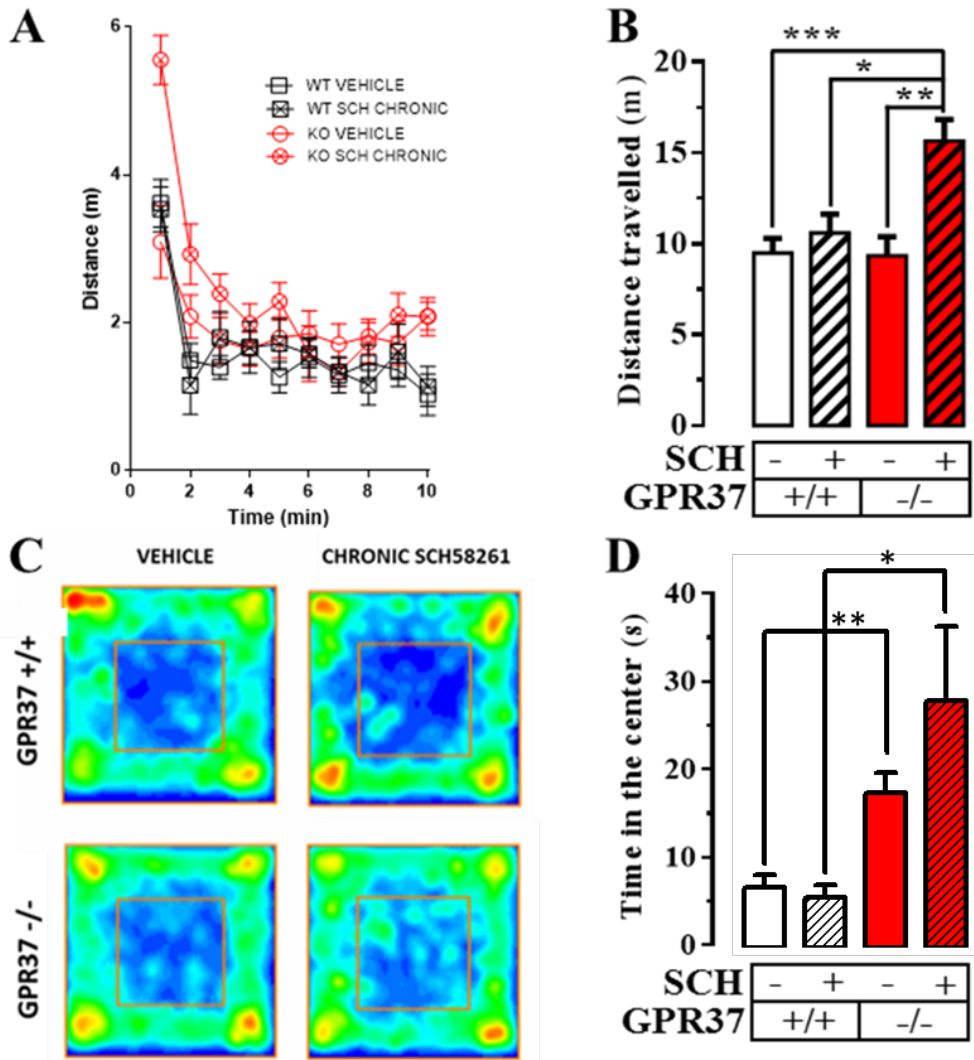


Figure 69. GPR37 deletion promotes $A_{2A}R$ -mediated locomotor sensitization. (A)

Spontaneous locomotor activity time course of GPR37^{+/+} and GPR37^{-/-} mice administered chronically with vehicle or SCH58261 (1 mg/kg). Data are expressed as mean \pm SEM of the distance travelled (n = 6-9). **(B)** Quantification of the horizontal locomotor activity during 5 min. The total distance travelled is expressed as mean \pm SEM (n = 6-9 animals). * $P < 0.05$, ** $P < 0.01$, *** $P < 0.001$ two-way ANOVA, followed by Bonferroni post-hoc test. **(C)** Representative 10 min trajectories (frequency of animal presence) in the open field arena of GPR37^{+/+} and GPR37^{-/-} mice administered chronically with either vehicle or SCH58261 (1 mg/kg). **(D)** Quantification of time spent in the central zone. Total time in the arena centre is expressed as mean \pm SEM (n = 6-9 animals) * $P < 0.05$, ** $P < 0.01$ two-way ANOVA, followed by Bonferroni post-hoc test.

Next, we aimed to assess whether the SCH58261 chronic treatment inducing locomotor sensitization in $GPR37^{-/-}$ mice might also affect another striatal behavioral task, namely the striatum-dependent cued navigation (243)(219)(244). To this end, $GPR37^{+/+}$ and $GPR37^{-/-}$ mice chronically treated with vehicle or SCH58261 were trained during 4 consecutive days in the cued water maze. Latency to find the escape platform improved across training trials, as expected (**Figure 70**). The two-way ANOVA analysis revealed no effect of either genotype, treatment and interaction between both factors at any of the testing days (**Figure 70**). Thus, the chronic SCH58261 treatment didn't modify striatum-dependent cued learning.

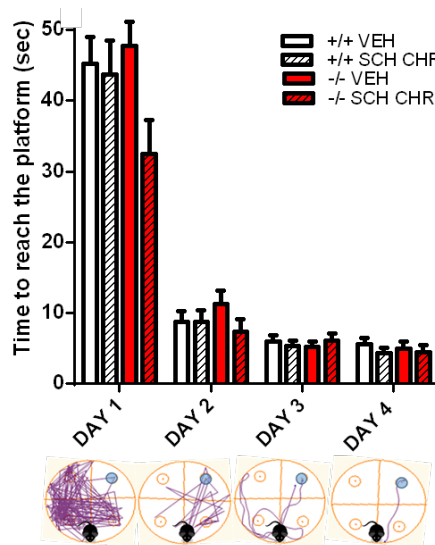


Figure 70. Chronic SCH58261 treatment do not alter striatum-dependent cued learning. MWM test learning curves showing escape latencies to reach the hidden platform during 4 testing days of $GPR37^{+/+}$ and $GPR37^{-/-}$ mice treated chronically with vehicle or SCH58261 (1mg/kg, i.p.). Animals performed 4 consecutive trials during 4 consecutive days. Time to reach the platform is expressed as mean \pm SEM (n= 6-7 animals). Representative routes showing mouse track during the 4 consecutive days.

Finally, we intended to assess whether the striatum-dependent behavioural changes upon chronic SCH58261 treatment (i.e. locomotor sensitization) was somehow related to an $A_{2A}R$ -mediated control of synaptic plasticity in corticostriatal excitatory synapses. To this end, we compared the LTD amplitude in corticostriatal slices from $GPR37^{+/+}$ and $GPR37^{-/-}$ mice treated chronically with vehicle or SCH58261. Indeed, similar input-output curves for the fEPSP population spike amplitude as function of the stimulus intensity was observed in $GPR37^{+/+}$ and $GPR37^{-/-}$ mice treated either with vehicle or SCH58261 (1 mg/kg/day, i.p., 10 days) (**Figure 71 A**), thus the chronic $A_{2A}R$ blockade does not modify

synaptic transmission. Interestingly, while in GPR37^{+/+} mice the SCH58261 chronic treatment did not modify LTD, in GPR37^{-/-} a reduction in LTD amplitude was observed (**Figure 71 B and C**). The two-way ANOVA analysis revealed effect of genotype [$F_{(1,22)} = 5.675, P = 0.0373$], treatment [$F_{(1,22)} = 5.162, P = 0.0332$] and interaction between both factors [$F_{(1,22)} = 4.915, P = 0.0373$]. Bonferroni post-hoc analysis showed significant differences between GPR37^{-/-} mice treated with SCH58261 and all the other experimental animal groups ($P < 0.05$) (**Figure 71 C**). Overall, these results demonstrated a GPR37-dependent SCH58261-mediated increase in LTD in the striatum and, thus, established a framework for A_{2A}R-dependent striatal neuroadaptations

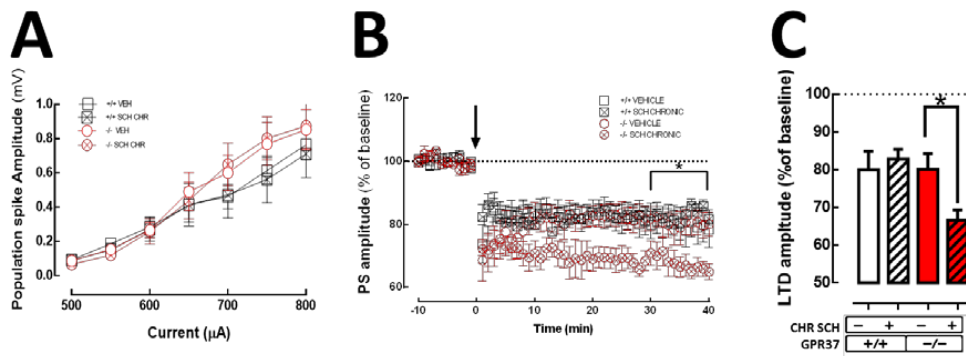


Figure 71. Effect of chronic A_{2A}R blockade on LTD in corticostriatal synapses of GPR37^{+/+} and GPR37^{-/-} mice. (A) Input–output curves of the population spike (PS) amplitude of fEPSP as a function of stimulus intensity before induction of LTD in corticostriatal slices from GPR37^{+/+} and GPR37^{-/-} mice treated with vehicle or SCH58261 (1 mg/kg/day, i.p., 10 days). **(B)** Plot of normalized PS amplitudes during experiments examining the effect of applying a LFS train (900 pulses at 1 Hz for 15 min) in DM striatum in GPR37^{+/+} and GPR37^{-/-} mice administered chronically with vehicle or SCH58261 (1 mg/kg/day, i.p., 10 days). LTD was consistently induced. **(C)** Quantification of the last 10 minutes after LTD induction shown in (B). Arrow indicates the time of LTD induction. Plotted data are mean \pm SEM ($n = 5-7$). * $P < 0.05$, two-way ANOVA, followed by Bonferroni post-hoc test.

Collectively, these results demonstrated that chronic treatment with a selective A_{2A}R antagonist induced sensitization of locomotor activity and increased LTD. This plasticity has the potential to powerfully regulate basal ganglia circuit function by setting the gain on incoming cortical and thalamic signals. Interestingly, alterations in striatal plasticity are thought to play a role in many movement disorders including Parkinson's disease, Huntington's disease, and dystonia.

Chapter II

GPR37-mediated modulation of the adenosinergic system in the hippocampus

Once we determined the impact of GPR37 in the striatal A_{2A}R functioning we next investigated the role of the GPR37 in the hippocampus and its relationship with the adenosinergic system.

First, we assessed the expression of GPR37 in hippocampal tissue. Thus, primary hippocampal cultures from GPR37^{+/+} and GPR37^{-/-} mice were cultured for 21 days *in vitro* before GPR37 expression was analyzed by immunofluorescence. Interestingly, positive immunolabeling for GPR37 was found, thus confirming the presence of this receptor in hippocampal neurons (**Figure 72**).

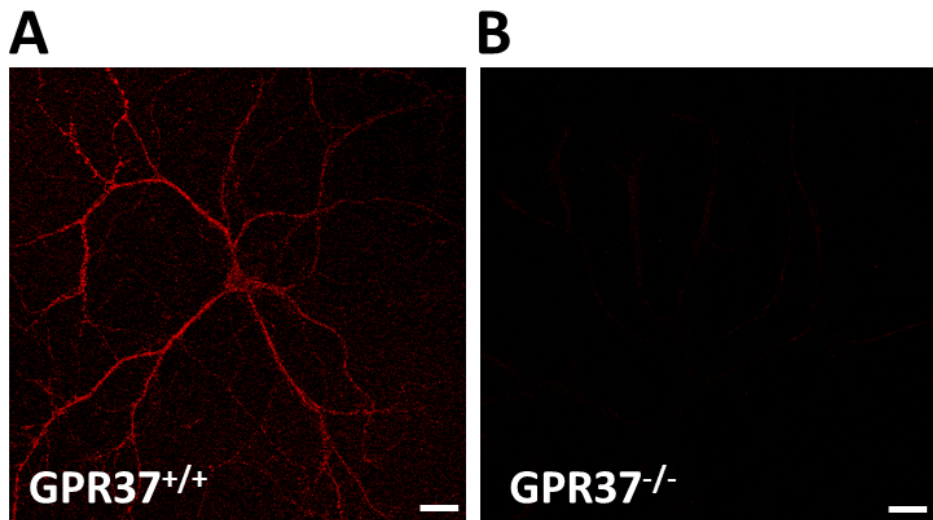


Figure 72. Distribution of GPR37 in cultured hippocampal neurons. Primary hippocampal neurons from either GPR37^{+/+} (**A**) or GPR37^{-/-} (**B**) mice were fixed, permeabilized, and immunostained as described in the “*Materials and Methods*” section. Scale bar: 10 µm. The immunocytochemistry results are representative of five independent cultures.

In order to investigate the regional distribution of GPR37 within the hippocampus we performed immunohistochemical studies in collaboration with Professor Rafael Luján (Facultad de Medicina, Universidad Castilla-La Mancha, Albacete, Spain). Interestingly, moderate GPR37-positive immunoreactivity was observed in the CA1 region (in the strata oriens, radiatum, and lacunosum-moleculare) and in the dentate gyrus (in the molecular layer and hilus) (**Figure 73 A**). The lowest immunoreactivity was observed in the CA3 stratum lucidum, with the remaining of the region displaying moderate immunolabeling. Conversely, in the pyramidal and granule cell layers no labeling was detected (**Figure 73 A**). Subsequently, we assessed the subcellular localization of GPR37 by means of immunogold electron microscopy. In the stratum radiatum of the hippocampal CA1 region, GPR37 immunoparticles were found both along the extrasynaptic plasma membrane of dendritic spines (**Figure 73 B, arrows**) and dendritic shafts (**Figure 73 C, arrows**) of pyramidal cells, which make contact with terminals from presumed CA3 pyramidal cells, as well as at intracellular sites (**Figure 73 D, crossed arrows**). Interestingly, quantitative analysis showed that 56% of all immunoparticles (323 out of 578 particles) were located along the plasma membrane of dendritic spines and dendritic shafts, while the remaining 44% of immunoparticles (255 out of 578 particles) were located at intracellular sites of those compartments. Presynaptically, GPR37-labeled immunogold particles (arrowheads) also localized in the extrasynaptic plasma membrane of axon terminals that establish asymmetrical synapses, thus excitatory, with spines (**Figure 73 E**).

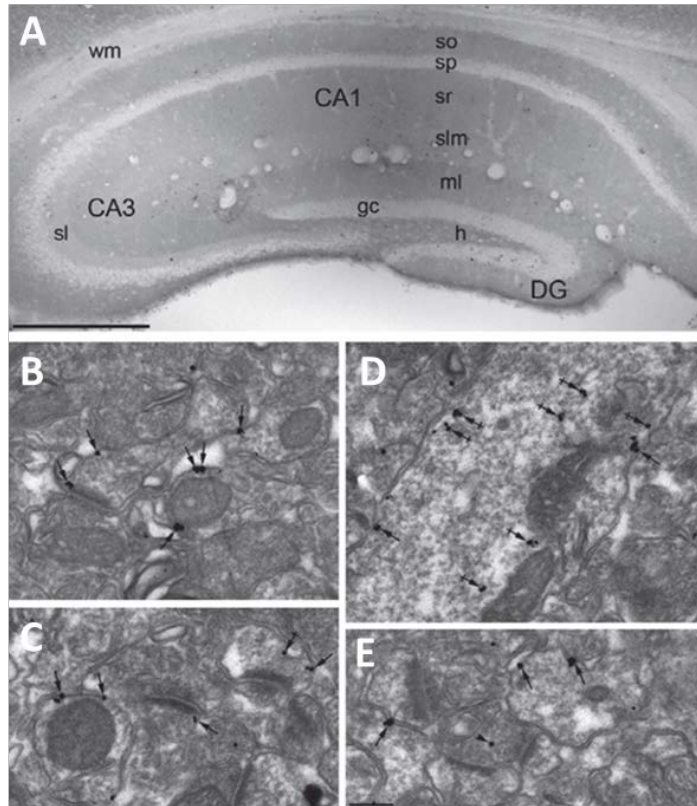


Figure 73. Distribution of immunoreactivity for GPR37 in the hippocampus. At the light microscopic level (**A**), immunoreactivity for GPR37 was widely distributed throughout the hippocampus. In the CA1 region, GPR37 immunolabeling was generally moderate in the strata oriens (so), radiatum (sr) and lacunosum-moleculare (slm). Similar immunoreactivities were observed in the CA3 region, with the exception of the stratum lucidum (sl) that showed the lowest immunoreactivity for GPR37. In the dentate gyrus, GPR37 immunolabeling was moderate in the molecular layer (ml) and in the hilus (h). Scale bar: A, 500 μ m. (**B-E**) Subcellular localization of GPR37 in the hippocampus. Electron micrographs of the stratum radiatum of the hippocampal CA1 region showed immunoparticles for GPR37, as detected using a preembedding immunogold method. Immunoparticles for GPR37 were observed along the extrasynaptic plasma membrane (arrows) of dendritic spines of pyramidal cells (s) contacted by terminals (at) of presumed CA3 pyramidal cells, as well as at intracellular sites (crossed arrows). Immunoparticles for GPR37 were also detected along the extrasynaptic plasma membrane (arrows) of dendritic shafts (Den) of pyramidal cells. Presynaptically, immunogold particles (arrowheads) were localized to the extrasynaptic plasma membrane of axon terminals (at) establishing asymmetrical synapses with spines (s). Scale bar: (B-E), 0.2 μ m. The results are representative of similar analysis carried out in 3 mice.

Finally, we attempted to determine the subsynaptic localization of GPR37 in hippocampal extracts. For this purpose, we performed subsynaptic fractionation of hippocampal nerve terminals, which allowed identifying the localization of GPR37 in pre-, post- and extrasynaptic enriched fractions (**Figure 74**). Interestingly, these immunoblots revealed an enrichment of GPR37 in the extrasynaptic fraction (**Figure 74 A**), thus corroborating the results obtained by means of electron microscopy. Accordingly, when GPR37 immunoreactivity was semi-quantified in the subsynaptic fractions, a preferential post-over presynaptic enrichment of the GPR37 was observed (**Figure 74 A-B**).

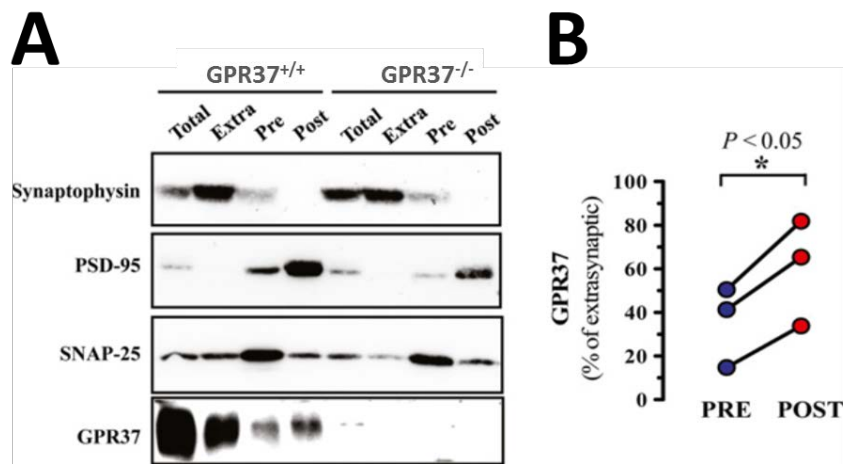


Figure 74. Subsynaptic distribution of GPR37 in the hippocampus. (A) Representative immunoblot showing GPR37 immunoreactivity in hippocampal synaptic fractions from GPR37^{+/+} and GPR37^{-/-} mice. Hippocampal synaptosomes (Total) were subcellularly fractionated (see “Materials and methods” section) into extrasynaptic (Extra), presynaptic active zone (Pre) and postsynaptic density (Post) fractions, which were analyzed by SDS-PAGE (20 μ g of protein/lane) and immunoblotted using the rabbit anti-GPR37 antibody as described the “Materials and Methods” section. **(B)** Relative quantification of GPR37 enrichment in hippocampal presynaptic and postsynaptic fractions. The intensities of the immunoreactive bands on the immunoblotted membranes corresponding to extrasynaptic, presynaptic (Pre), and postsynaptic (Post) fractions were measured by densitometric scanning. Values were normalized using the amount of GPR37 in the extrasynaptic fraction. Data from three independent experiments are shown. The asterisk indicates statistically significant difference: $p < 0.05$; paired Student’s t-test.

After establishing the subcellular and subsynaptic localization of GPR37 in the hippocampus, we aimed to determine if GPR37 controlled hippocampal synaptic plasticity (**Figure 75**). Comparison of PPF in the CA1 area of GPR37^{+/+} and GPR37^{-/-} mice showed that GPR37 deletion did not alter the hippocampal short-term plasticity at any of the inter-pulse intervals tested (i.e., 25, 50, 100 or 200 ms) (**Figure 75 A-B**).

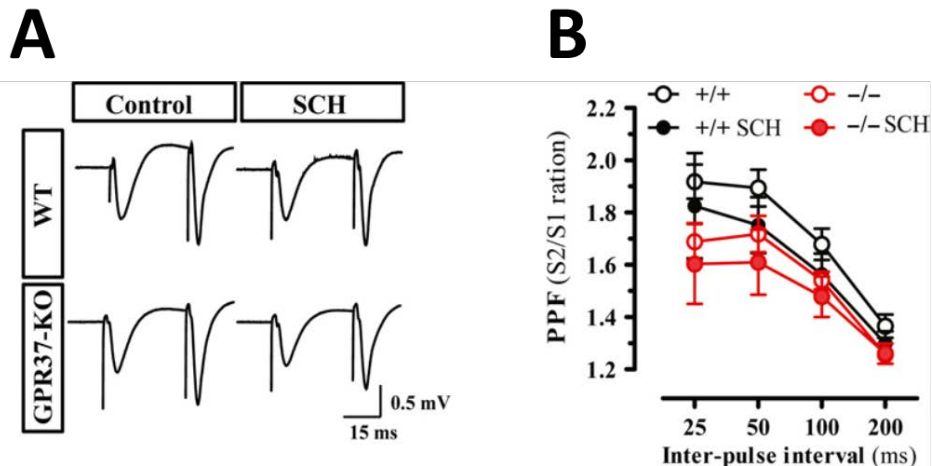


Figure 75. Deletion of GPR37 does not affect short term synaptic plasticity in the hippocampus. Effects of GPR37 deletion on short-term synaptic plasticity (paired pulse facilitation) in mouse hippocampal slices in the absence and in the presence of the A_{2A}R antagonist SCH58261 (SCH, 50 nM). **(A)** Representative traces of fEPSP paired with an inter-pulse interval of 25 ms recorded in the stratum radiatum of the CA1 area upon stimulation of the afferent Schaffer fibers. **(B)** The ratio of the second vs. the first fEPSP (P2/P1 ratio) with different inter-pulse intervals (25, 50, 100 and 200 ms) did not show significant differences between GPR37^{+/+} and GPR37^{-/-} mice either in the absence or presence of SCH58261 (right panel). The data are mean \pm SEM of 4–6 experiments carried out in different mice.

Next, we compared long-term plasticity both in GPR37^{+/+} and GPR37^{-/-} mice and no changes were observed in the amplitude of LTP (161% \pm 13% vs. 160% \pm 11%, respectively; n = 6) (**Figure 76 A-B**). Finally, we assessed the role of GPR37 in long term synaptic depression and we found that there were no significant differences in hippocampal depotentiation upon GPR37 deletion (97% \pm 2% vs. 103% \pm 3%, respectively) (**Figure 76 C-D**). Overall, GPR37 does not seem to directly play a role in the control of hippocampal synaptic plasticity.

Since GPR37 interacts with A_{2A}R and A_{2A}R play a pivotal role controlling hippocampal synaptic plasticity, we next aimed to evaluate whether the GPR37 deletion affected A_{2A}R-mediated modulation of hippocampal synaptic plasticity. To this end, we compared the effect on LTP of the selective A_{2A}R antagonist SCH58261 (50 nM) in slices from GPR37^{+/+} and GPR37^{-/-} mice. As shown in **Figure 75**, GPR37 deletion did not alter the impact of SCH58261 in hippocampal short-term plasticity at any of the inter-pulse intervals. When assessing long-term plasticity, A_{2A}R blockade significantly decreased LTP amplitude in GPR37^{+/+} mice (161% ± 13% vs. 116% ± 3%, *P* < 0.01), and this effect was similar to that obtained in GPR37^{-/-} mice (160% ± 11% vs. 126% ± 9%, *P* < 0.05) (**Figure 76 A-B**). However, when analyzing depotentiation, we observed that although in GPR37^{+/+} mice the amplitude of depotentiation was not altered by SCH58261 (97% ± 2% vs. 101% ± 4%, *P* > 0.05), in GPR37^{-/-} mice there was a significant increase in depotentiation upon SCH58261 treatment (103% ± 3% vs. 83% ± 3%, *P* < 0.05) (**Figure 76 C-D**). Overall, these results suggested that GPR37 may modulate some of the A_{2A}R-mediated effects on synaptic plasticity.

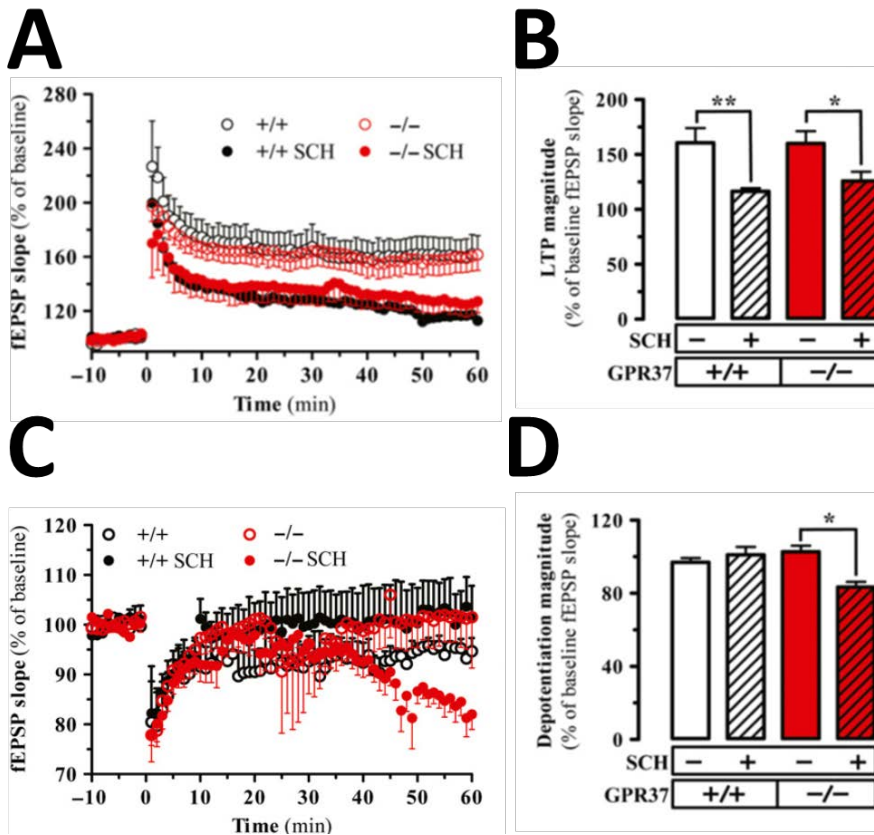


Figure 76. Deletion of GPR37 does not affect long term synaptic plasticity but alters the A_{2A}R-mediated control of depotentiation in hippocampal slices. (A) Average time course experiments of LTP induction, i.e., the variation in fEPSP slope over time upon induction of LTP with a HFS train (one train of 100 pulses of 1 Hz for 1 s) applied at time zero in hippocampal slices from WT and GPR37-KO animals either in the absence or in the presence of SCH58261 (50 nM). **(B)** The average LTP amplitude was significantly decreased by SCH58261 both in WT and GPR37-KO animals, whereas the elimination of GPR37 did not change LTP amplitude (right panel). The asterisks denote data significantly different: **p* < 0.05, ***p* < 0.01, one-way ANOVA with a Newman-Keuls post hoc test. **(C)** The left panel shows average time course depotentiation experiments, triggered by a low-frequency stimulation train (900 pulses of 1 Hz for 15 min) applied at time zero (60 min following the induction of LTP) in hippocampal slices from WT and GPR37-KO mice either in the absence or in the presence of SCH58261 (50 nM). Note that the baseline was normalized to 100% to allow a straightforward visual comparison between the different groups. **(D)** The right panel shows that the knock-out of GPR37 did not modify the amplitude of depotentiation in the absence of SCH58261, whereas the blockade of A_{2A}R with SCH58261 significantly increased the amplitude of depotentiation only in GPR37-KO but not in WT mice. The data are mean ± SEM of 4–6 experiments carried out in different mice. The asterisks denote data significantly different: **p* < 0.05, one-way ANOVA with a Newman-Keuls post hoc test.

Changes of GPR37 levels have been associated to behavioral alterations (245), a fact that prompted us to probe for modifications caused by the absence of GPR37 in hippocampal-dependent functions, including learning and memory as well as anxiety. Accordingly, we first assessed hippocampal-related working/reference memory by comparing the performance of WT and GPR37-KO mice in the novel object recognition test. Analysis of the preference for a novel object did not yield any differences between GPR37^{+/+} and GPR37^{-/-} mice (60% ±2% vs. 61% ±3%, respectively, **Figure 77**). Interestingly, while administration of SCH58261 (1 mg/kg, ip) to GPR37^{+/+} mice did not alter the preference for a novel object, in GPR37^{-/-} mice it was reduced when compared to vehicle-treated animals (49% ±3% vs. 61% ±3%, respectively; *P* < 0.01) (**Figure 77**).

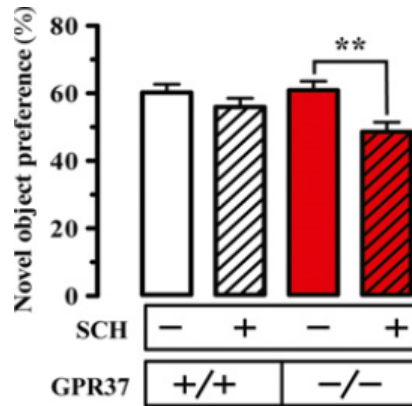


Figure 77. Effect of SCH 58261 in object recognition memory in GPR37^{+/+} and GPR37^{-/-} mice. GPR37^{+/+} and GPR37^{-/-} mice were treated with vehicle or SCH 58261 (1 mg/kg, i.p.) 15 min before novel object recognition test. Subsequently, the time exploring a novel object (novel object preference) was quantified during a 5 min session and then expressed as percentage of the total time exploring objects. The data are mean \pm SEM of ≥ 10 mice. The asterisks denote significant differences: * $P < 0.05$, ** $p < 0.01$, *** $p < 0.001$, one-way ANOVA with a Newman-Keuls post hoc test.

Next, we assessed the impact of GPR37 deletion in anxiety, another hippocampus-associated behavioral response (246). To this end, we used the Marble Burying test (MBT) and the Elevated Plus Maze (EPM) paradigm. In the MBT (**Figure 78 A**), GPR37^{-/-} mice displayed an anxiolytic behavior (less marbles buried, 4.4 ± 0.8 vs. 7.0 ± 0.6 in WT; $P < 0.01$). A similar effect was observed in the EPM test: thus, GPR37^{-/-} mice were less anxious, as reflected by the significantly greater time spent in the open arm when compared to GPR37^{+/+} mice ($80\% \pm 7\%$ vs. $55\% \pm 6\%$, respectively; $P < 0.05$) (**Figure 78 B**). These results suggested that GPR37 expression seems to be anxiogenic. As there are compelling evidences for a role of the A_{2A}R in stress, depression and anxiety (247)(248)(112), we evaluated the potential role of the A_{2A}R in the GPR37-mediated anxiety. Interestingly, while the administration of SCH58261 (1 mg/kg, i.p.) to GPR37^{+/+} animals did not affect anxiety-related behavior, it reverted the anxiolytic behavior of GPR37 expression (**Figure 78 A-B**). Thus, SCH58261 treated GPR37^{-/-} mice buried more marbles (8.2 ± 0.3 , $n = 9$; $p < 0.001$) in the MBT and spent less time ($52\% \pm 8\%$; $p < 0.05$) in the open arm in the EPM test compared to vehicle-treated GPR37^{-/-} mice, reaching a performance like that of GPR37^{+/+} mice (**Figure 78 B**). This ability of SCH58261 to rescue the anxiolytic behavior selectively in GPR37^{-/-} mice suggested a potential functional interplay between GPR37 and A_{2A}R. Although we did not detail the interaction between GPR37 and A_{2A}R in the control of motor function, the observation

that SCH58261-treated GPR37^{-/-} mice had a total number of entries in the EPM similar to non-treated GPR37^{-/-} mice (18.2 ±1.1 vs. 18.5 ±1.0, respectively) was indicative of a direct interaction of GPR37 and A_{2A}R in the control of mood-related behavior, independently of any additional interaction in the control of motor function.

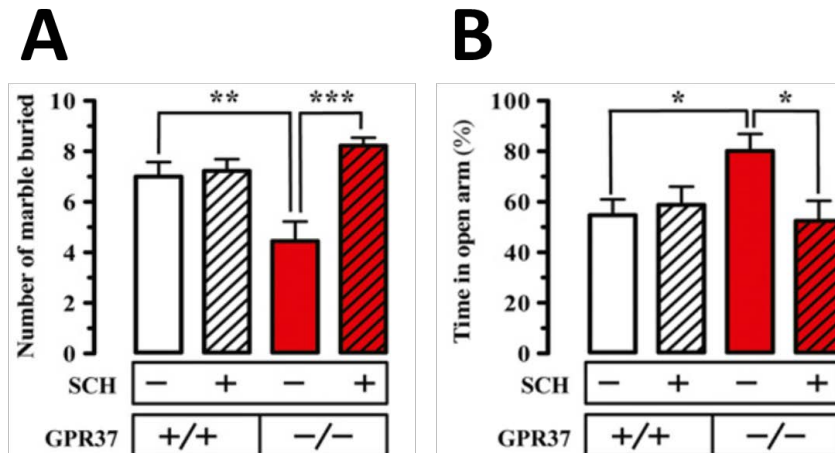


Figure 78. Effect of SCH 58261 in hippocampal-related behavior in GPR37^{+/+} and GPR37^{-/-} mice. GPR37^{+/+} and GPR37^{-/-} mice were treated with vehicle or SCH 58261 (1 mg/kg, i.p.) 15 min before behavioral evaluation. **(A)** In the marble burying test (MBT), the number of marbles buried during 30 min was quantified and represented as mean ± SEM. **(B)** In the elevated plus maze (EPM) test, the time spent in the open arms was monitored during 10 min and expressed as percentage of the total time spent in all arms. The data are mean ± SEM of ≥ 10 mice. The asterisks denote significant differences: *p < 0.05, **p < 0.01, ***p < 0.001, one-way ANOVA with a Newman-Keuls post hoc test.

Overall, we provided the first mapping of GPR37 within the hippocampus, where GPR37 is widely expressed and localized at the level of the extrasynaptic plasma membrane of dendritic spines, dendritic shafts, and axon terminals. GPR37 per se does not appear to play a role in learning and memory, since GPR37 deletion did not alter the performance in different hippocampal related memory tasks.

Chapter III

Ecto-GPR37 as a novel biomarker for Parkinson's disease

There are many evidences pointing to the relationship of GPR37 with PD neuropathology. Mostly, GPR37 has been shown to be up-regulated in AR-JP patients (143)(145) and accumulated in necropsies from PD patients with dementia (148) (see *introduction*). Thus, there are strong evidences indicating that GPR37 expression is altered in PD. Accordingly, we aimed to evaluate whether GPR37 expression is altered in substantia nigra necropsies from healthy and PD subjects. To this end, we first assessed the GPR37 band pattern detected by western-blot analysis of striatal membranes from mice using both our N- and C-terminal antibodies. Surprisingly, while the anti-N-terminal GPR37 antibody revealed a broad protein band of 55-63 kDa, the anti-C-terminal GPR37 antibody showed a band of 40 kDa (**Figure 79**). The specificity of these protein band detection was achieved by using striatal membranes from GPR37^{-/-} in the western-blot. This intriguing result revealed a peculiar GPR37 expression in native tissue, thus suggesting the existence of different coexisting GPR37 protein forms.

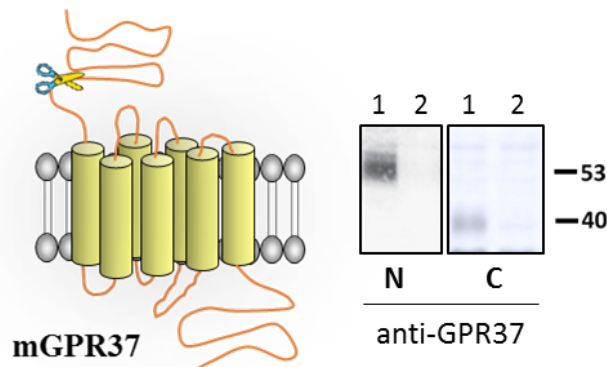


Figure 79. Detection of GPR37 in membrane extracts from mouse striatum. Membrane extracts (50 μ g) from the striatum of GPR37^{+/+} (lane 1) or GPR37^{-/-} mice (lane 2) were analyzed by SDS-PAGE and immunoblotted using either a rabbit anti-N-terminal mGPR37 (1 μ g/ml) or a rabbit anti-C-terminal GPR37 (1 μ g/ml). The primary bound antibody was detected using a horseradish peroxidase (HRP)-conjugated goat anti-rabbit antibody (1/30.000).

Subsequently, we assessed the GPR37 expression in human substantia nigra necropsies (**Figure 80**). Interestingly, the immunoblot using the anti-N-terminal GPR37 antibody revealed a major broad band between 53-63 kDa and another intense band at 40 kDa corresponding probably to the mature and N-terminal truncated human GPR37 respectively (**Figure 80**). Other less abundant protein bands at 67, 70 and 75 kDa were observed. Conversely, when the immunoblot was performed using the anti-C-terminal GPR37 antibody a 40 kDa main band was observed and a less abundant 53-63 kDa band was observed (**Figure 80**). Overall, these results revealed also the existence of similar coexisting GPR37 protein forms in human brain tissue, namely substantia nigra.

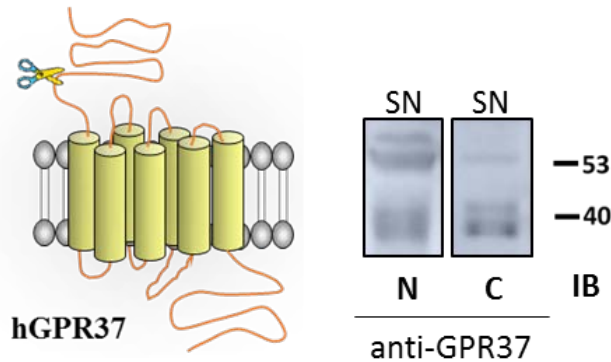


Figure 80. Detection of GPR37 in membrane extracts from human substantia nigra. Membrane extracts (50 μ g) from the human substantia nigra was analyzed by SDS-PAGE and immunoblotted using either a rabbit anti-N-terminal hGPR37 (1 μ g/ml) or a rabbit anti-C-terminal GPR37 (1 μ g/ml) (**B**). The primary bound antibody was detected using a horseradish peroxidase (HRP)-conjugated goat anti-rabbit antibody (1/30.000).

The different immunoblot pattern bands observed between mature and N-terminal truncated GPR37 in mouse and human native tissue could be due to a different N-terminal receptor processing by the metalloproteases, due to the different primary N-terminal antibodies used for the human and mouse GPR37 detection or due to differences between human and mouse samples collection. Next, we performed immunoblot analysis of PD post-mortem human brain samples to detect the protein expression levels of GPR37. Both mature and N-terminus truncated GPR37 protein levels were analyzed in the substantia nigra and increased levels of GPR37 were detected in Parkinson's disease individuals at stages 5-6 when compared with middle-aged healthy controls (HC) (**Figure 81**).

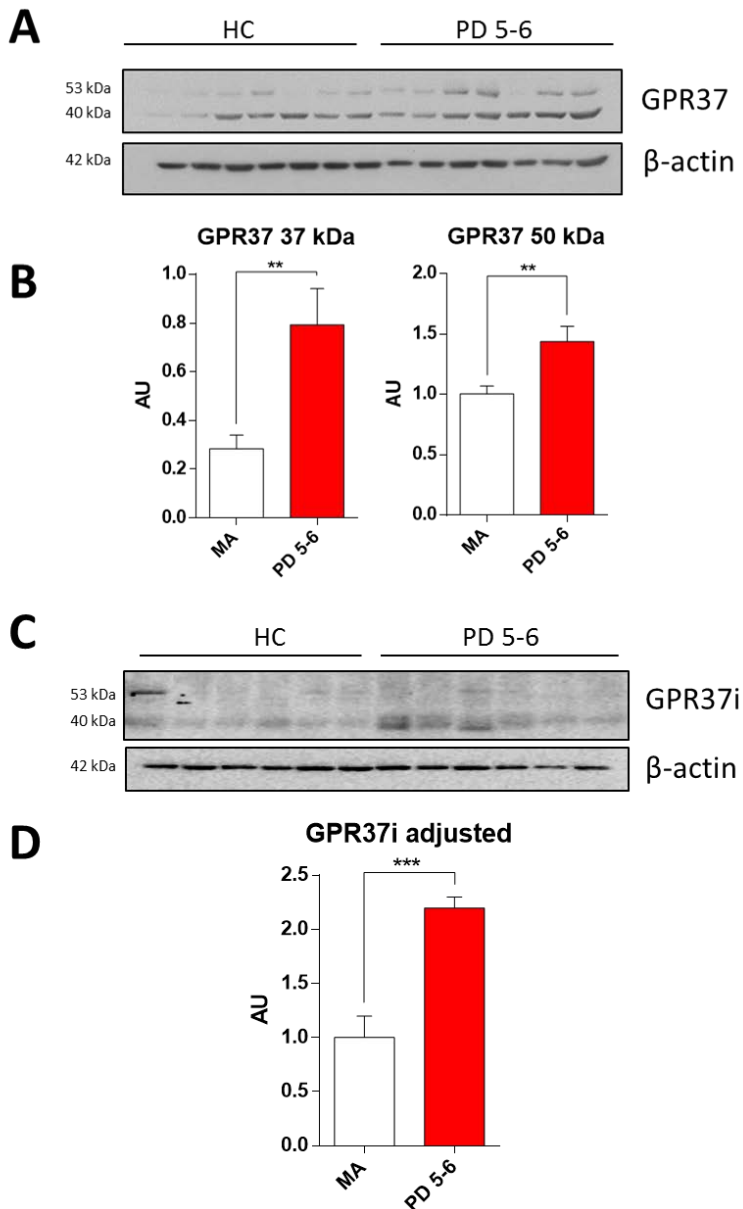


Figure 81. Analysis of GPR37 in substantia nigra membrane extracts from PD and HC human subjects. Protein expression levels of mature and N-terminus truncated GPR37 in total homogenate fractions of substantia nigra in healthy control cases and Parkinson's disease subjects. A significant increase in PD at stages 5-6 is detected in this region in comparison to HC cases. **(A-B)** Immunoblotting analysis using the N-terminal GPR37 antibody. **(C-D)** Immunoblotting analysis using the C-terminal GPR37 antibody. Protein normalization between samples was performed using β -actin. Statistical *t*-test was performed to compare groups. Significant p-values: * $p < 0.05$, ** $p < 0.01$, *** $p < 0.001$.

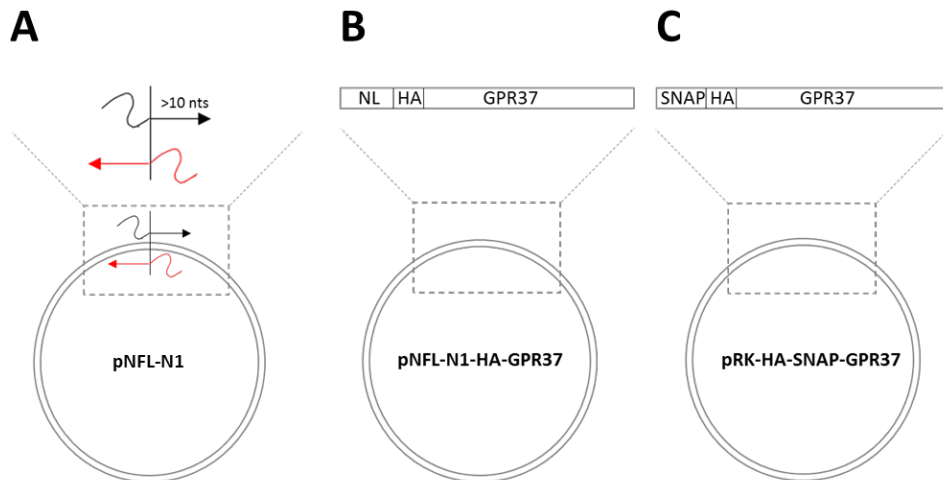
However, since these analysis were performed post-mortem, they do not provide information concerning the time-course of GPR37 relationship in PD neuropathology. Indeed, a main aim in PD current research consists of finding early biomarkers for the pathology. Biochemical and molecular markers for PD have been actively investigated in CSF and other body fluids. The most extensively studied candidate, in CSF, α -synuclein, is the major protein component of Lewy bodies and Lewy neurites, the pathological hallmarks of PD. The current consensus is that CSF α -synuclein concentrations are generally lower in PD patients due to α -synuclein accumulation in LB. However, both the sensitivity and specificity of these kinds of determinations are only moderate, and no correlation with PD progression has been observed (249)(250).

Recently, it was described that GPR37 is substrate from a proteolytic cleavage, which leads to the release of an N-terminal short domain (251). These information confirmed our previous results, in which by using an antibody targeting the C-terminal GPR37 domain we were able to observe both in mice and human native tissue a 40 kDa specific band. Interestingly, this band was 15-20 kDa shorter than the band observed with the N-terminal GPR37 antibody, thus suggesting the cleavage of the receptor once expressed at the cell surface, as previously reported in heterologous system (**Figure 79-80**). Accordingly, based on the data available, it seemed reasonable to attempt determining the GPR37 cleaved ecto-domain in different fluids, i.e. CSF, and if possible, to assess possible changes in different stages of PD.

Accordingly, we designed a novel strategy to detect ecto-GPR37 fragments in CSF using an in home-made Enzyme-linked immunosorbent assay (ELISA). ELISA is used to measure metabolites, hormones and proteins in cell, tissue, organ or body fluids (i.e. blood, CSF or urine). There are many variations on the ELISA method. In concrete, competitive ELISA is a strategy that consists of labeling purified antigen instead of the antibody. Unlabeled antigen from samples and the labeled antigen compete for binding to the capture specific antibody. A decrease in signal indicates the presence of the antigen in samples when compared to assay wells with labeled antigen alone. For the ecto-GPR37 Competitive ELISA assay we needed 3 elements: an specific antibody for the ecto-GPR37 capture and the labeled-unlabeled antigen for the quantification. The capture antibody would be the N-terminal GPR37 antibody produced in our lab raised against the human or mouse GPR37 and labeled-unlabeled antigen were produced taking advantage of the endogenous metalloproteinase activity of HEK-293T cell line. GPR37 overexpression in HEK-293T, undergoes N-terminal proteolytic cleavage of the GPR37. This procedure yields a cell line capable of producing spontaneously the ecto-

GPR37. To produce the labeled and unlabeled antigen we constructed several vectors that allow cloning of NanoLuciferase-HA (NL-HA) or SNAP-HA, respectively at the N-terminus of the orthologue mouse and human GPR37. Nanoluciferase (NL) is a newly developed small luciferase with the brightest bioluminescence reported to date. NL quantification was assessed by measuring luminescence at 480 nm in the presence of the substrate coelenterazine-h. SNAP-tag, a 20 kDa protein, was used as the unlabelled antigen due to the similar molecular weight to NL.

First, the hemagglutinin (HA) peptide, a 3 kDa amino acid sequence was introduced by point mutation in the pNFL-N1 vector (Promega) (**Figure 82 A**). This HA-tag was used to facilitate human and mouse NL ecto-GPR37 purification using HA-agarose resin after production in HEK-293T. The pRK-HA-SNAP vector was already available in the laboratory.



HA-tag: **TATCCGTATGATGT**GCCGGATTATGCG

Reverse: 5' **ACATCATACGGATACCCGCTCGAGCCGCCAG** 3'

Forward: 5' **GCCGGATTATGCGGCGATCGCTTCGGAATTCAGAGCTCAAC** 3'

Figure 82. Plasmids used for ecto-GPR37 Competitive ELISA reagents generation.

A) Graphic representation of the custom primers designed for the HA-tag insert mutagenesis in the pNFL-N1 plasmid. Half HA-tag was fused to forward and reverse primers without overlapping any nucleotide and HA-tag was introduced into the pNanoLucF1-secN plasmid using the Q5® Site-Directed Mutagenesis Kit. **B)** pNFL-N1-HA-GPR37 was transfected in HEK-293T cells to generate the NL-HA-ectoGPR37 (labelled antigen). **C)** pRK-HA-SNAP-GPR37 was transfected in HEK-293T cells to generate the HA-SNAP-ectoGPR37 (unlabelled antigen).

Labelled and non-labelled ecto-GPR37 products were produced and purified as follows. First, the cDNAs encoding NL-HA human- or mouse-GPR37 (labeled antigen) and SNAP-HA human- or mouse-GPR37 (unlabeled antigen) were overexpressed in HEK-293T cells (**Figure 82 B-C**). Thereafter, supernatant was collected and centrifuged to remove cellular debris and concentrated by means of centrifugal filter tubes. Once concentrated, the different proteins (ecto-domains of the GPR37, eGPR37) were purified by using an HA-agarose resin, which permitted to obtain free from impurities the NL-HA ecto-GPR37 or SNAP-HA ecto-GPR37 products. Luminescence from the NL-HA ecto-GPR37 fractions (1 mL) was rapidly assessed and the right expression of the protein confirmed by gel electrophoresis and immunoblotting. On the other hand, SNAP-HA ecto-GPR37 fractions were directly analyzed by Western Blot. The enriched 1 ml fractions containing the ecto-GPR37 products were mixed and dialyzed overnight in ELISA Wash Buffer at 4°C. The characterization of NL-HA-ecto-GPR37 and SNAP-HA-GPR37 was performed both for the mouse (**Figure 83**) and human (**Figure 84**) GPR37 homologue. Finally, luminescence measurements (when possible) and immunoblotting analysis, NL and SNAP human and mouse ecto-GPR37 products were characterized and stored at -20°C until use.

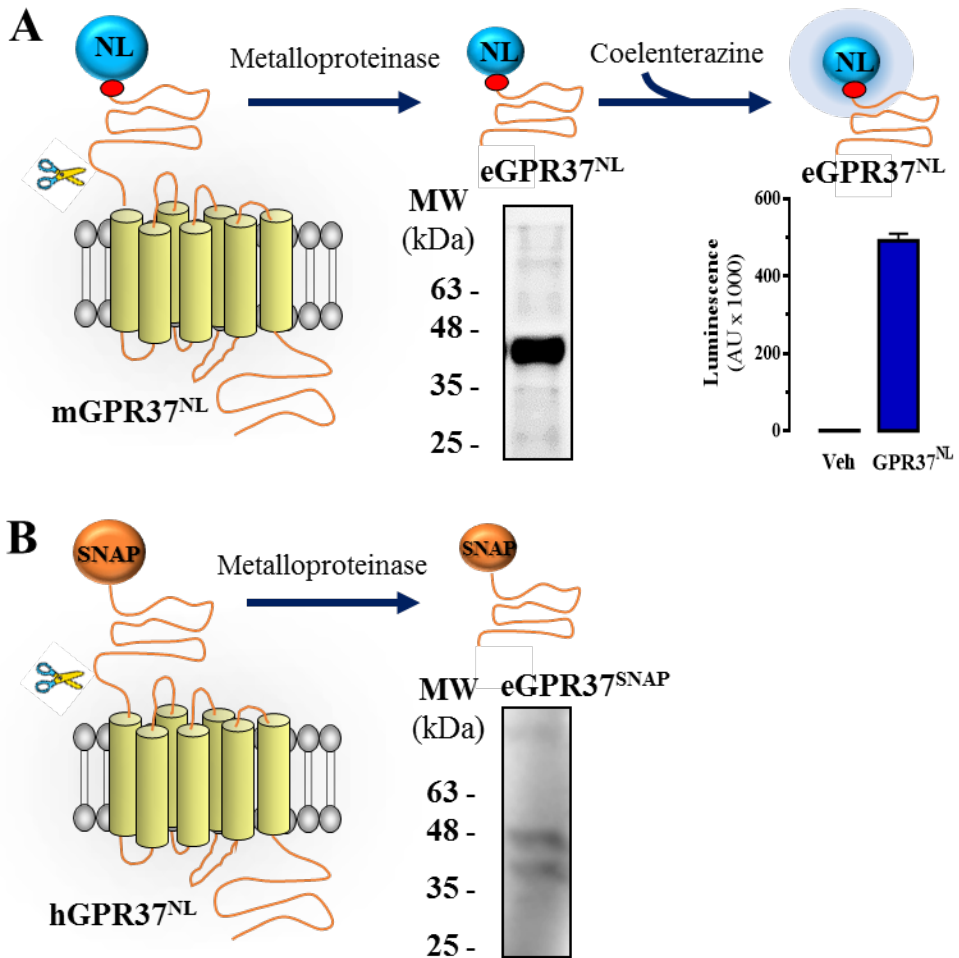


Figure 83. NL-HA and SNAP-HA mouse ecto-GPR37 purification and characterization. **A)** NL-HA mouse ecto-GPR37 was bound to the HA-agarose resin and eluted in 1 ml fractions by chemical elution. Fractions were analyzed both by immunoblotting and luminescence measurements and stored at -20°C until use. **B)** SNAP-HA mouse ecto-GPR37 were bound to the HA-agarose resin and eluted in 1 ml fractions by chemical elution. Fractions were analyzed by Western Blot and stored at -20°C until use.

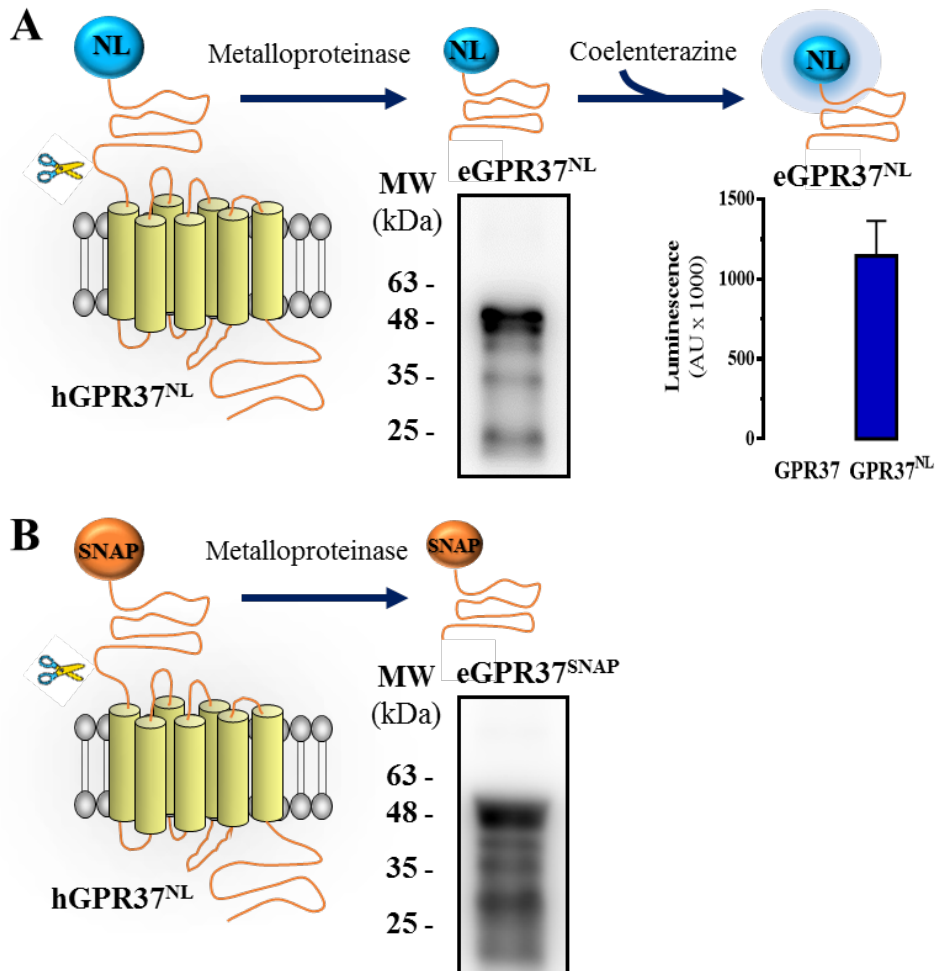


Figure 84. NL-HA and SNAP-HA human ecto-GPR37 purification and characterization. A) NL-HA human ecto-GPR37 was bound to the HA-agarose resin and eluted in 1 ml fractions by chemical elution. Fractions were analyzed both by immunoblotting and luminescence measurements and stored at -20°C until use. **B)** SNAP-HA human ecto-GPR37 were bound to the HA-agarose resin and eluted in 1 ml fractions by chemical elution. Fractions were analyzed by Western Blot and stored at -20°C until use.

In addition to luminescence measurements and immunoblotting analysis, the labelled (NL) and unlabelled (SNAP) mouse and human ecto-GPR37 products were characterized by LC-MSMS analysis. Interestingly, after trypsin digestion, LC-MSMS was performed by the Proteomic platform (Parc Científic de Barcelona) and showed that different N-terminal GPR37 peptides were present in the mouse ecto-GPR37 (**Figure 85**) and human ecto-GPR37 (**Figure 86**) purified products. Of note, these results were consistent with that obtained in immunoblotting experiments, in which a multiband pattern was obtained indicating a multiple proteolytic cleavage processing of the ecto-GPR37 (**Figure 83-84**).

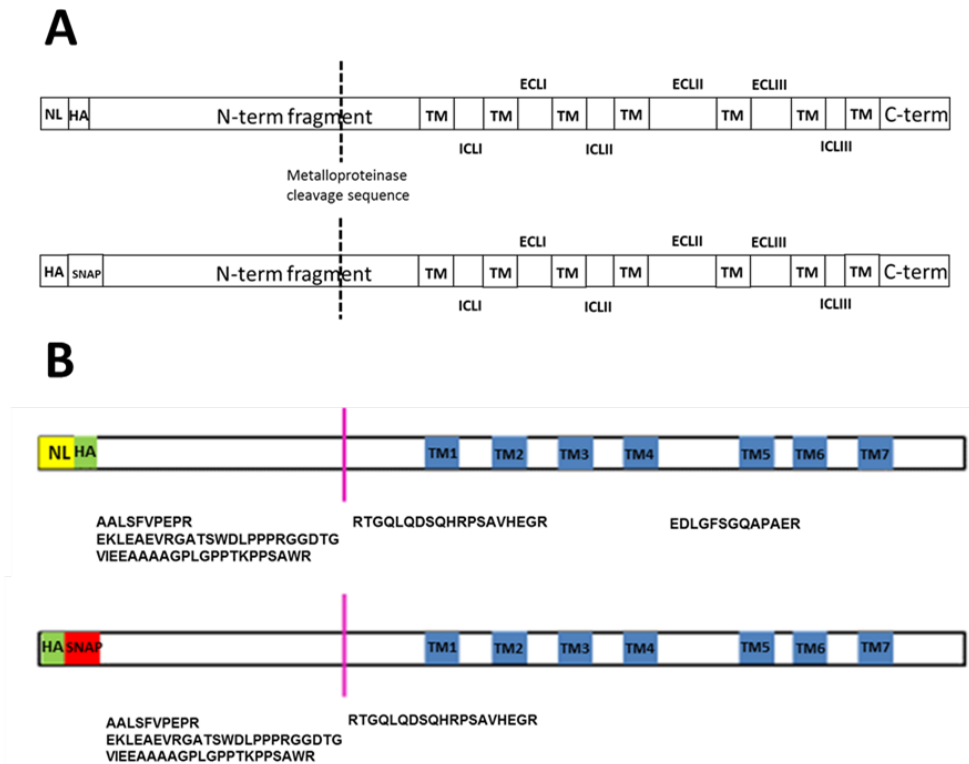


Figure 85. LC-MSMS analysis from the mouse ecto-GPR37 ELISA reagents: A. Schematic representation of the NL-HA and HA-SNAP mGPR37 overexpressed in HEK-293T. **B.** Purified mouse ecto-GPR37^{NL} and ecto-GPR37^{SNAP} were digested with trypsin and resulting peptides were analyzed and compared with a database containing the mouse GPR37 sequence.

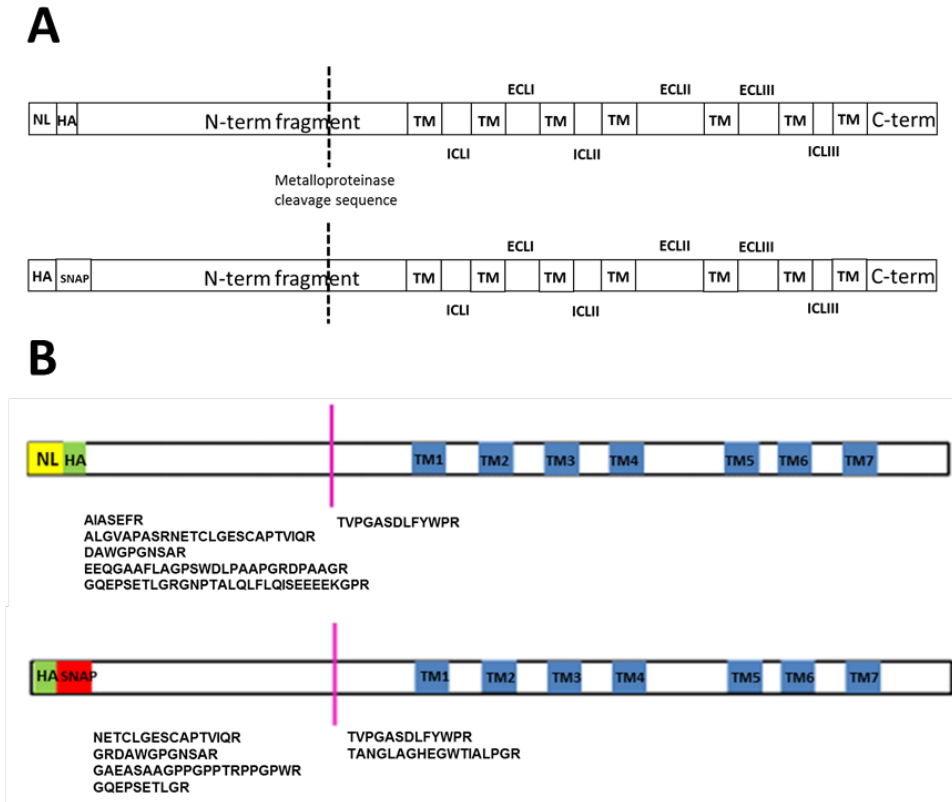


Figure 86. LC-MSMS analysis from the human ecto-GPR37 ELISA reagents: A. Schematic representation of the NL-HA and HA-SNAP mGPR37 overexpressed in HEK-293T. **B.** Purified human ecto-GPR37^{NL} and ecto-GPR37^{SNAP} were digested with trypsin and resulting peptides were analyzed and compared with a database containing the human GPR37 sequence.

Once we obtained the different ecto-GPR37 products, we aimed to validate whether they specifically bound the ELISA plate. Of note, we used streptavidin-coated plates to ensure high efficiency and selective binding of our proteins. Thus, the streptavidin coated plates were first blocked with DMEM complete. Thereafter, an anti-rabbit IgG-Biotin antibody was added. And finally, it was added a specific rabbit anti N-terminal human or mouse GPR37 (or a nonspecific antibody anti IgG as negative control). Once the plate was prepared, it was challenged the purified NL-HA human or mouse ecto-GPR37 and after extensive washing luminescence measured. Interestingly, it was observed a high specific signal-to-noise ratio. While increasing amounts of the NL-HA ecto-GPR37 produced a high positive and saturable luminescence signal when the N-terminal GPR37 antibody was bound to the plate, a quasilinear luminescence signal was observed when the C-terminal GPR37 or an IgG antibody was used (**Figure 87**).

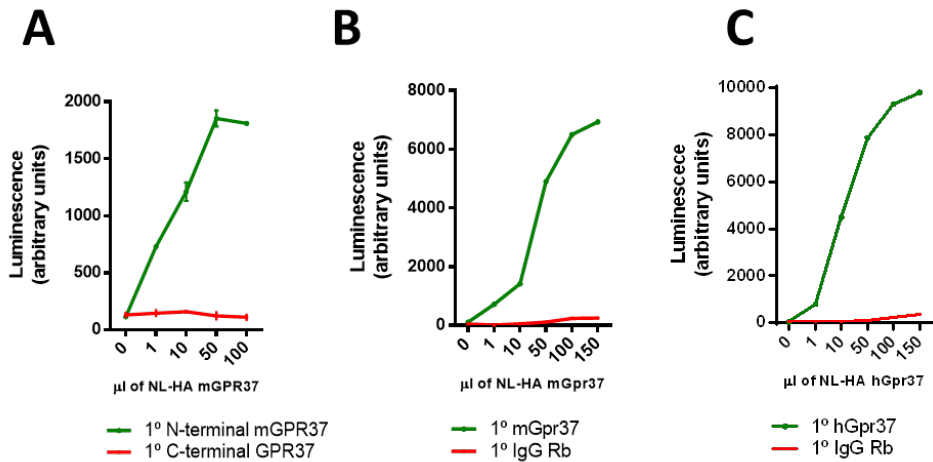


Figure 87. Specificity of the ecto-GPR37 Competitive Elisa. Specificity of the mouse (A) and human (B) ecto-GPR37 ELISA technique was validated by using the primary rabbit anti N-terminal mouse or human GPR37 antibody or a non-related (anti IgG) antibody as negative binding control. Plotted on the y-axis is the corresponding luminescence and on the x-axis the amount of NL-HA ecto-GPR37 used.

Noteworthy, the specificity of the assay was also assessed by using a negative control, a NL-containing construct with another receptor, namely the NL-A1R. Thus, when incubating the plate with the supernatant obtained from NL-A1R an increase in luminescence was not observed (Figure 88). Similarly, a dose-dependent increase in luminescence was not obtained when incubating the plate with a short version of the mouse GPR37 (without the ecto-GPR37) (Figure 88).

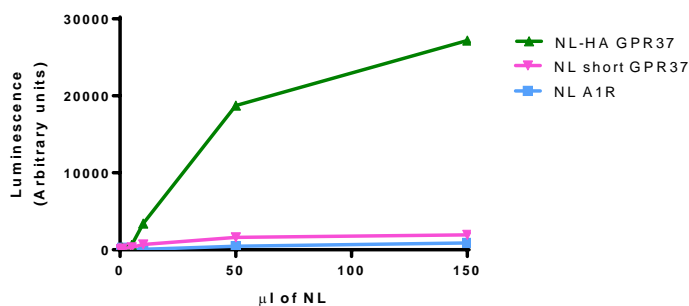


Figure 88. Specificity of the ecto-GPR37 Competitive Elisa. Specificity of the human ecto-GPR37 ELISA technique was validated by using the rabbit anti N-terminal human GPR37 antibody with the NL-HA human ecto-GPR37, with the supernatant obtained from NL-A1R or with supernatant obtained from a short version of the mouse GPR37 (without the ecto-GPR37). Plotted on the y-axis is the corresponding luminescence and on the x-axis the amount of NL used.

Then, we assed the quantification of the ecto-GPR37 in biological samples (following schematic representation of **Figure 89**).

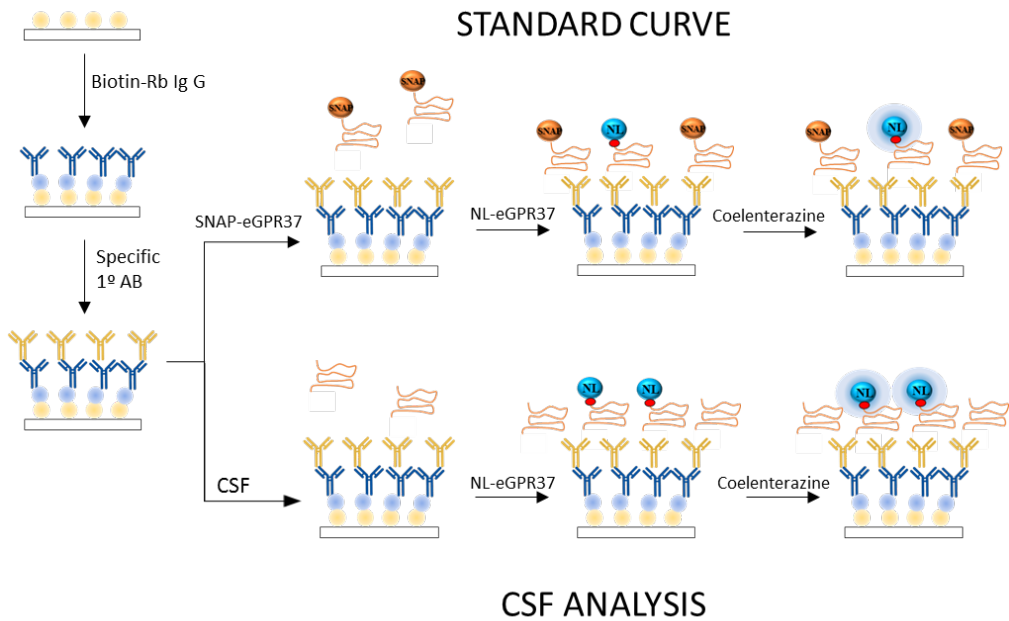


Figure 89. Step by step diagrammatic illustration of ecto-GPR37 Competitive ELISA method. As described previously in the section Competitive ELISA, Streptavidin plates were treated incubated with Biotin-Rb IgG and secondly the primary rabbit specific antibody was added (i.e. N-terminal GPR37, C-terminal GPR37 or IgG). Next, plates were incubated overnight with SNAP-GPR37 or CSF. The following day, NL-GPR37 was incubated and after NL substrate addition, luminescence signal was measured. and signal was inversely proportional to the amount of eGPR37 present in the sample.

Small peptides from the ecto-GPR37 have been previously described in human CSF. Thus, we collected CSF from GPR37 $+/+$ and GPR37 $-/-$ mice. Increasing amounts of GPR37 $+/+$ and GPR37 $-/-$ CSF were analyzed. In parallel, a standard curve was generated by incubating increasing amounts of SNAP-HA mouse ecto-GPR37. Interestingly, significant differences were obtained between GPR37 $+/+$ and GPR37 $-/-$ CSF. While increasing amounts of GPR37 $+/+$ CSF decreased luminescence signal, increasing amounts from GPR37 $-/-$ CSF did not decrease the luminescence (**Figure 90**). In parallel, we performed bicinchoninic acid (BCA) assay for the quantitation of the total protein present in the CSF and no significant differences were observed between GPR37 $+/+$ ($0.499 \pm 0,01332 \mu\text{g}/\mu\text{l}$) and GPR37 $-/-$ ($0.479 \pm 0,01450 \mu\text{g}/\mu\text{l}$) CSF.

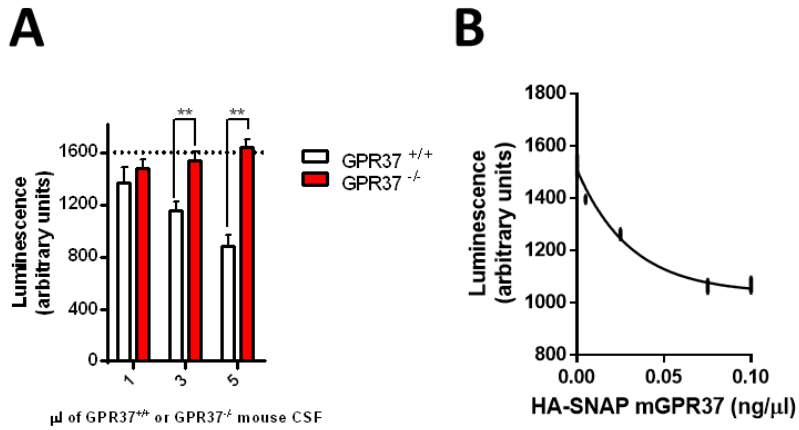


Figure 90. Determination of ecto-GPR37 in mouse GPR37^{+/+} and GPR37^{-/-} CSF. **A.** Increasing amounts of GPR37^{+/+} and GPR37^{-/-} mouse CSF were incubated and luminescence signal was measured. **B.** Standard curve using increasing amounts of SNAP-HA mouse GPR37. Plotted on the y-axis is the corresponding luminescence and on the x-axis the amount of NL used. **p < 0.01, t Student.

Next, we analyzed the presence of the ecto-GPR37 in serum from GPR37^{+/+} and GPR37^{-/-} mice and no differences were observed (**Figure 91**). Quantification of the total protein present in serum was also assed and no differences between GPR37^{+/+} (44.35±0.806 µg/µl) and GPR37^{-/-} (44.17±0.726 µg/µl) were observed.

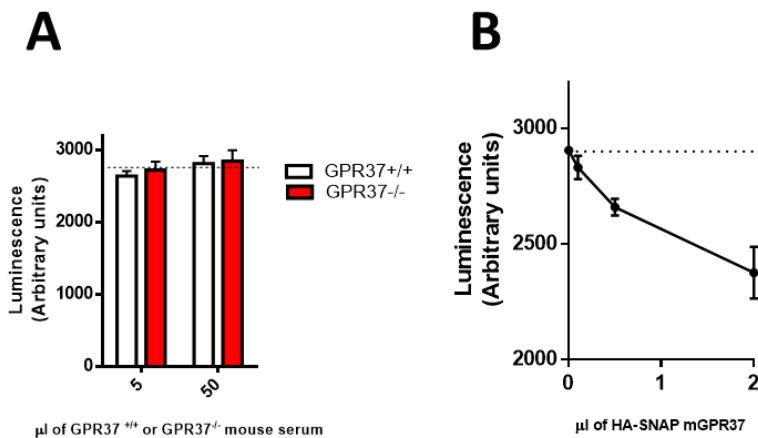


Figure 91. Determination of ecto-GPR37 in mouse GPR37^{+/+} and GPR37^{-/-} serum. **A.** Increasing volumes of GPR37^{+/+} and GPR37^{-/-} mouse serum were incubated and luminescence signal was measured. **B.** Standard curve was generated in parallel by using increasing amounts of SNAP-HA mouse GPR37. Plotted on the y-axis is the corresponding luminescence and on the x-axis the amount of NL used.

Finally, we measured the ecto-GPR37 in CSF human samples from PD and healthy subjects. PD and HC CSF samples had a similar collection post-mortem time (6.7 ± 1.7 vs 6.7 ± 0.7 , respectively). Similar to previously described, Streptavidin coated plates were blocked and incubated with the anti-rabbit IgG-Biotin antibody and secondly the specific rabbit anti N-terminal human GPR37. Then, 3 μ l of human CSF were incubated overnight. Following day, NL-HA human ecto-GPR37 was incubated for 1 hour and after extensive washing luminescence was measured (**Figure 92**). Interestingly, significant differences in luminescence signal were obtained between PD and healthy subjects. Lower luminescence signals were obtained in PD suggesting increased levels of ecto-GPR37 in the CSF (**Figure 92**).

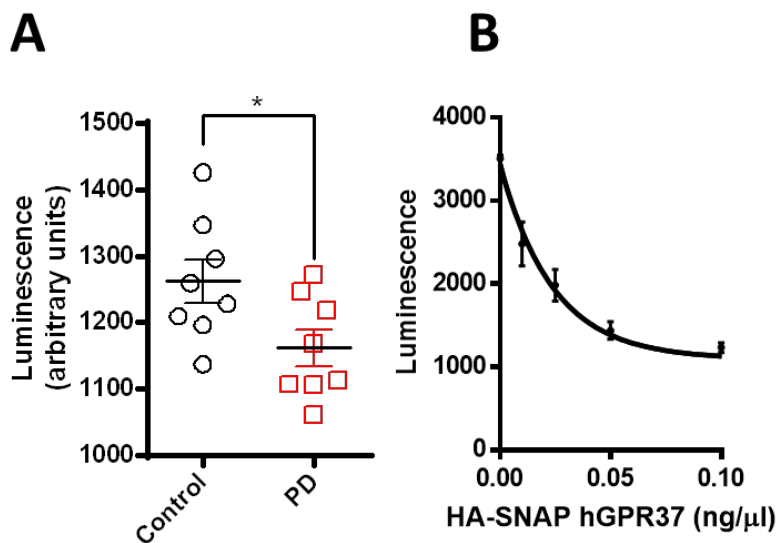


Figure 92. Detection of human ecto-GPR37 in CSF from post-mortem healthy and PD patients. A. Detection of ecto-GPR37 in CSF from healthy (control) and Parkinson disease (PD) necropsies. $P < 0.05$ t Student. **B)** Standard curve was generated in parallel by using increasing amounts of SNAP-HA human GPR37. Plotted on the y-axis is the corresponding luminescence and on the x-axis the amount of NL used.

In conclusion, increased GPR37 levels have been observed in SN post-mortem samples of PD patients when compared with HC. Ecto-GPR37 is generated in plasma membrane of neurons after cleavage of the N-terminal fragment by specific metalloproteinases and subsequently this ecto-GPR37 peptides are liberated to the CSF. We have developed a method to detect this ecto-GPR37 in CSF and ecto-GPR37 could potentially be used for PD diagnosis.

VI. Discussion

GPCRs are the largest family of signaling proteins, encoded in animals by 3–5% of all genes. Mammals have ~800–1000 GPCR subtypes, which display the propensity to bind and respond to a high number of ligands (i.e. agonists, antagonists or allosteric modulators), facilitating a plethora of functional outcomes (252)(253)(3). In addition, GPCRs exhibit the ability of functioning not only as individual receptors but also forming complexes with others (i.e. homo- or heterodimers, higher-order oligomers), a fact that may still increase the diversity of functions elicited (56)(254)(255). All together, GPCRs are the main current targets in drug development for a myriad of pathologies (i.e. PD, AD, cardiovascular diseases, etc) (256)(257).

GPR37 is an orphan GPCR highly expressed in different brain regions, such as corpus callosum, cerebellum, striatum and hippocampus, but the physiological function of this receptor has not been elucidated yet. On the other hand, GPR37 has been associated to PD neuropathology. For instance, it has been reported GPR37 up-regulation in brains, and also the presence of GPR37 in Lewy bodies, from PD patients. To elucidate the role of GPR37 in PD development, most studies have focused on revealing the interaction of this receptor with different neurotransmission systems. In such way, it has been proposed that GPR37 may interact with D₂R and A_{2A}R to form receptor-receptor complexes. Indeed, the existence of a direct receptor-receptor interaction between A_{2A}R and D₂R in the striatum was recently demonstrated and proposed, thus it could be postulated that the involvement of GPR37 in PD is related to its interaction with striatal A_{2A}R and/or D₂R (258)(63).

Our first aim consisted of elucidating the existence and functional consequences of a direct GPR37-A_{2A}R receptor-receptor interaction in the striatum. In addition, it was recently reported, by using a modified Membrane Yeast Two-Hybrid (MYTH) approach, that GPR37 may be a putative A_{2A}R interacting partner. Indeed, the direct GPR37-A_{2A}R receptor-receptor interaction was validated in HEK-293T cells by means of different biochemical and biophysical techniques (223). Also, it was previously described that co-expression of GPR37 with A_{2A}R, and also D₂R, had notable effects on plasma membrane expression of GPR37 (153). Accordingly, we aimed to further explore the biological relevance of this direct receptor-receptor interaction *in vivo*. First, we studied the subsynaptic distribution of GPR37 in striatum. Our results, using both immunogold labeling and biochemical analysis, showed that GPR37 is enriched at the postsynaptic over the presynaptic level, which represents a similar distribution to that observed for the A_{2A}R in the striatum. These results are in controversy with those previously published, in which it was described a presynaptic enrichment of GPR37 in synapses (63). Here, it is

important to note that a number of technical issues are critical to obtain reliable data. Thus, pre- and postsynaptic solubilization is directly related to pH, which is a key point in the subsynaptic fractionation protocol. In such way, if extra-, pre- and postsynaptic fractions are not properly solubilized and an enrichment of the synaptic markers is not observed in the predicted fraction, the subsynaptic localization of the different receptors under study may not be precise. Furthermore, our results are supported by two different approximations giving a strong robustness (76)(259).

Next, we assessed the existence of GPR37/A_{2A}R heteromers in the mouse striatum. We designed a multi-modal approach in which different techniques were used, namely Co-IP, double-labeling immunogold electron microscopy and P-LISA. Importantly, striatum from GPR37^{-/-} mice were used as negative control to assess specificity of the different methods. Our results strongly support the existence of a close proximity between these two receptors in the mouse striatum. Needless to say, a direct PPI can not be ensured by Co-IP, but it strongly suggests close proximity between two different proteins. Of note, mild detergents should be used in order to preserve membrane complexes (260). On the other hand, both immunogold labeling and P-LISA permitted a more consistent conclusion. Hence, the spatial resolution of double immunogold labeling is ~21 nm and the maximal distance between the secondary antibodies in the P-LISA assay is ~16 nm. Thus, these methodologies are quite close to the resolution of the most reliable approach used to undeniably demonstrate GPCR oligomerization, this is, resonance energy transfer, which allow to reveal protein-protein interactions in the order of ~10 nm. Notably, we and others recently demonstrated the reliability of the different techniques used in this work to reveal the existence of direct receptor-receptor interactions in native tissue (225)(261), thus we can conclude that this approach also validated the existence of GPR37/A_{2A}R heteromers in striatum.

Apart from demonstrating GPR37/A_{2A}R oligomerization, we were also able to unravel some of the characteristics of such protein-protein interaction. In such way, the following findings shed light regarding the function for the new striatal GPR37/A_{2A}R heteromer: i) GPR37 and A_{2A}R showed high and selective anatomical proximity within striatal spines and, therefore, its distribution in the striatum is similar to the previously described for the D₂R-A_{2A}R oligomer; ii) GPR37 deletion potentiated A_{2A}R cell surface targeting in striatal slices. This finding, together with the previously described increased DAT membrane expression in the presynaptic fraction in striatum of GPR37^{-/-} mice (63), could explain the enhanced response to A_{2A}R ligands; iii) A_{2A}R-mediated signaling was enhanced in nerve terminals and in primary cultures from GPR37^{-/-} mice. All together, these data highlighted

a bidirectional interaction between GPR37 and A_{2A}R in which they would modulate the heteromer partner functioning. Thus, putting together the present and previous results in which it was reported a A_{2A}R chaperone-like function that rescues GPR37 from intracellular accumulation (52), it would seem likely that receptor membrane expression and function is finely controlled by the formation of the GPR37/A_{2A}R oligomer.

Once ascertained the existence of striatal GPR37/A_{2A}R heteromers, we aimed to assess the impact of this oligomer in behavioral functions. With this purpose, we evaluated two behavioral responses strongly related with the striatum: locomotor activity and cued learning (262)(219)(263). Notably, we used A_{2A}R ligands to study the impact of GPR37/A_{2A}R oligomerization, since still does not exist a specific ligand for GPR37. In such way, different peptides have been proposed to proceed to GPR37 de-orphanization. The first ligand proposed to be the endogenous partner of GPR37 was HA (264). However, independent studies failed when attempting to replicate the finding that HA is a ligand for GPR37. Thus, it was not possible to find evidences for either HA-mediated internalization, ERK1/2 phosphorylation or cAMP stimulation (265). More recently, GPR37 and GPR37L1 were simultaneously paired with the endogenous protein prosaptide (or the synthetic analog TX14A) based on ERK1/2 phosphorylation and inhibition of forskolin-stimulated cAMP in HEK-293T cells co-expressing each receptor (141). Again, the claim that prosaposin and prosaptide are endogenous ligands for GPR37 and GPR37L1 is under debate. Thus, these results have not been independently validated by other groups and are yet to be ratified by the International Union of Basic and Clinical Pharmacology (IUPHAR) Nomenclature Committee. Hence, it seems clear that further studies are still required to understand the complex interplay between prosaptide and GPR37, and consequently to find out the endogenous ligand for GPR37, which indeed would accelerate and facilitate deciphering the role of this receptor in the brain.

Several evidences have revealed a role for A_{2A}R, which are localized at high density in the striatum, on the modulation of striatal processes such as locomotor activity. Importantly, the mechanism by which adenosine affects motor functions has been attributed to its ability to modulate dopamine-mediated signaling. Thus, apart from the above-mentioned direct receptor interaction between A_{2A}R and D₂R, it has been described that A_{2A}R stimulation reduce the affinity of dopamine for D₂R, or that D₂R activation partially inhibits and slows the binding association of A_{2A}R agonists (266). Interestingly, it was described that both systemic or intrastriatal administration of CGS21680, a selective A_{2A}R agonist, reduced spontaneous locomotor activity in rodents

and at higher doses, induced catalepsy (93); while the administration of SCH58261, a selective A_{2A}R antagonist, enhanced spontaneous locomotor activity and reduced haloperidol-induced catalepsy (232). In addition, increasing evidences suggest that A_{2A}Rs may also operate independently from D₂Rs to modulate locomotor activity. Thus, it has been shown that adenosine through A_{2A}R controls locomotion in conditions where dopamine or D₂R activity is lowered or absent (i.e. in PD patients, haloperidol-induced catalepsy model) (267). Here, we showed data supporting the notion that GPR37 is a negative modulator of A_{2A}R cell function *in vivo*. Hence, GPR37 deletion potentiated A_{2A}R antagonist-mediated increased locomotor activity and showed enhanced agonist-induced catalepsy, probably due to the observed increase of A_{2A}R membrane expression levels. Importantly, catalepsy is considered to be associated with reduced dopaminergic transmission, thus a functional interplay between GPR37, A_{2A}R and D₂R may be inferred from these results.

Importantly, in GPR37^{-/-} mice we did not observe changes, with respect to wild type mice, in spontaneous locomotor activity. These results may be in controversy with some reported data. Thus, GPR37^{-/-} mice were previously shown to display some motor alterations (149). Needless to say, although the mouse strain used in the two studies was similar, the reporter gene and vectors used for the generation of the null mice were different. Alternatively, some of the divergences in terms of locomotor activity for GPR37^{-/-} mice could be related to gender and age. Hence, a study described that while adult (4–6-month-old) females did not display any locomotor alteration in the open field arena over a 15-min period (245), 3-month-old GPR37^{-/-} males showed reduced locomotor activity over a 20–30-min period, but not when evaluating a 10-min period. Collectively, these differences may account for the divergences observed in the spontaneous locomotor activity of the GPR37^{-/-} mice. Moreover, the age of the animals used in our behavioral tests was distinct. In our hands, the spontaneous locomotor activity of 2-month-old GPR37^{-/-} males was not altered when a 10-min period was evaluated. Taking everything into account, GPR37^{-/-} clearly showed increased striatal A_{2A}R enhanced activity in synaptosomes and striatal primary cultures, and showed increased response after acute treatment with both A_{2A}R agonists or antagonists in striatum-related behavioral tasks.

The striatum, the main input structure of the basal ganglia, is not only responsible for motor control but it is also involved in learning/reward behavior. Indeed, striatal A_{2A}R are critical regulators of corticostriatal synaptic plasticity. Previous results supported the notion that changes in GPR37 expression affected A_{2A}R activity (153), thus we studied

the involvement of GPR37 in the A_{2A}R control of synaptic plasticity. Importantly, in GPR37^{-/-} mice we did not observe changes on the cued reference memory with respect to wild type mice. Previously it was reported that acute blockade of adenosine receptors does not alter LTD induction or expression (212). As A_{2A}R activation per se had no effect on glutamate release or basal excitatory synaptic transmission, the principal role of A_{2A}R in striatal glutamatergic afferents might not be a direct control of neurotransmitter release but rather a fine-tuning of other modulatory systems (268). Therefore, we first evaluated the effects of acute treatment of SCH58261, but we did not observe an effect in synaptic plasticity. Next we treated GPR37^{+/+} and GPR37^{-/-} mice chronically. In this chronic model, we observed that GPR37^{-/-} showed locomotor sensitization and increased synaptic depotentiation. It has been previously described that chronic treatment with SCH58261 increased dopamine levels in striatum and elicited locomotor sensitization (200). Also, several in vitro studies have shown that activation of DRs are a critical requirement for LTD to occur at corticostriatal synapses (269). Indeed it has been observed that D₁R and D₂R antagonists block the induction of LTD, and this form of synaptic plasticity is absent in mice lacking D₂R. Indeed, some studies related the chronic blockade of A_{2A}R with increased phosphorylation of DARPP-32, which plays an important role in neuronal plasticity (270) and participates in the generation and expression of behavioral sensitization to psychostimulants (271). Furthermore, high dopamine levels cause a weakening of indirect-pathway synapses and strengthening of direct-pathway synapses, leading to increased locomotor behavior required to forage for food. Indeed, the behavioral state of an animal can influence the direction of striatal plasticity observed. In animal behavioral models, it was observed that chronic treatment with A_{2A}R antagonists caused motor sensitization, increased dopamine levels in striatum and D2/D3 increased affinity for dopamine (272)(273).

A number of studies have shown that sensitization of locomotor activity indicates the incentive motivation properties of abuse drugs, which is believed to contribute to the intensification of drug craving and compulsive drug-seeking behavior (274). Also, it has been observed that repeated administration of cocaine and amphetamine resulted in psychomotor sensitization and was associated with increased DARPP-32 phosphorylation (275). The main effect of cocaine in dopaminergic terminals is the blockade of the presynaptic transporter-mediated dopamine uptake, which leads to an increase in dopamine availability at the synaptic cleft and the consequent stimulation of D₂R. We thus evaluated the effects of cocaine, and in agreement with other studies showing that acute administration of cocaine in corticostriatal synapses decreases synaptic transmission, we observed that in our animals, cocaine-induced depression of

synaptic transmission and this synaptic transmission depression was enhanced by the lack of GPR37 (276). This effect is unlikely to be presynaptic, since the genetic deletion of GPR37 did not interfere cocaine-induced paired-pulse facilitation, as observed when comparing PPS of GPR37^{-/-} and control littermates. The relevance of GPR37 in the context of cocaine addiction has to be properly addressed but the increase of the acute impact of cocaine in slices from GPR37^{-/-} mice indicates that it might facilitate the triggering of the synaptic plasticity events taking place during the chronification of the process.

Our major aim consisted of assessing the impact of GPR37 in the striatum, since this is the main brain region involved in PD. However, we were also interested in elucidating the presence and function of GPR37, and the interaction with A_{2A}R, in other brain nuclei. Accordingly, our second aim consisted of exploring the role of GPR37 in the hippocampus and attempting to elucidate a possible functional interaction with the A_{2A}R controlling some hippocampal-related functions (i.e. memory and anxiety). We first studied the distribution of GPR37 in the hippocampus and its subsynaptic distribution. Interestingly, we observed that GPR37 was broadly distributed throughout the hippocampus, being present in the CA1 and CA3 as well as in the dentate gyrus. Although high levels of GPR37 mRNA were found by others in glial cells of the fiber tracts (277), we observed that GPR37 was preferentially localized postsynaptically, when compared with the presynaptic fraction of dendritic spines and dendritic shafts of pyramidal cells, while low immunogold labeling was found in glial cells. In addition, GPR37 was localized at the plasma membrane in a similar proportion as found intracellularly. These findings are consistent with previous reports, which showed an accumulation of GPR37 in intracellular compartments (278)(144), from where the receptor was trafficked to/from the plasma membrane (279).

Next, we studied the role of GPR37 in hippocampal-based memory tasks, which are learning and memory (246). Our behavioral assessment showed no effect of GPR37 deletion on working/reference memory. Similarly, no significant effect of GPR37 deletion was found both in terms of short-term synaptic plasticity and LTP and its reversal, depotentiation. These results suggested that GPR37 does not play a prominent role in hippocampal dependent memory functions, and that per se, the elimination of GPR37 does not alter synaptic plasticity. On the other hand, GPR37^{-/-} mice displayed an anxiolytic behavior compared to GPR37^{+/+} mice. Thus, both the MBT and the EPM paradigms showed that deleting GPR37 triggered a significant decrease in anxiety. These results contrast to those reported previously (245), in which increased anxiety was

observed in GPR37^{-/-} mice. These differences may be attributed to several reasons including age or gender; our data, for instance, were obtained from 2-month-old males differently from those previously obtained in aged (16–18-month-old animals) female GPR37^{-/-} mice. Nevertheless, it seems clear that GPR37 deletion impacts on anxiety behavior. Consequently, it would be interesting to further study the mechanisms mediating this effect (i.e., changes of the behavior of GPR37^{-/-} mice previously stressed).

Similar to GPR37, A_{2A}R has been linked to stress and anxiety (248)(97). Indeed, A_{2A}R deletion produces an anxiogenic phenotype (247), while the over-expression of A_{2A}R causes anxiolytic effects (112). These observations, together with the fact that co-expression of A_{2A}R with GPR37 impacts the surface density of this last receptor (52), may suggest a possible interaction of both receptors to control hippocampal-related anxiety behavior. Interestingly, our results supported the notion that changes in GPR37 expression affect the activity of A_{2A}R. Thus, knocking out GPR37 bolstered the effect of the A_{2A}R antagonist, SCH58261, in synaptic depotentiation. In addition, SCH58261 reduced the novel object recognition memory only in GPR37^{-/-} mice, an unexpected result in view of the well described pro-cognitive effects of A_{2A}R antagonists (69). This ambiguous result evidences an intricate GPR37 involvement in working memory processing, which might indeed involve other neurotransmitters (i.e., dopamine, serotonin) and brain areas (i.e., cortex, striatum). Another surprising finding was the observation that A_{2A}R blockade restored the effects of GPR37 deletion in anxious behavior. Indeed, whereas we observed that GPR37^{-/-} mice had a decreased anxiety profile, A_{2A}R blockade reverted the phenotype of GPR37^{-/-} mice to values similar to those observed in GPR37^{+/+} mice. Hence, the emergence of the anxiolytic phenotype in GPR37^{-/-} mice was A_{2A}R-dependent. Collectively, these findings put forward the idea that GPR37 might play a key role in the genuine A_{2A}R function. Hence, our data not only point to a key role of GPR37 on anxiety behavior but they also exclude the participation of this receptor on working/reference memory. In addition, our results may help to further elucidate the mechanisms by which GPR37 modulates these functions, which include the observed functional interplay between GPR37 and A_{2A}R. Such interaction would require further exploration to help proposing new targets for the treatment of pathologies associated with hippocampal neuronal dysfunction and mood-related disorders.

These last novel findings regarding the role of GPR37 controlling different brain regions (i.e. hippocampus) may extend the relevance of this receptor. Nevertheless, at this moment, most studies are focused on revealing the role of GPR37 in PD neuropathology. Indeed, conventional therapies for PD, which are primarily devoted to replace and

support dopaminergic neurotransmission, display a number of drawbacks, thus novel targets are needed to reach better treatments for the disease. Interestingly, one of the new therapeutic proposed targets is the adenosinergic system (192). In fact, $A_{2A}R$ antagonists have not only been postulated but they have also been licensed as antiparkinsonian drugs. Remarkably, it is believed that the $A_{2A}R/D_2R$ heterodimer may be behind the observed antiparkinsonian effects of $A_{2A}R$ antagonists, a mechanism that is thought to be related to the well-known D_2R - $A_{2A}R$ transinhibition phenomenon (91). In addition, the striatal D_2R - $A_{2A}R$ heterodimer has been shown to be downregulated in experimental parkinsonism, a fact that parallels a concomitant increase in $A_{2A}R$ constitutive activity (225)(280). Accordingly, the ability of striatal GPR37 to oligomerize with $A_{2A}R$, and possibly with D_2R , might constitute a way for fine-tuning multiple receptor-signaling pathways and harmonizing dopaminergic neurotransmission. Certainly, manipulating GPR37/ $A_{2A}R$ heteromer stoichiometry could impact on D_2R functioning through putative postsynaptic GPR37/ D_2R / $A_{2A}R$ -containing complexes present in GABAergic striatopallidal neurons (198). In such way, it could be hypothesized that while increasing GPR37/ $A_{2A}R$ oligomerization would rise D_2R function, downregulation of the GPR37/ $A_{2A}R$ heteromer would lead to reduced D_2R signaling. This last hypothesis still needs to be experimentally probed, but it seems clear that the GPR37/ $A_{2A}R$ heteromer, which here we have demonstrated is formed in native conditions, may constitute a novel and very attractive target for the design of new pharmacological strategies to manage pathologies affecting dopaminergic neurotransmission, such as PD. However, in the absence of a functional specific ligand for GPR37, such cross-talk studies on the putative GPR37/ D_2R and GPR37/ $A_{2A}R$ heterodimers are not possible at the present time.

Noteworthy, apart from the lack of effective treatments for PD and other neurodegenerative diseases, one of the main problems of PD consists of its delayed diagnosis, which normally occurs after motor signs first appear when just about 50% of SN dopamine neurons are lost (281). The early and accurate diagnosis of PD would be the first step towards optimal patient management. Thus, it is necessary to develop new biomarkers at early stages of the disease in order to improve the early diagnosis of PD. To date, there are no definitive biomarkers for PD diagnosis, but several biomarkers for PD have been proposed in CSF, which is an accessible source of brain-derived proteins and reflects molecular changes that take place in the CNS. The detection of CSF α -synuclein in PD patients yielded promising but inconclusive results due to discrepant findings depending on assay formats and tremendous overlap of single values in patients and controls (282)(249)(249). Therefore, the use of α -synuclein alone is not sufficient as a single biomarker and it must therefore be used in combination with other reliable

biomarkers. Another proposed biomarker candidate for PD found in CSF is DJ-1, a multifunctional protein that plays an important role in oxidative stress. Interestingly, some studies have demonstrated that DJ-1 levels are decreased in the CSF of PD patients (283). Needless to say, extraction of CSF by lumbar puncture, an invasive procedure, limits routine analysis. On the other hand, inconsistency in the levels of variation between studies are also an important drawback, which may be related to limited sample size and population variations. Methodological issues, including differences in collection, handling and storage of CSF samples or the use of antibodies that detect different species of the antigen, might also cause inconsistent results. Another critical factor is represented by blood contamination, which may cause substantial concentration modifications. Recently, some biomarkers have also been proposed in other body fluids including serum and saliva. Nevertheless, since multiple disease processes may coexist in PD course, combination of different biomarkers that reflect each contributing pathogenic mechanism is likely to be the most appropriate approach.

Interestingly, it was recently described the N-terminal cleavage of GPR37 by specific metalloproteinases (liberating/shedding a peptide named ecto-GPR37) (284). Similarly, GPR37L1 and ETBR, receptors with significant sequence homology to GPR37 but with a significantly shorter N-termini than that of GPR37, have also been reported to undergo N-terminal cleavage in several studies and in various species (251)(285). Differences in length of these N-termini suggest that the mechanism and functional role of the cleavage are likely to be dissimilar. ETBR is cleaved at the plasma membrane by a mechanism that depends on agonist binding. Conversely, the proteolytic processing of GPR37 seems to occur constitutively, since only a very small fraction of the full-length receptor can be detected at the cell surface. Accordingly, it has been hypothesized that receptor cleavage is related to its functional activity. In addition, other GPCR, (i.e. β 1 adrenergic and V2 vasopressin receptors) have been reported to suffer N-termini cleavage and this process occurs in an activation-dependent manner following ligand binding (286). In the case of the parathyroid hormone receptor (PTHrP), the cleavage leads to reduced protein stability and possible degradation of the receptor protein (287), while the exposed new N-termini of the cleaved protease-activated receptors may act as tethered ligands for the cognate receptors (288)(289). It has also been described that cleaved GPR37 N-terminal ectodomain could be recovered from the conditioned medium of HEK-293T in the absence, but not in the presence, of metalloproteinase inhibitors (284). In the case of GPR37, the question about the functional significance of the proteolytic processing is further complicated by the fact that very little is known about the natural physiological function of the receptor. Interestingly, several peptides representing the GPR37 or ETBR

N-terminal domain were recently identified from human cerebrospinal fluid (290)(291). Importantly, GPR37 N-terminal processing should be taken into account in experimental design in order to prevent biased interpretation of observed results, especially when using antibodies directed against the receptor ectodomain. Thus, a number of works early reported GPR37 intracellular accumulation (292)(293). These studies were based on GPR37 overexpression in HEK-293T and GPR37 localization was analyzed using GPR37 N-terminal tags. As membrane GPR37 is mainly found in the N-terminal cleaved form, the conclusion was that receptor was accumulated intracellularly. Our results obtained using immunogold labeling and biotinylation experiments showed similar proportions between the GPR37 localized at the membrane and that at intracellular compartments. Our results suggest that GPR37 would not be accumulated intracellularly, at least in physiological conditions.

According to the description of N-terminal cleavage of GPR37, we focused on assessing the possible use of ecto-GPR37 as a possible biomarker for PD. First, we aimed to reveal changes in GPR37 protein expression levels in post-mortem samples. Thus, we took advantage of the specific antibodies generated in our lab to study the expression levels of GPR37 in PD patients. First, the two polyclonal antibodies directed against distinct regions of the GPR37 (N- and C-terminal domains) were used to characterize the pattern bands for the GPR37 in human samples. GPR37 western blot analysis of post-mortem human brain tissue (i.e. SN and caudate) with the N-terminal GPR37 antibody revealed five specific bands of ~100, 75, 67, 53 and 40 kDa. The 67 kDa band is close to the expected size for the GPR37, and the ~75 and 100 kDa could correspond to the glycosylated receptor. The ~53 and 40 kDa bands correspond to different N-terminal cleaved GPR37 species. A similar pattern bands was recognized with the C-terminal antibody. Surprisingly, proportions between the different GPR37 bands described previously were found in different brain regions. Our results obtained in human tissue are similar to a recently published study where the pattern band of GPR37 overexpressed in HEK-293T cells was studied (284). In this work, GPR37 was tagged with a cMyc-tag in the N-terminal and with a Flag-tag in the C-terminal region and western blot analysis of immunoprecipitated GPR37 with the cMyc antibody revealed two specific bands of ~67 and 96 kDa, the sizes of which are close to the expected size of the receptor polypeptide. The same three bands were recognized with the Flag antibody, indicating that they correspond to full-length receptor forms. Importantly, the Flag antibody, but not the cMyc antibody, detected also a very intense and heterogeneous band of 53 kDa and a much less abundant one of about 34 kDa. These two receptor species are likely to represent proteolytically processed forms of GPR37 missing part of the extracellular N

terminal domain. In parallel, striatum from GPR37^{+/+} and GPR37^{-/-} (used as a robust negative control for validating antibody specificity) western blot analysis with the rabbit anti-N-terminal mouse GPR37 antibody revealed a specific unique band of ~63 kDa, the size of which is close to the expected size for the GPR37. Similarly, a unique band of ~40 kDa was recognized with the C-terminal antibody. These differences in the mouse and human GPR37 pattern band could be due to a different glycosylation and proteolytic cleavage process of the receptors or due to technical issues (consequence of working with post-mortem human tissue, which is collected after different post-mortem intervals).

Once validated the specificity of the GPR37 antibodies, we analyzed protein levels of both full length and metalloprotease cleaved GPR37 (identified as a ~67 and ~40 kDa specific band, respectively). Interestingly, increased protein levels of both full length and mature GPR37 were obtained in SNc from PD samples compared with healthy controls. Since GPR37 is cleaved by metalloproteases in the plasma membrane, we hypothesized that this ecto-GPR37 was released in the extracellular space and could be detected in different body fluids (i.e. CSF). Thus, we designed and generated a homemade competitive ELISA assay (NanoLuc ELISA) for the detection of the ecto-GPR37. First, in order to characterize ecto-GPR37 peptides we analyzed conditioned medium of HEK-293T cells transiently transfected with human or mouse GPR37. Proteomic analysis identified several N-termini GPR37 peptides, some of them belonging to GPR37 sequence following GPR37 described metalloprotease cleavage (284). Thus, our results effectively showed that after first metalloprotease cleavage, ecto-GPR37 would be further processed into short peptides. Interestingly, from the peptides identified in our study, all of them belonged to the GPR37 N-termini, except one that belonged to the ECL2. This finding could be explained due to GPCRs tertiary structure, indicating that GPR37 N-termini interacts with the ECL2. In family A GPCRs, ECL2 is usually the longest ECL, and it has been observed for some GPCRs (i.e. rhodopsin), that ECL2 interacts with N-terminal region to form an effective 'lid', or 'plug' (49) that controls GPCR activity.

Importantly, one of the peptides identified in our study was previously found in human CSF (290). Accordingly, we analyzed the potential presence of the ecto-GPR37 in CSF and other fluids (serum, saliva) in mouse (to validate the technique and optimize volume and incubation times) and human samples. Specificity of the technique was first assessed using samples from GPR37^{-/-} mice. Next, we analyzed presence of ecto-GPR37 in GPR37^{+/+} mice body fluids. We only observed differences in ecto-GPR37 levels in CSF while no differences were observed in serum or saliva when comparing

GPR37^{+/+} and GPR37^{-/-}. This result could be explained by three reasons: i) Ecto-GPR37 is not capable of crossing the BBB; ii) Ecto-GPR37 is present in serum/saliva at low concentrations and the technique is not sensitive enough; iii) Experimental conditions should be optimized for ecto-GPR37 detection in serum/saliva (quantification of plasma and serum and saliva occasionally encounters problems that are caused by the matrix effect).

Once validated the feasibility of detecting the ecto-GPR37 in mouse CSF, we assessed the presence of ecto-GPR37 in human CSF. Interestingly, similar ecto-GPR37 levels were found in mouse and human CSF. Finally, we performed the assay in human healthy controls and PD patients samples. CSF protein levels of ecto-GPR37 were increased in late stage PD patients compared to those of healthy controls. Overall, we validated our NanoLuc-ELISA to detect ecto-GPR37 in human CSF, which may be considered as a putative marker for PD. Interestingly, compared to other immunoassay or biochemical methods, the present modified NanoLuc-ELISA display a number of advantages. Thus, NanoLuc-ELISA tests is rapid and highly sensitive. In such way, 3 μ l of CSF were enough for specific ecto-GPR37 quantification, while in other similar methods used to detect substances in the body, such as traditional ELISA, 50 μ l are normally required (294). In addition, another advantage of the NanoLuc Competitive ELISA is that homemade production of the labeled substrate reduce costs of the technique. Nevertheless, in order to finally consider GPR37/ecto-GPR37 as a specific biomarker for PD, more patients and at early stages of the PD neuropathology should be analyzed. A reliable GPR37 biomarker might also be predictive of cognitive impairment, very frequent as PD progresses, and shown to correlate with Braak's α -synuclein stages. Furthermore, since GPR37 is widespread expressed in brain and proteolyzed in physiological conditions, ecto-GPR37 protein levels could be used to monitor other neurodegenerative diseases (i.e. demyelinating diseases as Amyotrophic Lateral Sclerosis, ALS).

Future directions

In this work we demonstrated the existence of the A_{2A}R-GPR37 oligomer in different brain regions (i.e. mice striatum and hippocampus). It would be crucial to understand the role of GPR37 in the A_{2A}R-D₂R oligomer regulation both in physiological and pathological conditions to develop new therapies for PD. Indeed, it should be further studied the modulatory role of GPR37 over the adenosinergic system in the hippocampus. Moreover, the function of GPR37 in other brain regions where it is highly expressed should be studied (i.e. corpus callosum and cerebellum). Noteworthy, during the development of this thesis, many efforts have been focused on finding the endogenous ligand for GPR37. Different peptides (i.e. HA, prosaptide) have been proposed as specific ligands for GPR37, but we have not been able to replicate these results neither in heterologous expression systems nor in striatal primary cultures. Indeed, we propose that it should be explored the potential role of the ecto-GPR37 as the endogenous ligand of the receptor.

Finally, our results demonstrated the presence of ecto-GPR37 in human CSF and that the alteration in ecto-GPR37 protein levels could be used as a potential biomarker for PD diagnosis. More studies are required in order to ascertain its potential use as a PD biomarker at early stages and the possibility to use serum/plasma and saliva for ecto-GPR37 detection. Future studies should explore the relevance of N-terminal GPR37 cleavage for the normal GPR37 activity. Indeed, some questions may be raised from the results obtained: Is GPR37 cleavage necessary for receptor activation? Is ecto-GPR37 mediating the neuroprotective effects of GPR37? Does ecto-GPR37 function as a neuroprotective/neurotrophic peptide or it is a ligand for other receptors which mediate this effect? Undoubtedly, answering all these questions would facilitate the comprehension of the role of GPR37 in the brain. Notably, in collaboration with Jiang-Fan Chen, from the Boston University School of Medicine, we have recently developed a light-sensitive chimeric Opto-GPR37, which could be used to decipher GPR37 function in different brain regions. This tool consists of a fusion gene encoding a chimaera (*Opto-GPR37*) where the intracellular loops 1, 2 and 3 and the C-terminal of rhodopsin were replaced with those of human GPR37 and the C-terminal sequence of bovine rhodopsin (TETSQVAPA) was added to the C-terminal of *opto-GPR37*. Opto-GPR37 may have generalizable applications for the spatiotemporal control of GPR37 signaling, thus it may help to decipher some of the GPR37 functions. This strategy has already been used to study other GPCRs in brain (i.e. A_{2A}R)(295)(296).

VII. Conclusions

1. GPR37 is expressed in many brain regions, including striatum and hippocampus. Within the striatum, GPR37 is mostly expressed in neurons (i.e. MSNs) where it shows a preferential postsynaptic versus presynaptic distribution. Interestingly, GPR37 and A_{2A}R form direct receptor-receptor complexes (i.e. heteromers) in striatal MSNs.
2. Deletion of GPR37 increases striatal A_{2A}R cell surface expression with a concomitant increase in A_{2A}R-function. Thus, GPR37^{-/-} mice are sensitized to striatal A_{2A}R-mediated signaling (i.e. increasing antagonist-mediated synaptic depotentiation and enhancing spontaneous locomotor activity).
3. In the hippocampus, GPR37 also shows a preferential postsynaptic distribution. Interestingly, while hippocampal GPR37 do not appear to play a role in learning and memory, it seems to potentiate anxiety.
4. GPR37 deletion sensitizes mice to hippocampal A_{2A}R-mediated signaling (i.e. increasing antagonist-mediated synaptic depotentiation and reducing novel object recognition memory).
5. GPR37 expression is increased in SN from PD patients. The GPR37 N-terminal domain is cleaved both in mice and human native tissue and ecto-GPR37 levels are detected in CSF. Furthermore, ecto-GPR37 levels in CSF from PD patients are increased, thus we have postulated ecto-GPR37 as a potential PD biomarker.

VIII: References

1. Hopkins AL, Groom CR. The druggable genome. *Nat Rev Drug Discov* [Internet]. 2002;1(9):727–30. Available from: <http://www.ncbi.nlm.nih.gov/pubmed/12209152>
2. Schöneberg T, Schulz A, Biebermann H, Hermsdorf T, Römpler H, Sangkuhl K. Mutant G-protein-coupled receptors as a cause of human diseases. *Pharmacol Ther.* 2004;104(3):173–206.
3. Paul A, Insel, Chih-Min Tang, Ines Hahntow and MCM. Impact of GPCRs in clinical medicine: genetic variants and drug targets. *Biochim Biophys Acta.* 2007;1768(4):994–1005.
4. Vassart G, Costagliola S. G protein-coupled receptors: mutations and endocrine diseases. *Nat Rev Endocrinol* [Internet]. 2011;7(6):362–72. Available from: <http://dx.doi.org/10.1038/nrendo.2011.20>
5. Marinissen MJ, Gutkind JS. G-protein-coupled receptors and signaling networks: emerging paradigms. *Trends Pharmacol Sci* [Internet]. 2001;22(7):368–76. Available from: <http://www.ncbi.nlm.nih.gov/pubmed/11431032>
6. Topiol S, Sabio M. X-ray structure breakthroughs in the GPCR transmembrane region. *Biochem Pharmacol.* 2009;78(1):11–20.
7. Katritch V, Cherezov V, Stevens RC. Structure-Function of the G-protein-Coupled Receptor Superfamily.
8. Spehr M, Munger SD. Olfactory receptors: GPCRs and beyond.
9. Lique Levoye A, Dam J, Ayoub MA, Guillaume J-L, Couturier C, Delagrangre P, et al. The orphan GPR50 receptor specifically inhibits MT 1 melatonin receptor function through heterodimerization. *EMBO J.* 2006;25(13):3012–23.
10. Cabrera-Vera TM, Vanhauwe J, Thomas TO, Medkova M, Preininger A, Mazzoni MR, et al. Insights into G Protein Structure, Function, and Regulation. *Endocr Rev.* 2003;24(6):765–81.
11. G proteins and GPCRs in normal cell growth and cancer. *TRENDS Pharmacol Sci* [Internet]. 2001 [cited 2016 Jul 5];22(7). Available from: <http://tips.trends.com>
12. Schä B, Marg B, Gschwind A, Ullrich A. Distinct ADAM Metalloproteinases Regulate G Protein-coupled Receptor-induced Cell Proliferation and Survival. *J Biol Chem.* 2004;279(46):47929–38.
13. Power Coombs MR, Belderbos ME, Gallington LC, Bont L, Levy O. Adenosine modulates Toll-like receptor function: basic mechanisms and translational opportunities. *Expert Rev Anti Infect Ther* [Internet]. 2011;9(2):261–9. Available from: <http://www.pubmedcentral.nih.gov/articlerender.fcgi?artid=4052217&tool=pmcentrez&rendertype=abstract>

14. Gether U. Uncovering molecular mechanisms involved in activation of G protein-coupled receptors. *Endocr Rev* [Internet]. 2000;21(1):90–113. Available from: http://www.ncbi.nlm.nih.gov/entrez/query.fcgi?cmd=Retrieve&db=PubMed&dopt=Citation&list_uids=10696571
15. Mirzadegan T, Benko G. Sequence Analyses of G-Protein-Coupled Receptors: Similarities to Rhodopsin. *Biochemistry* [Internet]. 2003;42(10):2759–67. Available from: http://pubs3.acs.org/acs/journals/doi/lookup?in_doi=10.1021/bi027224+
16. Kobilka BK. G Protein Coupled Receptor Structure and Activation.
17. Rosenbaum DM, Rasmussen SGF, Kobilka BK. The structure and function of G-protein-coupled receptors. *Nature* [Internet]. 2009;459(7245):356–63. Available from: <http://dx.doi.org/10.1038/nature08144>
18. Palczewski K, Kumasaka T, Hori T, Behnke CA, Motoshima H, Fox BA, et al. Crystal Structure of Rhodopsin: A G Protein - Coupled Receptor. *Science* (80-). 2000;289:739–45.
19. Warne T, Serrano-Vega MJ, Baker JG, Moukhametzianov R, Edwards PC, Henderson R, et al. Structure of a β 1-adrenergic G-protein-coupled receptor. *Nature* [Internet]. 2008;454(7203):486–91. Available from: <http://www.nature.com/doi/finder/10.1038/nature07101>
20. Cherezov V, Rosenbaum DM, Hanson MA, Rasmussen SGF, Thian FS, Kobilka TS, et al. High-Resolution Crystal Structure of an Engineered Human β 2-Adrenergic. *Science* (80-) [Internet]. 2007;318(November):1258–66. Available from: <http://eutils.ncbi.nlm.nih.gov/entrez/eutils/elink.fcgi?dbfrom=pubmed&id=17962520&retmode=ref&cmd=prlinks>
21. Underwood JG, Bragg AE, Neumark DM, Zgierski MZ, Seideman T, Stolow A, et al. The 2.6 Angstrom Crystal Structure of a Human A2A Adenosine Receptor Bound to an Antagonist. 2008;(2).
22. Lodowski DT, Palczewski K. The Impact of G Protein-coupled Receptor (GPCR) Structures on Understanding Signal Transduction. *G Protein-Coupled Receptor From Struct to Funct* [Internet]. 2011;1–27. Available from: <papers://6ef7d602-1904-44f2-bd27-ffa0776e3fdb/Paper/p14>
23. Kolakowski LF J. GCRDb: a G-protein-coupled receptor database. *Recept Channels* [Internet]. 1994;2(March):1–7. Available from: <http://www.scirp.org/journal/ojgen/%5Cnhttp://www.scirp.org/journal/ojgen>
24. Schiöth HB, Fredriksson R. The GRAFS classification system of G-protein coupled receptors in comparative perspective. *Gen Comp Endocrinol*.

- 2005;142(1–2 SPEC. ISS.):94–101.
25. Mitri C, Parmentier ML, Pin JP, Bockaert J, Grau Y. Divergent evolution in metabotropic glutamate receptors: A new receptor activated by an endogenous ligand different from glutamate in insects. *J Biol Chem*. 2004;279(10):9313–20.
 26. Niswender CM, Conn PJ. Metabotropic Glutamate Receptors: Physiology, Pharmacology, and Disease. *Annu Rev Pharmacol Toxicol*. 2010;50:295–322.
 27. Raymond C, Stevens, Vadim Cherezov, Vsevolod Katritch, Ruben Abagyan, Peter Kuhn HR and KW. GPCR Network: a large scale collaboration on GPCR structure and function. *Nat Rev Drug Discov*. 2013;12(1):25–34.
 28. Lagerström MC, Schiöth HB. Structural diversity of G protein-coupled receptors and significance for drug discovery. *Nat Rev Drug Discov* [Internet]. 2008;7(4):339–57. Available from: <http://www.ncbi.nlm.nih.gov/pubmed/18382464>
 29. Coughlin SR. Thrombin signalling and protease-activated receptors. *Nature*. 2000;407(6801):258–64.
 30. Bartfai T. Neuropeptides and Neuropeptide Receptors : Drug Targets , and Peptide and Non-Peptide Ligands. 2012;9:2367–87.
 31. Chini B. The Binding Site of Neuropeptide Vasopressin V1a Receptor. *J Biol Chem* [Internet]. 1995;270(43):25771–7. Available from: <http://www.jbc.org/content/270/43/25771.full>
 32. Stoveken HM, Bahr LL, Anders MW, Wojtovich AP, Smrcka A V., Tall GG. Dihydromunduletone is a Small-Molecule Selective Adhesion G Protein-Coupled Receptor Antagonist. *Mol Pharmacol* [Internet]. 2016; Available from: <http://molpharm.aspetjournals.org/cgi/doi/10.1124/mol.116.104828>
 33. Liebscher I, Sch??n J, Petersen SC, Fischer L, Auerbach N, Demberg LM, et al. A Tethered Agonist within the Ectodomain Activates the Adhesion G Protein-Coupled Receptors GPR126 and GPR133. *Cell Rep*. 2014;9(6):2018–26.
 34. Paavola KJ, Hall RA. Adhesion G protein-coupled receptors: signaling, pharmacology, and mechanisms of activation. *Mol Pharmacol* [Internet]. 2012;82(5):777–83. Available from: <http://www.pubmedcentral.nih.gov/articlerender.fcgi?artid=3477231&tool=pmcencetrez&rendertype=abstract>
 35. Langenhan T, Aust G, Hamann J. Sticky Signaling — Adhesion Class G Protein – Coupled Receptors Take the Stage. 2013;6(276):1–22.
 36. Zhao GQ, Zhang Y, Hoon MA, Chandrashekar J, Erlenbach I, Ryba NJP, et al. The receptors for mammalian sweet and umami taste. *Cell*. 2003;115(3):255–66.
 37. Cardoso JCR, Clark MS, Viera FA, Bridge PD, Gilles A, Power DM. The secretin

- G-protein-coupled receptor family: Teleost receptors. *J Mol Endocrinol*. 2005;34(3):753–65.
38. Watkins HA, Au M, Hay DL. The structure of secretin family GPCR peptide ligands: Implications for receptor pharmacology and drug development. *Drug Discov Today [Internet]*. 2012;17(17–18):1006–14. Available from: <http://dx.doi.org/10.1016/j.drudis.2012.05.005>
 39. Li C, Iii C. Adenylyl cyclase. 2012;1–4.
 40. Diel S, Klass K, Wittig B, Kleuss C. G β y activation site in adenylyl cyclase type II: Adenylyl cyclase type III is inhibited by G β y. *J Biol Chem*. 2006;281(1):288–94.
 41. Tu H, Rondard P, Xu C, Bertaso F, Cao F, Zhang X, et al. Dominant role of GABAB2 and G β y for GABAB receptor-mediated-ERK1/2/CREB pathway in cerebellar neurons. *Cell Signal*. 2007;19(9):1996–2002.
 42. Luttrell LM, Hawes BE, van Biesen T, Luttrell DK, Lansing TJ, Lefkowitz RJ. Role of c-Src tyrosine kinase in G protein-coupled receptor- and Gbetagamma subunit-mediated activation of mitogen-activated protein kinases. *J Biol Chem*. 1996;271(32):19443–50.
 43. Philip F, Kadamur G, Silos RG, Woodson J, Ross EM. Synergistic activation of phospholipase C- β 3 by G α q and G β y describes a simple two-state coincidence detector. *Curr Biol*. 2010;20(15):1327–35.
 44. Pierce KL, Lefkowitz RJ. Classical and new roles of beta-arrestins in the regulation of G-protein-coupled receptors. *Nat Rev Neurosci*. 2001;2(10):727–33.
 45. Rocca SMCJ Della, Lin F, Kawakatsu H, Owada K, Luttrell DK, Caron MC, et al. β -arrestin-Dependent Formation of β 2 adrenergic receptor-Src Protein Kinase Complexes. 1999;283(January):655–61.
 46. Ahn S, Maudsley S, Luttrell LM, Lefkowitz RJ, Daaka Y. Src-mediated tyrosine phosphorylation of dynamin is required for β 2- adrenergic receptor internalization and mitogen-activated protein kinase signaling. *J Biol Chem [Internet]*. 1999;274(3):1185–8. Available from: <http://www.jbc.org/content/274/3/1185.full.pdf>
 47. Zheng H, Loh HH, Law PY. Posttranslation modification of G protein-coupled receptor in relationship to biased agonism. *Methods Enzymol*. 2013;522:391–408.
 48. Schwarz F, Aebi M. Mechanisms and principles of N-linked protein glycosylation. *Curr Opin Struct Biol [Internet]*. 2011;21(5):576–82. Available from: <http://dx.doi.org/10.1016/j.sbi.2011.08.005>

49. Wheatley M, Wootten D, Conner MT, Simms J, Kendrick R, Logan RT, et al. Lifting the lid on GPCRs: The role of extracellular loops. *Br J Pharmacol*. 2012;165(6):1688–703.
50. Lanctot PM, Leclerc PC, Clément M, Auger-Messier M, Escher E, Leduc R, et al. Importance of N-glycosylation positioning for cell-surface expression, targeting, affinity and quality control of the human AT1 receptor. *Biochem J* [Internet]. 2005;390(Pt 1):367–76. Available from: <http://www.pubmedcentral.nih.gov/articlerender.fcgi?artid=1188272&tool=pmcencetrez&rendertype=abstract>
51. Kountz TS, Lee KS, Aggarwal-Howarth S, Curran E, Park JM, Harris DA, et al. Endogenous N-terminal domain cleavage modulates $\alpha 1D$ -adrenergic receptor pharmacodynamics. *J Biol Chem*. 2016;291(35):18210–21.
52. Dunham JH, Meyer RC, Garcia EL, Hall RA. GPR37 surface expression enhancement via N-terminal truncation or protein-protein interactions. *Biochemistry*. 2009;48:10286–97.
53. Trudel M, Yao Q, Qian F. The Role of G-Protein-Coupled Receptor Proteolysis Site Cleavage of Polycystin-1 in Renal Physiology and Polycystic Kidney Disease. *Cells* [Internet]. 2016;5(1):3. Available from: <http://www.mdpi.com/2073-4409/5/1/3>
54. O'Hara PJ, Sheppard PO, Thorgersen H, Venezia D, Haldeman BA, McGrane V, et al. The ligand-binding domain in metabotropic glutamate receptors is related to bacterial periplasmic binding proteins. *Neuron*. 1993;11:41–52.
55. Schwarz DA, Barry G, Eliasof SD, Petroski RE, Conlon PJ, Maki RA. Characterization of γ -aminobutyric acid receptor GABA(B(1e)), a GABA(B(1)) splice variant encoding a truncated receptor. *J Biol Chem*. 2000;275(41):32174–81.
56. Bouvier M. Oligomerization of G-protein-coupled transmitter receptors. *Nat Rev Neurosci* [Internet]. 2001;2(4):274–86. Available from: <http://dx.doi.org/10.1038/35067575>
57. Lodowski DT, Salom D, Le Trong I, Teller DC, Ballesteros JA, Palczewski K, et al. Crystal packing analysis of Rhodopsin crystals. *J Struct Biol*. 2007;158(3):455–62.
58. Piirainen H, Hellman M, Tossavainen H, Permi P, Kursula P, Jaakola VP. Human adenosine A2A receptor binds calmodulin with high affinity in a calcium-dependent manner. *Biophys J* [Internet]. 2015;108(4):903–17. Available from: <http://dx.doi.org/10.1016/j.bpj.2014.12.036>
59. Whitson SR, LeStourgeon WM, Krezel AM. Solution structure of the symmetric

- coiled coil tetramer formed by the oligomerization domain of hnRNP C: Implications for biological function. *J Mol Biol.* 2005;350(2):319–37.
60. Angers S, Salahpour A, Bouvier M. Dimerization: an emerging concept for G protein-coupled receptor ontogeny and function. *Annu Rev Pharmacol Toxicol.* 2002;42(1):409–35.
 61. GPCR Signalling Complexes – Synthesis , Assembly , Trafficking and Specificity. Springer; 2012.
 62. Kim O-J, Ariano M a, Lazzarini R a, Levine MS, Sibley DR. Neurofilament-M interacts with the D1 dopamine receptor to regulate cell surface expression and desensitization. *J Neurosci* [Internet]. 2002;22(14):5920–30. Available from: <http://www.ncbi.nlm.nih.gov/pubmed/12122054>
 63. Marazziti D, Mandillo S, Di Pietro C, Golini E, Matteoni R, Tocchini-Valentini GP. GPR37 associates with the dopamine transporter to modulate dopamine uptake and behavioral responses to dopaminergic drugs. *Proc Natl Acad Sci U S A* [Internet]. 2007;104(23):9846–51. Available from: <http://www.pubmedcentral.nih.gov/articlerender.fcgi?artid=1887553&tool=pmcentrez&rendertype=abstract>
 64. Décaillot FM, Rozenfeld R, Gupta A, Devi LA. Cell surface targeting of mu-delta opioid receptor heterodimers by RTP4. *Proc Natl Acad Sci U S A* [Internet]. 2008;105(41):16045–50. Available from: <http://www.pubmedcentral.nih.gov/articlerender.fcgi?artid=2572960&tool=pmcentrez&rendertype=abstract>
 65. P. Jeffrey Conn¹, Craig W. Lindsley¹, Jens Meiler² and CMN. Opportunities and challenges in the discovery of allosteric modulators of GPCRs for treating CNS disorders. *Nat Rev Drug Discov.* 2014;13(9):692–708.
 66. Fernández-Dueñas V, Gómez-Soler M, Morató X, Núñez F, Das A, Kumar TS, et al. Dopamine D2 receptor-mediated modulation of adenosine A_{2A} receptor agonist binding within the A_{2A}R/D₂R oligomer framework. *Neurochem Int.* 2013;63(1):42–6.
 67. Lewis MA, Hunihan L, Watson J, Gentles RG, Hu S, Huang Y, et al. Discovery of D1 Dopamine Receptor Positive Allosteric Modulators: Characterization of Pharmacology and Identification of Residues that Regulate Species Selectivity. *J Pharmacol Exp Ther* [Internet]. 2015;354(3):340–9. Available from: <http://jpet.aspetjournals.org/content/354/3/340.abstract>
 68. Dunwiddie T V, Masino S a. The role and regulation of adenosine in the central nervous system. *Annu Rev Pharmacol Toxicol.* 2001;41(1):145–74.
 69. Cunha RA, Ferre S, Vaugeois JM, Chen JF. Potential therapeutic interest of

- adenosine A2A receptors in psychiatric disorders. *Curr Pharm Des* [Internet]. 2008;14(15):1512–24. Available from: <http://www.ncbi.nlm.nih.gov/pubmed/18537674>
70. Fredholm BB. Physiological and pathophysiological roles of adenosine. *Sleep Biol Rhythms*. 2011;9(SUPPL. 1):24–8.
 71. Fredholm BB, Chen JF, Cunha RA, Svenningsson P, Vaugeois JM. Adenosine and Brain Function. *Int Rev Neurobiol*. 2005;63(May 2014):191–270.
 72. Nishizaki T, Nagai K, Nomura T, Tada H, Kanno T, Tozaki H, et al. A new neuromodulatory pathway with a glial contribution mediated via A2a adenosine receptors. *Glia*. 2002;39(2):133–47.
 73. Badalà F, Nouri-mahdavi K, Raof DA. Adenosine receptor signaling in the brain immune system. *Trends Pharmacol Sci*. 2005;26(10):511–6.
 74. Feoktistov I, Goldstein AE, Ryzhov S, Zeng D, Belardinelli L, Voyno-Yasenetskaya T, et al. Differential expression of adenosine receptors in human endothelial cells: Role of A2B receptors in angiogenic factor regulation. *Circ Res*. 2002;90(5):531–8.
 75. Rebola N, Rodrigues RJ, Lopes L V., Richardson PJ, Oliveira CR, Cunha RA. Adenosine A1 and A2A receptors are co-expressed in pyramidal neurons and co-localized in glutamatergic nerve terminals of the rat hippocampus. *Neuroscience*. 2005;133(1):79–83.
 76. Rebola N, Canas PM, Oliveira CR, Cunha RA. Different synaptic and subsynaptic localization of adenosine A2A receptors in the hippocampus and striatum of the rat. *Neuroscience*. 2005;132(4):893–903.
 77. Shindou T, Nonaka H, Richardson PJ, Mori A, Kase H, Ichimura M. Presynaptic adenosine A2A receptors enhance GABAergic synaptic transmission via a cyclic AMP dependent mechanism in the rat globus pallidus. *Br J Pharmacol*. 2002;136:296–302.
 78. Cunha RA, Ribeiro JA. Purinergic modulation of [3H]GABA release from rat hippocampal nerve terminals. *Neuropharmacology*. 2000;39(7):1156–67.
 79. Rodrigues RJ, Canas PM, Lopes L V., Oliveira CR, Cunha RA. Modification of adenosine modulation of acetylcholine release in the hippocampus of aged rats. *Neurobiol Aging*. 2008;29(10):1597–601.
 80. Rodrigo A. Cunha, Bjorn Johansson, Bertil B. Fredholm, J. Alexandre Ribeiro AMS. Adenosine A2A receptors stimulate acetylcholine release from nerve terminals of the rat hippocampus. *Neurosci Lett*. 1995;196:41–4.
 81. Zhu C, Steiner JA, Munn JL, Daws LC, Hewlett WA, Blakely RD. Rapid Stimulation of Presynaptic Serotonin Transport by A 3 Adenosine Receptors.

- 2007;322(1):332–40.
82. Okada M, Nutt DJ, Murakami T, Zhu G, Kamata a, Kawata Y, et al. Adenosine receptor subtypes modulate two major functional pathways for hippocampal serotonin release. *J Neurosci* [Internet]. 2001;21(2):628–40. Available from: <http://www.ncbi.nlm.nih.gov/pubmed/11160442>
 83. MÃ¶ssner R, Albert D, Persico AM, Hennig T, Bengel D, Holtmann B, et al. Differential regulation of adenosine A1 and A2A receptors in serotonin transporter and monoamine oxidase A-deficient mice. *Eur Neuropsychopharmacol* [Internet]. 2000;10(6):489–93. Available from: [http://www.sciencedirect.com/science?_ob=ArticleURL&_udi=B6T26-41WBN9S-B&_user=10&_coverDate=12/31/2000&_rdoc=10&_fmt=high&_orig=browse&_srch=doc-info\(#toc#4910#2000#999899993#221238#FLA#display#Volume\)&_cdi=4910&_sort=d&_docanchor=&_ct=15&_acct=C00005022](http://www.sciencedirect.com/science?_ob=ArticleURL&_udi=B6T26-41WBN9S-B&_user=10&_coverDate=12/31/2000&_rdoc=10&_fmt=high&_orig=browse&_srch=doc-info(#toc#4910#2000#999899993#221238#FLA#display#Volume)&_cdi=4910&_sort=d&_docanchor=&_ct=15&_acct=C00005022)
 84. Allgaier C, Hertting G, Kùgelgen O V. The adenosine receptor-mediated inhibition of noradrenaline release possibly involves a N-protein and is increased by α 2-autoreceptor blockade. *Br J Pharmacol*. 1987;90(2):403–12.
 85. Fredholm BB, IJzerman a P, Jacobson K a, Klotz KN, Linden J. International Union of Pharmacology. XXV. Nomenclature and classification of adenosine receptors. *Pharmacol Rev*. 2001;53(4):527–52.
 86. Jaakola V, Griffith MT, Hanson MA, Cherezov V, Ellen YT, Lane JR, et al. The 2.6 Å Crystal Structure of a Human A2A Adenosine Receptor Bound to an Antagonist. 2009;322(5905):1211–7.
 87. Sun B, Bachhawat P, Chu ML-H, Wood M, Ceska T, Sands ZA, et al. Crystal structure of the adenosine A_{2A} receptor bound to an antagonist reveals a potential allosteric pocket. *Proc Natl Acad Sci* [Internet]. 2017;114(8):201621423. Available from: <http://www.pnas.org/lookup/doi/10.1073/pnas.1621423114>
 88. Ferré S, Lluís C, Justinova Z, Quiroz C, Orru M, Navarro G, et al. Adenosine-cannabinoid receptor interactions. Implications for striatal function. *Br J Pharmacol*. 2010;160(3):443–53.
 89. Perreault ML, Hasbi A, O'Dowd BF, George SR. The dopamine d1-d2 receptor heteromer in striatal medium spiny neurons: evidence for a third distinct neuronal pathway in Basal Ganglia. *Front Neuroanat* [Internet]. 2011;5(May):31. Available from: <http://www.pubmedcentral.nih.gov/articlerender.fcgi?artid=3130461&tool=pmcentrez&rendertype=abstract>

90. Ferré S, Ciruela F, Canals M, Marcellino D, Burgueno J, Casadó V, et al. Adenosine A2A-dopamine D2 receptor-receptor heteromers. Targets for neuro-psychiatric disorders. *Park Relat Disord*. 2004;10(5):265–71.
91. Ferre S, Quiroz C, Woods AS, Cunha RA, Popoli P, Ciruela F, et al. An update on adenosine A2A-dopamine D2 receptor interactions: implications for the function of G protein-coupled receptors. *Curr Pharm Des* [Internet]. 2008;14(15):1468–74. Available from: <http://www.pubmedcentral.nih.gov/articlerender.fcgi?artid=2424285&tool=pmcentrez&rendertype=abstract>
92. Khisti RT, Khisti RT, Chopde CT, Chopde CT, Abraham E, Abraham E. GABAergic involvement in motor effects of an adenosine A(2A) receptor agonist in mice. *Neuropharmacology* [Internet]. 2000;39:1004–15. Available from: <http://www.ncbi.nlm.nih.gov/pubmed/10727710>
93. Shiozaki S, Ichikawa S, Nakamura J, Kitamura S, Yamada K, Kuwana Y. Actions of adenosine A(2A) receptor antagonist KW-6002 on drug-induced catalepsy and hypokinesia caused by reserpine or MPTP. *Psychopharmacology (Berl)*. 1999;147(1):90–5.
94. Braun A a, Skelton MR, Vorhees C V, Williams MT. Comparison of the elevated plus and elevated zero mazes in treated and untreated male Sprague-Dawley rats. *Pharmacol Ther*. 2012;97(3):406–15.
95. Kulkarni SK, Singh K, Bishnoi M. Involvement of adenosinergic receptors in anxiety related behaviours. *Indian J Exp Biol*. 2007;45(5):439–43.
96. Ruby CL, Adams CA, Mrazek DA, Choi D-S. Adenosine Signaling in Anxiety. Ed by Vladimir V Kalinin. 2011;(March 2017):51.
97. Gomes C V, Kaster MP, Tomé AR, Agostinho PM, Cunha R a. Adenosine receptors and brain diseases: neuroprotection and neurodegeneration. *Biochim Biophys Acta* [Internet]. 2011;1808(5):1380–99. Available from: <http://www.ncbi.nlm.nih.gov/pubmed/21145878%5Cnhttp://dx.doi.org/10.1016/j.bbamem.2010.12.001>
98. El Yacoubi M, Ledent C, Parmentier M, Costentin J, Vaugeois JM. Evidence for the involvement of the adenosine A2A receptor in the lowered susceptibility to pentylenetetrazol-induced seizures produced in mice by long-term treatment with caffeine. *Neuropharmacology*. 2008;55(1):35–40.
99. El Yacoubi M, Ledent C, Parmentier M, Costentin J, Vaugeois JM. Adenosine A2A receptor deficient mice are partially resistant to limbic seizures. *Naunyn Schmiedebergs Arch Pharmacol*. 2009;380(3):223–32.
100. Dhaenens CM, Burnouf S, Simonin C, Van Brussel E, Duhamel A, Defebvre L,

- et al. A genetic variation in the ADORA2A gene modifies age at onset in Huntington's disease. *Neurobiol Dis* [Internet]. 2009;35(3):474–6. Available from: <http://dx.doi.org/10.1016/j.nbd.2009.06.009>
101. Kurumaji A, Toru M. An increase in [3H] CGS21680 binding in the striatum of post-mortem brains of chronic schizophrenics. *Brain Res.* 1998;808(2):320–3.
 102. Boison D, Singer P, Shen H, Feldon J, Yee BK. Adenosine hypothesis of schizophrenia –opportunities for pharmacotherapy. *Neuropharmacology* [Internet]. 2013;62(3):1527–43. Available from: <http://dx.doi.org/10.1016/j.neuropharm.2011.01.048>
<http://www.sciencedirect.com/science/article/pii/S0028390811000591>
 103. Citri A, Malenka RC. Synaptic Plasticity: Multiple Forms, Functions, and Mechanisms. *Neuropsychopharmacology* [Internet]. 2008;33(1):18–41. Available from: <http://www.nature.com/doi/10.1038/sj.npp.1301559>
 104. Wieraszko A, Seyfried TN. Increased amount of extracellular ATP in stimulated hippocampal slices of seizure prone mice. *Neurosci Lett.* 1989;106(3):287–93.
 105. Wieraszko A, Goldsmith G, Seyfried TN. Stimulation-dependent release of adenosine triphosphate from hippocampal slices. *Brain Res.* 1989;485(2):244–50.
 106. Costenla AR, Cunha RA, De Mendonça A. Caffeine, adenosine receptors, and synaptic plasticity. *J Alzheimer's Dis.* 2010;20(SUPPL.1).
 107. Lopes L V., Cunha RA, Kull B, Fredholm BB, Ribeiro JA. Adenosine A2A receptor facilitation of hippocampal synaptic transmission is dependent on tonic A1 receptor inhibition. *Neuroscience.* 2002;112(2):319–29.
 108. Costenla AR, De Mendonça A, Ribeiro JA. Adenosine modulates synaptic plasticity in hippocampal slices from aged rats. *Brain Res.* 1999;851(1–2):228–34.
 109. Rodrigues TM, Jerónimo-Santos A, Sebastião AM, Diógenes MJ. Adenosine A2A Receptors as novel upstream regulators of BDNF-mediated attenuation of hippocampal Long-Term Depression (LTD). *Neuropharmacology* [Internet]. 2014;79:389–98. Available from: <http://dx.doi.org/10.1016/j.neuropharm.2013.12.010>
 110. Talia N, Lerner, Eric A, Horne, Nephi Stella and ACK. Endocannabinoid signaling mediates psychomotor activation by adenosine A2A antagonists. *Clin Lymphoma.* 2010;10(30):2160–4.
 111. Calabresi P, Maj R, Pisani A, Mercuri NB, Bernardi G. Long-Term synaptic depression in the striatum: Physiological and Pharmacological characterization. *J Neurosci.* 1992;12(11):4224–33.

112. Coelho JE, Alves P, Canas PM, Valadas JS, Shmidt T, Batalha VL, et al. Overexpression of adenosine A2A receptors in rats: Effects on depression, locomotion, and anxiety. *Front Psychiatry*. 2014;5(JUN):1–8.
113. Zhou S-J, Zhu M-E, Shu D, Du X-P, Song X-H, Wang X-T, et al. Preferential enhancement of working memory in mice lacking adenosine A(2A) receptors. *Brain Res* [Internet]. 2009;1303:74–83. Available from: <http://dx.doi.org/10.1016/j.brainres.2009.09.082>
114. Chen JF, Xu K, Petzer JP, Staal R, Xu YH, Beilstein M, et al. Neuroprotection by caffeine and A(2A) adenosine receptor inactivation in a model of Parkinson's disease. *J Neurosci*. 2001;21(10):RC143.
115. Elsworth JD, Roth RH. Dopamine synthesis, uptake, metabolism, and receptors: relevance to gene therapy of Parkinson's disease. *Exp Neurol* [Internet]. 1997;144(1):4–9. Available from: <http://www.ncbi.nlm.nih.gov/pubmed/9126143>
116. Missale C, Nash SR, Robinson SW, Jaber M, Caron MG. Dopamine receptors: from structure to function. *Physiol Rev* [Internet]. 1998;78(1):189–225. Available from: <http://europepmc.org/abstract/MED/9457173>
117. Mansour A, Watson S. Dopamine receptor expression in the central nervous system. *Psychopharmacol fourth Gener ...* [Internet]. 1995; Available from: [http://www.bnl.gov/thanoslab/Dopamine Receptor Expression in the Central Nervous System.pdf](http://www.bnl.gov/thanoslab/Dopamine%20Receptor%20Expression%20in%20the%20Central%20Nervous%20System.pdf)
118. Tóth BE, Vecsernyés M, Zelles T, Kádár K, Nagy GM. Role of peripheral and brain-derived dopamine (DA) in immune regulation. *Adv Neuroimmune Biol*. 2012;3(2):111–55.
119. Hall H, Sedvall G, Magnusson O, Kopp J, Halldin C, Farde L. Distribution of D1- and D2-dopamine receptors, and dopamine and its metabolites in the human brain. Vol. 11, *Neuropsychopharmacology : official publication of the American College of Neuropsychopharmacology*. 1994. p. 245–56.
120. Levey AI, Hersch SM, Rye DB, Sunahara RK, Niznik HB, Kitt CA, et al. Localization of D1 and D2 dopamine receptors in brain with subtype-specific antibodies. *Proc Natl Acad Sci U S A* [Internet]. 1993;90(19):8861–5. Available from: http://www.ncbi.nlm.nih.gov/entrez/query.fcgi?cmd=Retrieve&db=PubMed&dopt=Citation&list_uids=8415621
121. Gagnon D, Petryszyn S, Sanchez MG, Bories C, Beaulieu JM, De Koninck Y, et al. Striatal Neurons Expressing D1 and D2 Receptors are Morphologically Distinct and Differently Affected by Dopamine Denervation in Mice. *Sci Rep* [Internet]. 2017;7(September 2016):41432. Available from:

- <http://www.nature.com/articles/srep41432>
122. Agnoli L, Mainolfi P, Invernizzi RW, Carli M. Dopamine D1-Like and D2-Like Receptors in the Dorsal Striatum Control Different Aspects of Attentional Performance in the Five-Choice Serial Reaction Time Task Under a Condition of Increased Activity of Corticostriatal Inputs. *Neuropsychopharmacology* [Internet]. 2013;38(5):701–14. Available from:
http://www.nature.com/npp/journal/v38/n5/full/npp2012236a.html?WT.ec_id=NP
[P-201304%5Cnhttp://www.nature.com/npp/journal/v38/n5/pdf/npp2012236a.pdf](http://www.nature.com/npp/journal/v38/n5/pdf/npp2012236a.pdf)
 123. Schuurkes JAJ, Helsen LFM, Ghoos ECR, Eelen JGMG, van Nueten JM. Stimulation of gastroduodenal motor activity: Dopaminergic and cholinergic modulation. *Drug Dev Res.* 1986;8(1–4):233–41.
 124. Giros B, Jaber M, Jones SR, Wightman RM, Caron MG. Hyperlocomotion and indifference to cocaine and amphetamine in mice lacking the dopamine transporter [Internet]. Vol. 379, *Nature.* 1996. p. 606–12. Available from:
http://www.ncbi.nlm.nih.gov/pubmed/8628395%5Cnhttp://www.ncbi.nlm.nih.gov/entrez/query.fcgi?cmd=Retrieve&db=PubMed&dopt=Citation&list_uids=8628395
 125. Joshua M, Adler A, Bergman H. The dynamics of dopamine in control of motor behavior. *Curr Opin Neurobiol.* 2009;19(6):615–20.
 126. Centonze D, Grande C, Saulle E, Martin AB, Gubellini P, Pavón N, et al. Distinct roles of D1 and D5 dopamine receptors in motor activity and striatal synaptic plasticity. *J Neurosci* [Internet]. 2003;23(24):8506–12. Available from:
<http://eutils.ncbi.nlm.nih.gov/entrez/eutils/eflink.fcgi?dbfrom=pubmed&id=13679419&retmode=ref&cmd=prlinks>
 127. Crocker AD. The regulation of motor control: an evaluation of the role of dopamine receptors in the substantia nigra. *Rev Neurosci* [Internet]. 1997;8(1):55–76. Available from: <http://www.ncbi.nlm.nih.gov/pubmed/9402645>
 128. Marek K. Dopaminergic Dysfunction in Parkinsonism: New Lessons from Imaging. *Neurosci* [Internet]. 1999;5(5):333–40. Available from:
<http://journals.sagepub.com/doi/10.1177/107385849900500519>
 129. Zhan L, Kerr JR, Lafuente MJ, Maclean A, Chibalina M V., Liu B, et al. Altered expression and coregulation of dopamine signalling genes in schizophrenia and bipolar disorder. *Neuropathol Appl Neurobiol.* 2011;37(2):206–19.
 130. Volkow ND, Fowler JS, Wang G-J, Swanson JM. Dopamine in drug abuse and addiction: results from imaging studies and treatment implications. *Mol Psychiatry* [Internet]. 2004;9(6):557–69. Available from:
<http://www.ncbi.nlm.nih.gov/pubmed/15098002>
 131. Ludolph AG, Kassubek J, Schmeck K, Glaser C, Wunderlich A, Buck AK, et al.

- Dopaminergic dysfunction in attention deficit hyperactivity disorder (ADHD), differences between pharmacologically treated and never treated young adults: A 3,4-dihydroxy-6-[18F]fluorophenyl-L-alanine PET study. *Neuroimage*. 2008;41(3):718–27.
132. Cepeda C, Murphy KPS, Parent M, Levine MS. The Role of Dopamine in Huntington ' s Disease. *Prog Brain Res*. 2014;211(310):235–54.
 133. Chen JY, Wang EA, Cepeda C, Levine MS. Dopamine imbalance in Huntington's disease: A mechanism for the lack of behavioral flexibility. *Front Neurosci*. 2013;7(7 JUL):1–14.
 134. Zeng Z, Su K, Kyaw H, Li Y. A novel endothelin receptor type-B-like gene enriched in the brain. *Biochem Biophys Res Commun* [Internet]. 1997;233(2):559–67. Available from: <http://www.ncbi.nlm.nih.gov/pubmed/9144577>
 135. Marazziti D, Golini E, Gallo A, Lombardi MS, Matteoni R, Tocchini-Valentini GP. Cloning of GPR37, a gene located on chromosome 7 encoding a putative G-protein-coupled peptide receptor, from a human frontal brain EST library. *Genomics* [Internet]. 1997;45(1):68–77. Available from: <http://www.ncbi.nlm.nih.gov/pubmed/9339362>
 136. Marazziti D, Gallo A, Golini E, Matteoni R, Tocchini-Valentini GP. Molecular cloning and chromosomal localization of the mouse Gpr37 gene encoding an orphan G-protein-coupled peptide receptor expressed in brain and testis. *Genomics*. 1998;53(3):315–24.
 137. Valdenaire O, Giller T, Breu V, Ardati A, Schweizer A, Richards JG. A new family of orphan G protein-coupled receptors predominantly expressed in the brain. *FEBS Lett*. 1998;424(3):193–6.
 138. Donohue PJ, Shapira H, Mantey SA, Hampton LL, Jensen RT, Battey JF. A human gene encodes a putative G protein-coupled receptor highly expressed in the central nervous system. *Brain Res Mol Brain Res* [Internet]. 1998;54(1):152–60. Available from: <http://www.ncbi.nlm.nih.gov/pubmed/9526070>
 139. Schaller HB and HC. Conserved amino acid sequence of a neuropeptide, the head activator, from coelenterates to humans. *Nature*. 1981;
 140. Rezgaoui M, S^osens U, Ignatov A, Gelderblom M, Glassmeier G, Franke I, et al. The neuropeptide head activator is a high-affinity ligand for the orphan G-protein-coupled receptor GPR37. *J Cell Sci* [Internet]. 2006;119(3):542–9. Available from: [http://jcs.biologists.org/content/119/3/542%5Cnfiles/181/Rezgaoui et al. - 2006 - The neuropeptide head activator is a high-affinity.pdf%5Cnfiles/183/542.html](http://jcs.biologists.org/content/119/3/542%5Cnfiles/181/Rezgaoui%20et%20al.%20-%202006%20-%20The%20neuropeptide%20head%20activator%20is%20a%20high-affinity.pdf%5Cnfiles/183/542.html)

141. Meyer RC, Giddens MM, Schaefer SA, Hall RA. GPR37 and GPR37L1 are receptors for the neuroprotective and glioprotective factors prosaptide and prosaposin. *Proc Natl Acad Sci U S A* [Internet]. 2013;110(23):9529–34. Available from:
<http://www.pubmedcentral.nih.gov/articlerender.fcgi?artid=3677493&tool=pmcentrez&rendertype=abstract>
142. Southern C, Cook JM, Neetoo-Isseljee Z, Taylor DL, Kettleborough CA, Merritt A, et al. Screening beta-Arrestin Recruitment for the Identification of Natural Ligands for Orphan G-Protein-Coupled Receptors. *J Biomol Screen* [Internet]. 2013;18(5):599–609. Available from:
<http://jbx.sagepub.com/content/18/5/599.full.pdf>
143. Imai Y, Soda M, Inoue H, Hattori N, Mizuno Y, Takahashi R. An unfolded putative transmembrane polypeptide, which can lead to endoplasmic reticulum stress, is a substrate of Parkin. *Cell*. 2001 Jun;105(7):891–902.
144. Murakami T, Shoji M, Imai Y, Inoue H, Kawarabayashi T, Matsubara E, et al. Pael-R is accumulated in Lewy bodies of Parkinson's disease. *Ann Neurol*. 2004 Mar;55(3):439–42.
145. Kitada T, Asakawa S, Hattori N, Matsumine H, Yamamura Y, Minoshima S, et al. Mutations in the parkin gene cause autosomal recessive juvenile parkinsonism. *Nature*. 1998;392(6676):605–8.
146. Shimura H, Hattori N, Kubo S, Mizuno Y, Asakawa S, Minoshima S, et al. Familial Parkinson disease gene product, parkin, is a ubiquitin-protein ligase. *Nat Genet*. 2000 Jul;25(3):302–5.
147. Zhang Y, Gao J, Chung KK, Huang H, Dawson VL, Dawson TM. Parkin functions as an E2-dependent ubiquitin- protein ligase and promotes the degradation of the synaptic vesicle-associated protein, CDCrel-1. *Proc Natl Acad Sci U S A*. 2000;97(24):13354–9.
148. Kitao Y, Imai Y, Ozawa K, Kataoka A, Ikeda T, Soda M, et al. Pael receptor induces death of dopaminergic neurons in the substantia nigra via endoplasmic reticulum stress and dopamine toxicity, which is enhanced under condition of parkin inactivation. *Hum Mol Genet*. 2007;16(1):50–60.
149. Marazziti D, Golini E, Mandillo S, Magrelli A, Witke W, Matteoni R, et al. Altered dopamine signaling and MPTP resistance in mice lacking the Parkinson's disease-associated GPR37/parkin-associated endothelin-like receptor. *Proc Natl Acad Sci U S A* [Internet]. 2004;101(27):10189–94. Available from:
<http://www.pubmedcentral.nih.gov/articlerender.fcgi?artid=454186&tool=pmcentrez&rendertype=abstract>

150. Lundius EG, Stroth N, Vukojević V, Terenius L, Svenningsson P. Functional GPR37 trafficking protects against toxicity induced by 6-OHDA, MPP+ or rotenone in a catecholaminergic cell line. *J Neurochem*. 2013;124(3):410–7.
151. Kubota K, Niinuma Y, Kaneko M, Okuma Y, Sugai M, Omura T, et al. Suppressive effects of 4-phenylbutyrate on the aggregation of Pael receptors and endoplasmic reticulum stress. *J Neurochem*. 2006;97(5):1259–68.
152. Omura T, Kaneko M, Okuma Y, Orba Y, Nagashima K, Takahashi R, et al. A ubiquitin ligase HRD1 promotes the degradation of Pael receptor, a substrate of Parkin. *J Neurochem*. 2006;99(6):1456–69.
153. Dunham JH, Meyer RC, Garcia EL, Hall RA. GPR37 surface expression enhancement via N-terminal truncation or protein-protein interactions. *Biochemistry*. 2009;48(43):10286–97.
154. Gandia J, Fernandez-Dueñas V, Morató X, Caltabiano G, González-Muñiz R, Pardo L, et al. The Parkinson's disease-associated GPR37 receptor-mediated cytotoxicity is controlled by its intracellular cysteine-rich domain. *J Neurochem*. 2013;125(3):362–72.
155. Milligan G. G protein-coupled receptor dimerization: function and ligand pharmacology. *Mol Pharmacol*. 2004;66(1):1–7.
156. Qiu C, Kivipelto M, Von Strauss E. Epidemiology of Alzheimer's disease: Occurrence, determinants, and strategies toward intervention. *Dialogues Clin Neurosci*. 2009;11(2):111–28.
157. Alves G, Forsaa EB, Pedersen KF, Dreetz Gjerstad M, Larsen JP. Epidemiology of Parkinson's disease. *J Neurol*. 2008;255(SUPPL. 5):18–32.
158. Bereczki D. The description of all four cardinal signs of Parkinson's disease in a Hungarian medical text published in 1690. *Park Relat Disord*. 2010;16(4):290–3.
159. Goetz CG. The history of Parkinson's disease: Early clinical descriptions and neurological therapies. *Cold Spring Harb Perspect Med*. 2011;1(1).
160. Cookson MR. Parkinsonism due to mutations in PINK1, Parkin, and DJ-1 and oxidative stress and mitochondrial pathways. *Cold Spring Harb Perspect Med*. 2012;2(9):1–11.
161. Petzold GC, Bohner G, Klingebiel R, Amberger N, van der Knaap MS, Zschenderlein R. The LRRK2 gene in Parkinson's disease: mutation screening in patients from Germany. *J Neurol Neurosurg Psychiatry*. 2006;77(7):889–91.
162. Thaler A, Ash E, Gan-Or Z, Orr-Urtreger A, Giladi N. The LRRK2 G2019S mutation as the cause of Parkinson's disease in Ashkenazi Jews. *J Neural Transm*. 2009;116(11):1473–82.
163. Desideri E, Martins LM. Mitochondrial stress signalling: HTRA2 and Parkinson's

- disease. *Int J Cell Biol.* 2012;2012.
164. Ross OA, Soto AI, Vilariño-güell C, Heckman MG, Diehl N, Hulihan MM, et al. Genetic variation of Omi/HtrA2 and Parkinson's disease. *2009;14(7):539–43.*
 165. Costa G, Abin-Carriquiry JA, Dajas F. Nicotine prevents striatal dopamine loss produced by 6-hydroxydopamine lesion in the substantia nigra. *Brain Res.* 2001;888(2):336–42.
 166. Jeyarasasingam G, Tompkins L, Quik M. Stimulation of non- $\alpha 7$ nicotinic receptors partially protects dopaminergic neurons from 1-methyl-4-phenylpyridinium-induced toxicity in culture. *Neuroscience.* 2002;109(2):275–85.
 167. Lolekha P, Phanthumchinda K, Bhidayasiri R. Prevalence and risk factors of Parkinson's disease in retired Thai traditional boxers. *Mov Disord.* 2010;25(12):1895–901.
 168. Deik A, Saunders-Pullman R, Luciano MS. Substance abuse and movement disorders: complex interactions and comorbidities. *Curr Drug Abuse Rev [Internet].* 2012;5(3):243–53. Available from: <http://www.pubmedcentral.nih.gov/articlerender.fcgi?artid=3966544&tool=pmcentrez&rendertype=abstract>
 169. Allam MF, Serrano A, Castillo D. Parkinson ' s disease risk factors : genetic , environmental , or both ? *2005;27:206–8.*
 170. Olanow CW, Perl DP, DeMartino GN, McNaught KSP. Lewy-body formation is an aggresome-related process: A hypothesis. *Lancet Neurol.* 2004;3(8):496–503.
 171. Dennis W. Dickson, MD,* Hirotake Uchikado, MD, PhD, Hiroshige Fujishiro, MD, PhD, and Yoshio Tsuboi M. Evidence in favor of Braak Staging of Parkinson's disease. *Mov Disord.* 2010;25(SUPPL. 1):78–82.
 172. Burke RE, Dauer WT, Vonsattel JPG. A critical evaluation of the Braak staging scheme for Parkinson's disease. *Ann Neurol.* 2008;64(5):485–91.
 173. Zhao YJ, Wee HL, Chan YH, Seah SH, Au WL, Lau PN, et al. Progression of Parkinson's disease as evaluated by Hoehn and Yahr stage transition times. *Mov Disord.* 2010;25(6):710–6.
 174. Baker MJtAZ, Hauser RA. Autonomic Nervous System Dysfunction in Parkinson ' s Disease. *Curr Treat.* 2003;
 175. Kim CS, Sung YH, Kang MJ, Park KH. Rapid Eye Movement Sleep Behavior Disorder in Parkinson's Disease: A Preliminary Study. *J Mov Disord [Internet].* 2016;9(2):114–9. Available from: <http://www.ncbi.nlm.nih.gov/pubmed/26936443%0Ahttp://www.pubmedcentral.nih.gov/articlerender.fcgi?artid=PMC4886198>

176. Shah M, Deeb J, Fernando M, Noyce A, Visentin E, Findley LJ, et al. Abnormality of taste and smell in Parkinson's disease. *Park Relat Disord*. 2009;15(3):232–7.
177. Field T. Smell and Taste Dysfunction as Early Markers for Neurodegenerative and Neuropsychiatric Diseases. *J Alzheimers Dis Park* [Internet]. 2015;5(1):186. Available from: <http://www.omicsonline.org/open-access/smell-and-taste-dysfunction-as-early-markers-for-neurodegenerative-and-neuropsychiatric-diseases-2161-0460-1000186.php?aid=42383>
178. Frisina PG, Borod JC, Foldi NS, Tenenbaum HR. Depression in Parkinson's disease: Health risks, etiology, and treatment options. *Neuropsychiatr Dis Treat*. 2008;4(1 A):81–91.
179. McDonald WM, Richard IH, DeLong MR. Prevalence, etiology, and treatment of depression in Parkinson's disease. *Biol Psychiatry*. 2003;54(3):363–75.
180. MCNamara P. The cognitive Neuropsychiatry of Parkinson's disease.
181. Kageyama T, Nakamura M, Matsuo A, Yamasaki Y, Takakura Y, Hashida M, et al. The 4F2hc/LAT1 complex transports L-DOPA across the blood-brain barrier. *Brain Res*. 2000;879(1–2):115–21.
182. Zou L, Jankovic J, Rowe DB, Xie W, Appel SH, Le W. Neuroprotection by pramipexole against dopamine- and levodopa-induced cytotoxicity. *Life Sci*. 1999;64(15):1275–85.
183. Thanvi B, Lo N, Robinson T. Levodopa-induced dyskinesia in Parkinson's disease: clinical features, pathogenesis, prevention and treatment. *Postgrad Med J* [Internet]. 2007;83(980):384–8. Available from: <http://www.ncbi.nlm.nih.gov/pmc/articles/PMC2600052/>
184. Bohnen N, Albin R. The Cholinergic System in Parkinson's Disease. *Behav Brain Res*. 2011;221(2):564–73.
185. Bohnen N, Müller M, Koeppe R, Studenski S, Kilbourn M, Frey K, et al. History of falls in Parkinson's disease is associated with reduced cholinergic activity. *Neurology*. 2009;73(20):1670–6.
186. Hung AS, Tsui TY, Lam JC, Wai MS, Chan WM, Yew DT. Serotonin and its receptors in the human CNS with new findings - a mini review. *CurrMedChem*. 2011;18(34):5281–8.
187. Politis M, Loane C. Serotonergic Dysfunction in Parkinson's Disease and Its Relevance to Disability. *Sci World J*. 2011;11:1726–34.
188. Porras G, Matteo V Di, Fracasso C, Lucas G, Spampinato U. 5-HT_{2A} and 5-HT_{2C/B} receptor subtypes modulate dopamine release induced in vivo by amphetamine and morphine in both the rat nucleus accumbens and striatum.

- Neuropsychopharmacology. 2002;26(1):311–24.
189. Johnson K a, Conn PJ, Niswender CM. Glutamate receptors as therapeutic targets for Parkinson's disease. *CNS Neurol Disord Drug Targets* [Internet]. 2009;8(6):475–91. Available from: <http://www.ncbi.nlm.nih.gov/pubmed/19702565><http://www.pubmedcentral.nih.gov/articlerender.fcgi?artid=PMC3005251>
 190. Ahmed I, Bose SK, Pavese N, Ramlackhansingh A, Turkheimer F, Hotton G, et al. Glutamate NMDA receptor dysregulation in Parkinson's disease with dyskinesias. *Brain*. 2011;134(4):979–86.
 191. Gasparini F, Di Paolo T, Gomez-Mancilla B. Metabotropic glutamate receptors for parkinson's disease therapy. *Parkinsons Dis*. 2013;2013(Table 1).
 192. Cieślak M, Komoszyński M, Wojtczak A. Adenosine A2A receptors in Parkinson's disease treatment. *Purinergic Signal*. 2008;4(4):305–12.
 193. Yin S, Zhang X, Chen S, Yang W, Zheng X, Zheng G. Adenosine A2A Receptor Gene Knockout Prevents I-3,4-Dihydroxyphenylalanine-Induced Dyskinesia by Downregulation of Striatal GAD67 in 6-OHDA-Lesioned Parkinson's Mice. *Front Neurol* [Internet]. 2017;8(March):88. Available from: <http://journal.frontiersin.org/article/10.3389/fneur.2017.00088/full>
 194. Hattori N, Kikuchi M, Adachi N, Hewitt D, Huyck S, Saito T. Adjunctive preladenant: A placebo-controlled, dose-finding study in Japanese patients with Parkinson's disease. *Parkinsonism Relat Disord* [Internet]. 2016;32:73–9. Available from: <http://linkinghub.elsevier.com/retrieve/pii/S1353802016303248>
 195. Pinna A. Adenosine A2A receptor antagonists in Parkinson's disease: Progress in clinical trials from the newly approved istradefylline to drugs in early development and those already discontinued. *CNS Drugs*. 2014;28(5):455–74.
 196. Brambilla D, Chapman D, Greene R. Adenosine mediation of presynaptic feedback inhibition of glutamate release. *Neuron*. 2005;46(2):275–83.
 197. Calon F, Dridi M, Hornykiewicz O, Bédard PJ, Rajput AH, Di Paolo T. Increased adenosine A2A receptors in the brain of Parkinson's disease patients with dyskinesias. *Brain*. 2004;127(5):1075–84.
 198. Beggiano S, Tomasini MC, Borelli AC, Borroto-Escuela DO, Fuxe K, Antonelli T, et al. Functional role of striatal A2A, D2, and mGlu5 receptor interactions in regulating striatopallidal GABA neuronal transmission. *J Neurochem*. 2016;19:254–64.
 199. El Yacoubi M, Ledent C, Parmentier M, Costentin J, Vaugeois JM. SCH 58261 and ZM 241385 differentially prevent the motor effects of CGS 21680 in mice: Evidence for a functional "atypical" adenosine A2A receptor. *Eur J Pharmacol*.

- 2000;401(1):63–77.
200. Hsu CW, Chen CY, Wang CS, Chiu TH. Caffeine and a selective adenosine A2A receptor antagonist induce reward and sensitization behavior associated with increased phospho-Thr75-DARPP-32 in mice. *Psychopharmacology (Berl)*. 2009;204(2):313–25.
 201. Administration of Substances to Laboratory Animals: Routes of Administration and Factors to Consider. *J Am Assoc Lab Anim Sci*. 2011;50(5):600–13.
 202. Haley TJ, McCormick WG. Pharmacological effects produced by intra-cerebral injections of drugs in the conscious mouse. *J Pharmacol*. 1957;12.
 203. P.D. Brown, S.L. Davies TS and IDM. Molecular Mechanisms of Cerebrospinal Fluid Production. *Neuroscience*. 2004;129(4):957–70.
 204. Gabriel LR, Wu S, Melikian HE. Brain slice biotinylation: an ex vivo approach to measure region-specific plasma membrane protein trafficking in adult neurons. *J Vis Exp [Internet]*. 2014;1506(86):1–6. Available from: <http://www.ncbi.nlm.nih.gov/pubmed/24747337>
 205. Deepika Ahuja MTS-R and JMP. SV40 large T antigen targets multiple cellular pathways to elicit cellular transformation. *Oncogene*. 2005;24.
 206. Gratacòs E, Checa N, Pérez-Navarro E, Alberch J. Brain-derived neurotrophic factor (BDNF) mediates bone morphogenetic protein-2 (BMP-2) effects on cultured striatal neurons. *J Neurochem [Internet]*. 2008 Jul 7 [cited 2016 Jul 5];79(4):747–55. Available from: <http://doi.wiley.com/10.1046/j.1471-4159.2001.00570.x>
 207. Gonçalves FQ, Pires J, Pliassova A, Beleza R, Lemos C, Marques JM, et al. Adenosine A2B receptors control A1 receptor-mediated inhibition of synaptic transmission in the mouse hippocampus. *Eur J Neurosci [Internet]*. 2015;41(October 2014). Available from: <http://doi.wiley.com/10.1111/ejn.12851>
 208. Taura J, Fernández-Dueñas V, Ciruela F. Visualizing G protein-coupled receptor-receptor interactions in brain using proximity ligation in situ assay. *Curr Protoc Cell Biol*. 2015;2015(June):17.17.1-17.17.16.
 209. Tönnies J, Stierli B, Cerletti C, Behrmann JT, Molnár E, Streit P. Regional distribution and developmental changes of GluR1-flop protein revealed by monoclonal antibody in rat brain. *J Neurochem [Internet]*. 1999;73(5):2195–205. Available from: <http://www.ncbi.nlm.nih.gov/pubmed/10537080>
 210. Fernández-Alacid L, Watanabe M, Molnár E, Wickman K, Luján R. Developmental regulation of G protein-gated inwardly-rectifying K⁺ (GIRK/Kir3) channel subunits in the brain. *Eur J Neurosci*. 2011;34(11):1724–36.
 211. Bortolotto ZA, Amici M, Anderson WW, Isaac JTR, Collingridge GL. Synaptic

- Plasticity in the Hippocampal Slice. *Curr Protoc Neurosci* [Internet]. 2001;Chapter 6:1–23. Available from:
<http://www.ncbi.nlm.nih.gov/pubmed/21207366>
212. Li W, Silva HB, Real J, Wang YM, Rial D, Li P, et al. Inactivation of adenosine A2a receptors reverses working memory deficits at early stages of Huntington's disease models. *Neurobiol Dis* [Internet]. 2015;79:70–80. Available from:
<http://dx.doi.org/10.1016/j.nbd.2015.03.030>
 213. Deacon RMJ. Digging and marble burying in mice: simple methods for in vivo identification of biological impacts. *Nat Protoc*. 2006;1(1):122–4.
 214. Bevins R a, Besheer J. Object recognition in rats and mice: a one-trial non-matching-to-sample learning task to study “recognition memory”. *Nat Protoc* [Internet]. 2006;1(3):1306–11. Available from:
<http://dx.doi.org/10.1038/nprot.2006.205>
 215. Dawson GR, Crawford SP, Collinson N, Iversen SD, Tricklebank MD. Evidence that the anxiolytic-like effects of chlordiazepoxide on the elevated plus maze are confounded by increases in locomotor activity. *Psychopharmacology (Berl)*. 1995;118(3):316–23.
 216. Dawson GR, Tricklebank MD. Use of the elevated plus maze in the search for novel anxiolytic agents. *Trends Pharmacol Sci*. 1995;16(2):33–6.
 217. Gupta G, Singh R, David SR, Verma RK. Effect of rosiglitazone, a ppar- γ ligand on haloperidol-induced catalepsy. *CNS Neurosci Ther*. 2013;19(9):724–5.
 218. Lee AS, Duman RS, Pittenger C. A double dissociation revealing bidirectional competition between striatum and hippocampus during learning. *Proc Natl Acad Sci U S A*. 2008;105(44):17163–8.
 219. Packard MG, McGaugh JL. Double dissociation of fornix and caudate nucleus lesions on acquisition of two water maze tasks: further evidence for multiple memory systems. *Behav Neurosci*. 1992;106(3):439–46.
 220. Kaskova ZM, Tsarkova AS, Yampolsky I V. 1001 Lights: Luciferins, Luciferases, Their Mechanisms of Action and Applications in Chemical Analysis, Biology and Medicine. *Chem Soc Rev* [Internet]. 2016;45(21):6048–77. Available from:
<http://dx.doi.org/10.1039/C6CS00296J>
 221. Stoddart LA, Johnstone EKM, Wheal AJ, Goulding J, Robers MB, Machleidt T, et al. Application of BRET to monitor ligand binding to GPCRs. *Nat Methods* [Internet]. 2015;12(7):661–3. Available from:
<http://dx.doi.org/10.1038/nmeth.3398>
 222. Jorge Gandia, Victor Fernandez-Dueñas, Xavier Morató, Gianluigi Caltabiano, Rosario Gonzalez-Muñiz, Leonardo Pardo IS and FC. The Parkinson's disease-

- associated GPR37 receptor-mediated cytotoxicity is controlled by its intracellular cysteine-rich domain. *J Neurochem.* 2013;125:362–72.
223. Sokolina K, Kittanakom S, Snider J, Kotlyar M, Maurice P, Gandía J, et al. Systematic protein–protein interaction mapping for clinically relevant human GPCRs. *Mol Syst Biol.* 2017;13:1–19.
224. Gandía J, Morató X, Stagljar I, Fernández-dueñas V. Adenosine A2A receptor-mediated control of pilocarpine-induced tremulous jaw movements is Parkinson's disease-associated GPR37 receptor-dependent. Available from: <http://msb.embopress.org/lookup/doi/10.15252/msb.20167430>
225. Fernández-Dueñas V, Taura JJ, Cottet M, Gómez-Soler M, López-Cano M, Ledent C, et al. Untangling dopamine-adenosine receptor-receptor assembly in experimental parkinsonism in rats. *Dis Model Mech.* 2015 Jan;8(1):57–63.
226. Dixon a K, Gubitza a K, Sirinathsinghji DJ, Richardson PJ, Freeman TC. Tissue distribution of adenosine receptor mRNAs in the rat. *Br J Pharmacol.* 1996;118(6):1461–8.
227. Rosin DL, Hettinger BD, Lee A, Linden J. Anatomy of adenosine A2A receptors in brain: morphological substrates for integration of striatal function. *Neurology.* 2003 Dec;61(11 Suppl 6):S12-8.
228. Lopes JP, Morató X, Souza C, Pinhal C, Machado NJ, Canas PM, et al. The role of parkinson's disease-associated receptor GPR37 in the hippocampus: Functional interplay with the adenosinergic system. *J Neurochem.* 2015;134(1):135–46.
229. Taura J, Fernández-Dueñas V, Ciruela F. Visualizing G Protein-Coupled Receptor-Receptor Interactions in Brain Using Proximity Ligation In Situ Assay. *Curr Protoc Cell Biol.* 2015 Jan;67:17.17.1-17.17.16.
230. Fuxe K, Agnati LF, Jacobsen K, Hillion J, Canals M, Torvinen M, et al. Receptor heteromerization in adenosine A2A receptor signaling: relevance for striatal function and Parkinson's disease. *Neurology.* 2003;61(11 Suppl 6):S19-23.
231. Fernández-Dueñas V, Gómez-Soler M, López-Cano M, Taura JJ, Ledent C, Watanabe M, et al. Uncovering Caffeine's Adenosine A2A Receptor Inverse Agonism in Experimental Parkinsonism. *ACS Chem Biol.* 2014 Nov;9(11):2496–501.
232. Wardas J, Pietraszek M, Dziedzicka-Wasylewska M. SCH 58261, a selective adenosine A2A receptor antagonist, decreases the haloperidol-enhanced proenkephalin mRNA expression in the rat striatum. *Brain Res.* 2003;977(2):270–7.
233. Ferré S. Adenosine-dopamine interactions in the ventral striatum. Implications

- for the treatment of schizophrenia. *Psychopharmacology (Berl)*. 1997 Sep;133(2):107–20.
234. Cabeza de Vaca S, Kannan P, Pan Y, Jiang N, Sun Y, Carr KD. The adenosine A2A receptor agonist, CGS-21680, blocks excessive rearing, acquisition of wheel running, and increases nucleus accumbens CREB phosphorylation in chronically food-restricted rats. *Brain Res*. 2007 Apr;1142:100–9.
235. Hauber W, Mönkle M. Motor depressant effects mediated by dopamine D2 and adenosine A2A receptors in the nucleus accumbens and the caudate-putamen. *Eur J Pharmacol*. 1997 Apr;323(2–3):127–31.
236. Wardas J, Konieczny J, Pietraszek M. Influence of CGS-21680, a selective adenosine A2A agonist, on the phencyclidine-induced sensorimotor gating deficit and motor behaviour in rats. *Psychopharmacology (Berl)*. 2003 Jul;168(3):299–306.
237. Clarke RBC, Adermark L. Acute ethanol treatment prevents endocannabinoid-mediated long-lasting disinhibition of striatal output. *Neuropharmacology* [Internet]. 2010;58(4–5):799–805. Available from: <http://dx.doi.org/10.1016/j.neuropharm.2009.12.006>
238. Kreitzer TNL and AC. RGS4 is required for dopaminergic control of striatal LTD and susceptibility to parkinsonian motor deficits. *Neuron*. 2012;73(2):347–59.
239. Martella G, Tassone A, Sciamanna G, Platania P, Cuomo D, Viscomi MT, et al. Impairment of bidirectional synaptic plasticity in the striatum of a mouse model of DYT1 dystonia: Role of endogenous acetylcholine. *Brain*. 2009;132(9):2336–49.
240. Cunha RA. Different cellular sources and different roles of adenosine: A1 receptor-mediated inhibition through astrocytic-driven volume transmission and synapse-restricted A2A receptor-mediated facilitation of plasticity. *Neurochem Int*. 2008;52(1):65–72.
241. Simões AP, Machado NJ, Gonçalves N, Kaster MP, Simões AT, Nunes A, et al. Adenosine A2A Receptors in the Amygdala Control Synaptic Plasticity and Contextual Fear Memory. *Neuropsychopharmacology* [Internet]. 2016;41(12):2862–71. Available from: <http://www.nature.com/doi/10.1038/npp.2016.98>
242. Hsu CW, Wang CS, Chiu TH. Caffeine and a selective adenosine A2A receptor antagonist induce sensitization and cross-sensitization behavior associated with increased striatal dopamine in mice. *J Biomed Sci*. 2010;17:4.
243. Pittenge LCBR and C. Cued and spatial learning in the water maze: equivalent learning in male and female mice. *Biophys Chem*. 2010;483(5):2432–7.
244. Lee AS, André JM, Pittenger C. Lesions of the dorsomedial striatum delay

- spatial learning and render cue-based navigation inflexible in a water maze task in mice. *Front Behav Neurosci* [Internet]. 2014;8(FEB):42. Available from: <http://www.scopus.com/inward/record.url?eid=2-s2.0-84894033522&partnerID=tZOtx3y1>
245. Mandillo S, Golini E, Marazziti D, Di Pietro C, Matteoni R, Tocchini-Valentini GP. Mice lacking the Parkinson's related GPR37/PAEL receptor show non-motor behavioral phenotypes: Age and gender effect. *Genes, Brain Behav*. 2013;12(4):465–77.
 246. Bannerman DM, Sprengel R, Sanderson DJ, McHugh SB, Rawlins JNP, Monyer H, et al. Hippocampal synaptic plasticity, spatial memory and anxiety. *Nat Rev Neurosci* [Internet]. 2014;15(3):181–92. Available from: <http://www.ncbi.nlm.nih.gov/pubmed/24552786>
 247. Catherine J. Wei, Elisabete Augusto, Catarina A. Gomes, Philipp Singer, Yumei Wang, Detlev Boison, Rodrigo A. Cunha, Benjamin K. Yee and J-FC. Regulation of fear responses by striatal and extra-striatal adenosine A2A receptors in forebrain. *June*. 2014;75(11):855–63.
 248. Kaster MP, Machado NJ, Silva HB, Nunes A, Ardaís AP, Santana M, et al. Caffeine acts through neuronal adenosine A 2A receptors to prevent mood and memory dysfunction triggered by chronic stress. *Proc Natl Acad Sci* [Internet]. 2015;112(25):201423088. Available from: <http://www.pnas.org/lookup/doi/10.1073/pnas.1423088112>
 249. Simonsen AH, Kuiperij B, Ali El-Agnaf OM, Engelborghs S, Herukka S-K, Parnetti L, et al. The utility of α -synuclein as biofluid marker in neurodegenerative diseases: a systematic review of the literature. *Biomark Med*. 2015;10(1):19–34.
 250. Parnetti L, Castrioto A, Chiasserini D, Persichetti E, Tambasco N, El-agnaf O, et al. Cerebrospinal fluid biomarkers in Parkinson disease. *Nat Publ Gr* [Internet]. 2013;9(3):131–40. Available from: <http://dx.doi.org/10.1038/nrneurol.2013.10>
 251. Coleman JLJ, Ngo T, Schmidt J, Mrad N, Liew CK, Jones NM, et al. Metalloprotease cleavage of the N terminus of the orphan G protein-coupled receptor GPR37L1 reduces its constitutive activity. *Sci Signal* [Internet]. 2016;9(423):ra36-ra36. Available from: <http://stke.sciencemag.org/content/9/423/ra36.abstract>
 252. Markovic D, Challiss R a J. Alternative splicing of G protein-coupled receptors: physiology and pathophysiology. *Cell Mol Life Sci*. 2009;66(August 2009):3337–52.
 253. Folabomi A. Oladosu, BS WM and AGN. Alternative Splicing of G-protein

- Coupled Receptors: Relevance to Pain Management. *Mayo Clin Proc.* 2015;90(8):1135–51.
254. Milligan G. G protein-coupled receptor hetero-dimerization: Contribution to pharmacology and function. *Br J Pharmacol.* 2009;158(1):5–14.
 255. Margeta-Mitrovic M, Jan YN, Jan LY. A trafficking checkpoint controls GABA(B) receptor heterodimerization. *Neuron.* 2000;27(1):97–106.
 256. Thathiah A, De Strooper B. The role of G protein-coupled receptors in the pathology of Alzheimer's disease. *Nat Rev Neurosci [Internet].* 2011;12(2):73–87. Available from: <http://dx.doi.org/10.1038/nrn2977>
 257. G. CF-P and J. GPCRs in cardiovascular pathologies. *Drug Discov Today.* 2012;49(9 (3)):743–50.
 258. Ferré S, Quiroz C, Orru M, Guitart X, Navarro G, Cortés A, et al. Adenosine A(2A) Receptors and A(2A) Receptor Heteromers as Key Players in Striatal Function. *Front Neuroanat [Internet].* 2011;5(June):36. Available from: <http://www.pubmedcentral.nih.gov/articlerender.fcgi?artid=3118889&tool=pmcentrez&rendertype=abstract>
 259. Phillips GR, Huang JK, Wang Y, Tanaka H, Shapiro L, Zhang W, et al. The presynaptic particle web: Ultrastructure, composition, dissolution, and reconstitution. *Neuron.* 2001;32(1):63–77.
 260. Xavier Morató, Dasiel O. Borroto-Escuela, Kjell Fuxe, Víctor Fernández-Dueñas and FC. Chapter 2: Co-immunoprecipitation from Brain. *Receptor and Ion Channel Detection in the Brain. Neuromethods.* 2016. 19-30 p.
 261. Trifilieff P, Rives M, Urizar E, Piskorowski RA, Vishwasrao HD, Castrillon J, et al. Detection of antigen interactions ex vivo by proximity ligation assay: endogenous dopamine D2-adenosine A2A receptor complexes in the striatum. *Biotechniques.* 2011;51(2):111–8.
 262. Neill DB, Ross JF, Grossman SP. Effects of lesions in the dorsal or ventral striatum on locomotor activity and on locomotor effects of amphetamine. *Pharmacol Biochem Behav [Internet].* 1974;2(5):697–702. Available from: <http://www.ncbi.nlm.nih.gov/pubmed/4610596>
 263. Knowlton MGP and BJ. Learning and memory functions of the basal ganglia. *Annu Rev Neurosci [Internet].* 2002;25(1):563–93. Available from: <http://www.annualreviews.org/doi/10.1146/annurev.immunol.22.012703.104702>
 264. Rezgoui M, Susens U, Ignatov A, Gelderblom M, Glassmeier G, Franke I, et al. The neuropeptide head activator is a high-affinity ligand for the orphan G-protein-coupled receptor GPR37. *J Cell Sci.* 2006 Feb;119(Pt 3):542–9.
 265. Smith NJ. Drug discovery opportunities at the endothelin B receptor-related

- orphan G protein-coupled receptors, GPR37 and GPR37L1. *Front Pharmacol.* 2015;6(NOV):1–13.
266. Ferre S, von Euler G, Johansson B, Fredholm BB, Fuxe K. Stimulation of high-affinity adenosine A2 receptors decreases the affinity of dopamine D2 receptors in rat striatal membranes. *Proc Natl Acad Sci U S A* [Internet]. 1991;88(16):7238–41. Available from: <http://www.pubmedcentral.nih.gov/articlerender.fcgi?artid=52269&tool=pmcentrez&rendertype=abstract>
267. Aoyama S, Kase H, Borrelli E. Rescue of locomotor impairment in dopamine D2 receptor-deficient mice by an adenosine A2A receptor antagonist. *J Neurosci* [Internet]. 2000;20(15):5848–52. Available from: <http://eutils.ncbi.nlm.nih.gov/entrez/eutils/elink.fcgi?dbfrom=pubmed&id=10908627&retmode=ref&cmd=prlinks>
268. Lindskog M, Svenningsson P, Pozzi L, Kim Y, Fienberg AA, Bibb JA, et al. Involvement of DARPP-32 phosphorylation in the stimulant action of caffeine. *Nature* [Internet]. 2002;418(6899):774–8. Available from: <http://www.nature.com/doi/10.1038/nature00817>
269. Centonze D, Picconi B, Gubellini P, Bernardi G, Calabresi P. Dopaminergic control of synaptic plasticity in the dorsal striatum. *Eur J Neurosci.* 2001;13(6):1071–7.
270. Gould TD, Manji HK. DARPP-32: A molecular switch at the nexus of reward pathway plasticity. *Proc Natl Acad Sci U S A* [Internet]. 2005;102(2):253–4. Available from: <http://www.pubmedcentral.nih.gov/articlerender.fcgi?artid=544318&tool=pmcentrez&rendertype=abstract>
271. Nairn AC, Svenningsson P, Nishi A, Fisone G, Girault JA, Greengard P. The role of DARPP-32 in the actions of drugs of abuse. *Neuropharmacology.* 2004;47(SUPPL. 1):14–23.
272. Simola N, Cauli O, Morelli M. Sensitization to caffeine and cross-sensitization to amphetamine: Influence of individual response to caffeine. *Behav Brain Res.* 2006;172(1):72–9.
273. Simola N, Tronci E, Pinna A, Morelli M. Subchronic-intermittent caffeine amplifies the motor effects of amphetamine in rats. *Amino Acids.* 2006;31(4):359–63.
274. Robinson TE, Berridge KC. The psychology and neurobiology of addiction: an incentive – sensitization view. *Addiction.* 2000;95(2):91–117.
275. Scheggi S, Rauggi R, Gambarana C, Tagliamonte A, De Montis MG. Dopamine

- and cyclic AMP-regulated phosphoprotein-32 phosphorylation pattern in cocaine and morphine-sensitized rats. *J Neurochem.* 2004;90(4):792–9.
276. Rial D, Morató X, Real JI, Gonçalves FQ, Stagljar I, Pereira FC, et al. Parkinson's disease-associated GPR37 receptor regulates cocaine-mediated synaptic depression in corticostriatal synapses. *Neurosci Lett.* 2017;638:162–6.
277. Leng N, Gu G, Simerly RB, Spindel ER. Molecular cloning and characterization of two putative G protein-coupled receptors which are highly expressed in the central nervous system. *Brain Res Mol Brain Res.* 1999;69(1):73–83.
278. Takahashi R, Imai Y. Pael receptor, endoplasmic reticulum stress, and Parkinson's disease. *J Neurol.* 2003;250(Suppl 3):III25-9.
279. Lundius EG, Vukojevic V, Hertz E, Stroth N, Cederlund A, Hiraiwa M, et al. GPR37 protein trafficking to the plasma membrane regulated by prosaposin and GM1 gangliosides promotes cell viability. *J Biol Chem.* 2014;289(8):4660–73.
280. Villar-Menéndez I, Porta S, Buirra SP, Pereira-Veiga T, Díaz-Sánchez S, Albasanz JL, et al. Increased striatal adenosine A2A receptor levels is an early event in Parkinson's disease-related pathology and it is potentially regulated by miR-34b. *Neurobiol Dis [Internet].* 2014;69:206–14. Available from: <http://dx.doi.org/10.1016/j.nbd.2014.05.030>
281. Cheng HC, Ulane C., Burke R. Clinical progression in Parkinson's disease and the neurobiology of Axons. *Ann Neurol.* 2010;67(6):715–25.
282. Sharma S, Moon CS, Khogali A, Haidous A, Chabenne A, Ojo C, et al. Biomarkers in Parkinson's disease (recent update). *Neurochem Int.* 2013;63(3):201–29.
283. Waragai M, Sekiyama K, Sekigawa A, Takamatsu Y, Fujita M, Hashimoto M. a-Synuclein and DJ-1 As Potential Biological Fluid Biomarkers for Parkinson'S Disease. *Int J Mol Sci.* 2010;11(11):4257–66.
284. Mattila SO, Tuusa JT, Petäjä-repo UE. Parkinson ' s disease-associated GPR37 undergoes metalloproteinase-mediated N-terminal cleavage and ectodomain shedding.
285. Grantcharova E, Furkert J, Peter Reusch H, Krell HW, Papsdorf G, Beyermann M, et al. The extracellular N terminus of the endothelin B (ETB) receptor is cleaved by a metalloprotease in an agonist-dependent process. *J Biol Chem.* 2002;277(46):43933–41.
286. Kjelsberg MA, Cotecchia S, Ostrowski J, Caron MG, Lefkowitz RJ. Constitutive activation of the b1-adrenergic receptor by all amino acid substitutions at a single site: Evidence for a region which constrains receptor activation. *J Biol Chem.* 1992;267(3):1430–3.

287. Klenk C, Schulz S, Calebiro D, Lohse MJ. Agonist-regulated cleavage of the extracellular domain of parathyroid hormone receptor type 1. *J Biol Chem*. 2010;285(12):8665–74.
288. Soh UJ, Dores MR, Chen B, Trejo J. Signal transduction by protease-activated receptors. *Br J Pharmacol*. 2010;160(2):191–203.
289. Stoveken HM, Hajduczuk AG, Xu L, Tall GG. Adhesion G protein-coupled receptors are activated by exposure of a cryptic tethered agonist. *Proc Natl Acad Sci [Internet]*. 2015;112(19):6194–9. Available from: <http://www.pnas.org/content/112/19/6194.abstract>
290. Shi M, Movius J, Dator R, Aro P, Zhao Y, Pan C, et al. Cerebrospinal fluid peptides as potential Parkinson disease biomarkers: a staged pipeline for discovery and validation. *Mol Cell Proteomics [Internet]*. 2015;14(3):544–55. Available from: <http://www.pubmedcentral.nih.gov/articlerender.fcgi?artid=4349976&tool=pmc.ncbi&rendertype=abstract>
291. Halim A, Rüetschi U, Larson G, Nilsson J. LC-MS/MS characterization of O-glycosylation sites and glycan structures of human cerebrospinal fluid glycoproteins. *J Proteome Res*. 2013;12(2):573–84.
292. Berger BS, Acebron SP, Herbst J, Koch S, Niehrs C. Parkinson's disease-associated receptor GPR37 is an ER chaperone for LRP6. *EMBO Rep [Internet]*. 2017;e201643585. Available from: <http://embor.embopress.org/lookup/doi/10.15252/embr.201643585>
293. Fujita-Jimbo E, Yu ZL, Li H, Yamagata T, Mori M, Momoi T, et al. Mutation in Parkinson Disease-Associated, G-Protein-Coupled Receptor 37 (GPR37/PaelR) Is Related to Autism Spectrum Disorder. *PLoS One*. 2012;7(12):3–8.
294. Compta Y, Valente T, Saura J, Segura B, Iranzo Á, Serradell M, et al. Correlates of cerebrospinal fluid levels of oligomeric- and total- α -synuclein in premotor, motor and dementia stages of Parkinson's disease. *J Neurol*. 2014;262(2):294–306.
295. Li P, Rial D, Canas PM, Yoo J, Li W, Zhou X, et al. Optogenetic activation of intracellular adenosine A2A receptor signaling in hippocampus is sufficient to trigger CREB phosphorylation and impair memory. 2016;20(11):1339–49.
296. Behavior G, Li Y, He Y, Chen M, Pu Z, Chen L, et al. Optogenetic Activation of Adenosine A 2A Receptor Signaling in the Dorsomedial Striatopallidal Neurons Suppresses. 2016;1003–13.

IX. Acknowledgements

Finalment, estic molt feliç d'arribar a aquest apartat de la Tesi, on puc agrair a tota la gent a qui admiro, estimo i aprecio tot el que m'han ajudat durant aquests anys. Els agraïments són aquella petita porció de la tesi doctoral on te n'adones que l'aspecte de la portada hauria de ser el següent:

Títol de la tesi

Família, Directors de tesi, companys i amics del laboratori, amistats, una immensitat de gent que ha participat en la teva formació prèvia, els gats i finalment el doctorand.

Primerament, m'agradaria agrair al Dr. Francisco Ciruela (Ying) l'oportunitat de realitzar la tesi doctoral al seu grup de recerca. Em va obrir les portes i gràcies a ell m'he enamorat de la Neurociència. També vull agrair tota l'ajuda rebuda d'en Víctor Fernández (Yang), tot un *Trail runner*, de qui he rebut de manera equimolar dosis de coneixements científics i teràpia psicològica. Ambdós han estat figures fonamentals durant tot el viatge i m'han ajudat a créixer en molts aspectes. També vull agrair la gran tolerància musical que han tingut amb els *hits musicals* que molt de tant en tant he sintonitzat al laboratori.

M'agradaria seguir amb la família. Mare, Tieta, cosins, la iaia "cul inquieta" i los primos de Hospi. Gràcies pel vostre suport incondicional tot i no entendre massa be què renoi feia tantes hores al laboratori, quina motivació hi trobava i per què encara no havia muntat la meva pròpia condoneria (Farmàcia). I a la família adoptiva: Belén, Fani+10, David, Pollo, Àlex, Nyicras, Dex i Fiona. Us estimo moltíssim!

Seguidament, m'agradaria donar les gràcies a la Dra. M^o Àngels Manresa Presas, amb qui vaig començar a gaudir de la "taula de laboratori" i l'olor a LB, a en Nel de Salort que va adquirir el títol de Sant al aguantar de manera estoica el període que em va tenir de pràctiques i a l'Artur Llobet amb qui vaig aprendre que les coses que fas s'han de mirar amb lupa.

Dels companys que m'han acompanyat durant el camí en podria nombrar "chorrocientos". De cadascun d'ells n'he après alguna cosa i me n'he quedat una part. Fran Pechotes Murcia (my bro), Anna Nualart, Helena *Tropicalis*, David Albrecht (te vendremos a ver y lo sabes!!), Rafael Rafe, Jonny El Melenes, Eli, Krys, Soto, Benja Jornet...una generació daurada i que sempre despertareu en mi una síndrome de Peter Pan! Gràcies a vosaltres, Bellvitge ha fet honor al seu nom i espero i obligo a la vida a que creui els nostres camins de nou.

Agrair també el suport que m'han donat al grup de Farmacologia. Salut, Lourdes i Laura ^{L^L}, Silvia i Àlex. Al Juràssic lab (Papito Jorge, Glory Kaiju, Maricel Pinche Way Gómez, Fabiana i Kristopher). I als contemporanis IronMarc, Merte la Nueva, JT de Son

Rapinya, René Crazy i Kristopher gràcies per aguantar-me CADA DIA. Em sento molt afortunat d'haver compartit una etapa tant important amb vosaltres (com a mínim en un dels universos). A los que ya no estan entre nosotros (Débora Lannister, Leandra, Paulo, Rahulk, Marta la nueva Nueva, Silvia i Kristopher) i als nouvinguts Altafaj lab, HL1éctor (tens un cor gegant!), Andreita (y su anecdotario de Bicorp), Fahad (el nostre traductor d'urdú), Paula i Kristopher.

També m'agradaria destacar el companyerisme que regna a la 4^a i 5^o planta. Els Estévez i Isidre's lab m'heu salvat mil i una vegades. I a títol particular, gràcies Paula per seguir-me la corrent amb el misteriós receptor GRP37 que no apareix ni al Pubmed. També ha estat un plaer compartir aquests anys amb vosaltres Pilingui i Ananda. I evidentment agrair al personal de l'Animal house tota la feina feta, especialment a la Pilar, Pedro, Lidia i Laia.

També voldria agrair el tracte rebut durant les estades externes. Prof. Rafael Luján, és un autèntic luxe haver tingut la oportunitat de compartir laboratori i aprendre de tu. Gràcies també a la resta de l'Albacete Lab, CRIBrothers i en especial a l'Ana Fajardo y su polvo cósmico (sona fatal!!). També m'agradaria agrair al Prof. Rodrigo Cunha que m'obris les portes del seu lab. Gràcies al laboratori de Purines del CNC de Coimbra per fer-me sentir tan còmode: Chico Queiroz fue un auténtico placer trabajar contigo, Paula Canas, Joao Pedro, Sofias entrenadoras Pokemon, Nelio i Samira. Moito obrigado!!

Finalment agrair a qui no tinc adjectius suficients per qualificar. La Sra. Preguntitas (Fani) tot el recolzament i *pressing* durant la part final de la tesi, per acompanyar-me en aquest camí i per suportar-me (en totes les accepcions de la paraula *suportar*) i per adaptar-te. Ets la peça que em fa tocar de peus a terra, em complementa, em fa créixer i ser molt millor persona.

En definitiva, gràcies a tots per ajudar-me a finalitzar la carrera de fons més dura que he realitzat fins al moment.